INTERNATIONAL JOURNAL

of

COMPUTERS COMMUNICATIONS & CONTROL

ISSN 1841-9836, e-ISSN 1841-9844

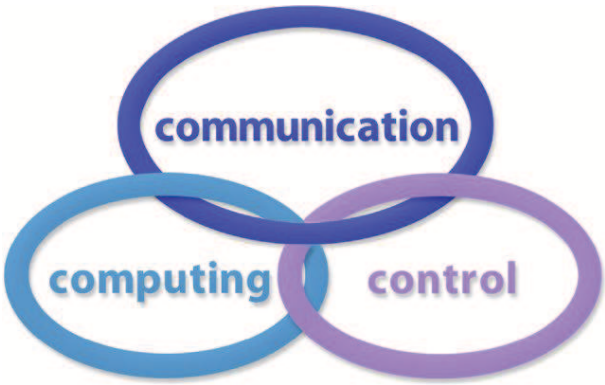

A Bimonthly Journal
With Emphasis on the Integration of Three Technologies

Year: 2019 Volume: 14 Issue: 5 Month: October

This journal is a member of, and subscribes to the principles of, the Committee on Publication Ethics (COPE).

http://univagora.ro/jour/index.php/ijccc/

CCC Publications

BRIEF DESCRIPTION OF JOURNAL

Publication Name: International Journal of Computers Communications & Control.
Acronym: IJCCC; **Starting year of IJCCC:** 2006.
ISO: Int. J. Comput. Commun. Control; **JCR Abbrev:** INT J COMPUT COMMUN.
International Standard Serial Number: ISSN 1841-9836, e-ISSN 1841-9844.
Publisher: CCC Publications - Agora University of Oradea.
Publication frequency: Bimonthly: Issue 1 (February); Issue 2 (April); Issue 3 (June); Issue 4 (August); Issue 5 (October); Issue 6 (December).
Founders of IJCCC: Ioan DZITAC, Florin Gheorghe FILIP and Misu-Jan MANOLESCU.

Indexing/Coverage:

- Since 2006, Vol. 1 (S), IJCCC is covered by Clarivate Analytics and is indexed in ISI Web of Science/Knowledge: Science Citation Index Expanded.

  2019 Journal Citation Reports® Science Edition (Clarivate Analytics, 2018):
  Subject Category: (1) Automation & Control Systems: Q4(2009, 2011, 2012, 2013, 2014, 2015), **Q3(2010, 2016, 2017, 2018)**; (2) Computer Science, Information Systems: Q4(2009, 2010, 2011, 2012, 2015), **Q3(2013, 2014, 2016, 2017, 2018)**.

  Impact Factor/3 years in JCR: 0.373(2009), 0.650 (2010), 0.438(2011); 0.441(2012), 0.694(2013), 0.746(2014), 0.627(2015), 1.374(2016), 1.29 (2017), **1.585 (2018)**.
  Impact Factor/5 years in JCR: 0.436(2012), 0.622(2013), 0.739(2014), 0.635(2015), 1.193(2016), 1.179(2017), **1.361(2018)**.

- Since 2008 IJCCC is indexed by Scopus: **CiteScore2018 = 1.56**.
  Subject Category:
  (1) Computational Theory and Mathematics: Q4(2009, 2010, 2012, 2015), **Q3(2011, 2013, 2014, 2016, 2017, 2018)**;
  (2) Computer Networks and Communications: Q4(2009), Q3(2010, 2012, 2013, 2015), **Q2(2011, 2014, 2016, 2017, 2018)**;
  (3) Computer Science Applications: Q4(2009), **Q3(2010, 2011, 2012, 2013, 2014, 2015, 2016, 2017, 2018)**.

  SJR: 0.178(2009), 0.339(2010), 0.369(2011), 0.292(2012), 0.378(2013), 0.420(2014), 0.263(2015), 0.319(2016), 0.326 (2017), 0.37 (2018).

- Since 2007, 2(1), IJCCC is indexed in EBSCO.

Focus & **Scope:** International Journal of Computers Communications & Control is directed to the international communities of scientific researchers in computers, communications and control, from the universities, research units and industry. To differentiate from other similar journals, the editorial policy of IJCCC encourages the submission of original scientific papers that focus on the integration of the 3 "C" (Computing, Communications, Control).

In particular, the following topics are expected to be addressed by authors:

(1) Integrated solutions in computer-based control and communications;

(2) Computational intelligence methods & Soft computing (with particular emphasis on fuzzy logic-based methods, computing with words, ANN, evolutionary computing, collective/swarm intelligence, membrane computing, quantum computing);

(3) Advanced decision support systems (with particular emphasis on the usage of combined solvers and/or web technologies).

EDITORIAL ADDRESS:
Agora University, Cercetare Dezvoltare Agora, Tineretului 8, 410526 Oradea, Bihor, Romania,
Tel./ Fax: +40 359101032, E-mail: ijccc@univagora.ro, rd.agora@univagora.ro
URL: http://univagora.ro/jour/index.php/ijccc/

EDITORIAL BOARD OF IJCCC (MEMBERS):

INTERNATIONAL JOURNAL OF COMPUTERS COMMUNICATIONS & CONTROL
ISSN 1841-9836, e-ISSN 1841-9844, Volume 14, Issue 5, October 2019.

Contents

INTERNATIONAL JOURNAL OF COMPUTERS COMMUNICATIONS & CONTROL
ISSN 1841-9836, e-ISSN 1841-9844, 14(5), 615-628, October 2019.

A Force/Position Hybrid Controller for Rehabilitation Robot

J. Hua, L.L. He, Z.Q. Kang, K.D. Yan

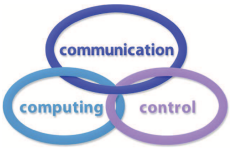

Jin Hua*
Xi'an University of Architecture and Technology,
School of Mechanical and Electrical Engineering
Xian 710055, China
Xi'an Technological University,
College of Electronic Information Engineering
Xi'an 710021, China
*Corresponding author: huahua_dz@aliyun.com

Lile He
Xi'an University of Architecture and Technology,
School of Mechanical and Electrical Engineering
Xi'an 710055, China

Zhiqiang Kang
Xi'an University of Architecture and Technology,
School of Mechanical and Electrical Engineering
Xi'an 710055, China

Keding Yan
Xi'an Technological University,
College of Electronic Information Engineering
Xi'an710021, China

Abstract: The growing ageing population in China poses a huge demand for rehabilitation care, which can be satisfied by the latest robot technology. Focusing on the motion system of a six degrees-of-freedom (DOF) robot, this paper explores the relationship between the force, torque, velocity and the postures of the end effector and joint. Drawing on robot control theories, the existing manipulator force/position hybrid controllers were reviewed, and a force/position hybrid controller was designed for path planning of rehabilitation robot. Then, the robot was modelled on the Robot Operating System (ROS), using the Unified Robot Description Format (URDF) file and the MoveIt! Setup Assistant. Finally, our controller was tested in the ROS virtual simulation environment. The results show that our controller can facilitate and optimize the design of the path of rehabilitation robot.
Keywords: rehabilitation robot, compliance control, Bezier curve, robot operating system (ROS).

1 Introduction

The ageing problem has become increasingly serious in China since the 1990s. From 1990 to 2014, the elderly population, defined as people aged 65 and over, increased from 62.99 million (5.57%) to 88.11 million (6.96%). The elderly population is expected to account for over 20%

in the total population of China by 2040. Currently, tens of millions of elderlies in China need rehabilitation care, posing a huge pressure on the medical and insurance systems.

Many industrial robots have been modified to provide rehabilitation care to the elderlies. For example, Li and Ye [8] created a motion relationship mapping model for upper limb joints, established several rehabilitation robots based on the relationship, and used joint torque signals to control the motion of the robots. Wang [18] developed a highly flexible pneumatic upper limb rehabilitation robot, which effectively prevents secondary damage to the affected limb. Pan and Song [12] designed an upper limb rehabilitation robot using impedance control strategy.

The existing rehabilitation robots mainly adopt the structure of a multi-degrees of freedom (DOF) exoskeleton with a single manipulator. The motions of the manipulator are controlled based on the signals of muscle force on the affected limb. This control mode cannot obtain the user's movement intention easily, or achieve good real-time response and accuracy.

Drawing on robot control theories, the existing manipulator force/position hybrid controllers were reviewed, and a force/position hybrid controller was designed for path planning of rehabilitation robot. Then, the robot was modelled on the Robot Operating System (ROS), using the Unified Robot Description Format (URDF) file and the MoveIt! Setup Assistant. Finally, our controller was tested in the ROS virtual simulation environment. The results show that our controller can facilitate and optimize the design of the path of rehabilitation robot.

2 Literature review

Robot technology is highly interdisciplinary and integrated. It covers many different fields, such as automatic control, computer technology, advanced sensing and mechanism. In recent years, more and more robots have been used to provide special services.

The compliance control is the key and difficult point in the research of robot technology. The compliance means the manipulator can adapt to the changes in the environment, keeping its contact force with the environment at a desired level. Over the years, many methods have been developed for compliance control of robot, including impedance control (converting feedback force into position or speed for dynamic adjustment), force/position mixed control, stiffness control [15], and implicit force control [9]. Being the hybrid of force control and position control, the compliance control can be achieved either actively or passively.

Under active compliance control, the robot perceives and regulates the contact force, completing the mixed control of its force and position. Considering the uncertainty of contact stiffness, Hogan [3] designs a force feedforward controller by inverse dynamics approach, and realizes parallel control of robot force and position. Sun and Chen [17] proposes a robot control method coupling motion prediction and impedance control, which ensures that the manipulator is flexible to react with unknown restricted mechanisms. Xu [22] puts forward a discrete-time sliding mode impedance controller with adaptive gain, and applies the controller to accurately control the force and position of a micro-gripper using piezoelectric bimorphs under uncertainties and interferences. Based on force/position hybrid control, Chang et al. [2] develops a fuzzy control method for redundant manipulator, which guarantees the accuracy of the end effector without sacrificing autonomy and flexibility. Singh and Sukavanam [16] creates a robust adaptive force/position hybrid control strategy based on neural network (NN). Under this strategy, the robot dynamics with uncertainties and disturbances are described by feedforward neural network (FNN), laying the basis for effective control of the force and position of the end effector. Hu et al. [4] conducts orthogonal separation of force control and position control in the time domain, and realizes grinding and polishing of the aspherical surface through mixed control of both force and position.

Under passive compliance control, the robot position is controlled by the rigid robot, while the contact force is controlled by a flexible joint added to the end of the robot. Compared with the active mode, passive compliance control is easy to implement, rich in economic benefits and widely applicable in industries. Nonetheless, the high demand on precision limits the use of passive compliance control in fast-responding applications. The most famous passive compliance controller is the remote center compliance (RCC) device developed by Whitney and Rourke [21]. The RCC device has been adopted for assembly operations to achieve compliance with any compliance center. However, this device cannot adapt well to operations with different stiffness requirements, due to its inflexible compliance center and fixed stiffness. Beijing University of Technology [14] designed a pneumatically-driven passive-compliance robotic hand that can control the contract force at a low level and complete precision hole and shaft assemblage. The robotic hand consists of an air bag and an air bearing. The former reduces the angular stiffness and the latter lowers the lateral stiffness. Harbin Engineering University [20] presented a passive-compliance flexible gripper for underwater search and object grabbing. The gripper has two fingers, a removable wrist, easily replaceable end effectors, a support mechanism, an active locking mechanism and a passive compliance mechanism. Despite the lack of a single DOF, the gripper can grab objects in different postures. Huang et al. [5] introduces a compliance mechanism to the abrasive belt of a robotic polishing system. The mechanism can adapt to the changing contact force of the system, eliminating the need of manual grinding of turbine blades. To cope with dynamic changes of the working environment and the uncertainties of human-computer interaction (HCI), Zhang et al. [23] designs a manipulator with passive compliance structure and active compliance control, and adds several elastic drive modules between the joint motor and connecting rod. Baksys et al. [1] set up an electric vibration table with a compliance device, examines the stress of the vibration table, and discloses the relationship between vibration frequency and assembly time. Kilikevicius and Baksys [7] analyzes the effects of dynamic systems and excitation parameters on passive compliance assembly by vibrating the casing in the axial direction on the platform basis. Huang et al. [6] puts forward a passive compliance control strategy for the position and force of a robotic polishing system, and installs a compliance device at the end effector for force control.

From the above, Because of the manipulator dynamics model contains the uncertainty structures and parameters, even more, the external disturbance, the method based on the model control will be resulted in the system control quality decline, more over instability from different degrees affection. Therefore, the adaptive control method which is selected in this paper, is proposed to deal with these uncertainties and external disturbances. The application of compliant control technology in service robot becomes hotter, but more difficult in the process of interacting with human. In this work, the force/position hybrid control method is adopted to solve the operation task of assisted rehabilitation movement. Combined with self-adaptation control, it structured the model which is contains the robot manipulator and the contact environment as a whole.

3 Design of force/position control algorithm for robotic manipulator

Mechanical impedance is the ratio of the increment of dynamic force in any DOF and the resulting increment of dynamic displacement. This ratio is generally a nonlinear coefficient. Therefore, when the manipulator is in contact with the working environment, both the position of the end effector and the dynamic relationship between the position and the contact force should be controlled to adjust the input torque of the manipulator.Currently, the two control

tasks are mainly implemented by two methods. The first method is the transform of the force signal into position or velocity, followed by the dynamic adjustment of the stiffness and damping part. The second method is the hybrid control of force/position.

The hybrid position/force control decomposes the task space into two orthogonal subspaces for position control and force control. The position is controlled in the tangent subspace under environmental constraints, while the force is controlled in the normal subspace under environmental constraints. In this way, the position/force control is decoupled.

Let K and P be the kinetic energy and potential energy of the manipulator, respectively. Then, the Lagrange equation of the manipulator can be expressed as $L = K - P$. Thus, the following equation can be derived:

$$\tau = \frac{d}{dt}\frac{dL}{d\dot{q}} - \frac{dL}{dq} \tag{1}$$

Therefore, the dynamic equation of the manipulator can be defined as:

$$\tau = M_i(q_i)\,\ddot{q}_i + h_i(q_i, \dot{q}_i) + G_i(q_i) \tag{2}$$

where $M(q)$, $h(q, \dot{q})$, $G(q)$ are the inertial matrix, centrifugal force and gravity vector of the manipulator, respectively. In the force space, the force acting on the end effector can be mapped to the equivalent joint space moment by the transposition J^T of the Jacobian matrix of the manipulator. When the end of the manipulator contacted with the external environment, there will be an F_e interaction between the manipulator and the external environment. Hence, in order to maintain the manipulator balance state, the output of torque controlling is expressed as follows:

$$\tau = M(q)\ddot{q} + h(q, \dot{q}) + G_q - J^T F_e \tag{3}$$

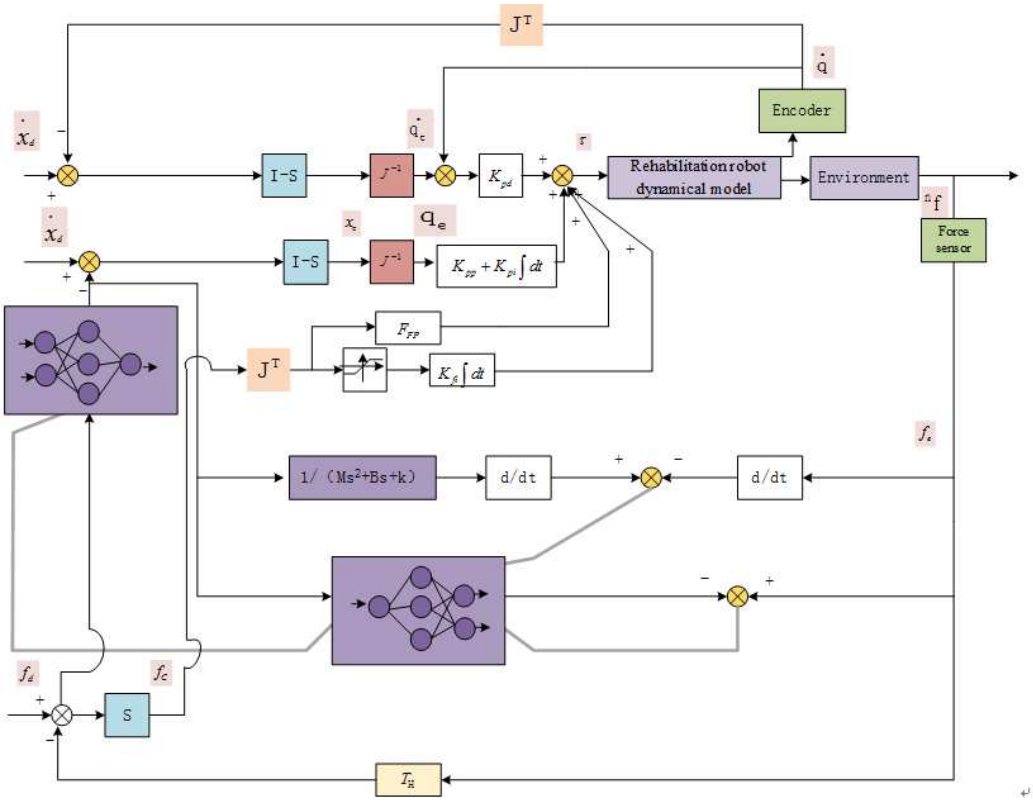

Figure 1: Design of Our Force / Position Hybrid Controller

The design of our force/position hybrid controller is shown in Figure 1. The output torque of the controller is the sum of the torque computed by the position control information via the inverse Jacobian matrixJ^{-1} and that computed by the force control information via J^T. The inverse Jacobian matrix stands for the mapping relationship between the change of the coordinate velocity of each member in the Cartesian coordinate system and the change of the joint angular velocity of that member.Considering that if only basic impedance control is used to maintain the dynamic relationship between the effector of the robot and the response contact force of the rehabilitation patients' limbs, although smooth contact is achieved to reduce the impact in contact, it cannot achieve good control of the rehabilitation intensity.So the controller is designed by adding artificial neural network, so as to correct the expected output impact using the error between the output of the reference model and the actual output.

In the traditional force/position control algorithm, the adaptive part of environmental parameters is improved. The contact force at the robot effector is measured by the six-dimensional force/torque sensor, which is used as the control part of the force feedback to the force/position hybrid controller. After learning the adaptive modified NN, the position will be changed.So, we select the parameter model of the environment as$M_d s^2 + B_d s + K$. When, M_d is the target inertia of the impedance model, B_d is the target damping, and K_d is the target stiffness matrix.

In the controller, S is a diagonal matrix. If $i = 6$, then the matrix is a unit matrix of $6 * 6$. Therefore, $\bar{S}$ can be obtained as:

$$\bar{S} = I - S \tag{4}$$

The essence of the hybrid control is to set the DOF for the desired path of the end effector, that is, to select the control component of the controller through S and $\bar{S}$.

The cartesian force, which on the end of the manipulator, maps the equivalent joint torque according to the transpose Jacobian matrix J^T . When the manipulator performs the action task, it is inevitable that it will have physical contact with the external environment or the operating object. As the task executing, manipulator will inevitably contact with the external environment or the operating object. That leads to the results of positional constraints in the positional space.

In addition to considering the dynamic model of the robot arm itself, the model of the interaction between the robot arm and the external environment should be established when modeling the control object, so as to realize the flexible control of the task action process by the dynamic model. Considering the dynamic model of the arm, while the model of the interaction between the robot and environment will be confirmed, so as to achieve the flexible control process by the whole dynamic model. The force sensor is mounted between the end gripper and the joint arm.The data, which acquired from the experiment in a certain rehabilitation teaching movement, are the position and the six-axis force obtain from the force sensor. From that measurement data, the interaction force of this kind rehabilitation exercise between the manipulator and the environment is obtained. In the diagram, the τ is the total driving torque of the six joints ($i = 6$). The joint position q and joint velocity can be measured by the photoelectric encoder. Acquired by six-axis torque sensor, ${}^{H}\mathrm{f}$ is converted to the effective vector ${}^{c}\mathrm{f}$ in cartesian coordinate system by using the coordinate transformation.

So suppose this is a S selection matrix, which elements in the diagonal matrix are set to 1, corresponding to its degree space are controlled by the applied force loop. For example, when:

$$S = diag[1, 0, 1, 0, 1, 1] \tag{5}$$

so $X_d = [x_d, 0, z_d, 0, \beta_d, \gamma_d]$, As known from the formula, the expected displacement of the Y-axis and the rotation around the Y axis should be ignored. As the same as in the position control ring. In addition, the original six-degree-of-freedom manipulator become a redundant mechanical manipulator. Meanwhile, the change of the expected force is controlled by the force closed loop.

The motion differential equation is:

$$\dot{X}_e = J\dot{\Theta} \tag{6}$$

so as to, $\dot{X}_e$ is the $m \times l$ dimensional vector, that is composed of linear velocity and angular velocity of the end effector, $\dot{\Theta}$ is the $n \times l$ dimensional vector, composed of angular velocity of each joint in manipulator, while, J is $m \times n$ matrix. When $J$is singular matrix, that means $m < n$, the joint angular velocity of redundant manipulator is:

$$\dot{\Theta} = J^{+}\dot{X}e + (I - J^{+}J)\dot{\varphi} \tag{7}$$

in this formula, J^{+} is the pseudo-inverse of J, if J is full rank, then $J^{+} = J^{T}(JJ^{T})^{-1}$. I is the identity matrix, $(I - J^{+}J)$ is the null space projection matrix, and is any joint angular velocity vector. When $\dot{\phi} = 0$, $\dot{\Theta}$ can be solved with the minimum norm solution. In other words, the motion of the end effector can be guaranteed under the control of the minimum joint velocity in joint space, or use $K\nabla H(\Theta)$ instead of$\dot{\Theta}$:

$$\dot{\Theta} = J^{+}\dot{X}_e + k(I - J^{+}J)\nabla H(\Theta) \tag{8}$$

where the $H(\Theta)$ can be optimized by the gradient projection method.

4 Robot trajectory planning based on Bezier curve

The Bezier curve can be defined as:

$$b(u) = \sum_{j=0}^{m} B_j^m(u)p_j, \quad 0 \le u \le 1 \tag{9}$$

wherep_j is the control point; $B_j^m(u)$is the M-order Bernstein polynomial:

$$B_j^m(u) = \frac{m!}{j!(m-j)!}u^j(1-u)^{m-j} \tag{10}$$

The polynomial form of the Bezier curve can be expressed as:

$$b(u) = \sum_{i=0}^{m} a_j u^i \tag{11}$$

where$a_j$is a coefficient determined by control pointP_j:

$$a_j = \frac{m!}{(m-i)!}\sum_{j=0}^{i}\frac{(-1)^{j+i}}{j!(i-j)!}P_j \tag{12}$$

According to the principle of Bezier curve principle, a planned path for the rehabilitation robot was obtained (Figure 2).

As shown in Figure 4, the planned path consists of a straight segment Q_AQ_B and an arc segment Q_BQ_C ; the origin and radius of the arc segment are O_A and R, respectively; the fifth-order Bezier transition segment is $Q'_BQ''_B$. The straight segment reaches the front of the target slag, which is at the center of the arc segment, while the arc segment bypasses the target slag to complete the slagging action.

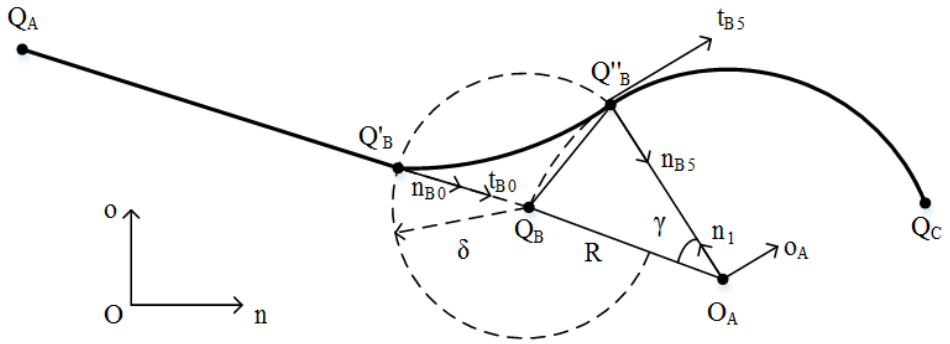

Figure 2: Trajectory Planning for The Rehabilitation Robot

Let δ be the tolerance of the fifth-order Bezier transition segment. Then, the $Q_BQ''_B$ of center angle γ can be obtained by triangulation:

$$\gamma = 2arctan(\delta/2R) \tag{13}$$

Let T be the transformation matrix from the global coordinate system $O-ZYX$ to the arc segment coordinate system $O_A - X_AY_AZ_A$. Then, the two ends of the fifth-order Bezier transition segment (Q_{B_0} and Q_{B_5}) can be respectively expressed as:

$$Q'_B = Q_B - \frac{Q_B - Q_A}{\mid Q_B - Q_A \mid}\delta \tag{14}$$

$$Q''_B = O + T(Rcos\gamma \quad Rsin\gamma \quad 0)^T \tag{15}$$

The six points of the fifth-order Bezier transition segment can be obtained as:

$$\begin{cases} Q_{B_0} = Q'_B \\ Q_{B_1} = Q_{B_0} + (\alpha_B/5)\cdot t_{B_0} \\ Q_{B_2} = 2Q_{B_1} - Q_{B_0} \\ Q_{B_5} = Q''_B \\ Q_{B_4} = Q_{B_5} - (\alpha_B/5)\cdot t_{B_5} \\ Q_{B_3} = 2Q_{B_4} - Q_{B_5} + 0.05(\frac{db}{du})^2|_{u=1}\cdot\frac{\vec{R}}{R^2} \end{cases} \tag{16}$$

where $u \in [0,1]$ is the fifth-order displacement parameter of Bezier curve $b = b(u)(u = u(t))$; α_B is the first-order differential vector; $\vec{R}$ is the vector pointing from the new start point of the arc segment to the center of the circle. The straight segment and Bezier curve contain the same unit tangential vector at the transition point$t$ and curvature vector n in Q'_B . The unit vector along the direction of Q'_BQ_B can be expressed as:

$$t_{B_0} = n_{B_0} = \frac{Q_B - Q'_B}{\delta} \tag{17}$$

The velocity at the intersection of the arc segment and the Bezier curve is the same as the direction:

$$t_{B_5} = o_A \tag{18}$$

To constraint the start and end of the straight segment, the continuous velocity and acceleration, straight segment displacement, acceleration, maximum velocity, maximum acceleration and

maximum jerk must satisfy: $u_0 = 0, u_1 = 1, \ddot{u}_0 = \ddot{u}_1 = 0, \dot{u}_{\max} = v_{\max}/l_{AB}, \ddot{u}_{\max} = a_{\max}/l_{AB}$ and$\dddot{u}_{\max} = j_{\max}/l_{AB}$.

To satisfy the velocity requirement, the straight segment and the fifth-order Bezier transition segment must satisfy:

$$\frac{dl_{AB}(u)}{dt}|_{u=1} = \frac{db(u)}{dt}|_{u=0} \tag{19}$$

Since the straight segment precedes the fifth-order Bezier transition segment, the velocity must satisfy:

$$\begin{cases} \dot{u_0} = 0 \\ \dot{u_1} = \mid \dot{b}(u)|_{u=0} \mid \cdot \lambda / l_{AB} \end{cases} \tag{20}$$

wherel_{AB} is the path function for straight segment; λ is the scale factor of the fifth-order Bezier transition segment. To constraint the start and end of the arc segment, the continuous velocity and acceleration, straight segment displacement, acceleration, maximum velocity, maximum acceleration and maximum jerk must satisfy:$u_0 = 0, u_1 = 1, \ddot{u}_0 = \ddot{u}_1 = 0, \dot{u}_{\max} = v_{\max}/r_{BC}, \ddot{u}_{\max} = a_{\max}/r_{BC}$ and$\dddot{u}_{\max} = j_{\max}/r_{BC}$.

In the path, the arc segment is at the end segment. Then, the velocity must satisfy:

$$\begin{cases} \dot{u_0} = \mid dotb(u)|_{u=1} \mid \cdot \lambda / r_{BC} \\ \dot{u_1} = 0 \end{cases} \tag{21}$$

where r_{BC} is the path function for the arc segment.

5 Experimental verification

5.1 ROS-based modelling of rehabilitation manipulator

The URDF is a standard ROS XML format in the ROS for robot modelling [24]. The ROS also provides a $C++$ parser for URDF files. This parser helps to implement motion planning or model-based computing. The model-based computing is easy to complete, for the information of the model is directly called in the algorithm code [11].

After URDF modelling, the MoveIt! Setup Assistant was employed to configure the robot model. Firstly, the Semantic Robot Description Format (SRDF) file was generated based on the user-imported robot model, creating a feature pack for the MoveIt! configuration. Then, the robot was configured, visualized and simulated. The resulting configuration files were stored in the "config" folder. The SRDF file saves all the information of the visual configuration, the URDF file stores the compiled information, the "kinematic.yaml" file retains the configuration of the kinematic solver kdl_kinmatics_plugin. In the "launch" folder, a series of launch files were generated automatically for the launch of the manipulator. The move_group is the core of the MoveIt! architecture [13]. Both kinematics solution and motion planning need the launch file move_group to start the manipulator. The MoveIt! Setup Assistant offers various algorithms for robot motion planning. Each of these algorithms is a plugin with a unique focus.

MoveIt! System Configuration Frameworkas shown in the Figure 3, the move_group [10] integrates various functions to the MoveIt! environment through plugins. Thus, all external information, including their interactions with the internal data must be implemented by MoveIt!. In this paper, the Open Motion Planning Library (OMPL) in MoveIt! is adopted to realize the robot functions [19]. The OMPL, as an open-source library, contains various cutting-edge algorithms. It is used by MoveIt! to plan the robot motion from start to destination.

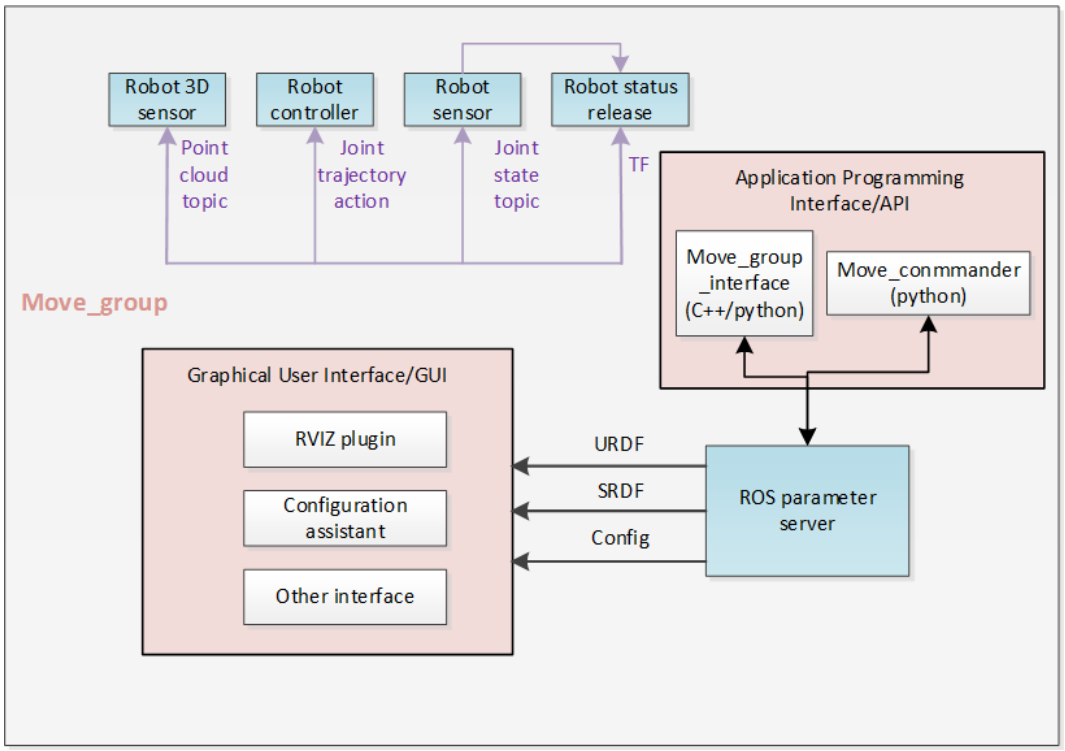

Figure 3: MoveIt! System Configuration Framework

5.2 Experimental design based on impedance control

In the ROS, the built-in rqt_plot provides the drawing functions. However, this function is too simple to visualize a huge amount of data. Hence, the Matlab was selected for data analysis. The whole operation flow chart as shown in the Figure 4. To avoid controlling the manipulator each time, the information about the topic joint_states was saved as a bag file. The command order as follows:

1). *rosbag record -O manipulater1.bag /joint_states.* "Create a trajectory motion simulation namedjoint_states. O is the indicator of the output file; manipulater1 is the name of the output file".

2). *rosbagplay youbot_action2.bag -clock.*"A terminal was turned on to play back the data, clock is the simulation time".

3). *rostopic echo /joint_states>record2.txt.* "The output text was saved to store the data".

Finally, the text was copied to windows, imported to excel and analyzed via Matlab simulation. Figure 5 shows the modelled rehabilitation manipulator in virtual environment.

When the robot performs the auxiliary operation of basic rehabilitation movement, it is necessary to perform the basic rehabilitation actions such as the circular motion of the joint on a fixed track and the linear motion of push, pull and drag on the muscle or joint of the recovered person.

5.3 Results analysis

When the robot performs the basic auxiliary rehab operation, it is necessary to imitate people like action such as the joint circular motioning, and a fixed plan tracking,and the linear motion like pushing, pulling from muscle. Then, the first-order and second-order differential vectors of the trajectory should be computed, that is reached there habilitation exercise positions.

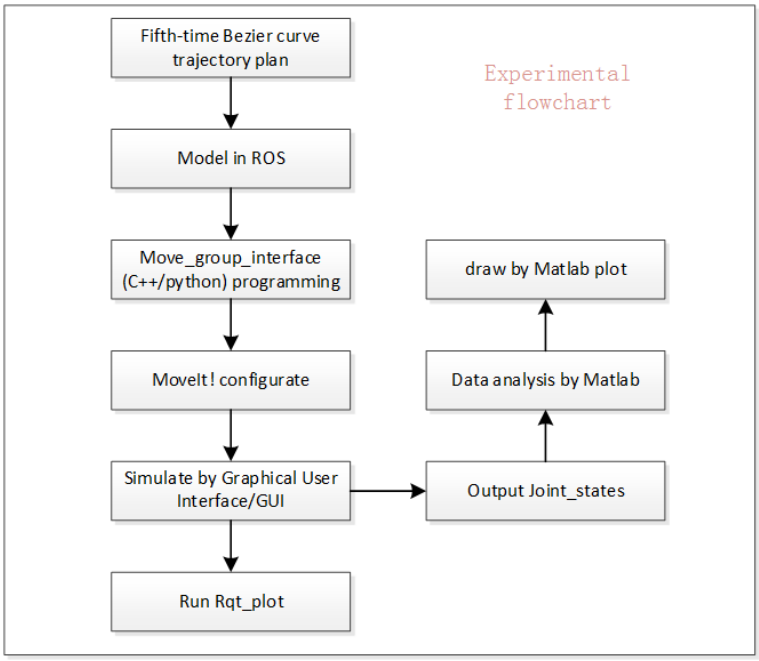

Figure 4: Experimental flowchart

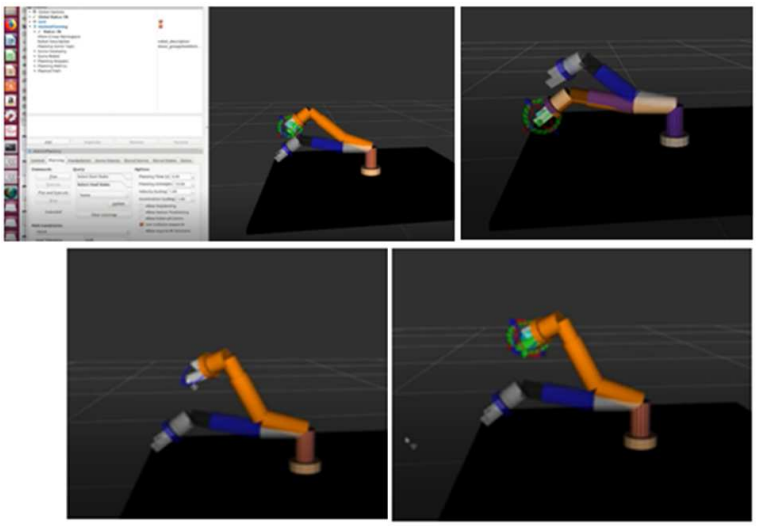

Figure 5: The Modelled Rehabilitation Manipulator

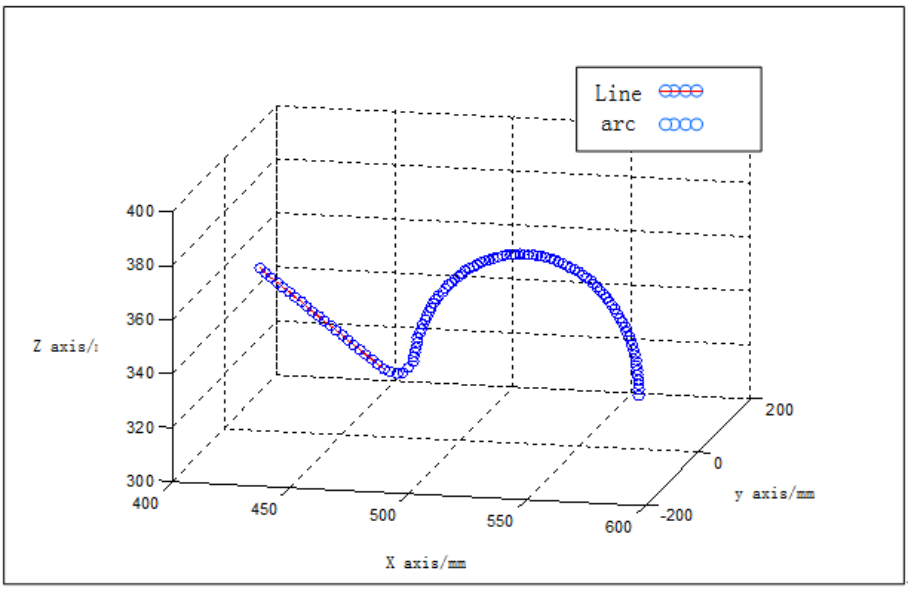

Figure 6: The Fifth-Time Bezier Curve of Rehabilitative Exercise

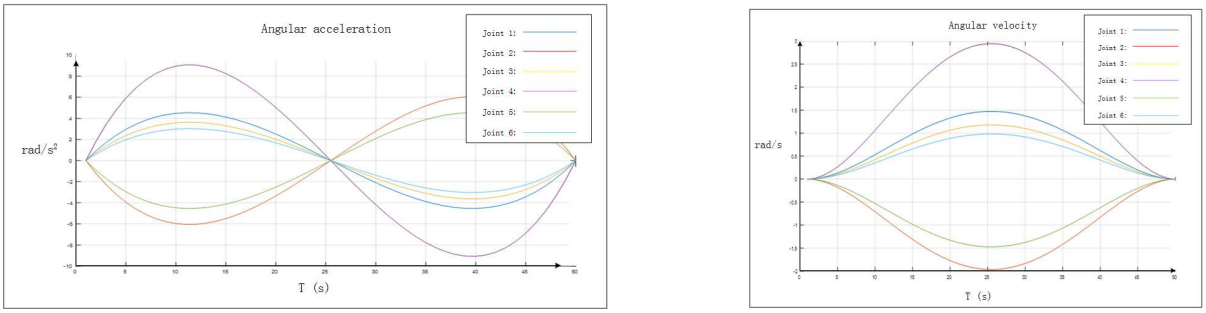

(a) (b)

Figure 7: The Acceleration(a), Velocity (b) Variations of the End Effector in One Control Cycle

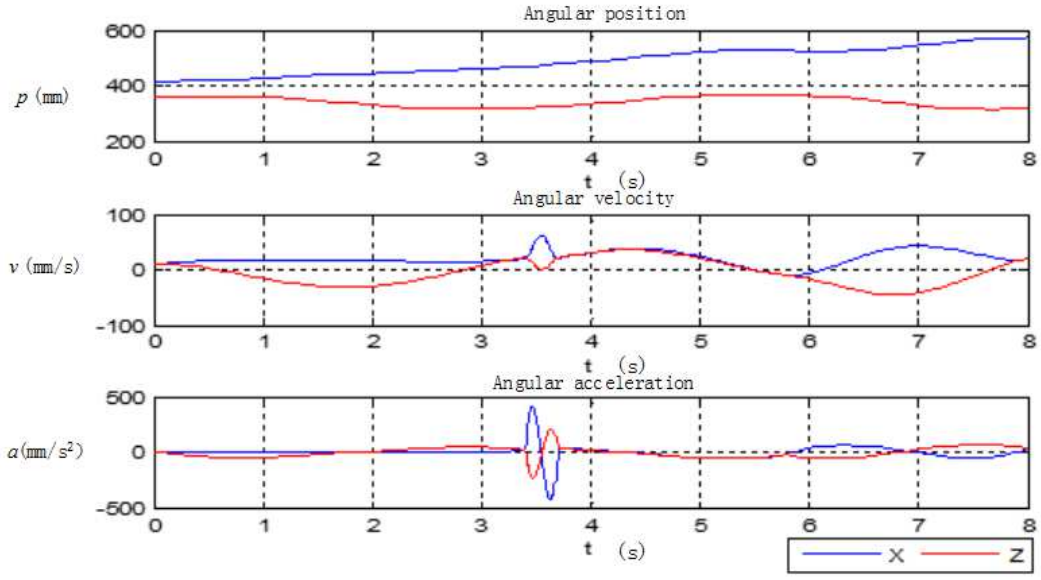

Figure 8: Position, Velocity and Acceleration of the End Effector

The straight segment and arc segment was linked up by the fifth-time Bezier curve. We defined variable δ was $10mm$.

The six points were calculated as the following information in the three-dimensional location:
$Q_{B_0} = (467.5932, 0, 325.3327), Q_{B_1} = (477.5448, 0, 324.2365)$,
$Q_{B_2} = (473.2109, 0, 323.7652), Q_{B_4} = (475.5001, 0, 324.5602)$,
$Q_{B_5} = (478.0034, 0, 325.8482)andQ_{B_6} = (480.3521, 0, 328.0214)$.

The result of planning trajectory based on the fifth-time Bezier curve is shown in Figure 6.

The position, velocity and acceleration variations were plotted (Figure 7). It can be seen that the acceleration of the end effector changed smoothly, which is conducive to the rehabilitation efficiency and comfort.

Figure 8 presents the position, velocity and acceleration of end effector in the x-z plane. The acceleration curve at the end of the manipulator shows that our method slows down the abrupt changes in acceleration caused by rapid velocity change, when the end effector suddenly changes in the x-z plane.

6 Conclusions

The hybrid control of position and force is essentially to select the DOF according to the desired path of the end effector, that is, to select the control component of the controller through S and $\bar{S}$. In this paper, a force/position hybrid controller is designed based on the principle of impedance control. The control DOFs were selected through reconstruction of the desired path, and then the S and $\bar{S}$ of the controller were identified. Next, our controller was tested in the ROS virtual simulation environment. The results show that our controller can facilitate and optimize the design of the path of rehabilitation robot.

Acknowledgement

This paper was supported by National sonar Key Laboratory Open Fund(6142109KF2018); National Fund Youth Project(11804263).

Bibliography

[1] Baksys, B.; Kilikevicius, S.; Chadarovicius, A. (2012). Experimental investigation of vibra assembly with passive compliance, *Mechanika*, 17(6), 608-611, 2012.

[2] Chang, J.; Wang, Y.Z.; Li, B. (2016). Accurate Operation Control Method Based on Hybrid Force/PositionAlgorithm for 7-DOF Manipulator, *ROBOT*, 38(5), 531-539, 2016.

[3] Hogan, N. (1985). Impedance control-An approach to manipulation. I - Theory. II - Implementation. III- Applications, *Journal of Dynamic Systems Measurement & Control*, 107(1), 1-24, 1985.

[4] Hu, L.Y.; Zhan, J.M.(2015). Studyon theorthogonalization forHybrid motion/force control and its application in aspheric surface polishing,International *Journal of Advanced Manufacturing Technology*, 77(5-8), 1259-1268, 2015.

[5] Huang, H.; Gong, Z.M.; Chen,X.Q.; Zhou, L.(2002). Robotic grinding and polishing for turbine-vane overhaul, *Journal of Materials Processing Technology*, 127(2), 140-145, 2002.

[6] Huang, T.; Sun, L.N.; Wang, Z.H.; Yu, X.Y.; Chen, G.D. (2017). Hybrid Force/Position Control Method for Robotic Polishing Based onPassive Compliance Structure, *ROBOT*, 39(6), 776-785 and 794, 2017.

[7] Kilikevicius, S.; Baksys, B. (2011). Dynamic analysis of vibratory insertion process, *Assembly Automation*, 31(3), 275-283, 2011.

[8] Li, Q.L.; Ye, T.M.(2009). Controlled assistance by an exoskeletal rehabilitation robot for upper limbs, *Journal of Harbin Engineering University*, 34(2), 166-177, 2009.

[9] Li, S.R.; Yin, H.Q.(2017). Adaptive position/force control for coordinated multiple flexible-jointmanipulators with time delay, *Control Theory and Applications*, 34(9), 1208-1214, 2017.

[10] Liu, Y.Q.; Tao, R.; Ding, F.; Zhang, J.X.; Chen, Y.J.; Liu, X.(2018). Research on vision servo 7DOF manipulator simulationbased on ROS and EtherCAT,*Journal of natural science of Heilongjiang university*, 35(1), 94-101, 2018.

[11] Lu, L.; Xie, S.X. (2018). Construction method of robot simulation model in ROS environment. *Modern Electronics Technique*, 41(7), 102-105, 110, 2018.

[12] Pan, L.Z.; Song, A.G.(2012). Real-time Safety Control of Upper-limb Rehabilitation Robot, *ROBOT*, 34(2), 197-210, 2012.

[13] Qi, Z.G.; Huang, P.F.; Liu, Z.X.; Han, D.(2019). Research on path planning method of spatial redundant manipulator. *ActaAutomaticaSinica*, 45(6), 1103-1110, 2019.

[14] Qin, H.Q.; Xiong, Q.Y.; Shi, X.(2014). Simulation research of force control system for manipulator based on Matlab, *Computer Engineering and Applications*, 50(12), 242-246, 2014.

[15] Roy, N.; Newman, P.; Srinivasa, S. (2012). *Rigidity maintenance control for multi-robot systems. Robotics: Science & Systems VIII*, MIT Press, 2012.

[16] Singh, H.P.; Sukavanam, N. (2013). Stability analysis of robust adaptive hybrid position/-force controller for robot manipulators using neural network with uncertainties,*Neural Computing & Applications*, 22(7-8), 1745-1755, 2013.

[17] Sun, Y.X.; Chen, W.D. (2011). Operating Unknown Constrained Mechanisms Based on Motion Prediction and Impedance Control, *ROBOT*, 33(5), 563-569, 2011.

[18] Wang, T. (2016). *Design of An Exoskeleton Rehabilitation Robot Replicating the Synergistic Characteristics of Upper Extremity Movements*, Huazhong University of Science and Technology, 2016.

[19] Wang, Z.G.; Freidovich, L.B.; Zhang, H.H.(2019). Periodic Motion Planning and Control for Double Rotary Pendulum via Virtual Holonomic Constraints,*IEEE/CAA Journal of AutomaticaSinica*, 6(1), 291-298, 2019.

[20] Wei, H.X.; Wang, X.D;Meng, Q.X.(2000). The study of a passive and pliant underwater claw, *MarineTechnology*,2000(3):17-20, 2000.

[21] Whitney, D.E.; Rourke, J.M.(1986). Mechanical behavior and design equations for elastomer shear pad remote center compliances, *Journal of Dynamic Systems Measurement & Control*, 108(3), 223-232, 1986.

[22] Xu, Q.S. (2013). Adaptive discrete-time sliding mode impedance control of a piezoelectric micrograpper, *Robotics IEEE Transactions on*, 29(3), 663-673, 2013.

[23] Zhang, X.L.; Gu, X.X.; Zhao, H.F.; Wang, K.(2016). Design of a Compliant Robotic Arm Based on Series Elastic Actuator,*ROBOT*, 38(4), 385-394, 2016.

[24] Zuo, X.R.; Han, L.L.; Zhuang, J.; Shi, Q.Q.; Huang, Y.(2015). Design of human-robot interaction system for space robot using robot operating system, *Computer engineering and design*, 36(12), 3370-3374, 2015.

INTERNATIONAL JOURNAL OF COMPUTERS COMMUNICATIONS & CONTROL
ISSN 1841-9836, e-ISSN 1841-9844, 14(5), 629-646, October 2019.

VINERS Method for the Multiple Criteria Analysis and Neuromarketing of Best Places to Live

A. Kaklauskas, D. Dzitac, J. Sliogeriene, N. Lepkova, I. Vetloviene

Arturas Kaklauskas*
Vilnius Gediminas Technical University, Vilnius, Lithuania
*Corresponding author: arturas.kaklauskas@vgtu.lt

Domnica Dzitac
New York University Abu Dhabi, Abu Dhabi, UAE
domnica.dzitac@nyu.edu

Jurate Sliogeriene
Vilnius Gediminas Technical University, Vilnius, Lithuania
jurate.sliogeriene@vgtu.lt

Natalija Lepkova
Vilnius Gediminas Technical University, Vilnius, Lithuania
natalija.lepkova@vgtu.lt

Ingrida Vetloviene
Vilnius Gediminas Technical University, Vilnius, Lithuania
ingrida.vetloviene@vgtu.lt

Abstract: The best and worst places to live have been analysed in the world for many years and multiple criteria analysis has been used for that purpose. The quality of housing and its environment, pollution, green places, public spaces, physical movement and health, crime rates and individual safety, the wellbeing of youngsters, unemployment, job value, economic scarcity, governance, circadian rhythm, weekly rhythm and other factors are the focus of such analyses that aim to determine levels of positive emotions and happiness in built environment. Questionnaires are the most common tool for such analyses, where inhabitants are asked to rank their happiness experience as a whole in built environment. Many studies demonstrate that happy people are effective in multiple areas of their life including job efficiency, salary, health, human relations, etc. The innovative aspect of this research stems from the fact that biometric technologies (affective attitudes, emotional and physiological states) and the VINERS method developed by the authors are used to determine the best places to live and to serve neuro ads of homes for sale. To do this, rational segments of homebuyers are determined according to their demographic profiles (age, gender, education, marital status, families with children, main source of income), consumer psychographics and behaviour (happy, sad and angry along with valence and heart rate) and then select a rational video ad for such rational segment. The aim of our research is to develop the VINERS Method for the Multiple Criteria Analysis and Neuromarketing of Best Places to Live (VINERS method) by combining the Somatic Marker Hypothesis, biometrics, neuromarketing and COPRAS method. This article presents a case study to demonstrate the VINERS method put to practice.
Keywords: COPRAS and VINERS methods, neuromarketing, multiple criteria analysis, best places to live.

1 Introduction

Many authors [5,7,14,15,24,33,34,42,45,49,55] have analysed the effect of built environment on the happiness of the people in it. That effect (from the perspective of developing a sustainable community) has also been analysed in the field of sustainability [7, 8, 35, 39].

Common presumption is that happiness is an individual characteristic and each person is the one responsible for his or her own happiness. Happiness is, however, a community characteristic as well, and factors external to the individual can have influence on its levels [8]. Leyden [30] have analysed ten major cities and discovered that self-reported happiness of people is associated with aspects they see as important in their built environments, including issues such as maintenance, convenient public transportation and access to cultural amenities. The empirical data have been collected in the ten cities and they strongly suggest that built environment has an effect on social connections to places that play a vital role in happiness in a city [30]. Florida et al. [16] have determined that the central role in the happiness of cities belongs to human capital, which outperforms income and all other variables. Other researchers [27, 45] have also determined that in places where educational attainment is higher people are happier. Does a modern hospital offer true healing? Healing Places analyses different environments and their effect on our physical, spiritual, mental, emotional and social healing. Four dimensions found in healing environments have been identified: built, natural, social and symbolic [18].

People tend to link city centres with feelings of excitement and/or anxiety, and see them as stimulating and lively. In the urban renaissance, an important role is played by evening activities because they keep a town or city alive way beyond normal business hours. A successful urban renaissance requires a more diverse pool of people attracted into city and town centres in the evening and at night [24]. Urry [49] took interest in the ways visitors (and local people too) experience a place. What pleasures the place offers? What are the emotions people feel when they enter a place that is relatively unfamiliar? Urry [49] focuses on popular tourist destinations and shows how specific sites are set up to saturate them with emotions, sometimes frightening and wild, sometimes relaxing and aesthetically pleasing. These emotions then become inseparable from how both tourists and residents imagine and portray those places. Milligan et al. [33] explore positive emotional experiences of older people in the shared community spaces of gardening and social clubs. Milligan et al. [33] demonstrate that the role of social spaces, and shared outdoor gardening activities in particular, can be important and constructive in contributing, in older people's lives, to feelings of self-worth and belonging and emotional expression. Emotions can be joyful, numbing or heartbreaking, but they all have the power to transform our lives, open new horizons or confine us, creating new fixtures or fissures we never expected to find [5].

This paper is structured as follows. This introduction is followed by Section 2 with a demonstration of the VINERS method. Section 3 deliver Case Studies. The paper ends with conclusions and follow-ups on forthcoming research in Section 4.

2 VINERS method

The Introduction presents studies showing that a specific demographic segment of buyers should seek housing in the neighborhoods, which they often experience positively. To put it another way, it's best to live feeling as best as possible.

The aim of our research is to develop the VINERS Method for the Multiple Criteria Analysis and Neuromarketing of Best Places to Live (VINERS method) by combining the Somatic Marker Hypothesis (1994), biometrics, neuromarketing and COPRAS methods [52] developed by the applicants. The new VINERS method would make it possible to determine a rational segment of homebuyers by their demographic profiles, consumer psychographics and behaviour and then

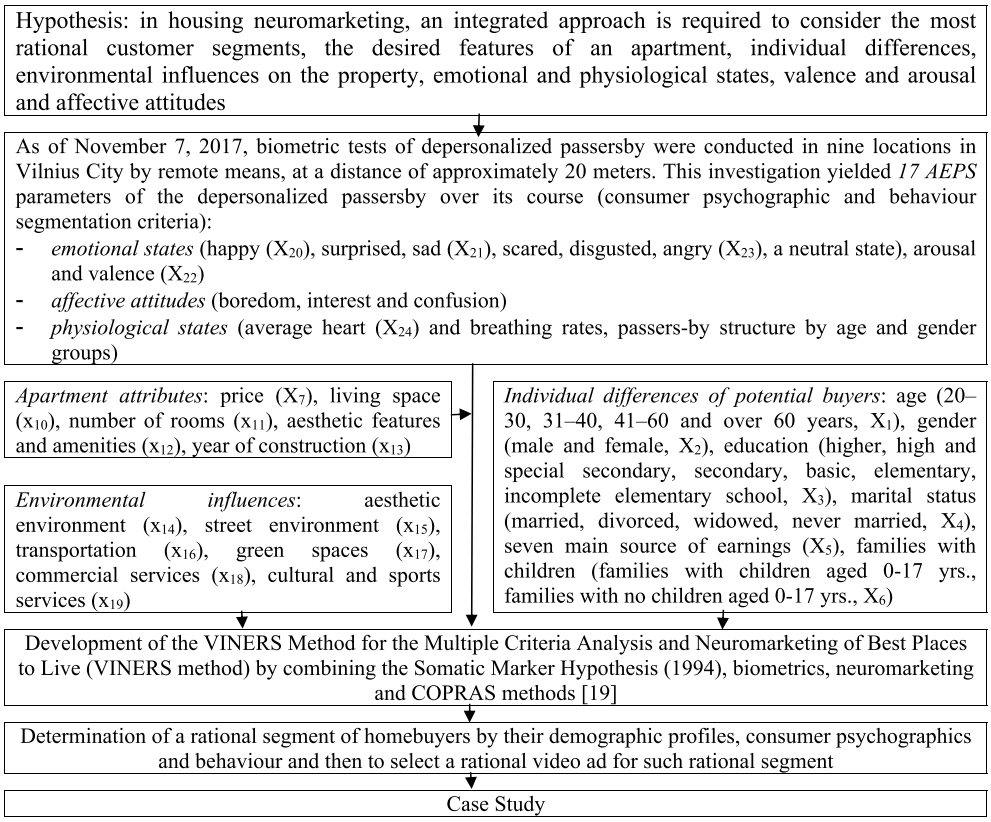

Figure 1: Development of the VINERS Method for the Multiple Criteria Analysis and Neuromarketing of Best Places to Live

to select a rational video ad for such rational segment.

A rational segment of homebuyers by their demographic profiles, consumer psychographics and behaviour can be determined by creating a multiple criteria neuro matrix.

In this research, we hypothesized that in housing neuromarketing an integrated approach is required to consider the most rational customer segments, the desired features of an apartment, individual differences, environmental influences on property, emotional and physiological states, valence and arousal and affective attitudes.

Our research launched on 6 November 2017 is tracking the 17 states of people at nine locations in Vilnius. The goal is to collect data for anonymised affective attitudes, emotional and physiological tests (see Figure 1). The data from our annual tracking activities done in Vilnius with FaceReader 7.1 and the respiration sensor X4M200 were used to establish the AEPS of passers-by taking into account their age and gender.

We have to determine the priority and utility degree of suggested video ads and for that purpose the following system of criteria has been produced to define the specific rational homebuyer segments by their demographic profiles, consumer psychographics and behavior (see Figure 1).

Statistics Lithuania has provided the statistical information about the individual differences of potential buyers (X_1-X_6, X_8, X_9) under deliberation. The data on apartment attributes (X_7, X_{10}-X_{13}) and environmental influences (X_{14}-X_{19}) came from eight experts on real estate marketing, brokerage and evaluating. Currently over 250 million anonymised affective attitudes, emotional and physiological states (see Figure 1) data entries have been accumulated. It would take a great deal of space to describe all the performed investigations. Therefore, to simplify the write-up of the performed investigation, the use was only of X_{20}-X_{24}, rather than all the

available AEPS data (see Table 1).

The research consists of data gathered on these depersonalized bystanders relevant to 17 parameters numbering over 250 million items. It would require considerable room to demonstrate

Table 1: The neuro decision matrix of alternative video ads and the results of its multiple criteria analysis

Criteria describing alternatives	**Sub-criteria describing alternatives**	**Measuring units**	**Weight**	*****	**Apartments video alternatives under comparison**					
					$\mathbf{A_1}$	...	...	$\mathbf{A_j}$	...	$\mathbf{A_n}$
Buyer's individual differences (demographic segmentation criteria)										
Age ($\mathbf{X_1}$)	X_{11} (20–30 years)	Points	q_{11}	+	x_{111}	...	...	x_{11j}	...	x_{11n}
	X_{12} (31–40 years)	Points	q_{12}	+	x_{121}	...	...	x_{12j}	...	x_{12n}
	X_{13} (41–60 years)	Points	q_{13}	+	x_{131}	...	...	x_{13j}	...	x_{13n}
	X_{14} (over 60 years)	Points	q_{14}	+	x_{141}	...	...	x_{14j}	...	x_{14n}
Gender ($\mathbf{X_2}$)	X_{21} (male)	Points	q_{21}	+	x_{211}	...	...	x_{21j}	...	x_{21n}
	X_{22} (female)	Points	q_{22}	+	x_{221}	...	...	x_{22j}	...	x_{22n}
Education ($\mathbf{X_3}$)	X_{31} (higher)	Points	q_{31}	+	x_{311}	...	...	x_{31j}	...	x_{31n}
	X_{32} (high/ special secondary)	Points	q_{32}	+	x_{321}	...	...	x_{32j}	...	x_{32n}
	X_{33} (secondary)	Points	q_{33}	+	x_{331}	...	...	x_{33j}	...	x_{33n}
	X_{34} (basic)	Points	q_{34}	+	x_{341}	...	...	x_{34j}	...	x_{34n}
	X_{35} (elementary)	Points	q_{35}	+	x_{351}	...	...	x_{35j}	...	x_{35n}
	X_{36} (incomplete elementary school)	Points	q_{36}	+	x_{361}	...	...	x_{36j}	...	x_{36n}
Marital status ($\mathbf{X_4}$)	X_{41} (married)	Points	q_{41}	+	x_{411}	...	...	x_{41j}	...	x_{41n}
	X_{42} (divorced)	Points	q_{42}	+	x_{421}	...	...	x_{42j}	...	x_{42n}
	X_{43} (widowed)	Points	q_{43}	+	x_{431}	...	...	x_{43j}	...	x_{43n}
	X_{44} (never married)	Points	q_{44}	+	x_{441}	...	...	x_{44j}	...	x_{44n}
Main source of earnings ($\mathbf{X_5}$)	X_{51} (salary/work compensation)	Points	q_{51}	+	x_{511}	...	...	x_{51j}	...	x_{51n}
	X_{52} (income from own or family business)	Points	q_{52}	+	x_{521}	...	...	x_{52j}	...	x_{52n}
	X_{53} (income from agricultural activities)	Points	q_{53}	+	x_{531}	...	...	x_{53j}	...	x_{53n}
	X_{54} (ownership or investment income)	Points	q_{54}	+	x_{541}	...	...	x_{54j}	...	x_{54n}
	X_{55} (pension)	Points	q_{55}	+	x_{551}	...	...	x_{55j}	...	x_{55n}
	X_{56} (governmental support)	Points	q_{56}	+	x_{561}	...	...	x_{56j}	...	x_{56n}
	X_{57} (support by family and/or other persons)	Points	q_{57}	+	x_{571}	...	...	x_{57j}	...	x_{57n}
Families with children ($\mathbf{X_6}$)	X_{61} (families with children aged 0-17 yrs.)	Points	q_{61}	+	x_{611}	...	...	x_{61j}	...	x_{61n}
	X_{62} (families with no children)	Points	q_{62}	+	x_{621}	...	...	x_{62j}	...	x_{62n}
Price ($\mathbf{X_7}$)	X_{71}	Points	q_{71}	-	x_{711}	...	...	x_{71j}	...	x_{71n}

Table 1: (Continued.)

Criteria describing alternatives	**Sub-criteria describing alternatives**	**Measuring units**	**Weight**	*	**Apartments video alternatives under comparison**					
					$\mathbf{A_1}$	...	...	$\mathbf{A_j}$	...	$\mathbf{A_n}$
Type of residential housing unit ($\mathbf{X_8}$)	X_{81} (one unit house)	Points	q_{81}	+	x_{811}	...	...	x_{81j}	...	x_{81n}
	X_{82} (two-unit house)	Points	q_{82}	+	x_{821}	...	...	x_{82j}	...	x_{82n}
	X_{83} (multi-unit building dwelling)	Points	q_{83}	+	x_{831}	...	...	x_{83j}	...	x_{83n}
Ownership form of residential dwelling ($\mathbf{X_9}$)	X_{91} (home owner resident)	Points	q_{91}	+	x_{911}	...	...	x_{91j}	...	x_{91n}
	X_{92} (resident in a rental unit)	Points	q_{92}	+	x_{921}	...	...	x_{92j}	...	x_{92n}
Dwelling characteristics										
Residential space ($\mathbf{X_{10}}$)		Points	q_{100}	+	x_{1001}	...	...	x_{100j}	...	x_{100n}
Number of rooms ($\mathbf{X_{11}}$)		Points	q_{110}	+	x_{1101}	...	...	x_{110j}	...	x_{110n}
Aesthetic and comfort features ($\mathbf{X_{12}}$)		Points	q_{120}	+	x_{1201}	...	...	x_{120j}	...	x_{120n}
Construction year ($\mathbf{X_{13}}$)		Points	q_{130}	+	x_{1301}	...	...	x_{130j}	...	x_{130n}
Environmental influences										
Aplinkos estetika ($\mathbf{X_{14}}$)		Points	q_{140}	+	x_{1401}	...	...	x_{140j}	...	x_{140n}
Street environment ($\mathbf{X_{15}}$)		Points	q_{150}	+	x_{1501}	...	...	x_{150j}	...	x_{150n}
Susisiekimas ($\mathbf{X_{16}}$)		Points	q_{160}	+	x_{1601}	...	...	x_{160j}	...	x_{160n}
Green areas ($\mathbf{X_{17}}$)		Points	q_{170}	+	x_{1701}	...	...	x_{170j}	...	x_{170n}
Commercial services ($\mathbf{X_{18}}$)		Points	q_{180}	+	x_{1801}	...	...	x_{180j}	...	x_{180n}
Cultural and sporting services ($\mathbf{X_{19}}$)		Points	q_{190}	+	x_{1901}	...	...	x_{190j}	...	x_{190n}
Consumer psychographic and behaviour segmentation criteria										
Happiness ($\mathbf{X_{20}}$)		Points	q_{200}	+	x_{2001}	...	...	$\mathbf{x_{200j}}$	...	$\mathbf{x_{200n}}$
Sadness ($\mathbf{X_{21}}$)		Points	q_{210}	+	x_{2101}	...	...	$\mathbf{x_{210j}}$	...	$\mathbf{x_{210n}}$
Valence ($\mathbf{X_{22}}$)		Points	q_{220}	+	x_{2201}	...	...	$\mathbf{x_{220j}}$	...	$\mathbf{x_{220n}}$
Angriness ($\mathbf{X_{23}}$)		Points	q_{230}	+	x_{2301}	...	...	$\mathbf{x_{230j}}$	...	$\mathbf{x_{230n}}$
Heart rate ($\mathbf{X_{24}}$)		Points	q_{240}	+	x_{2401}	...	...	$\mathbf{x_{240j}}$	...	$\mathbf{x_{240n}}$
Priority of the project alternative					$\mathbf{P_1}$		...	$\mathbf{P_j}$	...	$\mathbf{P_n}$
Degree of utility of the project					$\mathbf{N_1}$		...	$\mathbf{N_j}$	...	$\mathbf{N_n}$

Tables 1–3 containing the data on these 17 parameters of depersonalized bystanders. Therefore fragments of variables relevant to the theoretical study on these data appear in Table 1. Tables 2 and 3 illustrate fragments calculated practically.

The system of criteria is then used as the basis for a multiple criteria neuro decision matrix where its columns represent n alternative video ads and its rows are filled with detailed quantitative information of each alternative. Our quantitative information includes the systems of criteria, measuring units, values and weights, and the minimising or maximising criterion.

In marketing segmentation, we take a large cohort of current and potential customers, and, based on the above features, divide it into customer sub-groups (segments). In general, the goal of segmentation is to identify the sub-groups of customers that are most likely to buy a dwelling or bring the best profit, and as a result these potential consumers can become target demographic, behavioral or other significant segments. In marketing segmentation, it is accepted

that different marketing segments need different advertising approaches with different green housing options (based on characteristics, prices, environmental influences, etc.). By applying marketing segmentation, we seek to create profiles of the main potential home buyers.

The authors analysed scientific articles and statistical data and their analysis shows that dwelling buyer needs and buying habits depend on age (X1), gender (X2), education (X3), marital status (X4) and other factors. Buyers in the age group between 18 and 34, for instance, are usually looking for cheaper properties and tend to commit smaller sums for home buying than older buyers; smaller incomes is a factor. Gender differences in the choice of home show that women are more interested in the size of the kitchen, bathroom and wardrobes. Men, on the other hand, tend to focus on recreational spaces, pools and tubs. The size of and requirements for real estate investments can be also inferred from marital status. [11] compared married and single buyers and determine that those that are married have larger incomes and, naturally, can afford better apartment. The affordability of apartment and the environment in which their children will grow are the two main points stressed by these buyers. Single buyers are quite different and their gender also plays a role: single men choose properties closer to entertainment, recreation and sports centres, whereas single women prefer properties closer to their friends or family. To do a good job, real estate brokers need to understand how buyers react to marketing stimuli such as needs, personality, motives, expectations and experiences. Exposed to the same kinds of stimuli individuals often identify them in different ways, often focusing on elements they find important [2]. Expectations among female participants are generally higher than among men, and also higher among younger participants than among older. The least-educated participants have the highest expectations regarding the time when they will buy their own property and with every step up the education ladder expectations fall lower. Students had the highest expectations related to transport links, proximity to shops, schools and kindergartens, socio-economic and financial factors, greater autonomy, and a sense of peace [21].

Eight experts of property marketing, brokers and valuators applied expert methods to determine criteria values and weights (see Tables 2 and 3). The eight real estate experts evaluated how specific characteristics of housing units correspond with the needs of specific buyers based on a 10-point scale (where 1 is not very important, and 10 is very important). Their basis for the evaluation included the aforementioned and worldwide practices as well as their long-time. A method of complex determination of the weights of the criteria taking into account their quantitative and qualitative characteristics [26] was applied for criteria weights calculations.

The COPRAS method [52] is applied to determine the priority and utility degree of a video ad. The utility degree (N_j) can be between 0% and 100% and it depends, directly and proportionally, on the relative impact the criterial values x_{ij} and weights q_i make on the end result. The COPRAS Method [52] ensures that an adequate system of criteria defines any analyzed alternatives. Additionally, the weights and degrees of utility of these alternatives are presumed to link, both by direct and proportional dependence, to the values and weights of those criteria.

3 Case study

As of November 7, 2017, biometric tests of depersonalized passersby were conducted in nine locations in Vilnius City by remote means, at a distance of approximately 20 meters. This investigation yielded 17 affective attitudes, physiological and emotional states parameters (see Figure 1) of the depersonalized passersby over its course. Over 250 million items of data were gathered on these 17 parameters of depersonalized passersby during the course of this investigation. Since these 17 parameters of depersonalized passersby would take a tremendous amount of space to demonstrate in Tables 1, 2 and 3 that are under deliberation, fragments of these data for a theoretical analysis are illustrated as variables in Table 1. Meanwhile fragments of practical

calculations appear as numbers in Tables 2 and 3.

3.1 Detailed system of criteria defining the alternative video ads

This study has looked at the following groups of criteria: individual differences of potential buyers, apartment attributes, environmental influences, and consumer psychographic and behaviour segmentation criteria.

Buyer's individual differences (demographic segmentation criteria)

When users are looking for suitable options of apartment, the process can be lengthy and complicated because they may have many factors to consider. They need to take into account their budget and what facilities they need such as supermarkets, public transport or public schools available for their children. Most home buyers also find it important to look for a property that will grow in value over time so that in a few years they can sell it and move up the property ladder easier [28].

Socioeconomic and demographic characteristics may influence how a resident evaluates the neighbourhood, as may a normative element of the apartment environment preferred based on the person's lifestyle, experience, and inclinations. The objective characteristics evaluated by the resident in residential environment are the attributes of a specific house and neighbourhood. When the subjective individual perception of the residential environment, including the quality of the neighbourhood, matches the person's needs and expectations, it results in residential satisfaction [43]. When a person is satisfied with his or her residential environment, it means the perceived situation and the desired situation are a close match; deviation from preferred conditions, on the other hand, leads to dissatisfaction [19].

A range of studies spanning several decades show that neighbourhood satisfaction depends on age, sex, marital status, income, education, and race [6,25,40,41,48] focused on older residents in Spain and found higher satisfaction among Madrid residents living alone or only with a spouse. The satisfaction was also higher among women [19].

Marriage, change in jobs, fertility, educational issues or living with old parents may make public rental apartment tenants reconsider the objective public rental apartment factors in light of changing personal requirements.

Looking at group and personal influences would mean focusing on mutual relationships between potential home buyers and their co-workers, family members, friends and other individuals. To limit the scope of this research, these factors were, therefore, excluded from the development of VINERS method, even though ethnicity, culture, group and personal influences affect the needs and behaviour of potential home buyers, as has been shown. These factors will be incorporated into the VINERS method at later stages of the research.

Dwelling characteristics and environmental influences

Intrinsic and extrinsic characteristics influence the choice of a home. Intrinsic are the factors that define the apartment unit itself (flat, house or building), i.e. the number of rooms, balconies, windows, the floor, aesthetic properties, decor, features and amenities, etc. Extrinsic are the features of the location, such as green spaces (public parks and gardens), urban quality (roads, buildings, squares), public transport, social context, proximity to commercial areas or other centralities, picturesque views, historical significance of the area, pollution (acoustic, atmospheric), and so on [10].

A rapid increase of railway lines, both operational and under construction, leads to an increase in the number of buildings that suffer adverse effects of ground-borne vibration (e.g.

indoor noise and shaking) [17].

Ventilation regulates indoor air parameters, such as air temperature, air speed, relative humidity and concentrations of chemical substances in the air, and this way creates thermally comfortable environments with acceptable indoor air quality [44].

Building height determines various parameters. Negative correlation, for instance, links air temperature, humidity, $PM_{2.5}$, PM_{10}, and C_{O2} to building height—the higher the building, the lower the values. In contrast, ozone generally increased with building height, and the values of NO2 were less consistent. The correlation between PM, CO_2, and O_3 concentrations and floor height was stronger than between local wind speed and direction and floor height [1].

Indoor temperature and humidity fluctuations can be moderated by means of building materials. Phase change materials can be used to moderate the indoor temperature variations and reduce the energy consumption of HVAC systems; they absorb or release large amount of thermal heat at a constant temperature in phase change process. Well known is also the fact that indoor air humidity may have a significant influence on the living environment and, thus, on the comfort and health of its occupants. Humidity is an important factor. It influences both indoor air quality and thermal comfort [50].

When households make the decision which home to buy, they consider such important factors as the costs of apartment, time and transport, and the benefits that the site offers [10]. Available amenities and local incomes are usually the key factors in choosing a location. Incomes, in part, depend on the interaction between the demand and supply of labour. In terms of the choice of a city, residents, workers and businesses also consider the overall quality of life offered by the city [10].

Papamanolis [37] believes that environmental factors constantly change. Those that affect buildings are all variable [38]; among them are air temperature, moisture, solar radiation, precipitation, wind, noise and air pollution. All of them display fluctuations in many aspects. The fluctuations in some cases span a wide range of values (e.g. in case of air temperature, solar radiation, humidity and wind speed), occasionally varying between negative and positive effects. Other factors, such as pollution and ambient noise, have fluctuations ranging from negligible to (usually) negative. Beyond the intensity, important is also the frequency with which environmental factors affecting buildings vary. The same can be said about air pollution, especially in urban areas. A storm or a pollution event is a good example. At the building shell surface, the wind can serve as a medium for ventilation, pollution dispersion, natural cooling or thermal exchange. It can also act as a factor involved in structural integrity. Fluctuating values of environmental factors directly affect functioning of the systems installed in buildings in order to control the impact. The response of systems to variable conditions is a critical factor in their efficiency. Only when they are adapted to address the effects of any prevailing factors, passive systems can be efficient. Active systems are different. They show more flexibility when they respond to the fluidity of the environmental impact. A good example of a system that "behaves" according to the prevailing conditions are dynamic louvers—they react to the actual conditions to make sure the control of daylight and solar heat gains is optimal. Every step towards higher levels of adaptability to a variety of conditions makes these systems more effective [37]. Inclusion of the environmental factors mentioned above in the neuro decision matrix would involve a wide scope of research.

Potential home buyers make decisions slowly due to the complexities of decision making, often associated with a need for a large amount of funds and acceptance of long term obligations. They analyze various alternatives and circumstances as well as compare and consider different offers. Researchers [13, 46, 47, 51] noticed the huge influence emotions play on decision making.

Exceptional as well as digital marketing means must be employed to interest buyers in proposed apartment units. These promise buyers more possibilities for choosing a desired dwelling.

Applications of integrated neuro-marketing means make it possible to evaluate the needs of potential real estate buyers relevant to their emotions, present the most suitable offers and encourage decision making.

Traditional marketing means are insufficient when wanting to interest buyers in new, innovative products and to orient them towards firm and perspective albeit untraditional decision making. Thus this study undertook an analysis of the video neuro-advertising used in the real estate market of Vilnius City. This video neuro-advertising was submitted to the inhabitants of four eldership districts of Vilnius (specifically to Naujamiestis, Verkiai, Old Town and Žirmūnai). The selection of these specific districts were due to their reflecting a social distribution that makes it possible to forecast the desired level of apartment for acquisition, specific needs for such and the abilities to accept adequate obligations. For example, homeowners in the Old Town manage the most expensive apartment in Vilnius (where the price per one square meter is, on average, 2900 Euros). These buyers are able to consider the highest-class projects being offered when their family structures and needs change. Conversely, in the Žirmūnai district, residential apartment constructed long ago dominate; these units are notable for their lesser liquidity and significantly lower prices (where the price per one square meter is, on average, around 1300 Euros). Real estate companies and brokers notice that residents change their apartment units 3-4 times on average during their entire lives. Therefore the interest in real estate offerings is always relevant to various groups of residents during different stages of their lives. That is the reason different residents of these Vilnius districts, representing various social groups, were selected for this study. Data on the selected district residents came for the Lithuanian Department of Statistics in 2018 [29] following the submission of a targeted query. The data received permitted dividing the residents by age, gender, education, marital status and family composition, main sources for earnings and the type of apartment in which the persons resided and the form of its ownership. Conducted interviews established their needs to acquire or change their apartment units.

Consumer psychographic and behavioral segmentation

A number of investigations in the area of consumer psychographic and behavioral segmentation have been performed [4, 12, 23]. For example, the research performed by [12] investigated emotions to determine if they can be considered as a suitable variable for segmenting museum visitors. The reports from the segment with more positive emotions indicated perceptions of the museum as being more attractive and unique at the museum, than the other segment did, along with a higher level of satisfaction [12].

3.2 First-step segmentation

In marketing segmentation, we take a large cohort of current and potential customers, and, based on the above features, divide it into customer sub-groups (segments). In general, the goal of segmentation is to identify the sub-groups of customers that are most likely to buy a dwelling or bring the best profit and as a result these potential consumers can become target demographics, behavioural or other significant segments. In marketing segmentation, it is accepted that different marketing segments need different advertising alternatives with different housing options (based on characteristics, prices, environmental influences, etc.). By applying marketing segmentation we seek to create profiles of the main potential home buyers.

Our research uses the two-step segmentation technique of potential home buyers. In geographic segmentation, the properties in question were grouped taking into account the urban districts (neighbourhoods). In the second stage dedicated to demographic, psychographic and behavioural segmentation, the aggregate neuro decision matrices created for each neighbourhood

in question were narrowed down to cover more specific buyer segments. By using the two segmentation stages real estate brokers can optimise their marketing resources and reach the most rational potential clients.

A team of eight property experts from Vilnius evaluated ads and matched them with a certain group of residents following the definition provided by Statistics Lithuania. Four relative age groups were established: Group I with people aged 20 to 30, Group II with people aged 31 to 40, Group III with people aged 41 to 60 and Group IV with people aged over 60.

Our approach includes the first step segmentation for which the object of our analysis, i.e. the urban district, was divided into four neighbourhoods (Naujamiestis, Verkiai, Old Town, Žirmūnai). Then, in the second stage, we reclassify the sub-segments established in the first stage and determine a rational number of segments (see Table 2).

Table 2: The fragment of aggregate general neuro decision-making matrix during the time of first-step segmentation in the Old Town District

Criteria describing alternatives	**Criteria No**	**Sub-criteria describing alternatives**	*	**Weight**	**Number of inhabitants**	**Housing unit video ad alternatives under comparison**								
						1	**2**	...	**15**	**16**	**17**	**18**	**19**	**20**
Buyer's individual differences (demographic segmentation criteria)														
Age (X_1)	1	20–30 years	+	0.0079	4635	3	6	...	3	5	1	6	1	8
	2	31–40 years	+	0.0047	2895	6	6	...	6	8	2	8	3	9
	3	41–60 years	+	0.0381	4981	4	5	...	8	9	7	6	8	4
	4	Over 60 years	+	0.027	3286	7	7	...	3	3	2	3	2	4
Gender (X_2)	5	Male	+	0.0097	7060	7	9	...	8	8	6	8	6	9
	6	Female	+	0.0128	8737	8	10	...	9	8	5	7	8	8
Education (X_3)	7	higher	+	0.060	7400	7	6	...	9	7	9	7	9	6
	8	high and special secondary	+	0.016	1938	7	8	...	5	7	4	7	4	8
	9	secondary	+	0.042	5227	6	7	...	2	7	1	7	2	8
	10	basic	+	0.012	1442	5	6	...	4	4	1	4	1	4
	11	elementary	+	0.012	1521	4	5	...	1	2	1	2	1	3
	12	incomplete elementary school	+	0.001	140	3	4	...	1	2	1	2	1	4
Marital status (X_4)	13	married	+	0.057	6995	7	6	...	7	9	8	9	8	9
	14	divorced	+	0.016	1988	9	9	...	4	6	7	6	7	6
	15	widowed	+	0.011	1352	7	8	...	5	7	5	8	4	8
	16	never married	+	0.053	6556	9	8	...	4	6	7	6	7	8
Main source of earnings (X_5)	17	salary/work compensation	+	0.069	8445	7	8	...	5	7	4	7	5	7
	18	(income from own or family business	+	0.004	534	8	8	...	9	8	9	7	9	7
	19	income from agricultural activities	+	0.0001	18	8	8	...	9	8	6	7	6	7
	20	ownership or investment income	+	0.0006	74	7	7	...	9	6	9	6	9	6
	21	pension	+	0.024	3021	4	5	...	2	2	1	3	1	4
	22	governmental support	+	0.004	551	1	5	...	1	1	1	1	1	1
	23	support by family and/or other persons	+	0.045	5493	1	4	...	1	1	1	1	1	1
Families with children (total 4152) (X_6)	24	families with children aged 0-17 yrs.	+	0.016	2023	6	6	...	7	9	7	9	7	8
	25	families with no children aged 0-17 yrs.	+	0.017	2129	8	8	...	6	7	8	7	8	7

Table 2: (Continued.)

Criteria describing alternatives	**Criteria No**	**Sub-criteria describing alternatives**	*	**Weight**	**Nnumber of inhabitants**	**Housing unit video ad alternatives under comparison**								
						1	**2**	...	**15**	**16**	**17**	**18**	**19**	**20**
Dwelling characteristics														
Price (X_7)	26	Average price (euro /sq. m.)	–	1		1830	1450	...	1770	1280	4050	1290	3710	1320
Type of residential housing unit (X_8)	27	one unit house	+	0.002	285	5	4	...	9	7	9	7	9	7
	28	two-unit house	+	0.003	335	6	4	...	9	7	9	7	9	7
	29	multi-unit building dwelling	+	0.138	16969	8	9	...	7	9	7	9	7	9
Ownership form of residential dwelling (18917) (X_9)	30	home owner resident	+	0.111	13681	8	7	...	7	9	6	9	6	8
	31	resident in a rental unit	+	0.027	3328	7	8	...	5	8	5	8	5	7
Building materials (X_{10})	32		+	0.18	Points	7	5	...	8	6	9	6	9	7
Noise and air pollution (X_{11})	33		+	0.10	Points	8	8	...	9	9	8	8	8	7
Energy consumption (floor heating, renewable energy sources and etc.) (X_{12})	34		+	0.27	Points	6	7	...	8	7	8	9	9	7
Aesthetic properties (X_{13})	35		+	0.05	Points	7	7	...	9	7	9	8	9	7
Environmental influences														
Urban quality (infrastructure) (X_{14})	36		+	0.22	Points	7	7	...	8	6	9	6	9	7
Green spaces (X_{15})	37		+	0.18	Points	7	7	...	9	7	6	7	7	6
Consumer psychographic and behaviour segmentation														
Happiness	38		+	0.1	Points	0.14	0.14	...	0.14	0.14	0.14	0.14	0.14	0.14
Arousal	39		+	0.1	Points	0.33	0.33	...	0.33	0.33	0.33	0.33	0.33	0.33
Boredom	40		-	0.1	Points	0.06	0.06	...	0.06	0.06	0.06	0.06	0.06	0.06
Interest	41		+	0.1	Points	0.01	0.01	...	0.01	0.01	0.01	0.01	0.01	0.01
Heart rate	42		+	0.1	Points	66	66	...	66	66	66	66	66	66
Breathing rate	43		+	0.1	Points	16.7	16.7	...	16.7	16.7	16.7	16.7	16.7	16.7
Priority of housing unit video alternatives under comparison						18	12	...	20	6	1	7	2	9
Utility degree of housing unit video alternatives under comparison (%)						74,17	75,88	...	74,17	78,48	100	78,28	94,49	77,7256

* The symbol " + / − " specifies that a bigger (smaller) criterion value corresponds to a bigger (smaller) importance for a user (stakeholder).
Comment: Criteria evaluations ranging from 1 to 10 points, where 1–not very important, and 10–very important. Per Department of Statistics data, distribution of residents by educational achievement does not apply to persons aged less than 10 years (not included in the calculations of residents in eldership districts). Distribution of residents by marital status does not apply to persons aged less than 15 years. The study does not include persons aged under 19 years, because they are not yet active participants in the real estate market.

A method of complex determination of the weights of the criteria taking into account their quantitative and qualitative characteristics [26] was applied for criteria weights calculations.

The group of experts were shown 20 video ads taken from property offerings assigned to the relevant group of potential homebuyers. A sum segmentation neuro decision matrix for the Old Town was compiled based on this data (see Table 2). On a 10-point scale, each expert assigned a certain number of points to each apartment in the matrix based on its acquisition/interest potential and taking into account the needs, financial capacity and family composition of typical social groups, as well as market trends, acquisitions and stereotypes. Similar sum segmentation neuro

decision matrixes were compiled for the other three districts of Vilnius (Verkiai, Naujamiestis and Žirmūnai). Table 3 has been analogically filled out.

The COPRAS technique [52] and the data from Table 2 has been used to determine the potential effect of the video ads being analyzed on passers-by. The seventeenth video ad (N_{17} = 100%) made the biggest potential impact on passers-by. The lowest potential impact on passers-by impressions and feelings was made by the fifteenth ad (N_{15} = 74,17%).

With the buyer segments in the Old Town determined (see Table 2), more rational marketing is then possible for the highest success. The individual buyer differences, environmental influences and apartment attributes related to each segment of buyers assists with more effective ad targeting.

To determine the buyer segments in the Old Town, we start with the broadest possible sample (see Table 2) and then narrow it down to establish more specific groups (see Table 3) because the majority of property agents have multiple buyer personas.

3.3 Second-step segmentation

The Old Town's sum neuro decision matrix created as part of the first-step segmentation (see Table 2) has been used as the basis for a more specific neuro decision matrix in the second stage. Table 3 shows one of the matrixes created in the second stage.

Fragments of available 250 millions AEPS data (see Figure 1) are displayed as variables in Tables 1–3, because displaying the 17 parameters of these depersonalized passersby data in Tables 1–3 which are under deliberation would take up a great deal of space. Meanwhile fragments of the practical calculations appear as numbers in Tables 2 and 3.

An analysis of male and female respondents of various ages was for establishing an integrated, rational segment of potential buyers and an effective advertisement for housing in the Old Town of Vilnius. The purpose of this analysis was to establish the project that would be most rational for advertising at this time to the group of a specific age. Three video alternatives were shown to the eight aforementioned experts.

The first alternative was Video 1 on the Live Square project (`https://livesquare.lt/en/`). Live Square apartments are modern and high-quality home spaces. Apartments with balconies and terraces are designed for three LIVE SQUARE residential buildings.

The second alternative was Video 2 on Magnus Rezidencija [Magnus Residence] (`http://gedimino47.lt/`). Magnus Rezidencija is an exceptional oasis of residential housing and commercial facilities on Gedimino Prospect, a central street of Vilnius City. Cozy terraces, high windows, bright staircases and a separate playground for children in a private yard have been equipped for this project. A safe neighborhood, privacy and convenience distinguish this project.

The third alternative is Centro Rezidencija [Central Residence] (`https://centrorezidencija.lt/galerija/`). This project consists of eight residential buildings consisting of 4 to 9 stories. Stage I of this project has concluded building 4-5 and 7-storey buildings that contain 115 housing units measuring from 35 to 68 square meters. The construction for Stage II of this project consists of three residential buildings: two have 7 storeys and one has 6 storeys. During this stage, the offer is for 133 housing units measuring from 29 to 85 square meters. Stage III of this project consists of three residential buildings, one is 8-stories and two are 9-stories high. The units offered for sale measure from 25 to 98 square meters. Central to every stage of Centro Rezidencija will be the formation of a closed, internal yard complete with safe playgrounds for children, rest zones and an environment arranged by landscaping specialists. There is an underground parking lot for automobiles beneath the buildings. It is easily accessible by elevator operating directly from the staircases.

Table 3: Neuro decision matrix created as part of second-step segmentation in the Old Town

Criteria describing alternatives	**Measuring units**	**Weight**	*****	**Video alternatives for the age groups**											
				Video 1				**Video 2**				**Video 3**			
				Age demographics for advertising (years, male & female)				**Age demographics for advertising (years, male & female)**				**Age demographics for advertising (years, male & female)**			
				x_{11} (20–30)	x_{12} (31–40)	x_{13} (41–50)	x_{14} (51–60)	x_{11} (20–30)	x_{12} (31–40)	x_{13} (41–50)	x_{14} (51–60)	x_{11} (20–30)	x_{12} (31–40)	x_{13} (41–50)	x_{14} (51–60)
Residential space	Points	0,1	+	7	8	8	6	7	8	9	6	8	9	9	7
Number of rooms	Points	0,1	+	6	7	7	5	7	8	8	8	7	9	9	8
Construction year	Points	0,02	+	10	10	9	6	10	10	10	7	10	10	10	8
Aplinkos estetika	Points	0,09	+	10	10	10	9	10	10	10	10	10	10	10	10
Street environment	Points	0,06	+	10	10	10	8	10	10	10	9	9	10	10	8
Public transport	Points	0,12	+	9	10	10	10	9	10	10	10	9	10	10	10
Price	Points	0,2	–	4	7	8	6	5	8	9	7	6	9	9	8
Green areas	Points	0,14	+	8	10	10	10	9	10	10	9	8	10	10	9
Commercial services	Points	0,09	+	8	9	9	8	9	10	10	9	8	10	10	9
Cultural and sporting services	Points	0,08	+	10	10	9	6	10	10	10	7	10	10	10	8
Heart rate	Points	0,05	+	71,65	74,49	84,31	82,80	79,46	76,39	82,94	91,12	77,85	78,16	76,01	70,18
Happy	Points	0,2	+	0,139	0,108	0,085	0,070	0,130	0,115	0,083	0,075	0,134	0,116	0,101	0,104
Sad	Points	0,05	+	0,191	0,141	0,121	0,109	0,192	0,160	0,157	0,112	0,190	0,157	0,146	0,149
Angry	Points	0,05	+	0,115	0,099	0,100	0,087	0,094	0,102	0,102	0,103	0,104	0,105	0,108	0,110
Valence	Points	0,15	+	-0,224	-0,097	-0,107	-0,099	-0,107	-0,098	-0,139	-0,118	-0,104	-0,096	-0,114	-0,101
Utility degree of housing unit video alternatives under comparison (%)				**100,0**	**64,45**	**59,30**	**71,84**	**82,79**	**59,30**	**55,64**	**64,45**	**71,84**	**55,64**	**55,64**	**59,30**
Priority of housing unit video alternatives under comparison				**1**	**6**	**7**	**4**	**2**	**9**	**12**	**5**	**3**	**10**	**11**	**8**

* The symbol "+/-" specifies that a bigger (smaller) criterion value corresponds to a bigger (smaller) importance for a user (stakeholder).

The COPRAS method [52] and the data from Table 3 has been used to define the possible result of the video ads being examined on passers-by. A multicriteria analysis of alternatives, performed with the application of the VINERS method, indicated that the group ranging in the ages of 20-30 years was the most receptive to the advertisement and showed the greatest interest in the projects under development (see Table 3).

4 Conclusions

The researches described in the introduction indicate that a specific demographic segment of buyers would be best off looking for a dwelling in the same area where they usually feel well. In other words, people are best off living where they feel best.

The best [20,32,36] and worst [9,20] places to live have been analysed in the world for many years and multiple criteria analysis has been used for that purpose [22]. Other studies [3,31,42,53] also have analysed the environment that contributes to higher or lower positive emotions and happiness.

Lu [31] made a review of 178 published articles and was the first to look beyond the physiological and environmental effects of air pollution and take a systematic look at its psychological (affective, behavioural, cognitive), social and economic effects. Air pollution contributes to

decreased happiness and life satisfaction and increased anxiety, annoyance, self-harm, mental disorders, and suicide [31]. Benita et al. [3] determined a positive correlation between immediate environmental factors, public spaces and happiness. Benita et al. [3] unique contribution is the estimation, by using nearly real-time data, of the impact places, environment, and personal characteristics make on momentary happiness. To make people more happy, which is important to their well-being, planners are recommended to focus on designs that support opportunities for social interaction, make people feel safer in the environment, and increase access to open green spaces [42]. Zhang et al. [54] estimate the monetary value of cutting $PM_{2.5}$, one of the main sources of air pollution in China. Zhang et al. [53] matched the hedonic happiness values from a representative country-level survey with daily air quality parameters by the dates and counties of interviews in China and determined how local concentration of particulate matter is related to individual happiness.

Over the course of the research, over 250 million items of data have been gathered on 17 AEPS parameters (see Figure 1) of these depersonalized passersby. Our investigation has looked at the dynamic links between positive emotions and happiness of people and their built environment. Our research shows that the innovative VINERS method is an essential new addition to multiple criteria neuromarketing analysis of integrated sustainable development, positive emotions, happiness and built environment. The research determines rational segments of homebuyers by their demographic profiles (age, gender, education, marital status, families with children, main source of income), consumer psychographics and behaviour (happy, sad and angry along with valence and heart rate). This article also presents a case study to demonstrate the VINERS method put to practice.

The research confirmed our hypothesis that in housing neuromarketing an integrated approach is required to consider the most rational customer segments, the desired features of an apartment, individual differences, environmental influences on property, emotional and physiological states, valence and arousal and affective attitudes. By applying the Neuro Decision Tables, the above data can be used in neuromarketing to discover the most rational customer segments and to perform multiple criteria analysis of video ads.

Certain limitations of the research were also noticed during the time of the case study. For example, this study only encompassed real estate examples, which the ViNeRS Method then verified. The future expectation is to apply the neuro decision matrix and the ViNeRS Method more broadly, performing neuro-marketing for business, services, industry, agricultural organizations, relationships and social units. Furthermore, it is foreseen to supplement the neuro decision matrix on real estate with new criteria for more accurate descriptions of the objects under deliberation.

When someone advertises a home for sale, they usually consider the individual differences of potential homebuyers, their desires for the flat or house (indoor environmental quality and human health; energy, water, and materials efficiency; recycled, reusable and low-impact building materials; waste reduction; low-carbon technologies; renewable energy sources), and the environmental influences (air, noise and water pollution, green architecture, green built environment, etc.) on the property. The affective reactions, physiological and emotional status, arousal and valence of potential buyers are only considered in real estate advertising in exceptional cases. But so far all these factors have never been considered as an integrated whole. This study aimed to take an integrated look at the physiological and emotional status of potential homebuyers, their affective reactions, individual differences, arousal and valence, as well as environmental influences on properties and the preferred features of homes. The above data in this study was used in multiple criteria analysis of video ads and neuromarketing; different customer segments were analyzed by means of Neuro decision matrices. This research adds new pieces to "the big picture" of neuromarketing in green housing sales. This study, however, does not fully answer

some questions and many new questions have surfaced. In future studies, for instance, we intend to include a more extensive application of biometric and affective computing technologies in the ViNeRS method.

Acknowledgment

This project has received funding from European Regional Development Fund (project No 01.2.2-LMT-K-718-01-0073) under grant agreement with the Research Council of Lithuania (LMTLT).

Bibliography

[1] Azimi, P.; Zhao, H.; Fazli, T.; Zhao, D.; Faramarzi, A.; Leung, L.; Stephens, B. (2018). Pilot study of the vertical variations in outdoor pollutant concentrations and environmental conditions along the height of a tall building, *Building and Environment*, 138, 124–134, 2018.

[2] Belch, G.E.; Belch, M.A. (2012). Advertising and Promotion: An integrated marketing communications perspective. McGraw-Hill Irwin, New York, 2012.

[3] Benita, F.; Bansal, G.; Tunçer, B. (2019). Public spaces and happiness: Evidence from a large-scale field experiment, *Health & Place*, 56, 9–18, 2019.

[4] Bigné, J. E.; Andreu, L. (2004). Emotions in segmentation: An empirical study, *Annals of Tourism Research*, 31(3), 682–696, 2004.

[5] Bondi, L.; Davidson, J.; Smith, M. (2016). Introduction: Geography's 'emotional turn', *In Emotional geographies*, Routledge, 15–30, 2016.

[6] Chapman, D. W.; Lombard, J. R. (2006). Determinants of neighborhood satisfaction in fee-based gated and non-gated communities, *Urban Affairs Review*, 41(6), 769–799, 2006.

[7] Cloutier, S.; Berejnoi, E.; Russell, S.; Morrison, B.A.; Ross, A. (2018). Toward a holistic sustainable and happy neighborhood development assessment tool: A critical review of relevant literature, *Ecological Indicators*, 89, 139–149, 2018.

[8] Cloutier, S.; Pfeiffer, D. (2015). Sustainability through happiness: A framework for sustainable development, *Sustainable Development*, 23(5), 317–327, 2015.

[9] Cook, R.; Wainer, H. (2017). Joseph Fletcher, thematic maps, slavery, and the worst places to live in the UK and the US, *Visible Numbers*, Routledge, 83–105, 2017.

[10] D'Acci, L. (2019). Quality of urban area, distance from city centre, and green housing value. Case study on real estate values in Turin, *Cities*, 91, 71–92, 2019.

[11] Dahl, S.; Gordon-Wilson, S.M. (2013). Advertising assertiveness and effectiveness: the role of product involvement, *Proceedings of the Academy of Marketing, Marketing Relevance*, Glamorgan, Wales, 1–6, 2013.

[12] Del Chiappa, G.; Andreu, L.; G. Gallarza, M. (2014). Emotions and visitors' satisfaction at a museum, *International Journal of Culture, Tourism and Hospitality Research*, 8(4), 420–431, 2014.

[13] Dzitac, D. (2019). Extending Curiosity: The Power of Exploring Options, Oral presentation at *NYU Global Engagement Symposium*, New York University, New York City, April 5th, 2019.

[14] Florida, R.L. (2009). Reports what qualities of cities and towns actually make people happy, 2009.

[15] Florida, R. L. (2009). *Who's your city?: How the creative economy is making where to live the most important decision of your life*, Vintage Canada, 2009.

[16] Florida, R.; Mellander, C.; Rentfrow, P. J. (2013). The happiness of cities, *Regional studies*, 47(4), 613–627, 2013.

[17] Galvín, P.; López Mendoza, D.; Connolly, D.P.; Degrande, G.; Lombaert, G.; Romero A. (2018). Scoping assessment of free-field vibrations due to railway traffic, *Soil Dynamics and Earthquake Engineering*, 114, 598–614, 2018.

[18] Gesler, W. (2003). *Healing Places Lanham MD*, Rowman and Littlefield, 2003.

[19] Gibler, K.M.; Taltavull de La Paz, P.; Zahirovic-Herbert, V. J. (2018). Residents' evaluation of advantages and disadvantages of golf community living in Alicante, Spain. *Green housing and the Built Environment*, 33(4), 731–748, 2018.

[20] Granger, M.; Price, G. N. (2015). Are States with Larger than Average Black Populations Really the Worst Places to live in the USA? A Spatial Equilibrium Approach to Ranking Quality of Life, *Journal of Public Management & Social Policy*, 20(2), 3, 2015.

[21] Grum, B.; Salaj, A.T. (2010). Expectations of potential acquisitions of residential real estate rights in the republic of Slovenia, according to gender, age, education and employment, *Geodetski vestnik*, 54(3), 501–516, 2010.

[22] Hoepfner, G. K.; Mata, F. (1993). A multi-criteria decision analysis methodology for selection of a preferred residence based on physical attributes, *Computers & industrial engineering*, 25(1-4), 365–368, 1993.

[23] Hosany, S.; Prayag, G. (2013). Patterns of tourists' emotional responses, satisfaction, and intention to recommend, *Journal of Business Research*, 66(6), 730–737, 2013.

[24] Hubbard, P. (2016). The geographies of 'going out': Emotion and embodiment in the evening economy, *In Emotional geographies*, Routledge, 131–148, 2016.

[25] James, R. N. (2008). Residential satisfaction of elderly tenants in apartment green housing, *Social Indicators Research*, 89, 421–437, 2008.

[26] Kaklauskas, A. (1999). *Multiple criteria decision support of building life cycle, research report presented for habilitation* (DrSc), Technological Sciences, Civil Engineering (02T). Technika: Vilnius Gediminas Technical University, Vilnius, 1999.

[27] Lawless, N. M.; Lucas, R. E. (2011). Predictors of regional well-being: A county level analysis, *Social Indicators Research*, 101(3), 341–357, 2011.

[28] Li, M.; Bao, Z.; Sellis, T.; Yan, S.; Zhang, R. (2018). HomeSeeker: A visual analytics system of real estate data, *Journal of Visual Languages & Computing*, 45, 1–16, 2018.

[29] Lithuanian Department of Statistics. (2018). Segmentation of consumers by age and gender at select districts. Accessed date: 29 September 2018

[30] Leyden, K.M.; Goldberg, A.; Michelbach, P. (2011). Understanding the pursuit of happiness in ten major cities, *Urban Aff. Rev.* 47 (6), 861–888, 2011.

[31] Lu, J. G. (2019). Air Pollution: A Systematic Review of Its Psychological, Economic, and Social Effects, *Current Opinion in Psychology*, In Press, Journal Pre-proof.

[32] Méndez, M. L.; Gayo, M. (2019). Inheritors, Achievers, and Incomers: Wrapping Up a Multidimensional Approach to Social Reproduction, *In Upper Middle Class Social Reproduction*, Palgrave Macmillan, Cham, 135–145, 2019.

[33] Milligan, C.; Bingley, A.; Gatrell, A. (2016). "Healing and feeling": The place of emotions in later life, *In Emotional geographies*, Routledge, 63–76, 2016.

[34] O'Brien, C. (2005). Sustainable happiness: harmonizing our internal and external landscapes, *2nd International Conference on Gross National Happiness*, Antigonish, Nova Scotia, 2005.

[35] O'Brien, C. (2008). Sustainable happiness: how happiness studies can contribute to a more sustainable future, *Can. sychol./Psychologie canadienne*, 49(4), 289, 2008.

[36] O'Hara, M. (2016). Make it personal: International Futures Forum's Approach to community transformation, *In Transforming Communication in Leadership and Teamwork*, Springer, Cham, 99–106, 2016.

[37] Papamanolis, N. (2014). An Overview of the Architectural Methods Used to Manage the Variable Environmental Influences on Buildings in the Mediterranean Region, *Journal of Architectural Engineering Technology*, 3(3), 2014.

[38] Papamanolis, N. (2006). An Approach to the Effects of Environmental Change on Building Design and Construction, *23rd Conference on Passive and Low Energy Architecture*, Geneva, Switzerland, 2006.

[39] Paralkar, S.; Cloutier, S.; Nautiyal, S.; Mitra, R. (2017). The sustainable neighborhoods for happiness (SNfH) decision tool: Assessing neighborhood level sustainability and happiness, *Ecological Indicators*, 74, 10–18, 2017.

[40] Parkes, A.; Kearns, A.; Atkinson, R. (2002). What makes people dissatisfied with their neighbourhoods? *Urban Studies*, 39, 2413–2438, 2002.

[41] Perez, F. R.; Fernandez-Mayoralas, G.; Rivera, F. E. P.; Abuin, J. M. R. (2001). Ageing in place: Predictors of the residential satisfaction of elderly, *Social Indicators Research*, 54, 173–208, 2001.

[42] Pfeiffer, D.; Cloutier, S. (2016). Planning for happy neighborhoods, *Journal of the American planning association*, 82(3), 267–279, 2016.

[43] Phillips, D. R.; Siu, O. L.; Yeh, A. G. O.; Cheng, K. H. C. (2005). The impacts of dwelling conditions on older persons' psychological well-being in Hong Kong: The mediating role of residential satisfaction, *Social Science and Medicine*, 60, 2785–2797, 2005.

[44] Pitarma, R.; Lourenço, M.; Ramos, J. (2016). Improving occupational health by modelling indoor pollutant distribution, *Facilities*, 34(5/6), 289–301, 2016.

[45] Rentfrow, P. J.; Mellander, C.; Florida, R. (2009). Happy states of America: A state-level analysis of psychological, economic, and social well-being, *Journal of Research in Personality*, 43(6), 1073–1082, 2009.

[46] Respizzi, S.; Covelli, E. (2015). The emotional coaching model: quantitative and qualitative research into relationships, communication and decisions in physical and sports rehabilitation, *Joints*, 3(4), 191–200, 2015.

[47] Tam, N.D. (2015). Quantitative Assessment of Sad Emotion, *Psychology and Behavioral Sciences*, 4(2), 36–43, 2015.

[48] Tan, T-H. (2012). Green housing satisfaction in medium- and high-cost green housing: The case of Greater Kuala Lumpur, Malaysia, *Habitat International*, 36(1), 108–116, 2012.

[49] Urry, J. (2016). The place of emotions within place, *In Emotional geographies*,Routledge, 91–98, 2016.

[50] Xu, X.; Zhong, Z.; Deng, S.; Zhang, X. (2017). A review on temperature and humidity control methods focusing on air-conditioning equipment and control algorithms applied in small-to-medium-sized buildings, *Energy and Buildings*, 162, 163–176, 2017.

[51] Yang, J.; Zhou, Q.; Liu, X.; Liu, M.; Qu, S.; Bi, J. (2018). Biased perception misguided by affect: How does emotional experience lead to incorrect judgments about environmental quality? *Global Environmental Change*, 53, 104–113, 2018.

[52] Zavadskas, E. K.; Kaklauskas, A.; Sarka, V. (1994). The new method of multicriteria complex proportional assessment of projects, *Technological and economic development of economy*, 3, 131–139, 1994.

[53] Zhang, X.; Zhang, X.; Chen, X. (2017). Valuing air quality using happiness data: the case of China, *Ecological economics*, 137, 29–36, 2017.

[54] Zhang, X.; Zhang, X.; Chen X. (2017). Happiness in the air: How does a dirty sky affect mental health and subjective well-being? *Environmental Economics and Management*, 85, 81–94, 2017.

[55] Zidansek, A. (2007). Sustainable Development and Happiness in Nations, *Energy*, 32, 91–897, 2007.

INTERNATIONAL JOURNAL OF COMPUTERS COMMUNICATIONS & CONTROL
ISSN 1841-9836, e-ISSN 1841-9844, 14(5), 647-659, October 2019.

Exploring Analytical Models for Performability Evaluation of Virtualized Servers using Dynamic Resource

Y Kirsal

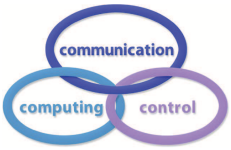

Yonal Kirsal*
Department of Electronics and Communication Engineering
European University of Lefke, Lefke, North Cyprus
TR-10 Mersin, Turkey
*Corresponding author:ykirsal@eul.edu.tr

Abstract: Virtualization of resources is a widely accepted technique to optimize resources in recent technologies. Virtualization allows users to execute their services on the same physical machine, keeping these services isolated from each other. This paper proposes the analytical models for performability evaluation of virtualized servers with dynamic resource utilization. The performance and avalability models are considered separately due to the behaviour of the proposed system. The well-known Markov Reward Model (MRM) is used for the solution of the analytical model considered together with an exact spectral expansion and product form solution. The dynamic resource utilization is employed to enhance the QoS of the proposed model which is another major issue in the performance characterization of virtulazilation. In this paper, the performability output parameters, such as mean queue length, mean response time and blocking probability are computed and presented for the proposed model. In addition, the performability results obtained from the analytical models are validated by the simulation (DES) results to show the accuracy and effectiveness of the proposed work. The results indicate the proposed modelling results show good agreement with DES and understand the factors are very important to improve the QoS.
Keywords: Analytical models, markov reward model, performability evaluation, virtulazilation, dynamic resource utilization.

1 Introduction

With the rapid growth of network applications, the management of resources and bandwidth in future system is becoming more complicated. Virtualization is one of the techniques that serve large number of tasks and multimedia applications with high demands by using a single physical machine [12]. Virtualization allows users to better utilize the resources that networks have available in a physical machine. The physical machine considered for virtualization purpose has a lot more resources than a personal computer such as a lot more CPU, RAM and the hard disk space. Thus, all of those resources can be emulated inside a software and with this software many virtual machines can be put on a single physical machine [18].

Virtualization allows service providers to lower their capital expenditures instead of buying many physical machines. In addition, centralized management with virtualization can be easily reachable instead of having to reach many individual physical machines providers only to manage one physical machine. In addition, all the updates or patches that the network to do for each of those individual machines can be done through from one central location. So, with the

centralized management service providers have lower operational expenses because it takes less effort to manage these multiple machines [1]. However, putting multiple machines on one machine is not anything new. Currently, service providers have servers running these virtual machines for their subscribers in cloud computing environment and need additional computing resources for different server. Thus, they begin to add other virtual machines and these could be larger virtual machines depending on the business need [15].

Obtaining the best QoS requirements and improve the system performance of virtualized servers in cloud computing is a challenging task. Even though it is not a new topic, QoS modelling and evaluation of virtualized servers in such environment is still one of the key issues in order to obtain QoS measurements. Modelling and performance evaluation of such system in an analytical point of view help to service providers to predict the complex system behaviour. This might lead to improve the system QoS characterization in different aspects. Therefore, the main focus in this paper is to model and analyse the QoS of the proposed work considering the availability issues of a physical and virtual machines together with dynamic resource utilization. In other words, the physical and virtual machine failures and repairs are considered in analytical point of view. In addition, dynamic resource utilization is also employed to enhance the QoS of the proposed model which is another major issue in the performance characterization. Using the proposed model, important performability measures, such as mean queue length, mean response time and blocking probability can be computed. The well-known Markov Reward Model (MRM) is used for the solution of the analytical model considered together with an exact spectral expansion and product form solution. The rest of the paper is organized as follows: Section II gives motivation of the proposed model. Section III describes the proposed model and the solution approach. Numerical results and discussions are given in Section IV. Conclusions and future-work are provided in Section VI.

2 Motivation

With the widespread deployment and development of cloud computing facilities, the importance of virtualized cloud systems has significantly grown. The resource allocation is one of the important factors which affect the QoS of the virtualized servers [7]. The modeling of resource allocation and evaluation in cloud computing is considered in [2,6,13,19,21]. An analytic probabilistic model is presented in [2] to calculate profit in a virtualized cloud data center. The proposed model accurately calculate the arrival rates based on the external and internal requests for virtualized cloud data centers. In [13] the authors proposed a web application model via simulation to get the behavioral patterns of different users and an performance analysis is done for resource utilization in cloud computing. The energy-efficient scheduling of virtual machine resource reservations in the cloud data center is presented in [19] focusing on CPU applications. The main aim is to schedule all reservations non-preemptively considering the limitations of a physical machine capacities to minimize the total energy consumption. The authors in [21] proposed an effective evolutionary approach for virtual machine allocation that can maximize the energy efficiency of a cloud data center. This is done by designing a simplified simulation using CloudSim that speed up the process of the proposed work. However, those proposed models do not consider availability issues of both virtual and physical machines for dynamic resource utilization.

In addition, many existing studies mainly focus on performance analysis of virtual servers in cloud computing systems [5, 6, 10, 11, 17, 20]. Performance modelling and evaluation of the virtual servers in the cloud computing is considered in [5]. However, two virtual machines and a physical machine have been considered for performance evaluation which is not practical case. In [6] and [17] a performance management system is proposed based on an analytical

queuing model on cloud. In those studies, the web applications are modeled as queues and virtual machines are modeled as service centers. Thus, the queuing theory models are applied to dynamically create and remove virtual machines in the cloud to enhance the system performance. The performance models for service migration have been addressed in [20] to predict the virtual machine migration time and the resources availability. However, the analysis done above studies considers only the pure performance model which ignore failure and recovery behaviour of the system. But in reality such systems are prone to failures due to hardware and software failures. An optimization method for the scheduling of scientific work flows on cloud systems is presented in [16]. A performability model is presented which provides the fitnesses of explored solutions by use of a meta-heuristic algorithm. In [9] a hierarchical model is employed for analysis of virtual machines failure and recovery with respect to the system behavior. In addition, the proposed model used in [9] for virtual machine mode was Continuous Time Markov Chain (CTMC) and a stochastic reward nets (SNR) is employed in [8] to model and analysis of the availability of a virtualized system.

In summary, however, the performability analysis of virtual machines with physical machine failure and recovery behaviour together with dynamic resource utilization have not been considered in none of the presented studies for an analytic probabilistic model. In this paper, the proposed model considers analytical models for performance and availability issues together with dynamic resource utilization in an attempt to understand, and improve system QoS. In addition, the analytical models results are validated by the discrete event simulation (DES) results to show the accuracy and effectiveness of the proposed work. The results indicate the proposed modelling results show good agreement with DES.

3 Proposed model and solution approach

In this section, the proposed analytical models and the solution approaches are presented to evaluate the QoS of the virtualized machines considering availability of physical as well as virtual machines together with dynamic resource utilization. In order to obtain realistic QoS output measurements dynamic resource utilization is also considered which can maximize the memory usage depending on the number of requests and failures within the proposed model. The main idea is to enhance the overall performance of the entire system by sharing the available resources. All the virtual machines used by the same physical machine are perfectly coordinated and synchronized. Hence, the tasks can be serviced more efficiently since the service ability will change dynamically when the virtual machine failures occur. The performance and availability models are considered separately due to the behavior of the proposed model. The exact spectral expansion solution approach is used to obtain steady state probabilities for the availability model, on the other hand, the steady state probabilities of the performance model are obtained by using the product form solution approach. Therefore, the MRM is employed to obtain performability output parameters for the proposed model. In MRM, the steady state probabilities of performance model are obtained (π_i^P) and are passed as reward rates to the availability model.

3.1 Model description

The handling of an incoming tasks for the proposed system with single physical machine (PM), a number of parallel homogeneous virtual machines (VMs) and a finite queue, L are illustrated in Fig. 1. Hence the total system capacity is K where K=L+VM. As shown in the figure, the arriving tasks reach first in a finite buffer and then distributed by the PM with a mean service time $1/\mu$ according to virtual machine availability. The PM will distribute the tasks for processing if and only if any of the VMs are available to handle a new task. Hence, each VM

can also service and process the tasks in the system with a mean service time $1/\mu$. A VM can only serve one task at a time.

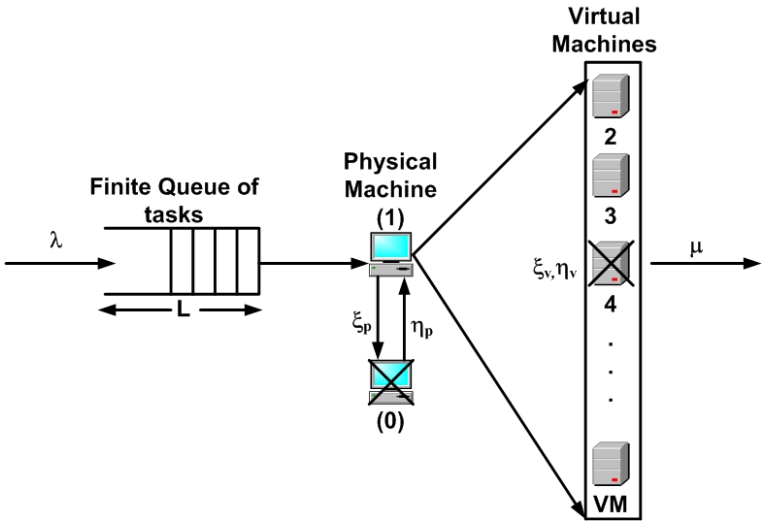

Figure 1: The proposed system

The resource allocations of such systems can be implemented in various ways depending on the system architecture. The dynamic resource allocation is presented which assures fair sharing of the CPU or the memory. The proposed allocation considers the avalability of the virtual machines and number of VMs in the system. It determines if the VM is busy or idle, if it is idle, it starts to transmit. If the VM is busy, the physical machine sends the tasks to VMs when they available. However, if the VM fails the shared CPU will not be wasted and can be dynamically used by the others available VMs until the failed VM will be repaired. Thus, the marginal distribution of the number of operative VMs is easily seen to be binomial [14]:

$$q_{i,.} = \sum_{j=0}^{\infty} q_{i,j} = \binom{VM}{i} \left(\frac{\eta_v}{\eta_v + \xi_v}\right)^i \left(\frac{\xi_v}{\eta_v + \xi_v}\right)^{VM-i} where \quad i = 0, 1, \ldots, VM. \tag{1}$$

Where q_i is the probability that i, VM are operative. Hence, the processing capacity of the system, which is defined as the average number of operative virtual machines, is equal to E(I)=VM($\eta_n/\eta_n+\xi_n$). The η_n and ξ_n are recovery and failure rates of virtual machines in the proposed system. The failure and recovery behaviour of the proposed system is explained in section 3.2 in more detail. However, for a good QoS measurements in such system the availability of virtual machines and impact of on system performance should be considered. Therefore, in order to get more realistic results, dynamic resource utilization (effective service rate) for the proposed system is calculated considering all possible combinations of the number of operative VMs. Then the expected effective service rate is calculated as follows:

$$\mu_{eff} = \sum_{i=0}^{VM} q_i \cdot \mu_i \tag{2}$$

Equation 2 is used to calculate effective service rate of the proposed work when a VM failure occurs and used to optimize the resource allocation in the proposed work. In other words, Let's define T as a service time of a virtual machine and T_{eff} as dynamic service time of virtual machine with a failure with means μ and μ_{eff}, respectively. Hence, for dynamic resource utilization the service time of a task is equal to the smaller one between T and T_{eff}. Since the random variables

T and T_{eff} have exponential distribution, the service times of a task is exponentially distributed with mean;

$$E[T] = \frac{1}{\mu} = E[min(T, T_{eff})] = \frac{1}{\mu + \mu_{eff}} \tag{3}$$

As shown in Fig. 1, the tasks join the system with the Poisson distribution, hence the average arrival rate is λ [4, 10, 11]. On the other hand, the physical and virtual machines in the system are prone to failures, each VMs and PM get corrupted with an average rate of ξ_v and ξ_p, respectively. The failed VMs and a PM then repaired with an average repair rate of η_v and η_p, respectively. The repair priority is given to PM since the VMs can not operate when a PM failure occurs. If there are tasks in the queue, the operative VM cannot be in a pending state. However, when any VM fails due to the corruption, new tasks can be served by the first available VM. It is also assumed that if an operative VM fails, it becomes available again at the breakpoint. If all VMs are busy or failed, the queue is growing with average rate of λ. In order to obtain more realistic QoS output parameters both performance and availability issues are considered together with dynamic resource allocation. The performance and availability models considered are presented with the resulting MRM solution approach in detail following sections.

3.2 The availability model of the proposed system

The availability model shows possible VMs and a PM failures and repairs in the proposed system. An exact spectral expansion solution approach is used for availability model to obtain the steady state probabilities. The both failures and repairs behaviour are shown in Fig. 2. As mentioned before, the distribution of time intervals between VMs and a PM failures are exponential and given by mean $1/\xi_v$ and $1/\xi_p$, respectively. At the end of the VMs and a PM failures, the VMs and a PM require an exponentially distributed repair time with mean $1/\eta_v$ and $1/\eta_p$. As clearly seen from the Fig. 2 that multi-repairman facility is assumed for all of the VMs in order to get realistic QoS measurements.

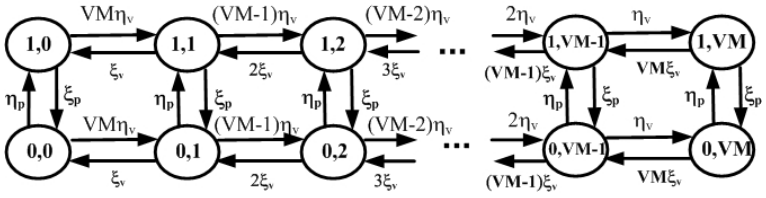

Figure 2: The availability model considered

Assume that $\pi^A_{i,j}$ represents the steady state probabilities of the availability model. Hence, the state of the availability model at time t can be described by a pair of integer valued random variables, $I(t)$ and $J(t)$, specifying the VMs and the PM failures and repairs, respectively. As clearly seen from the Fig. 2, $J(t)$ describes the PM failures and has two modes. Let $J(t)$=0,1 denote a binary value indicating whether or not the system is down due to a PM failure. In other words, *0* indicates the whole system is down due to a PM failure and *1* indicates all VMs are operate. On the other hand, $I(t)$ represents the operative states of the VMs and there are $VM + 1$ configurations. Thus, $I(t) = 0, 1, \cdots, VM$. Hence, $Z = [I(t), J(t)]$; $t \geq 0$ is an irreducible Markov process on a lattice strip that models the system. Its state space is (0, 1, $\cdots$, $VM+1$) x (0, 1). In other words, the failure and repair behaviour of the VMs can be represented in the horizontal as well as the failure and recovery behaviour of the PM in the vertial direction of a lattice strip. The three matrixes of the spectral expansion can be defined when the state

diagram is obtained. Hence, A, B, and C are the matrixes that indicate of the transition rates of the proposed model. The definition and the formation of the matrixes can be found in [3,11]. Therefore, clearly, the elements of A,B and C depend on the parameters VM, ξ_v, η_v, η_p,ξ_p. The transition matrices of a system with VM machines are of size $(VM+1)\times(VM+1)$. It is possible to specify the numbering of the matrices as $(0,1,2,\cdots,VM+1)$ for states $(0,1,2,\cdots,VM+1)$ respectively. The state transition matrices A, A_j, B, B_j, C, and C_j can be given as follows:

$$A = A_j = \begin{pmatrix} 0 & VM\eta_v & 0 & 0 & 0 & 0 & 0 \\ \xi_v & 0 & (VM-1)\eta_v & 0 & 0 & 0 & 0 \\ 0 & 2\xi_v & 0 & (VM-2)\eta_v & 0 & 0 & 0 \\ 0 & 0 & 3\xi_v & 0 & \ddots & 0 & 0 \\ 0 & 0 & 0 & \ddots & 0 & 2\eta_v & 0 \\ 0 & 0 & 0 & 0 & (VM-2)\xi_v & 0 & \eta_v \\ 0 & 0 & 0 & 0 & 0 & (VM-1)\xi_v & 0 \\ 0 & 0 & 0 & 0 & 0 & 0 & VM\xi_v \end{pmatrix}$$

$$B = B_j = \begin{pmatrix} \eta_p & 0 & 0 & 0 & 0 \\ 0 & \eta_p & 0 & 0 & 0 \\ 0 & 0 & \ddots & 0 & 0 \\ 0 & 0 & 0 & \eta_p & 0 \\ 0 & 0 & 0 & 0 & \eta_p \end{pmatrix}$$

$$C = C_j = \begin{pmatrix} 0 & 0 & 0 & 0 & 0 & 0 & 0 \\ 0 & \xi_p & 0 & 0 & 0 & 0 & 0 \\ 0 & 0 & \xi_p & 0 & 0 & 0 & 0 \\ 0 & 0 & 0 & \ddots & 0 & 0 & 0 \\ 0 & 0 & 0 & 0 & \xi_p & 0 & 0 \\ 0 & 0 & 0 & 0 & 0 & \xi_p & 0 \\ 0 & 0 & 0 & 0 & 0 & 0 & 0 \end{pmatrix}$$

Therefore, the proposed system can be solved using the well-known exact spectral expansion solution method. Thus, the steady state probabilities for the availability model, $\pi^A_{i,j}$ can be obtained using the steady state solution. The solution is given for systems with bounded queuing capacities. The steady-state probabilities of the system considered can be expressed as:

$$p_{i,j} = lim_{t\to\infty}^{P(I(t)=i,J(t)=j)}; \quad 0 \le i \le VM+1, \quad 0 \le j \le 1 \tag{4}$$

Let's define certain diagonal matrices of size $(VM+1)\times(VM+1)$ as follows:

$$D^A_j(i,i) = \sum_{k=0}^{VM+1} A_j(i,k); \quad D^A(i,i) = \sum_{k=0}^{VM+1} A(i,k); \tag{5}$$

$$D^B_j(i,i) = \sum_{k=0}^{VM+1} B_j(i,k); \quad D^B(i,i) = \sum_{k=0}^{VM+1} B(i,k); \tag{6}$$

$$D^C_j(i,i) = \sum_{k=0}^{VM+1} C_j(i,k); \quad D^C(i,i) = \sum_{k=0}^{VM+1} C(i,k); \tag{7}$$

and $Q_0 = B$, $Q_1 = A - D^A - D^B - D^C$, $Q_2 = C$. Hence, all state probabilities in a row can be defined as:

$$v_j = (p_{0,j}, p_{1,j}, \cdots, p_{VM+1,j}); j = 0, 1 \tag{8}$$

The steady-state balance equations for bounded queuing systems ($0 \leq j \leq 1$) can now be written as follows:

$$v_0[D_0^A + D_0^B] = v_0 A_0 + v_1 C_1 \tag{9}$$

$$v_j[D_j^A + D_j^B + D_j^C] = v_{j-1} B_{j-1} + v_j A_j + v_{j+1} C_{j+1}; \quad 0 \leq j \leq 1 \tag{10}$$

$$v_L[D^A + D^C] = v_{L-1} B + v_L A \tag{11}$$

The normalizing equation is given as follows:

$$\sum_{j=0}^{L} v_j e = \sum_{j=0}^{1} \sum_{i=0}^{VM+1} P(i,j) = 1.0 \tag{12}$$

From the equations above, the following equation can be written:

$$v_j Q_0 + v_{j+1} Q_1 + v_{j+2} Q_2 = 0; \quad 0 \leq j \leq 1 \tag{13}$$

Furthermore, the characteristic matrix polynomial $Q(\lambda)$ can be defined as:

$$Q_\lambda = Q_0 + Q_1 \lambda + Q_2 \lambda^2; \quad \bar{Q}_\beta = Q_2 + Q_1 \beta + Q_0 \beta^2; \tag{14}$$

where

$$\Psi Q_\lambda = 0; \quad |Q_\lambda| = 0; \quad \phi \bar{Q}_\beta = 0; |\bar{Q}_\beta| = 0; \tag{15}$$

λ and Ψ are eigenvalues and left-eigenvectors of Q_λ and β and ϕ are eigenvalues and left-eigenvectors of $\bar{Q}_\beta$, respectively. Note that, ϕ and β are vectors defined as:

$$\phi = \phi_0, \phi_1, \ldots, \phi_{S+1} \tag{16}$$

$$\beta = \beta_0, \beta_1, \ldots, \beta_{S+1} \tag{17}$$

Furthermore, $v_j = \sum_{k=0}^{VM+1} (a_k \Psi_k \lambda_k^{j+1} + b_k \phi_k(i) \beta_k^{2-j})$,0≤j≤ 1 and in the state probability form,

$$p_{i,j} = \sum_{k=0}^{VM+1} (a_k \Psi_k \lambda_k^{j-M+1} + b_k \phi_k(i) \beta_k^{2-j}) \quad 0 \leq j \leq 1 \tag{18}$$

Where $\lambda_k (k = 0, 1, \ldots, VM+1)$ and $\beta_k (k = 0, 1, \ldots, VM+1)$ are $VM+1$ eigenvalues [3,4,11]. The more details of the exact spectral expansion method can be found in [3]. Therefore, all steady state probabilities of the availability model, $\pi_{i,j}^A$ can be obtained using the exact spectral expansion method.

3.3 The performance model of the system

The performance model considers the arrival and service rates transitions of the single PM and multiple VMs in this section. The state transition diagram of performance model of a proposed system is given in Fig. 3.

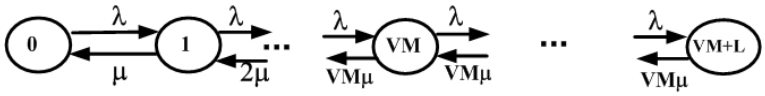

Figure 3: The performance model considered

Let's define the states i (i=0,1,2,$\cdots$,VM+L) as the number of tasks in the system at time t. In order to obtain perofrmability measures of the proposed model, the performance model is solved using general product form solution technique to get steady state probabilities. Once all π_i^P obtained, they pass as reward rates to the availability model. ρ is the traffic intensity in the system where ρ=λ/μ. Hence, the state probabilities, π_i^P can be obtained and are given in equation 19 [9, 10].

$$\pi_i^P = \begin{cases} \frac{\rho^i}{i!} \cdot \pi_0^P & 0 \leq i \leq VM \\ \\ \frac{\rho^i}{VM^{i-VM}.VM!} \cdot \pi_0^P & VM < i \leq VM + L \end{cases} \tag{19}$$

In equation 19, π_i^P is the probability that there are i tasks in the proposed system and π_0^P can be defined as follows:

$$\pi_0^P = \left[\sum_{i=0}^{VM-1} \frac{\rho^i}{i!} + \sum_{i=VM}^{VM+L} \frac{\rho^i}{VM^{i-VM}.VM!} \right]^{-1} \tag{20}$$

Hence, the average number of tasks in the proposed system, N_{VM} can then be calculated as $N_{VM} = \sum_{i=0}^{VM+L} i \cdot \pi_i^P$ which gives:

$$N_{VM} = \left[\sum_{i=0}^{VM} i \cdot \frac{\rho^i}{i!} + \sum_{i=VM}^{VM+L} i \cdot \frac{\rho^i}{VM^{i-VM}.VM!} \right] \cdot \pi_0^P \tag{21}$$

Similarly, the blocking probability P_B of the system can be calculated as:

$$P_B = P(VM + L) = \frac{\lambda^{VM+K}}{VM^L VM! \mu^{VM+L}} \cdot \pi_0^P \tag{22}$$

Using Little's formula, the average value of time of a task in a the system is can be calculated as follows:

$$MRT = \frac{MQL}{(1 - P_B)\lambda} \tag{23}$$

Therefore, a MRM approach can be used to obtain the overall performability output parameters such as mean queue length, blocking probability and mean response time. Equation 21 gives the MQL assuming that all VMs are operative. However, since only i VMs are operative at any time, the MQL can now be represented by N_i where i is the number of operative VM. Thus overall MQL can be calculated as follows;

$$MQL = \sum_{i=0}^{K} N_i \sum_{j=0}^{1} \pi_{i,j}^A \tag{24}$$

Similarly, the blocking probability, P_B and MRT of the proposed system can be evaluated as follow:

$$P_B = \sum_{i=0}^{K} P_{B,i} \sum_{j=0}^{1} \pi_{i,j}^{A} \tag{25}$$

$$MRT = \sum_{i=0}^{K} MRT_i \sum_{j=0}^{1} \pi_{i,j}^{A} \tag{26}$$

4 Results and discussion

In this section, numerical results are presented to understand the beahviour of the system and show the affect of the availability issues for virtualized servers with dynamic resource utilization. The performance and availability models are considered separately and a MRM is employed for steady state solution. As stated before, the results obtained from the analytical model and the simulation for each analysis are presented in order to validate as well as to show accuracy of the proposed analytical model. Numerical results are presented here for performability measures of virtualized servers with dynamic resource utilization. The parameters used are mainly taken from the literature in order to be consistent [2, 4–6, 8–13, 17, 19, 20]. The mean service rate is mainly application dependent.

In Fig. 4 QoS results are presented as a function of the arrival rate for the proposed system with VM=50 and L=100 where, K=VM+L=150. The other parameters are $\mu = 0.016(tasks/sec)$, η_v=$\eta_p = 0.5/h$,ξ_v=$\xi_p = 0.001/h$ and mean arrival rate per tasks varies from 0.05 tasks per second. QoS output parameters, mean queue length and blocking probability, have been computed for both fixed resource allocation (FRA) and dynamic resource allocation (DRA) in Fig. 4(a) and 4(b), respectively in order to show efficiency of the dynamic resource allocation in the proposed system. It can be clearly seen that dynamic resource allocation gives more promising performance results compared to fixed resource allocation scheme in terms of mean queue length and blocking probability. Fig. 4 shows that as the rate of the incoming tasks increases, mean queue length and blocking probability results are also increases for both reservation schemes. However, when the virtual as well as the physical machine failures are considered, the system with dynamic resource allocation policy performs better than fixed resource allocation especially for the loaded system. This is due to the service utilization continues to increase by dynamic resource allocation. Thus, the tasks can be serviced since the service ability will change dynamically when the virtual machine failures occur. On the other hand, all virtual machines have an equal share of resources in FRA and some of the resources will be wasted due to failures. As the rate of the incoming requests increases this difference becomes less evident since the queuing capacity, K=150 becomes the main limiting factor. Hence, please note that DRA is used for the rest of the analysis since it gives better QoS output results compare to FRA when the both failures are considered.

In Figs. 5 and 6, QoS output measurements are presented as a function of mean arrival rate for the proposed model with different virtual machines and a physical machine failure rates, respectively. The mean queue length, blocking probability and mean response time results are shown in Fig. 5(a), 5(b) and 5(c), respectively with different virtual machines failures. The parameters are VM=50, K=150, $\mu = 0.016(tasks/sec)$, η_v=$\eta_p = 0.5/h$, $\xi_p = 0.001/h$ and mean arrival rate per tasks varies from 0.05 tasks per second. As clearly seen that even though the dynamic resource utilization is used, the failures of the virtual machines significantly effect the system performance. In Fig. 5 the pure perforamnce results gives best QoS output measurements

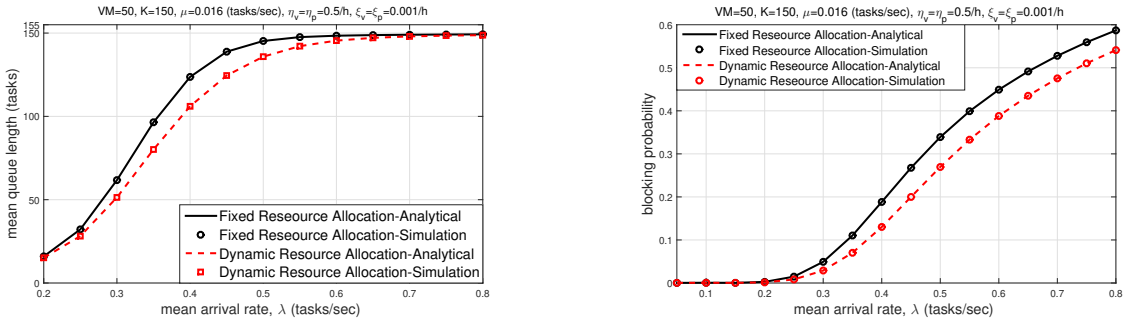

(a) (b)

Figure 4: QoS results of the proposed model with fixed resource allocation and dynamic resource allocation: (a) Mean queue length; (b) Blocking probability

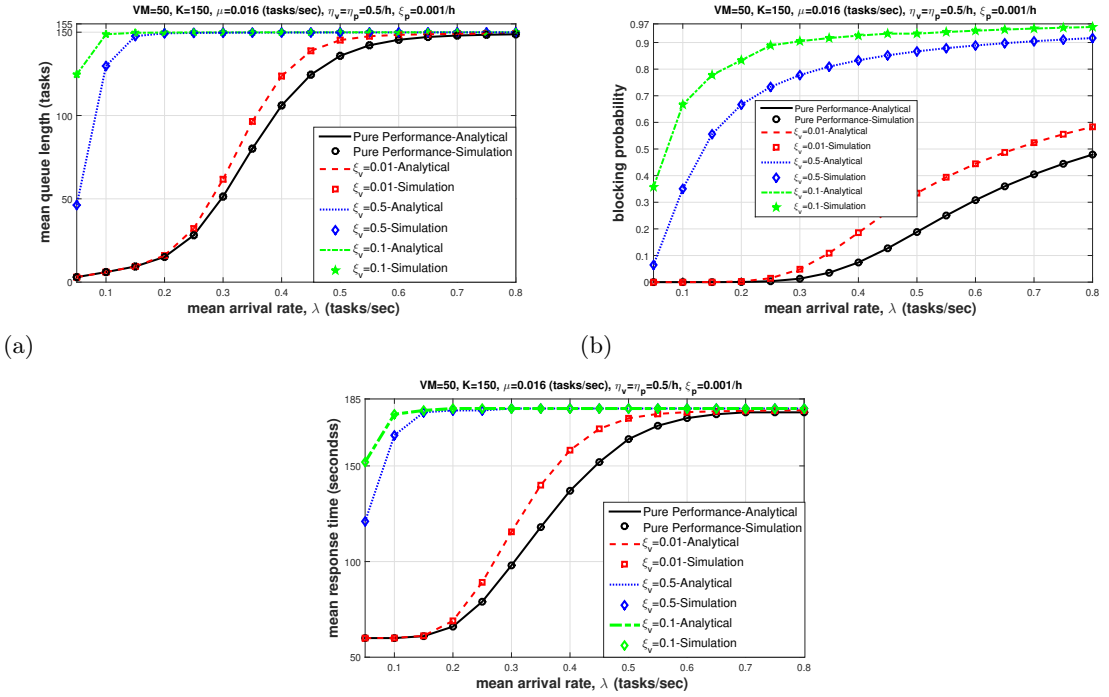

(a) (b)

(c)

Figure 5: QoS results of the proposed model with different failure rates: (a) Mean queue length; (b) Blocking probability; (c) Mean response time

for each analysis since the system never fails. However, the results show in Fig. 5 that as virtual machine failure rate increases the QoS degradation becomes more evident. For instance, for $\xi_v = 0.1/h$ and $\xi_v = 0.5/h$ the all QoS values dramatically increases. In other words, the tasks will be piled up in the system quickly as shown in Fig. 5(a) when the virtual machine failure increases. The system will not serve the tasks and the system reaches the maximum capacity quickly (i.e, K=150). In Fig. 5(b), the system started to block incoming tasks due to frequent virtual machine failures hence the blocking probability increases as the virtual machine failure increases. Similarly, the system will not able to serve the tasks due to virtual machine failures hence the mean response time of the proposed system also increases as shown in Fig. 5(c).

On the other hand, in Fig. 6 the affect of the physical machine failures are shown. Similarly

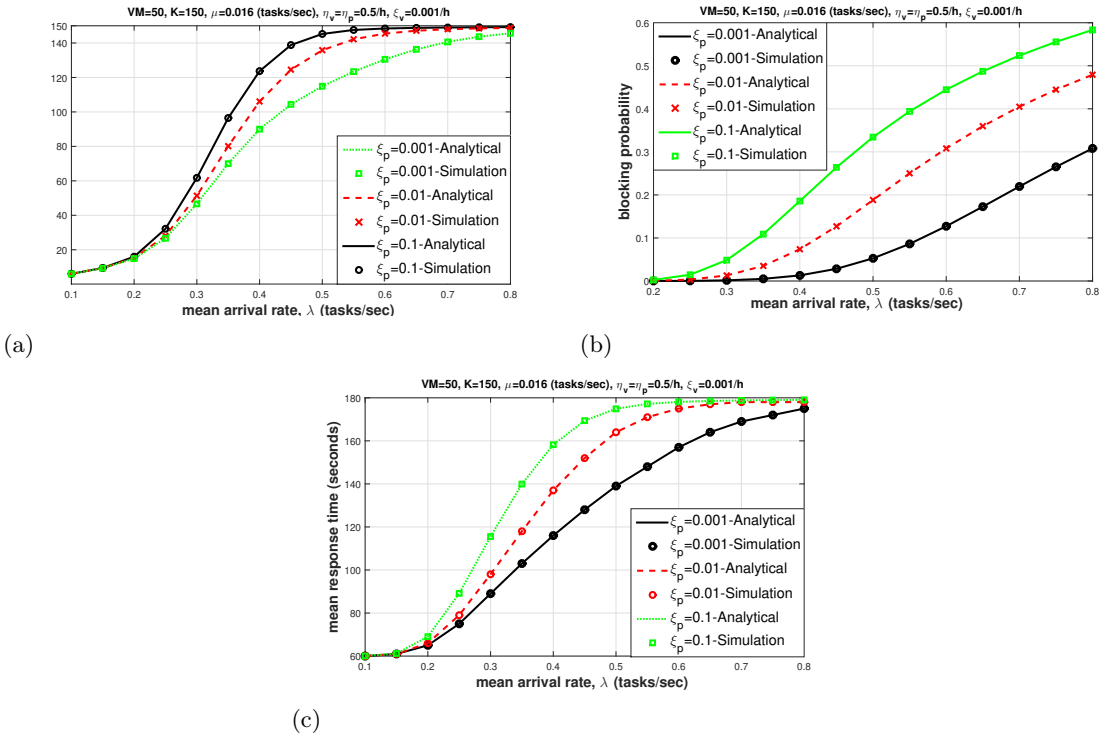

Figure 6: QoS results of the proposed model with physical machine failure rates: (a) Mean queue length; (b) Blocking probability; (c) Mean response time

to the Fig. 5, the mean queue length, the blocking probability and the mean response time results are presented in Fig. 6 with a physical machine failure and repair. The parameters used are the same as used in Fig. 5. However, in this analysis the virtual machine failures are kept constant, $\xi_v = 0.001/h$ and a physical machine failure varies from 0.001 to 0.1. As clearly seen from the Fig. 6, the system QoS degrades with a physical machine failure in terms of mean queue length, blocking probability and mean response time in Figs. 6(a), 6(b) and 6(c), respectively. When a physical machine fails all of the virtual machines do not operate, hence the failure of the physical machine limits the access to the virtual machines. As the failure rate of a physical machine increases all of the performability measures increases and the QoS is getting worst. In other words, less physical machine failure, the better the system performance gets. In the case of a physical machine fails, it will cause of blocking the incoming tasks as shown in Fig. 6(b), increase of the tasks in the queue as well as late responses from the system as shown in Fig. 6(a) and 6(c), respectively.

Therefore, it is very important to understand the failure and recovery of both VM and PM as well as dynamic resource utilization so that such practical systems could be incorporated improved in terms of QoS for such systems.

5 Conclusions

In this paper, the analytical models have been modelled for performance and availability issues together with dynamic resource utilization in order to understand and improve system QoS parameters. The behaviour of failure and recovery of the virtual machines and a physical machine are considered as an availability model and the exact spectral expansion solution approach is used to obtain steady state probabilities. The steady state probabilities of the performance model

are obtained by using the product form solution approach. Therefore, the MRM is employed to obtain performability output parameters for the proposed model. In addition, dynamic resource utilization is also employed to enhance the QoS of the proposed model.

The main focus in the analysis is given to performability output parameters such as mean queue length, blocking probability and mean response time. Numerical results obtained clearly show that, the virtual machine and especially a physical machine failures affect the system QoS significantly. The failures of a physical machine cause more significant performance degradation. It can be clearly seen from the numerical results that dynamic resource allocation gives more promising performance results compared to fixed resource allocation. The QoS results obtained from the analytical model are compared to the DES results in order to show the accuracy and effectiveness of the proposed models. Findings show that the analytical models and a MRM technique presented show good agreement with DES. The models presented in this paper are flexible and useful for modelling systems with similar behaviour and queuing considerations.

Bibliography

[1] Borangiu, T.; Trentesaux, D.; Thomas, A.; Leitao, P.; Barata, J. (2019). Digital transformation of manufacturing through cloud services and resource virtualization, *Computers in Industry*, 108, 150-162, 2019.

[2] Bi, J.; Yuan, H.; Tan, W.; Zhou, M.C.; Fan, Y.; Zhang, J.; Li, J.G. (2017). Application-Aware Dynamic Fine-Grained Resource Provisioning in a Virtualized Cloud Data Center, *IEEE Transactions on Automation Science and Engineering*, 14(2), 1172–1184, 2017.

[3] Chakka, R. (1995). *Performance and reliability modelling of computing systems using spectral expansion*, Ph.D. thesis, University of Newcastle, Upon Tyne, UK, 1995.

[4] Ever, Y.K.; Kirsal, Y.; Ever, E.; Gemikonakli, O. (2015). Analytical modelling and performability evaluation of multi channel WLANs with global failures. *International Journal of Computers Communications & Control*, 10(10), 551–566, 2015.

[5] Gemikonakli, O.; Ever, E.; Gemikonakli, E. (2009). Performance modelling of virtualized servers. *International Conference on Computer Modelling and Simulation*, 434–438, 2009.

[6] Goswami, V.; Patra, S.S.; Mund, G.B. (2012). Performance analysis of cloud with queue dependent virtual machines. *International Conference on Recent Advances in Information Technology (RAIT)*, 357–362, 2012.

[7] Iyer, R.; Illikkal, R.; Tickoo, O.; Zhao, L.; Apparao, P.; Newell, D. (2009). VM3: Measuring, modeling and managing VM shared resources. *Computer Networks*, 53(17), 2873–2887, 2009.

[8] Kim, D. S.; Hong, J. B.; Nguyen, T. A.; Machida, F.; Park, J. S.; Trivedi, K. S. (2016). Availability modeling and analysis of a virtualized system using stochastic reward nets. *In IEEE International Conference on Computer and Information Technology (CIT)*, 210–218, 2016.

[9] Kim, D. S.; Machida, F.; Trivedi, K. S. (2009). Availability modeling and analysis of a virtualized system. *In IEEE Pacific Rim International Symposium on Dependable Computing*,365–371, 2009.

[10] Kirsal, Y. (2016). Analytical modelling of a new handover algorithm for improve allocation of resources in highly mobile environments. *International Journal of Computers Communications & Control*, 11(6), 789–803, 2016.

[11] Kirsal, Y.; Paranthaman, V. V.; Mapp, G. (2018). Exploring Analytical Models for Proactive Resource Management in Highly Mobile Environments. *International Journal of Computers Communications & Control*, 13(5), 837–852, 2018.

[12] Liu, N.; Li, X.; Wang, Q. (2011). A resource and capability virtualization method for cloud manufacturing systems, *IEEE Int. Conf. on Systems, Man, and Cybernetics*, 1003–1008, 2011.

[13] Magalhaes, D.; Calheiros, R. N.; Buyya, R.; Gomes, D. G. (2015). Workload modeling for resource usage analysis and simulation in cloud computing, *Computers and Electrical Engineering*, 47, 69–81, 2015.

[14] Mitrani. I. (2001). *Queues with Breakdowns, Performability Modelling:Techniques and Tools*, Wiley, Chichester, 2001.

[15] Odun-Ayo, I.; Ajayi, O.; Falade, A. (2018). Cloud Computing and Quality of Service: Issues and Developments,*In International Multi-Conference of Engineers and Computer Scientists*, 2018.

[16] Oliveira, D.; Brinkmann, A.; Rosa, N.; Maciel, P. (2019). Performability evaluation and optimization of workflow applications in cloud environments, *Journal of Grid Computing*, 1–22, 2019.

[17] Peng, C. H.; Chong, L.S. (2010). A queueing-based model for performance management on cloud. *International Conference on Advanced Information Management and Service (IMS)*, 83–88, 2010.

[18] Sotomayor, B.; Montero, R.S.; Llorente, I.M. (2009). Virtual infrastructure management in private and hybrid clouds, *IEEE Internet Comput.*, 13(5), 14–22, 2009.

[19] Tian, W.; He, M.; Guo, W.; Huang, W.; Shi, X.; Shang, M.; Buyya, R. (2018). On minimizing total energy consumption in the scheduling of virtual machine reservations. *Journal of Network and Computer Applications*, 113, 64–74, 2018.

[20] Wu, Y.; Zhao, M. (2011). Performance modeling of virtual machine live migration. *In IEEE 4th International Conference on Cloud Computing*, 492–499, 2011.

[21] Zhang, X.; Wu, T.; Chen, M.; Wei, T.; Zhou, J.; Hu, S.; Buyya, R. (2019). Energy-aware virtual machine allocation for cloud with resource reservation. *Journal of Systems and Software*, 147, 147–161, 2019.

INTERNATIONAL JOURNAL OF COMPUTERS COMMUNICATIONS & CONTROL
ISSN 1841-9836, e-ISSN 1841-9844, 14(5), 660-671, October 2019.

Intrusion Detection for Mobile Ad Hoc Networks Based on Node Reputation

T. Lin, P. Wu, F.M. Gao, T.S. Wu

Tao Lin
1. School of Automation, Chongqing University, Chongqing 400044, China
2. Chongqing College of Electronic Engineering, Chongqing 401331, China
lintaoemail@126.com

Peng Wu*
1. School of Automation, Chongqing University, Chongqing 400044, China
2. Chongqing Chuanyi Automation Co., Ltd., Chongqing 401121, China
*Corresponding author: pwu@cqu.edu.cn

Fengmei Gao
Chongqing College of Electronic Engineering, Chongqing 401331, China
gfmemail@126.com

Tianshu Wu
College of Computer Science, Chongqing University, Chongqing 400044, China
723412117@qq.com

Abstract: The mobile ad hoc network (MANET) is more vulnerable to attacks than traditional networks, due to the high mobility of nodes, the weakness of transmission media and the absence of central node. To overcome the vulnerability, this paper mainly studies the way to detect selfish nodes in the MANET, and thus prevent network intrusion. Specifically, a data-driven reputation evaluation model was proposed to detect selfish nodes using a new reputation mechanism. The mechanism consists of a monitoring module, a reputation evaluation module, penalty module and a response module. The MANET integrated with our reputation mechanism was compared with the traditional MANET through simulation. The results show that the addition of reputation mechanism can suppress the selfish behavior of network nodes and enhance network security.
Keywords: Mobile ad hoc network (MANET), intrusion detection, reputation mechanism, node reputation.

1 Introduction

A mobile ad hoc network (MANET) is self-organized through the collaboration between numerous dynamic nodes, eliminating the need of fixed infrastructure or manual intervention [2] [3] [13]. In the MANET, multiple intelligent nodes are dynamically connected within a limited range. Each node at once serves as host and router, and can send and receive data. Thus, there is no central entity in the network.

The communication in the MANET is completed through the cooperation among network nodes. However, the cooperation failure may occur if the MANET is intruded. In this case, the

nodes will cease to route, send or receive data packets, which undermines the network performance.

Network intrusion cannot be prevented effectively by traditional security mechanisms, because such mechanisms are unable to eliminate the selfish, non-cooperative behavior of MANET nodes. This calls for new security mechanisms to protect network security. In the absence of pre-agreed trust relationship, reputation mechanism is a promising way to prevent network intrusion and non-cooperation of selfish nodes [5]. If the nodes in the network can't cooperate with each other, they can't route, send and receive data packets. It will seriously affect the performance of the network, and result in a great threat to the security of the network.

To suppress the selfish behavior of MANET nodes, this paper mainly calculates the reputation value, constructs a reputation mechanism, and applies the model to detect selfish nodes. The research results show that the proposed reputation mechanism can detect and deal with selfish behavior of nodes in time, and enhance the security performance of MANET. The most innovative point of this paper is to propose a data-driven reputation evaluation model to evaluate the reputation of nodes, and to detect selfish nodes through a new reputation mechanism.

2 Literature review

The security of ad hoc network has become a research hotspot in recent years. Many security mechanisms have been developed for ad hoc network. However, these mechanisms cannot be directly applied to the MANET. Thus, it is necessary to design a unique security mechanism that fits in with the MANET. Intrusion detection refers to identifying behaviors like the misuse of or attempt to exploit the vulnerabilities in preventive mechanism through persistent monitoring of events in the network. For the MANET, intrusion detection can be non-cooperative or cooperative [1]. Network intrusion is often accompanied by the selfish behavior of nodes. So far, the selfish behavior of MANET nodes has been deeply explored, giving birth to various solution. These solutions mainly rely on credibility, reputation or game.

Credibility-based solutions use virtual or real money to pay the network nodes for forwarding data to other nodes [11]. Camp et al. [4] designed a credibility-based system, which incentives nodes to forward data packets with virtual currency. Sun et al. [14] proposed a system that encourages mobile nodes to cooperate honestly, without needing to install tamper-proof hardware in any node. Patel et al. [10] pointed out the defects of credibility-based systems: the complete path from the source to the destination must be known in advance, i.e. adopting the source routing protocol.

Reputation-based solutions evaluate the reputation of each node according to its communication behavior. Each node uses the monitoring module to observe whether its neighbors forward packets from other nodes, and uses the response module to change or update the reputation table. The most famous reputation-based solution is the watchdog scheme [7], which detects whether a node is anomalous based on the packet forwarding of its neighbors. Pan et al. [9] presented a secure and objective credit-based incentive mechanism that encourages network nodes to transmit data packets and act more altruistically.

Game-based solutions draw on the features of the credibility- and reputation-based solutions, and take root in game theory model. Jaramillo et al. [6] modelled various interactions in wireless ad hoc networks as credibility- and reputation-based games, and analyzed the forwarding behavior of selfish nodes. Tang et al. [15] designed a self-learning repetitive game framework, in which each distributed node obeys research cooperation and development protocols. Umar et al. [16] created a coalition game-based method, in which the boundary nodes help the backbone nodes in the network to transmit information. Subramaniyan et al. [12] put forward a new

game theory solution to detect selfish nodes, and thus realized secure transmission of data in the network with a low cost and minimal idle time.

3 Data-driven reputation evaluation model

The distributed control structure is very suitable for the MANET. There are two types of distributed control structures, namely, fully distributed control structure (plane structure) and hierarchical distributed control structure (hierarchical structure) [8]. The plane structure and hierarchical structures of the MANET are shown in Figures 1 and 2, respectively.

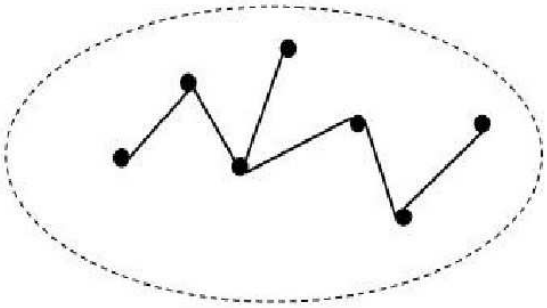

Figure 1: Plane structure of the MANET

In the plane structure, the network is rather simple and each node has equal status. This structure has high robustness and virtually no bottleneck. The network nodes are linked up via multiple paths, laying the basis for optimal routing and load balancing. However, the plane structure should not have too many nodes. Otherwise, the control overhead will increase markedly and the routing will be easily terminated. Hence, a plane structure with relatively few nodes is safe and suitable for small-scale MANETs.

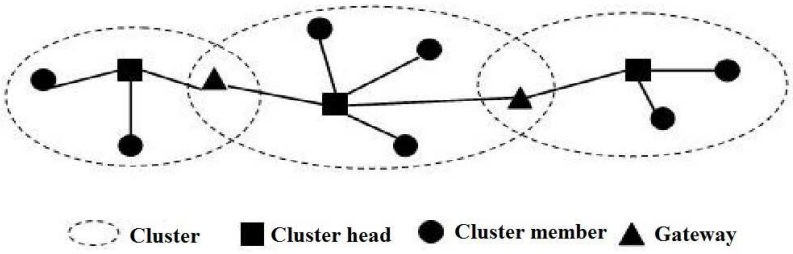

Figure 2: Hierarchical structure of the MANET

In the hierarchical structure, the MANET can be divided into multiple clusters, each of which consists of many members and one head node. The head node is mainly responsible for forwarding data between clusters, and can be set in advance or selected by algorithm. Unlike the head node, the member nodes do not need to save or update routing information, and thus enjoy high extensibility. Since the head node can be selected at any time, the hierarchical structure boasts a strong ability against destruction. Therefore, the hierarchical structure is appropriate for large-scale MANETs.

The special structure of the MANET makes the network vulnerable to multiple attacks. The attacks may come from the inside or outside of the network. The internal attacks may

occur when malicious network nodes attack the routing information or selfish nodes refuse to participate in routing. If the MANET is attacked by selfish nodes, the attacking nodes should be identified and disposed of rapidly, such as to protect network security and prevent outage.

As mentioned before, each node in the MANET has two roles: host and router. Due to the resource constraints, a MANET node may commit selfish behaviors to maximize its own interests. For example, the selfish node may refuse to participate in routing or forward data to other nodes. The selfish behaviors pose a serious threat to network performance.

The reputation mechanism can effectively suppress the selfish behavior of MANET nodes. To detect network intrusions, the reputation mechanism requires accurate evaluation of the reputation of network nodes. In this paper, a data-driven reputation evaluation model is proposed to compute, share, judge and update the reputation of each node.

In this model, when a normal node is requested to communicate with other nodes, it will firstly determine if the node requesting communication is trustworthy, and then choose a neighbor with high reputation value for routing communication, while updating its reputation table according to the situation of network communication; when a selfish node is requested to communicate with other nodes, it will forward data selectively without evaluate the reputation of the requester, which seriously undermines the network performance. Figure 3 explains the basic flow of communication two nodes in the proposed model.

In this paper, the calculation of node reputation is data-driven, i.e. the data were collected and processed, and updated iteratively for reputation calculation. In each iteration, the reputation value of a node was computed based on the real-time data being collected and classified. After time t, the node reputation was re-evaluated based on the reputation value in the previous iteration.

Suppose S is the source node of the communication request and D is the destination node of the communication request. If D is a normal node, node D calculates the reputation of S node according to the reputation evaluation process shown in Figure 3, and determines whether to communicate with it based on the S reputation value.

The features of ad hoc network determine that it takes more energy for a node to transmit data packets than to transmit routing packets. Thus, the reputation value of a node was calculated considering the number of data packets transmitted by the node. The classified data were computed directly to yield the reputation value of a node forwarding data packets (h_1), that of a node forwarding routing packets (r_1), that of a node receiving data packets (h_2) and that of a node receiving routing packets from other nodes (r_2). The four reputation values can be calculated by:

$$h_1 = \frac{N_{Tdata-others}}{N_{Tdata-self} + N_{Tdata-others}} \tag{1}$$

$$r_1 = \frac{N_{Tctrl-others}}{N_{Tctrl-self} + N_{Tctrl-others}} \tag{2}$$

$$h_2 = \frac{N_{Rdata-others}}{N_{Rdata-self} + N_{Rdata-others}} \tag{3}$$

$$r_2 = \frac{N_{Rctrl-others}}{N_{Rctrl-self} + N_{Rctrl-others}} \tag{4}$$

where $N_{Tdata-self}$ and $N_{Tdata-others}$ are the total number of packets generated by a node forwarding itself and forwarding other nodes, respectively; $N_{Tctrl-self}$ and $N_{Tctrl-others}$ are the total number of routing packets generated by a node forwarding itself and forwarding other nodes, respectively; $N_{Rdata-self}$ and $N_{Rdata-others}$ are the total number of packets a node receives from

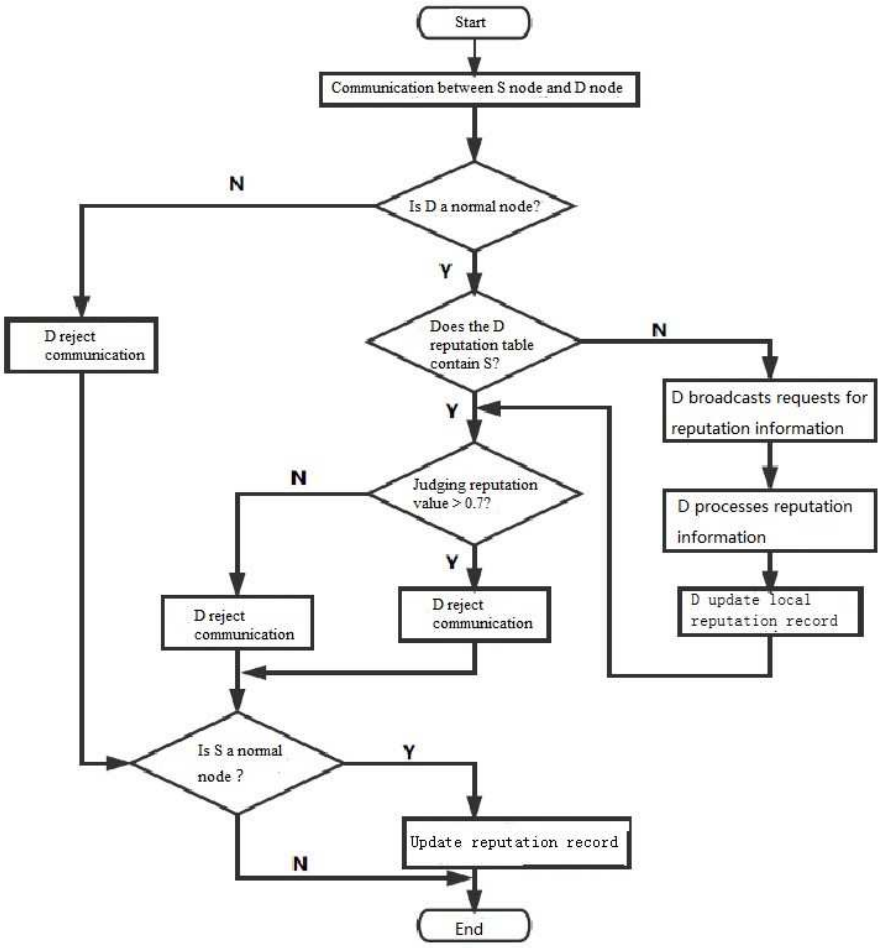

Figure 3: Basic flow of communication between two nodes

itself and from other nodes, respectively; $N_{Rctrl-self}$ and $N_{Rctrl-others}$ are the total number of routing packets a node receives from itself and from other nodes, respectively;

To calculate the reputation value of a node sending and receiving data packets to or from other nodes, h_1 and h_2 were added up to get the reputation value of the node sending and receiving data packets to or from monitored nodes. Similarly, r_1 and r_2 were added up to get the reputation value of the node sending and receiving routing packets to or from monitored nodes. The two reputation values can be defined as:

$$h_{data} = h_1 + h_2 \tag{5}$$

$$r_{control} = r_1 + r_2 \tag{6}$$

The direct reputation value of a node depends on the number of packets and the number of routing packets sent and received to or from other nodes.

Since an ad hoc network node consumes more energy to transmit data packets than to transmit routing packets, the weight factor ρ was introduced:

$$\rho = \frac{N_{Tdata} + N_{Rdata}}{N_{Tdata} + N_{Tctrl} + N_{Rdata} + N_{Rctrl}} \tag{7}$$

where N_{Tdata} and N_{Tctrl} are the total number of packets and routing packets forwarded by the node, respectively; N_{Rdata} and N_{Rctrl} are the total number of packets and routing packets received by the node, respectively. Then, the direct reputation value R_T of the node can be computed by:

$$R_T = \begin{cases} (1-\rho) \times h_{data} + \rho \times r_{control}, & 0 < \rho < 0.5 \\ \rho \times h_{data} + (1-\rho) \times r_{control}, & \rho \geq 0.5 \end{cases} \tag{8}$$

Let R_0 be the default reputation value of all network nodes, that is, the direct reputation value of each network node at time t. For a new node entering the network or each node at the start of network activity, the total direct reputation value of the node equals the default reputation value, i.e. $R_T = R_0$. After time t, the node can compute the reputation values of its neighboring by monitoring their communication behaviors. The new reputation value R_1, which equals R_T, can be computed by:

$$R_1 = \vartheta R_0 + (1-\vartheta) R_{p1} \tag{9}$$

where $\vartheta \in [0,1]$; R_{p1} is the reputation value of neighbors at time t. With the growing amount of information about node activity, the direct reputation value of the node will be updated periodically at a specific time. After time $t+1$, the new reputation value R_2 can be obtained by:

$$R_2 = \vartheta R_1 + (1-\vartheta) R_{p2} \tag{10}$$

The direct reputation value derived from the latest monitoring results can be defined as:

$$R_n = \vartheta^n R_0 + \vartheta^{n-1}(1-\vartheta) R_{p1} + \vartheta^{n-2}(1-\vartheta) R_{p2} + \cdots + \vartheta^{n-i}(1-\vartheta) R_{pi} \tag{11}$$

where n is a positive integer indicating the number of iterations.

This formula lays the basis for node reputation calculation in the MANET. In our model, each node stores the reputation values of other nodes in the local reputation table. The values recorded in the table are known as the local reputation values.

4 MANET intrusion detection based on node reputation

Based on the above reputation evaluation model, a novel reputation mechanism was developed to detect selfish nodes in the MANET and thus identify network intrusions. A penalty module and a response module were introduced to deal with abnormal nodes, and improve the evaluation of reputation values. The penalty module mainly compares the evaluated reputation values against the penalty rules, while the response module executes commands and deals with selfish nodes according to the message from penalty module and reputation evaluation. The workflow of the reputation mechanism after the addition of the two modules is described in Figure 4.

In the MANET, all the nodes are of equal status. There is no reliable third-party authentication authority, or preset trust relationship between the nodes. Therefore, the reputation value of a node can only be evaluated based on its communication status in the network. In our reputation mechanism, the reputation evaluation module is mainly composed of four processes: reputation calculation, sharing, judgment and updating. As shown in Figure 5, the module firstly processes data by data-driven method, then identifies the selfish network nodes, and finally submits the results to the penalty module.

The reputation evaluation module stores the evaluated reputation value in the reputation table, and regularly transmits the latest table to the penalty module. Next, the penalty module will process the message from the reputation evaluation module, get the corresponding evaluation results, and evaluate the trustworthiness of the node.

The reputation evaluation module also stores the total direct reputation value in the reputation table and updates the table regularly. If the target node forwards data and routing information to other nodes, its total reputation value will increase. Once a node is marked as an intrusive node, it will be blacklisted at once, and its information will be sent to the response module.

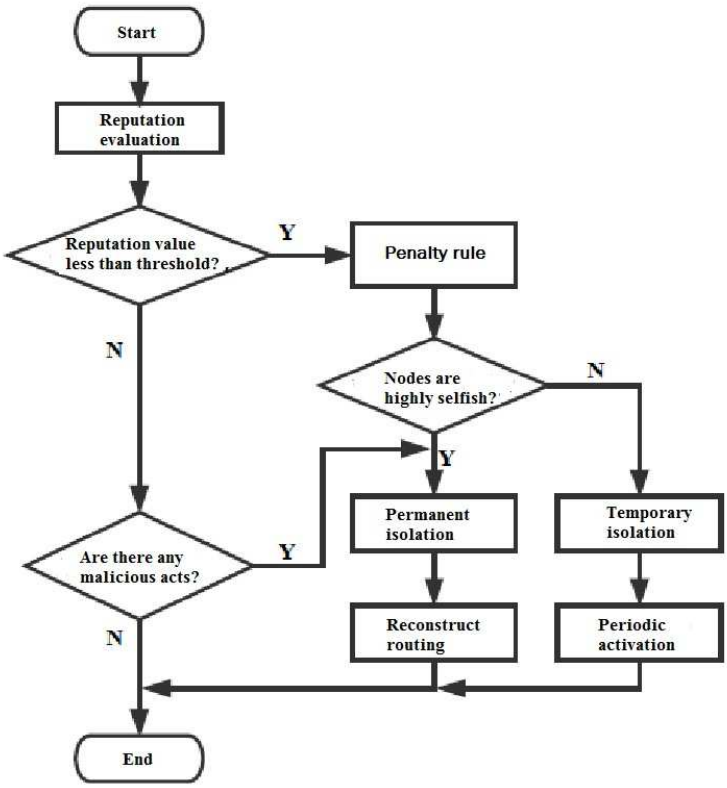

Figure 4: Workflow of the reputation mechanism after the addition of the two modules

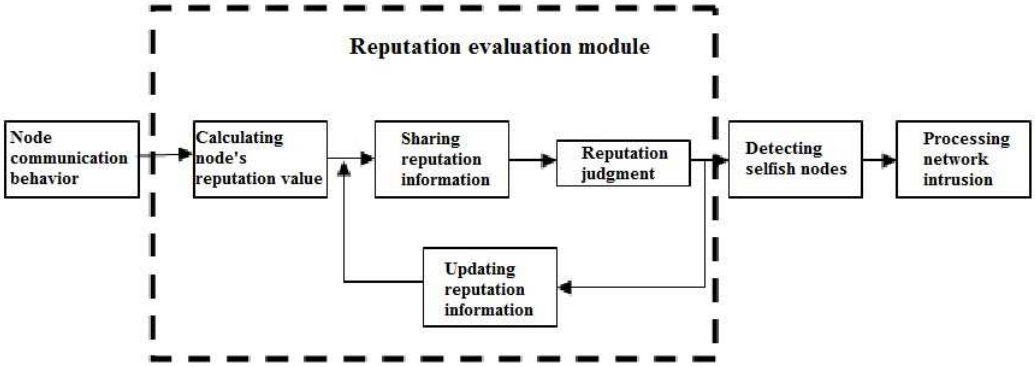

Figure 5: Workflow of reputation evaluation module

The response module mainly takes actions according to the messages from reputation eval-

uation module and penalty module. Once a node is judged as selfish, it will be added into the observation table of the penalty module, and then be processed by the response module. In general, the selfish nodes can be permanently isolated from the network or temporarily banned from the network. In this paper, it is proposed that a selfish node can join the network again but with limited times, that is, the node cannot enter the network beyond the set limit on the number of entries. The workflow of the response module is given in Figure 6 below.

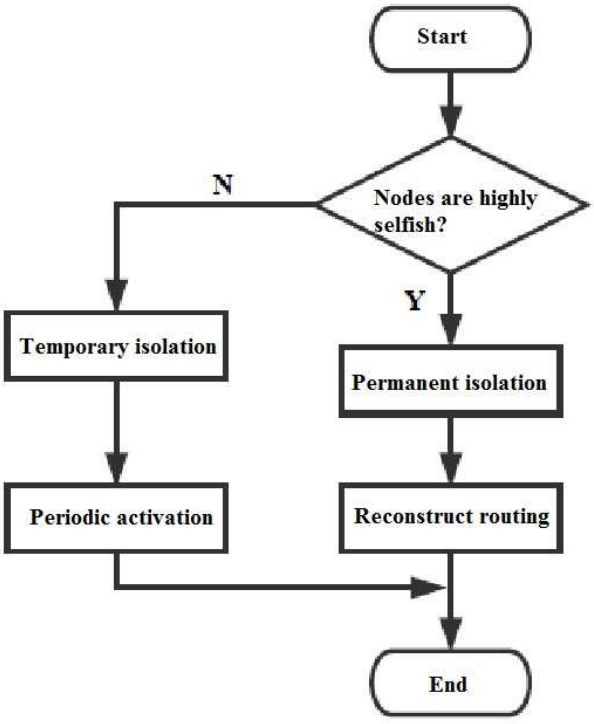

Figure 6: Workflow of the response module

5 Simulation experiment and performance analysis

To validate our reputation mechanism in Linux, the MANET was simulated on Network Simulator 2 (NS2), taking the dynamic source routing (DSR) as the routing protocol. The DSR protocol was simulated with and without reputation mechanism, both in the absence of selfish nodes and the presence of different number of selfish nodes. The parameters of the simulation environment are listed in Table 1 below.

As shown in Figure 7, the traditional DSR network delivered packets basically at the same rate with the DSR network integrated with reputation mechanism, in the absence of selfish nodes. This means the addition of the reputation mechanism has little effect on the delivery rate of packets.

As shown in Figure 8, with the growth in the number of selfish nodes, the packet delivery rates of both networks exhibited a gradual decline. The decline was steeper in the traditional DSR network, while the packet delivery rate in the network with reputation mechanism remained above 0.6. The possible reasons are as follows. In the traditional network, the selfish nodes only receive packets but do not forward packets, pushing up the resource consumption of normal nodes. Meanwhile, in the network with reputation mechanism, the selfish nodes are effectively

Table 1: Parameters of the simulation environment

Parameters	**Value**
Simulation area	900m*900m
Number of nodes	50
Propagation model	Two-Ray Ground Reflection
Packet size	512 bytes
MAC type	802.11
Signal coverage radius	300m
Maximum number of connections	20
ϑ	0.15

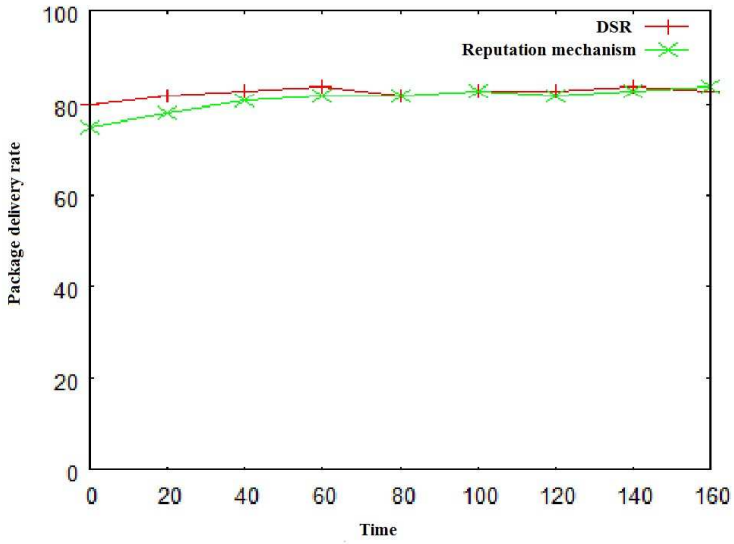

Figure 7: Relationship between packet delivery rate and time

removed and isolated.

As shown in Figure 9, the routing overheads in both networks were gradually falling, with the growth in the number in selfish nodes. The decline of routing overheads can be attributed to the following facts: With the elapse of time, the network nodes will establish routing paths and store routing information with each other, thus reducing the routing overhead. Of course, the network with reputation mechanism had a slightly lower routing overhead than the traditional network.

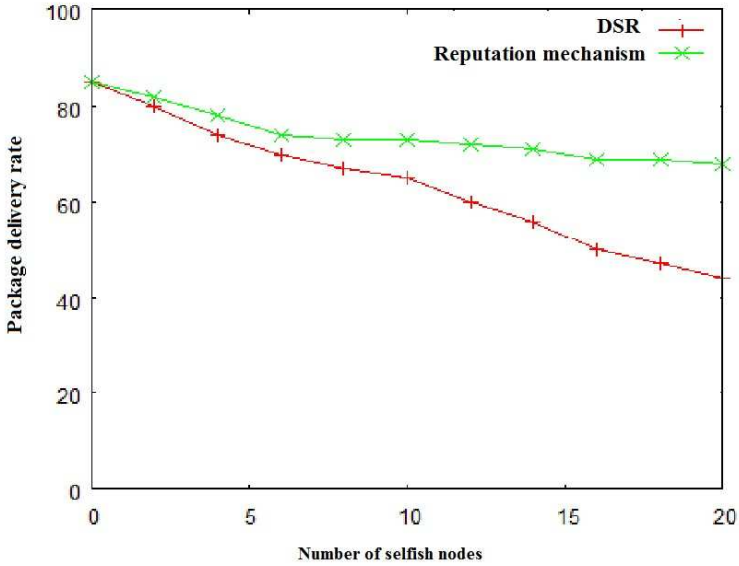

Figure 8: Relationship between packet delivery rate and the number of selfish nodes

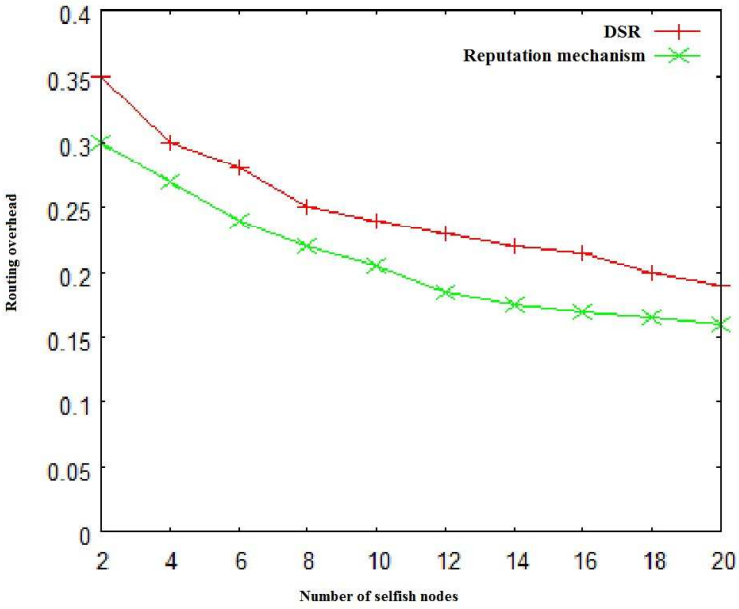

Figure 9: Relationship between routing overhead and the number of selfish nodes

6 Conclusion

This paper mainly studies the way to detect selfish nodes in the MANET, and thus prevent network intrusion. Specifically, a data-driven reputation evaluation model was proposed to detect selfish nodes. Then, based on the proposed model, a new reputation mechanism is proposed. The mechanism consists of a monitoring module, a reputation evaluation module, penalty module and a response module. The MANET integrated with our reputation mechanism was compared with the traditional MANET through simulation. The results show that the addition of reputation mechanism can suppress the selfish behavior of network nodes and enhance network security.

Funding

This work was supported by the Scientific and Technological Research Program of Chongqing Municipal Education Commission (Grant Numbers are KJ1602901 and KJQN201803102 respectively), Chongqing College of Electronic Engineering Scientific Research Project (Grant Number is XJZK201809) and Xinxiang Medical University Education and Teaching Reform Research Project (Grant Number is 2017-XYJG-41).

Author contributions. Conflict of interest

The authors contributed equally to this work. The authors declare no conflict of interest.

Bibliography

[1] Almousa, Z.; Nasir Q. (2015). cl-CIDPS: A cloud computing based cooperative intrusion detection and prevention system framework, *Communications in Computer & Information Science*, 523, 181-194, 2015.

[2] Al-Sultan, S.; Al-Doori, M. M.; Al-Bayatti, A. H.; Zedan, H. (2014). A comprehensive survey on vehicular Ad Hoc network, *Journal of Network & Computer Applications*, 37(1), 380-392, 2014.

[3] Azees, M.; Jegatha, D. L.; Vijayakumar, P. (2016). A comprehensive survey on security services in vehicular ad-hoc networks (VANETs), *IET Intelligent Transport Systems*, 10(6), 379-388, 2016.

[4] Camp, T.; Boleng, J.; Davies, V. (2002). A survey of mobility models for ad hoc network research, *Wireless Communications and Mobile Computing*, 2(5), 483-502, 2002.

[5] He, S.; Chen, J.; Li, X.; Shen, X. M.; Sun, Y. X. (2012). Leveraging prediction to improve the coverage of wireless sensor networks, *IEEE Transactions on Parallel & Distributed Systems*, 23(4), 701-712, 2012.

[6] Jaramillo, J. J.; Srikant, R. (2010). A game theory based reputation mechanism to incentivize cooperation in wireless ad hoc networks, *Ad Hoc Networks*, 8(4), 416-429, 2010.

[7] Moati, N.; Otrok, H.; Mourad, A.; Robert, J. M. (2014). Reputation-based cooperative detection model of selfish nodes in cluster-based QoS-OLSR protocol, *Wireless Personal Communications*, 75(3), 1747-1768, 2014.

[8] Moussaoui, A.; Semchedine, F.; Boukerram, A. (2014). A link-state QoS routing protocol based on link stability for mobile Ad Hoc networks, *Journal of Network & Computer Applications*, 39(1), 117-125, 2014.

[9] Pan, D.; Zhang, H.; Chen, W. J.; Lu, K. (2015). Transmission of multimedia contents in opportunistic networks with social selfish nodes, *Multimedia Systems*, 21(3), 277-288, 2015.

[10] Patel, N.; Srivastava, S. (2012). Packet forwarding strategies for cooperation enforcement in mobile Ad Hoc wireless networks, *Lecture Notes in Computer Science*, 7154, 200-211, 2012.

[11] Rodriguez-Mayol, A.; Gozalvez, J. (2014). Reputation based selfishness prevention techniques for mobile ad-hoc networks, *Telecommunication Systems*, 57(2), 181-195, 2014.

[12] Subramaniyan, S.; Johnson, W.; Subramaniyan, K. (2014). A distributed framework for detecting selfish nodes in MANET using record- and trust-based detection (RTBD) technique, *EURASIP Journal on Wireless Communications and Networking*, (1), 205-221, 2014.

[13] Sun, G.; Bin, S. (2017). Router-level internet topology evolution model based on multi-subnet composited complex network model, *Journal of Internet Technology*, 18(6), 1275-1283, 2017.

[14] Sun, J.; Zhang, C.; Zhang, Y.; Fang, Y. G. (2011). SAT: A security architecture achieving anonymity and traceability in wireless mesh networks, *IEEE Transactions on Dependable and Secure Computing*, 8(2), 295-307, 2011.

[15] Tang, C.B.; Li, X.; Wang, Z. (2017). Cooperation and distributed optimization for the unreliable wireless game with indirect reciprocity, *Science China (Information Sciences)*, (11), 129-145, 2017.

[16] Umar, R.; Mesbah, W. (2018). Throughput-efficient coalition formation of selfish/altruistic nodes in ad hoc networks: A hedonic game approach, *Telecommunication Systems*, 67(1), 1-17, 2018.

INTERNATIONAL JOURNAL OF COMPUTERS COMMUNICATIONS & CONTROL
ISSN 1841-9836, e-ISSN 1841-9844, 14(5), 672-691, October 2019.

Risk Evaluation in Failure Mode and Effects Analysis Based on D Numbers Theory

B. Liu, Y. Deng

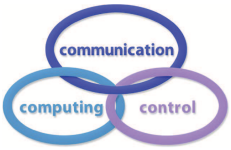

Baoyu Liu
1. Institute of Fundamental and Frontier Science
University of Electronic Science and Technology of China
Chengdu, 610054, China
2. School of Data and Computer Science
Sun Yat-sen University, China
Guangzhou, China
Baoyu.L@hotmail.com

Yong Deng*
Institute of Fundamental and Frontier Science
University of Electronic Science and Technology of China
Chengdu, 610054, China
*Corresponding author: prof.deng@hotmail.com

Abstract:
Failure mode and effects analysis (FMEA) is a useful technology for identifying the potential faults or errors in system, and simultaneously preventing them from occurring. In FMEA, risk evaluation is a vital procedure. Many methods are proposed to address this issue but they have some deficiencies, such as the complex calculation and two adjacent evaluation ratings being considered to be mutually exclusive. Aiming at these problems, in this paper, A novel method to risk evaluation based on D numbers theory is proposed. In the proposed method, for one thing, the assessments of each failure mode are aggregated through D numbers theory. For another, the combination usage of risk priority number (RPN) and the risk coefficient newly defined not only achieve less computation complexity compared with other methods, but also overcome the shortcomings of classical RPN. Furthermore, a numerical example is illustrated to demonstrate the effectiveness and superiority of the proposed method.

Keywords: failure mode and effects analysis, Dempster-Shafer evidence theory, D numbers, risk evaluation, aggregate assessment.

1 Introduction

Failure mode and effects analysis (FMEA) is an efficient technology for identifying potential faults, problems, risk, and errors from the system, procedure, and service. It improves the reliability by preventing these faults, problems, risks, and errors from occurring. Risk evaluation is a pivotal procedure in FMEA. Nowadays, FMEA is developed so fast that it is extensively applied in many fields, such as medical care [3,29,32,49,60], society [51], environmental protection [1, 8], financial service [65], industry [2, 24, 69, 78], and so on.

A traditional method for risk evaluation in FMEA is the classical risk priority number (RPN), which is obtained by multiplying the grades of the occurrence assessment, severity assessment, and detection assessment. Therefore, how to aggregate the assessment information of

these three risk factors is a significant issue, especially when it comes to the information with uncertainty. Focusing on this problem, many math models such as fuzzy sets [14, 16, 17, 79], R numbers [53], D numbers [20], Z numbers [21,26,27,39,76] and evidence theory [10,55], have been applied to the real applications [37, 50]. In [28], Kim et al. present a general model to explain the functional relationship among the three factors, and use the model to discuss the unique role of each factor for comparing the risk of different failure modes. In [77], a new method to risk evaluation based on Dempster-Shafer evidence theory is proposed. Some other evidential FEMA are presented recently [5].

Nevertheless, although classical RPN is easy to use because of its succinct form, it is still criticized for its weaknesses. For example, the experts usually give the assessment with uncertainty or fuzzy information, but classical RPN is not appropriated to treat the fuzzy assessment. Furthermore, different combination of risk factors might acquire the same RPN, however, the potential risk might be totally different so that they might have different priorities. With the aim of overcoming these weaknesses, many methods, such as Chin's method [9], are proposed. However, existing methods almost is not only too complex to calculation, but also do not take the non-exclusiveness between two adjacent rankings into account. Actually, because of the subjectivity of the experts, two adjacent estimation scales are supposed to be not exclusive mutually. In order to solve the problems, a novel method based on D number theory [13] is proposed in this paper. On the one hand, the assessments for each failure mode are aggregated through constructing and combining D numbers because two propositions are allowed to be non-exclusive in D numbers theory. On the other hand, RPN is applied in the proposed method so as to reduce the computation complexity, simultaneously, novel compute mode to RPN and risk coefficient present in this paper is capable to get rid of the weaknesses of the classical RPN. Last but not the least, an illustrative example is used to show the effectiveness and superiority of the proposed method.

The remainder of this paper is organized as follows. Key concepts and previous theories are reviewed in short in Section 2. In Section 3, A novel risk evaluation in failure mode and effects analysis based on D numbers theory is proposed. To demonstrate the effectiveness and superiority of the proposed method, a numerical example is illustrated in Section 4. Last but not the least, A brief conclusion is drawn in Section 5.

2 Preliminaries

2.1 Dempster-Shafer evidence theory

The real application is inevitable to deal with uncertainty [4, 6, 45–47]. Dempster-Shafer evidence theory (D-S theory) [10, 55], is a significant theory to handle uncertainty information [11]. Compared with Bayesian theory, it needs weaker conditions so that it is often deemed as an extension of the Bayesian theory. D-S theory is widely applicated in many fields, such as decision making [6,22,30,44,71], pattern recognition [40,41,43,73], evidential reasoning [15,42,74,83–85], risk and reliability [52, 54], information fusion [59, 61, 75], uncertainty modelling [19, 25, 58] and conflict management [36, 68, 81].

Definition 1. Let $\Theta = \{H_1,\ H_2,\ \cdots,\ H_N\}$ be a finite nonempty set, which consist of N mutually exclusive elements. Let $P(\Theta)$ be the power set of Θ, which is composed of 2^N elements. The basic probability assignment (BPA) function is defined as a mapping of the power set $P(\Theta)$ to a number between 0 to 1, that is $m : P(\Theta) \to [0, 1]$, and which satisfies the following conditions:

$$m(\emptyset) = 0; \tag{1}$$

$$\sum_{A\in P(\Theta)} m\left(A\right)=1. \tag{2}$$

The mass m(A) represents how strongly the evidence supports to A.

Definition 2. Let $m_1,\ m_2$ be two BPAs defined on the frame of discernment Θ. The Dempster's combination rule, denoted by $m=m_1\bigoplus m_2$, is defined as follows:

$$m\left(A\right)=\begin{cases}\frac{1}{k-1}\sum_{B\cap C=A} m_1(B)m_2(C), & A\neq\emptyset\\ 0, & A=\emptyset\end{cases} \tag{3}$$

with

$$K=\sum_{B\cap C=\emptyset} m_1(B)m_2(C) \tag{4}$$

where K is a normalization constant which reflects the conflict of two bodies of evidence.

Actually, $0\leq K\leq 1$. $K=0$ shows the absence of conflict between two bodies of evidence. While $K=1$ shows complete conflict between m_1 and m_2. Besides, when $K=1$, the Dempster's combination rule is not any longer applicable, a possible explanation is open world assumption [32, 33]. In order to make decision in terms of the BPA, a method called pignistic probability transformation is present in [57], which derive a distribution of probabilities from the BPA. The pignistic probability transformation function is defined as follows:

Definition 3. Let m be a BPA on the frame of discernment Θ, a pignistic probability transformation function $BetP_m:\ \Theta\longrightarrow[0,1]$ associated to m is defined by

$$BetP_m\left(x\right)=\sum_{x\in A,\ A\in\Theta}\frac{1}{|A|}\frac{m(A)}{1-m(\emptyset)} \tag{5}$$

where $m\left(\emptyset\right)\neq 1$ and $|A|$ is the cardinality of proposition A.

2.2 Fuzzy set theory

Fuzzy sets were proposed independently by Zadeh [79] in 1965 as an extension of the classical notion of set. Fuzzy set theory is widely applied in many fields [23, 33, 72]. It reflects the stay of the object and its fuzzy concept as a fuzzy set. Then, it sets up the appropriate membership functions through fuzzy set about operation and transform, and analyzes the fuzzy object based on the fuzzy mathematics. In the objective world, there are many fuzzy phenomena. For example, when evaluating a person's appearance, people usually use linguistic variables whose values are represented by words or sentences in a natural or artificial language, such as "very pretty", "pretty", "general", "ugly", and "very ugly".

Definition 4. Denote L as the universe of discourse, a fuzzy set A is described by a membership function μ_A satisfying

$$\mu_A:\ L\longrightarrow[0,1]$$

where $\mu_A(x)$ is called the membership degree of $x\in L$ belonging to fuzzy set A.

For $L=\{x_1,\ \ldots,x_i,\ \ldots,\ x_n\}$, the fuzzy set (A,μ_A) is represent by

$$\frac{\mu_A\left(x_1\right)}{x_1},\ldots,\frac{\mu_A\left(x_i\right)}{x_i},\ \ldots,\frac{\mu_A\left(x_n\right)}{x_n}.$$

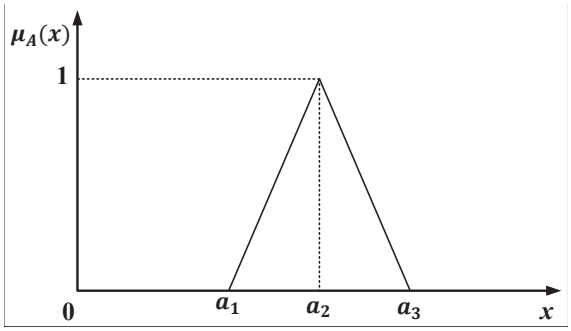

Figure 1: Graphical presentation of the triangular fuzzy number

It is obvious that a fuzzy set is characterized entirely by its membership function. When $\mu_A(x)$ get value from $\{0, 1\}$, fuzzy set A degrade into a classical set. A is a fuzzy subset of the real number R, and its membership function satisfies

$$\mu_A(x) : R \longrightarrow [0, 1]$$

where x is real number and there exists an element x_0 such that $\mu_A = 1$. Triangular fuzzy numbers are the most extensively applied fuzzy numbers. A triangular fuzzy number is usually expressed as $A = (a_1, a_2, a_3)$, as graphically shown in Figure 1, which has the following membership function

$$\mu_A(x) = \begin{cases} 0, & x < a_1 \\ \frac{x-a_1}{a_2-a_1}, & a1 \le x \le a2 \\ \frac{a3-x}{a3-a2}, & a_2 \le x \le a_3 \\ 0, & x > a_3 \end{cases} \tag{6}$$

where $a_1 < a_2 < a_3$.

In practice, fuzzy numbers are bound up with linguistic variables to describe the fuzzy evolution to objects.

2.3 Risk priority number

The real systems are too complicated to be modelled. Risk priority number (RPN) is a traditional and typical method to model and evaluate risk in FMEA. RPN is calculated by multiplying the grades of occurrence assessment (O), severity assessment (S), and detection assessment (D). That is

$$\text{RPN} = \text{O} \times \text{S} \times \text{D} \tag{7}$$

where O stands for the probability of occurrence of failure mode, S refers to the severity of failure mode and D refers to the probability of failure being detected. The three risk factors are evaluated by FMEA experts using a 1 to 10 numeric scale. Besides, occurrence assessment is expressed in Table 1. The larger RPN is, the more important degree it is supposed to be assigned, referring to the failure mode should be more priority to be corrected. Although this method is easy to use because of its sententious form, traditional RPN is still criticized for its weaknesses. For example, traditional RPN does not take the weights of three risk factors into consideration. Besides, different combination of risk factors might acquire the same RPN, however, the potential risk might be totally different so that they might have different priorities.

2.4 D numbers

D number, is a useful tool to model uncertain information, which overcomes the shortcomings of Dempster-Sharfer theory [20]. Nowadays, D number is widely used in many fields such as decision making [7, 19, 31], risk assessment [18, 29, 35, 67], reliability analysis [70, 80], data fusion [8, 62, 66]. It is defined as follows:

Definition 5. Let Ω be a finite nonempty set, D number is a mapping $D:\ \Omega \longrightarrow [0,1]$, such that

$$\sum_{B\subseteq\Omega} D(B) \leq 1 \text{ and } D(\emptyset) = 0 \tag{8}$$

where $\emptyset$ is the empty set and B is a subset of Ω.

If $D(B) = 1$, the information is regarded to be complete while $D(B) < 1$, it is considered to be incomplete. Most importantly, different from D-S theory, D number does not request the elements of set Ω to be mutually exclusive. In order to express the non-exclusiveness in Ω, a fuzzy membership function is used to measure the exclusive/non-exclusive degree [82].

Definition 6. Let A_i and A_j be two non-empty elements in 2^Ω, the non-exclusive degree between A_i and A_j is characterized by a fuzzy membership function $u_{\neg E}$ as follows:

$$u_{\neg E} : 2^\Omega \times 2^\Omega \longrightarrow [0,1] \tag{9}$$

with

$$u_{\neg E}(A_i, A_j) = \begin{cases} 1, & A_i \cap A_j \neq \emptyset \\ p, & p \in [0,1],\ A_i \cap A_j = \emptyset \end{cases} \tag{10}$$

besides,

$$u_{\neg E}(A_i, A_j) = \max_{x\in A_i,\ y\in A_j} \{u_{\neg E}(x,y)\} \tag{11}$$

Let u_E be the exclusive degree between A_i and A_j, then $u_E = 1 - u_{\neg E}$.

An illustrative example is given as follows to express the calculation of the non-exclusive degree.

Table 1: Assessment rankings for occurrence in FMEA

Ranking	Probability of Occurrence	Possible Failure Rate
10	Extremely high: failure almost inevitable	$\geq 1/2$
9	Very high	$1/3$
8	Repeated failures	$1/8$
7	High	$1/20$
6	Moderately high	$1/80$
5	Moderate	$1/400$
4	Relatively low	$1/2000$
3	Low	$1/15000$
2	Remote	$1/150000$
1	Nearly impossible	$\leq 1/150000$

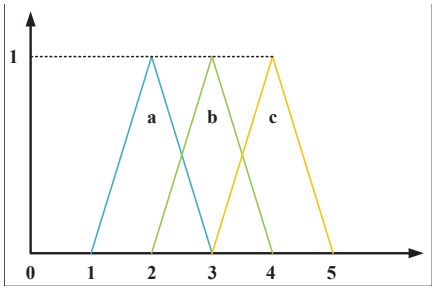

Figure 2: Graphically presentation of fuzzy variables in Table 2

Example 7. *Suppose there is a non-empty set* $\Omega = \{a, b, c\}$*, where* a, b, c *are three fuzzy variables represented by triangular fuzzy numbers given in Table 2 and shown in Figure 2. The non-exclusiveness degree can be calculated as follows [12]:*

$$u_{\neg E}(A, B) = \frac{Area_{A\cap B}}{Area_A + Area_B - Area_{A\cap B}} \tag{12}$$

where the areas of fuzzy numbers A *and* B *are characterized by* $Area_A$ *and* $Area_B$*, and the area of the overlap of* A *and* B *is* $Area_{A\cap B}$*. Thus, according to Eq.12, we have*

$$\begin{aligned}
u_{\neg E}(a, b) &= \frac{Area_{a\cap b}}{Area_a + Area_b - Area_{a\cap b}} = \frac{0.25}{1+1-0.25} \approx 0.1429 \\
u_{\neg E}(b, c) &= \frac{Area_{b\cap c}}{Area_b + Area_c - Area_{b\cap c}} = \frac{0.25}{1+1-0.25} \approx 0.1429 \\
u_{\neg E}(a, b, c) &= \max\{u_{\neg E}(a, b), u_{\neg E}(b, c)\} = \max\{0.1429, 0.1429\} = 0.1429 \\
u_{\neg E}(a, \{a, b\}) &= \max\{u_{\neg E}(a, a), u_{\neg E}(a, b)\} = \max\{1, 0.1429\} = 1
\end{aligned}$$

Similar with Dempster combination rule, the combination rule is discussed under two cases: complete information and incomplete information.

Definition 8. (complete information). Let D_1 and D_2 be two numbers over Ω with $\sum_{A\subseteq\Omega} D_1(A) = 1$ *and* $\sum_{A\subseteq\Omega} D_2(A) = 1$, the combination of D_1 and D_2, indicated by $D = D_1 \bigodot D_2$, is defined by

$$D(A) = \begin{cases} 0, & A = \emptyset \\ \frac{1}{1-K_D}\Big(\sum\limits_{B\cap C=A} u_{\neg E}(B, C)\, D_1(B)\, D_2(C) + \\ \sum\limits_{B\cup C=A, B\cap C=\emptyset} u_{\neg E}(B, C)\, D_1(B)\, D_2(C)\Big), & A \neq \emptyset \end{cases} \tag{13}$$

with

$$K_D = \sum_{B\cap C=\emptyset} (1 - u_{\neg E}(B, C))\, D_1(B)\, D_2(C) \tag{14}$$

Table 2: The fuzzy number of fuzzy variables

Fuzzy Variables	Fuzzy Numbers
a	(1, 2, 3)
b	(2, 3, 4)
c	(3, 4, 5)

It is worth mentioning that this combination rule can be degenerated to the classical Dempster's rule if $u_{\neg E} = 0$ for any $B \cap C = \emptyset$. a numerical example is used to illustrate the combination of two D numbers under the complete information situation as follows:

Example 9. *There are two D numbers over* $\Omega = \{a, b\}$*:*

$$\begin{aligned} D_1(a) &= 0.4, & D_1(b) &= 0.6 \\ D_2(a) &= 0.9, & D_2(b) &= 0.1 \end{aligned}$$

And assume $u_{\neg E}(a, b) = 0.1429$*. Thus, we have* $D\prime = D_1 \bigodot D_2$ *that*

$$\begin{aligned} K_{D\prime} &= (1 - 0.1429) \times [0.4 \times 0.1 + 0.6 \times 0.9] = 0.4971 \\ D\prime(a) &= \frac{1}{1 - 0.4971} \times 1 \times 0.4 \times 0.9 = 0.7159 \\ D\prime(b) &= \frac{1}{1 - 0.4971} \times 1 \times 0.6 \times 0.1 = 0.1193 \\ D\prime(a, b) &= \frac{1}{1 - 0.4971} \times 0.1429 \times [0.4 \times 0.1 + 0.6 \times 0.9] = 0.1648 \end{aligned}$$

Definition 10. (incomplete information). Let D_1 and D_2 be two numbers over Ω with $\sum_{A \subseteq \Omega} D_1(A) < 1$ *and* $\sum_{A \subseteq \Omega} D_2(A) < 1$, the combination of D_1 and D_2, defined by $D = D_1 \bigodot D_2$ and calculated as follows:

$$D(A) = \begin{cases} 0, & A = \emptyset \\ f(Q_1, Q_2) \frac{D_t(A)}{\sum_{B \subseteq \Omega} D_t(B)}, & A \neq \emptyset \end{cases} \tag{15}$$

with

$$D_t(A) = \sum_{B \cap C = A} u_{\neg E}(B, C) D_1(B) D_2(C) + \sum_{B \cup C = A, B \cap C = \emptyset} u_{\neg E}(B, C) D_1(B) D_2(C), \forall\ A \in \Omega$$

and

$$Q_1 = \sum_{A \subseteq \Omega} D_1(A), \quad Q_2 = \sum_{A \subseteq \Omega} D_2(A) \tag{16}$$

where $f(Q_1, Q_2)$ is a function satisfying $0 \leq f(Q_1, Q_2) \leq \max\{Q_1, Q_2\}$, $f(Q_1, Q_2) = 1$ if $Q_1 = 1$ and $Q_2 = 1$.

Next, a simple example is used to illustrate the combination process of D numbers according to Definition 10.

Example 11. *There are two D numbers over* $\Omega = \{a, b\}$*:*

$$\begin{aligned} D_1(a) &= 0.7, & D_1(b) &= 0.2 \\ D_2(a) &= 0.5, & D_2(b) &= 0.3 \end{aligned}$$

Assume $u_{\neg E}(a,b) = 0.1429$*, and let* $f(Q_1, Q_2) = Q_1 \times Q_2$*. Thus, we have* $D = D_1 \bigodot D_2$ *that*

$$\begin{aligned} f(Q_1, Q_2) &= (0.7 + 0.2) \times (0.5 + 0.3) = 0.72 \\ D_t(a) &= 0.7 \times 0.5 = 0.35 \\ D_t(b) &= 0.2 \times 0.3 = 0.06 \\ D_t(a,b) &= 0.1429 \times (0.7 \times 0.3 + 0.2 \times 0.5) \approx 0.044 \end{aligned}$$

Thus,

$$\begin{aligned} \sum_{B \subseteq \Omega} D_1(B) &= 0.35 + 0.06 + 0.044 = 0.454 \\ D(a) &= f(Q_1, Q_2) \frac{D_t(a)}{\sum\limits_{B \subseteq \Omega} D_1(B)} \approx 0.555 \\ D(b) &= f(Q_1, Q_2) \frac{D_t(b)}{\sum\limits_{B \subseteq \Omega} D_1(B)} \approx 0.095 \\ D(a,b) &= f(Q_1, Q_2) \frac{D_t(a,b)}{\sum\limits_{B \subseteq \Omega} D_1(B)} \approx 0.070 \end{aligned}$$

If there are n D numbers expressed as $D_1,\ D_2,\ \cdots,\ D_n$, whose weights are $w_1, w_2,\ \cdots,\ w_n$, satisfying $\sum_{i=1}^{n} w_i = 1$. At first, the average D number among $D_1, D_2,\ \cdots, D_n$ is defined as

$$\bar{D}(A) = \sum_{i=1}^{n} w_i D_i(A), \forall A \subseteq \Omega. \tag{17}$$

Then, the result of combination $D_1, D_2,\ \cdots, D_n$ is acquired by combining average D number $\bar{D}$ with itself $n-1$ times.

$$D = \bar{D} \bigodot \bar{D} \bigodot \cdots \bigodot \bar{D} \tag{18}$$

where $\bigodot$ is the combination rule given in Definition 8 and Definition 10.

3 Proposed method

Failure mode and analysis (FMEA) is an efficient technology to identify and remove potential faults, errors and risk from systems. In FMEA, risk evaluation is a significant procession. Traditionally, risk priority number (RPR) is used to evaluate risk, which is calculated by multiplying the grades of occurrence assessment (O), severity assessment (S), and detection assessment (D). Although classical RPN is easy to use for its concise form, it is still criticized for its weaknesses. For example, traditional RPN does not take the weights of three risk factors into consideration. Besides, different combination of risk factors might acquire the same RPN, however, the potential risk might be totally different so that they might have different priorities. So far, many methods are presented. Nevertheless, most of them not only have rather complex algorithm, but also do not consider the non-exclusiveness between two rankings in assessment.

With the aim of solving these problems, in this paper, a novel method to risk evaluation based on D numbers theory is proposed. First of all, each assessment rating is treated as a fuzzy

variable which is represented as a fuzzy number. Then, non-exclusive degree between two ratings can be calculated. Next, for each failure mode, the assessments of experts are aggregated by D numbers theory. The assessments are treated as D numbers and then are combined by using D numbers combination rule. Furthermore, RPNs are calculated for ranking the failure mode. Last but not the least, when coming to the same RPN of some failure modes, a variable, named risk coefficient, is defined to rank the failure modes with the same RPN. The large risk coefficient is, the more important degree it is supposed to be assigned, referring to the failure mode should be more priority to be corrected.

Step 1. Make sure the triangular fuzzy numbers for each rankings in assessment and calculate the non-exclusive degrees by 12.

Step 2. The assessments of experts are regarded as D numbers, that is, for each failure mode, the assessments of each expert is constructed as a D number. Therefore, the aggregation of experts' assessment of each failure mode by combining the corresponding D numbers. If information is complete, the equations in Definition 8 are used to the combination. If the information is incomplete, the equations in Definition 10 are applied to the combination. What is more, if different experts have different weights, it is supposed to put the 17 into use.

Step 3. For the results of Step 2, use 5 to calculate pignistic probability transformation (PPT).

Step 4. Calculate RPN. Firstly, calculate the mathematical expectation of each assessment. Then, use Eq. (7) to calculate the RPN of each failure mode.

Step 5. Calculate risk coefficient.

Definition 12. Let s be the standard deviation of the ratings of three assessments, defined as risk coefficient.

As mentioned above, different combination of risk factors might acquire the same RPN, however, the potential risk might be totally different. In this paper, risk coefficient, the standard deviation of the ratings of three assessments, is used to evaluate such kinds of failure modes. As a matter of fact, this method is reasonable. For example, there are two failure modes, the assessments of which are shown in Table 3.

Table 3: The assessments of three risk factors

	occurrence assessment	severity assessment	detection assessment
FM1	1	10	6
FM2	2	6	5

Apparently, two failure modes have the same RPN. However, as is shown in Table 3, compared with FM2, FM1 has the better grade in occurrence assessment but performs worse in severity and detection assessment. Therefore, FM1 should be more priority to be corrected. When observing and analyzing the data, it is not difficult to find that the distribution of FM2's data is more concentrated, which has smaller standard deviation. Besides, it is worth mentioning that standard deviation is usually used to measure the risk in financial field. Thus, it is reasonable that the standard deviation of the ratings of three assessments is applied to measure the risk in risk evaluation.

Step 6. Rank the failure modes though RPN. The larger RPN is, the more priority failure mode is supposed to be corrected. If the failure modes have the same RPN, their rankings depend on risk coefficient defined in Definition 12. The failure modes with the lager risk coefficient are assumed to be more significant and should be given higher priorities.

Table 4: The results of the risk evaluation

Item	Rating of risk factor								
	Expert 1			Expert 2			Expert 3		
	O	S	D	O	S	D	O	S	D
1	3:40% 4:60%	7	2	3:90% 4:10%	7	2	3:80% 4:20%	7	2
2	2	8	4	2	8:70% 9:30%	4	2	8	4
3	1	10	3	1	10	3	1	10	3
4	1	6:80% 7:20%	3	1	6	3:70% 2:30%	1	6	3
5	1	3	2:50% 1:50%	1	3	1:70% 2:30%	1	3:60% 2:40%	1
6	2	6	5	2	6	5	2	6	5
7	1	7	3	1	7	3	1	7	3
8	3	5:60% 6:40%	1	3	5:80% 6:20%	1	3	5:80% 7:20%	1
9	2:90% 1:10%	10:60% 9:40%	4	2:75% 1:25%	10:90% 9:10%	4	2:80% 1:20%	10:90% 9:10%	4
10	1	10	6	1	10	6	1	10	6
11	1	10	5	1	10	5	1	10	5
12	1	10	6:60% 5:40%	1	10	5:80% 4:20%	1	10	6:70% 5:30%
13	1	10	5:80% 4:20%	1	10	5	1	10	5
14	1	10	6	1	10	6:80% 7:20%	1	10	6
15	2	7:95% 6:5%	3	2	7	3	2	7	3:70% 4:30%
16	2:90% 1:10%	4	3	2:75% 1:25%	4	3	2:80% 1:20%	4	3:80% 2:20%
17	2	5:90% 6:10%	3	2	5:90% 6:10%	3	2	5:60% 6:40%	3

4 Numerical example

In order to demonstrate the effectiveness and superiority of the proposed method, a numerical example in [77] is solved in this section. Supposing there are three experts who evaluate 17 failure modes and identify the ratings of the three risk factors. The assessment results are expressed in Table 4. In this illustrative example, the weights of experts and risk factors are supposed to be equal to 1. Taking the failure mode 1 for example, the detailed computing is expressed as follows:

Step 1. The ratings are represented by triangular fuzzy numbers listed in Table 5 and shown in Figure 3. From Table 4, the occurrence assessments of three experts are $(3:40\%, 4:60\%)$, $(3:90\%, 4:10\%)$ and $(3:80\%, 4:20\%)$. Therefore, according to the Eq. (12), the non-

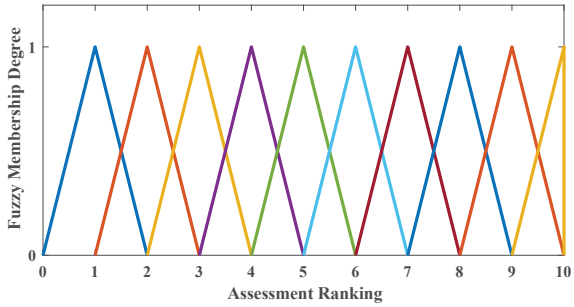

Figure 3: Graphically presentation of fuzzy variables in Table 5

Table 5: The fuzzy numbers of the assessment ratings

Assessment Ratings	Fuzzy Numbers
1	(0, 1, 2)
2	(1, 2, 3)
3	(2, 3, 4)
4	(3, 4, 5)
5	(4, 5, 6)
6	(5, 6, 7)
7	(6, 7, 8)
8	(7, 8, 9)
9	(8, 9, 10)
10	(9, 10, 10)

exclusiveness degrees are calculated as follows:

$$u_{\neg E}(3,3)=1, \qquad u_{\neg E}(4,4)=1, \qquad u_{\neg E}(3,\{3,4\})=1$$
$$u_{\neg E}(4,\{3,4\})=1, \qquad u_{\neg E}(3,4)=\frac{0.25}{1+1-0.25}\approx 0.1429$$

Step 2. Construct D numbers and combine D numbers. According to Section 3, corresponding to the evaluations of three experts, three D numbers are constructed as follows:

$$D_1(3)=0.4, \qquad D_1(4)=0.6$$
$$D_2(3)=0.9, \qquad D_2(4)=0.1$$
$$D_3(3)=0.8, \qquad D_3(4)=0.2$$

Then, because these D numbers have complete information, the combination among D_1, D_2 and D_3 is calculated by 10-14, that is $D_1 \bigodot D_2 \bigodot D_3$.

At first, calculate $D' = D_1 \bigodot D_2$:

$$K_{D'} = (1-0.1429)\times[0.4\times 0.1+0.6\times 0.9]=0.4971$$
$$D'(3)=\frac{1}{1-0.4971}\times 1\times 0.4\times 0.9=0.7159$$
$$D'(4)=\frac{1}{1-0.4971}\times 1\times 0.6\times 0.1=0.1193$$
$$D'(3,4)=\frac{1}{1-0.4971}\times 0.1429\times[0.4\times 0.1+0.6\times 0.9]=0.1648$$

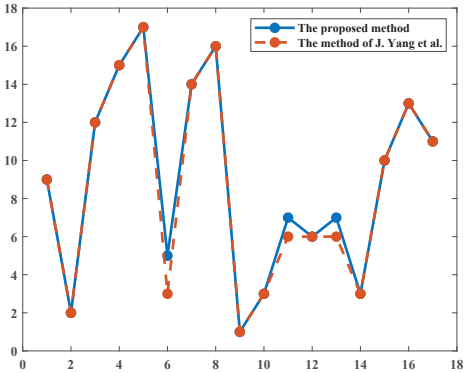

Figure 4: The risk priority of the failure modes using two methods

Next, calculate $D = D' \bigodot D_3$:

$$K_D = (1 - 0.1429) \times [0.7159 \times 0.2 + 0.1193 \times 0.8] = 0.2045$$

$$D(3) = \frac{1}{1 - 0.2045} \times [1 \times 0.7159 \times 0.8 + 1 \times 0.1648 \times 0.8] = 0.8857$$

$$D(4) = \frac{1}{1 - 0.2045} \times [1 \times 0.1193 \times 0.2 + 1 \times 0.1648 \times 0.2] = 0.0714$$

$$D(3,4) = \frac{1}{1 - 0.2045} \times 0.1429 \times [0.7159 \times 0.2 + 0.1193 \times 0.8] = 0.0429$$

Step 3. Calculate pignistic probability transformation (PPT) of the result of Step 2 by 5

$$BetP(3) = 0.8857 + \frac{0.0429}{2} \approx 0.9071 BetP(4) = 0.8857 + \frac{0.0429}{2} \approx 0.0929$$

Step 4. The mathematical expectation of the occurrence assessment is $3 \times 0.9071 + 4 \times 0.0929 = 3.0929$. Besides, three experts have the same evaluation to the severity assessment (S) and detection assessment (D) of failure mode 1, what is more, the evaluation are real numbers, 7 and 2, without any uncertainty. Thus, in these two assessments, the results through Step 1 to 4 are still 7 and 2.

Step 5. Calculate the RPN of failure mode 1 (RPN_1) by 7.

$$RPN_1 = O_1 \times S_1 \times D_1 = 3.0929 \times 7 \times 2 = 43.3006$$

Step 6. Calculate the risk coefficient of the failure mode 1.

$$\bar{x}_1 = \frac{3.0929 + 7 + 2}{3} \approx 4.0310$$

$$s_1 = \sqrt{\frac{1}{3} \cdot [(3.0929 - 4.0310)^2 + (7 - 4.0310)^2 + (2 - 4.0310)^2]} \approx 2.6287$$

The data of other failure modes are treated through Step 1 to 6 as mentioned above. Then, according to the RPNs and risk coefficients, the risk priorities of the failure modes are obtained, which are shown in Table 6. Meanwhile, in order to demonstrate the effectiveness of the proposed method, the results are compared with that of the J. Yang et al.'s method [77].

As shown in Table 6, the results of two methods are similar. Apart from failure mode 6, 11 and 13, other failure modes have the same risk priority rankings in both two methods. In addition, it is indicated that the five of highest risk priority rankings are failure mode 9, 2, 10,

Table 6: The results of the risk evaluation

Failure mode	RPN	Risk coefficient	The rankings of the proposed method	The rankings of the J. Yang et al.'s method
1	43.3006	2.6287	9	9
2	64	3.0551	2	2
3	30	4.7258	12	12
4	18	2.5166	15	15
5	3.0726	1.1478	17	17
6	60	2.0817	5	3
7	21	3.0551	14	14
8	15.0657	2.0110	16	16
9	78.10103376	4.1593	1	1
10	60	4.5092	3	3
11	50	4.5092	7	6
12	51.452	4.5047	6	6
13	50	4.5092	7	6
14	60	4.5092	3	3
15	42	2.6458	10	10
16	23.5152	1.0203	13	13
17	30.4038	1.5643	11	11

14, and 6, which refers that these 5 faults are most likely to occur. Furthermore, in both two methods, failure mode 16, 7, 4, 8, and 5 have the five of lowest priorities, indicating that these 5 failures are almost impossible to happen.

Figure 4 shows the comparison of risk priorities of two methods, in which the ranking is on the abscissa axis while the failure mode is on the vertical axis. As shown in Figure 4, two curves have the similar trend, which indicates that the proposed method is as effective as J. Yang et al.'s method.

Nevertheless, the results also reflect the different evaluations using two methods, which precisely demonstrates the superiority of the proposed method. As seen in Figure 4, using J. Yang et al.'s method, failure mode 11, 12, 13 have the same risk priority, while failure mode 12 has the larger risk priority compared with failure mode 11 and failure mode 13 in the proposed method. Because the highest rating of failure mode 12 in detection assessment is 6, which is higher than that of failure mode 11, 13 in detection assessment. Thus, failure mode 12 is obviously supposed to have higher risk priority compare with failure mode 11 and failure mode 13. What is more, in J. Yang et al.'s method, failure mode 6, 10, 14 have the same risk priority, but in the proposed method, failure mode 6 has the lower risk priority compared with failure mode 10 and failure mode 14. Although these failure modes have the same RPN, compared with failure mode 10 and failure mode 14, failure mode 6 has two lower risk ratings in severity assessment and detection assessment and merely a lager rating in occurrence assessment. Therefore, failure mode 6 is supposed to have the lower risk priority compared with failure mode 10 and failure mode 14.

5 Conclusion

In this paper, a novel method to risk evaluation in failure mode and effects analysis based on D numbers theory is proposed. In the proposed method, the application of the D numbers not only aggregates the fuzzy assessment in risk evaluation, but also takes the non-exclusiveness into account. Besides, the shortcomings of RPN are overcome successfully. Furthermore, the numerical example has demonstrated that the proposed method achieves less computation complexity compared with most existing method to risk evaluation in FMEA. In conclusion, the proposed method is an advanced and efficient method to risk evaluation in FMEA.

Acknowledgement

The work is partially supported by National Natural Science Foundation of China (Grant No. 61573290,61973332).

Conflict of Interest

The authors declare no conflict of interest.

Bibliography

[1] Adar, E.; Ince, M.; Karatop, B.; Bilgili, M. S. (2017). The risk analysis by failure mode and effect analysis (fmea) and fuzzy-fmea of supercritical water gasification system used in the sewage sludge treatment. *Journal of Environmental Chemical Engineering*, 5 (1), 1261–1268, 2017.

[2] Ahn, J.; Noh, Y.; Park, S. H.; Choi, B. I.; Chang, D.; Ahn, J.; Noh, Y.; Park, S. H.; Choi, B. I.; Chang, D. (2017). Fuzzy-based failure mode and effect analysis (fmea) of a hybrid molten carbonate fuel cell (mcfc) and gas turbine system for marine propulsion. *Journal of Power Sources*, 364, 226–233, 2017.

[3] Alimohammadzadeh, K.; Bahadori, M.; Jahangir, T.; Ravangard, R. (2017). Assessing common medical errors in a children's hospital nicu using failure mode and effects analysis (fmea). *Trauma Monthly*, in Press, 2017.

[4] Biswas, S. K.; Devi, D.; Chakraborty, M. (2018). A hybrid case based reasoning model for classification in internet of things (iot) environment. *Journal of Organizational and End User Computing (JOEUC)*, 30 (4), 104–122, 2018.

[5] Cao, X.; Deng, Y. 2019. A new geometric mean fmea method based on information quality. *IEEE Access*, 7 (1), 95547–95554, 2019.

[6] Capuano, N.; Chiclana, F.; Herrera-Viedma, E.; Fujita, H.; Loia, V. (2018). Fuzzy rankings for preferences modeling in group decision making. *International Journal of Intelligent Systems*, 33 (7), 1555–1570, 2018.

[7] Chatterjee, K.; Zavadskas, E. K.; Tamosaitiene, J.; Adhikary, K.; Kar, S. (2018). A hybrid MCDM technique for risk management in construction projects. *Symmetry*, 10 (2), 46, 2018.

[8] Chen, Y. C.; Tsai, P. Y. (2017). Evaluating the operational risks of biomedical waste using failure mode and effects analysis. *Waste Manag Res*, 35 (6), 593–601, 2017.

[9] Chin, K. S.; Wang, Y. M. ; Poon, G. K. K. et al. (2009). Failure mode and effects analysis using a group-based evidential reasoning approach[J]. *Computers and Operations Research*, 36 (6), 1768–1779, 2009.

[10] Dempster, A. P. (1967). Upper and lower probabilities induced by a multivalued mapping, *Annals of Mathematical Statistics*, 38 (2), 325–339, 1967.

[11] Deng, X.; Jiang, W. (2018). Dependence assessment in human reliability analysis using an evidential network approach extended by belief rules and uncertainty measures. *Annals of Nuclear Energy*, 117, 183–193, 2018.

[12] Deng, X.; Jiang, W. (2019). Evaluating green supply chain management practices under fuzzy environment: a novel method based on D number theory. *International Journal of Fuzzy Systems*, 21, 1389–1402, 2019.

[13] Deng, X.; Deng, Y. (2014). D numbers theory: a generalization of dempster-shafer theory. *Computer Science*, 2014.

[14] Dzitac, I.; Filip, F. G.; Manolescu, M.-J. (2017). Fuzzy logic is not fuzzy: World-renowned computer scientist Lotfi A. Zadeh. *International Journal of Computers Communications & Control*, 12 (6), 748–789, 2017.

[15] Fang, R.; Liao, H.; Yang, J.-B.; Xu, D.-L. (2019). Generalised probabilistic linguistic evidential reasoning approach for multi-criteria decision-making under uncertainty. *Journal of the Operational Research Society*, in press, 2019.

[16] Fei, L.; Wang, H.; Chen, L.; Deng, Y. (2019). A new vector valued similarity measure for intuitionistic fuzzy sets based on owa operators. *Iranian Journal of Fuzzy Systems*, 16 (3), 113–126, 2019.

[17] Feng, F.; Fujita, H.; Ali, M. I.; Yager, R. R.; Liu, X. (2018). Another view on generalized intuitionistic fuzzy soft sets and related multiattribute decision making methods, *IEEE Transactions on Fuzzy Systems*, 27 (3), 474–488, 2018.

[18] Gao, X.; Deng, Y. (2019). The generalization negation of probability distribution and its application in target recognition based on sensor fusion. *International Journal of Distributed Sensor Networks*, 15 (5), 2019.

[19] Gao, X.; Deng, Y. (2019). The negation of basic probability assignment, *IEEE Access*, 7 (1), 107006–107014, 2019.

[20] Guan, X.; Liu, H.; Yi, X.; Zhao, J. (2018). The Improved Combination Rule of D Numbers and Its Application in Radiation Source Identification. *Mathematical Problems in Engineering*, 2018, 10 pages, 2018.

[21] Jiang, W.; Cao, Y.; Deng, X. (2019). A Novel Z-network Model Based on Bayesian Network and Z-number. *IEEE Transactions on Fuzzy Systems*, 2019.

[22] Jiang, W.; Wei, B. (2018). Intuitionistic fuzzy evidential power aggregation operator and its application in multiple criteria decision-making. *International Journal of Systems Science*, 49 (3), 582–594, 2018.

[23] Jiang, W.; Wei, B.; Liu, X.; Li, X.; Zheng, H. (2018). Intuitionistic fuzzy power aggregation operator based on entropy and its application in decision making, *International Journal of Intelligent Systems*, 33 (1), 49–67, 2018.

[24] Jin, T.; Chen, C.; Chen, L.; Tian, H.; Zhu, D.; Jia, X. (2018). Failure mode and effects analysis of CNC machine tools based on spa, *International Conference on System Reliability & Safety*, 107–111, 2018.

[25] Kang, B.; Deng, Y. (2019). The maximum Deng entropy, *IEEE Access*, 7 (1), 10.1109/ACCESS.2019.2937679, 2019.

[26] Kang, B.; Deng, Y.; Hewage, K.; Sadiq, R. (2019a). A method of measuring uncertainty for Z-number. *IEEE Transactions on Fuzzy Systems*, 27 (4), 731–738, 2019.

[27] Kang, B.; Zhang, P.; Gao, Z.; Chhipi-Shrestha, G.; Hewage, K.; Sadiq, R. (2019b). Environmental assessment under uncertainty using dempster–shafer theory and z-numbers. *Journal of Ambient Intelligence and Humanized Computing*, Published online, doi: 10.1007/s12652–019–01228–y, 2019.

[28] Kim, K. O.; Zuo, M. J.; Kim, K. O.; Zuo, M. J. (2018). General model for the risk priority number in failure mode and effects analysis. *Reliability Engineering & System Safety*, 169, 321–329, 2018.

[29] Lee, Y. C.; Kim, Y.; Huynh, J. W.; Hamilton, R. J. (2017). Failure modes and effects analysis for ocular brachytherapy. *Brachytherapy*, 16 (6), 1265–1279, 2017.

[30] Li, M.; Xu, H.; Deng, Y. (2019). Evidential decision tree based on belief entropy. *Entropy*, 21 (9), 897, 2019.

[31] Li, X.; Chen, X. (2018). D-Intuitionistic hesitant fuzzy sets and their application in multiple attribute decision making. *Cognitive Computation*, 10 (3), 496–505, 2018.

[32] Li, X.; He, M.; Wang, H. (2017). Application of failure mode and effect analysis in managing catheter-related blood stream infection in intensive care unit. *Medicine*, 96 (51), e9339, 2017.

[33] Li, Y.; Deng, Y. (2019). Intuitionistic Evidence Sets, *IEEE Access*, 7 (1), 106417–106426, 2019.

[34] Lin, S.; Li, C.; Xu, F.; Liu, D.; Liu, J. (2018). Risk identification and analysis for new energy power system in China based on D numbers and decision-making trial and evaluation laboratory (DEMATEL). *Journal of Cleaner Production*, 180, 81–96, 2018.

[35] Liu, B.; Hu, Y.; Deng Y. (2018). New Failure Mode and Effects Analysis based on D Numbers Downscaling Method, *International Journal of Computers Communications & Control*, 13(2), 205–220, 2018.

[36] Liu, F.; Gao, X.; Zhao, J.; Deng, Y. (2019a). Generalized belief entropy and its application in identifying conflict evidence. *IEEE Access* 7 (1), 126625–126633, 2019.

[37] Liu, H.; Li, Z.; Song, W.; Su, Q. (2017). Failure mode and effect analysis using cloud model theory and PROMETHEE method. *IEEE Trans. Reliability*, 66 (4), 1058–1072, 2017.

[38] Liu, P.; Zhang, X. (2019). A multicriteria decision-making approach with linguistic D numbers based on the Choquet integral. *Cognitive Computation*, 11 (4), 560–575, 2019.

[39] Liu, Q.; Tian, Y.; Kang, B. (2019b). Derive knowledge of z-number from the perspective of dempster-shafer evidence theory. *Engineering Applications of Artificial Intelligence*, 85, 754–764, 2019.

[40] Liu, Z.; Liu, Y.; Dezert, J.; Cuzzolin, F. (2019c). Evidence combination based on credal belief redistribution for pattern classification. *IEEE Transactions on Fuzzy Systems*, DOI: 10.1109/TFUZZ.2019.2911915, 2019.

[41] Liu, Z.; Pan, Q.; Dezert, J.; Han, J.-W.; He, Y. (2018a). Classifier fusion with contextual reliability evaluation. *IEEE Transactions on Cybernetics*, 48 (5), 1605–1618, 2018.

[42] Liu, Z.-G.; Pan, Q.; Dezert, J.; Martin, A. (2018b). Combination of classifiers with optimal weight based on evidential reasoning. *IEEE Transactions on Fuzzy Systems*, 26 (3), 1217–1230, 2018.

[43] Luo, C.; Chen, Y.; Xiang, H.; Wang, W.; Wang, Z. (2018). Evidence combination method in time domain based on reliability and importance. *Journal of Systems Engineering and Electronics*, 29 (6), 1308–1316, 2018.

[44] Luo, Z.; Deng, Y. (2019). A matrix method of basic belief assignment's negation in Dempster-Shafer theory. *IEEE Transactions on Fuzzy Systems*, 10.1109/TFUZZ.2019.2930027, 2019.

[45] Meng, D.; Li, Y.; Zhu, S.-P.; Lv, G.; Correia, J.; de Jesus, A. (2019). An enhanced reliability index method and its application in reliability-based collaborative design and optimization. *Mathematical Problems in Engineering*, 2019, 10 pages, 2019.

[46] Meng, D.; Liu, M.; Yang, S.; Zhang, H.; Ding, R. (2018). A fluid–structure analysis approach and its application in the uncertainty-based multidisciplinary design and optimization for blades. *Advances in Mechanical Engineering*, 10 (6), 2018.

[47] Meng, D.; Yang, S.; Zhang, Y.; Zhu, S.-P. (2019). Structural reliability analysis and uncertainties-based collaborative design and optimization of turbine blades using surrogate model. *Fatigue & Fracture of Engineering Materials & Structures*, 42(6), 1219–1227, 2019.

[48] Mo, H.; Deng, Y. (2019). An evaluation for sustainable mobility extended by D numbers. *Technological and Economic Development of Economy*, 25 (5), 802–819, 2019.

[49] Moreno, R. V.; Riera, S. I.; Alvarez, E. M.; Mendoza, J. A. B.; Vazquez, S. T.; Castellano, L. D.; Gonzalez, J. C. M. (2016). Improvement of the safety of a clinical process using failure mode and effects analysis: Prevention of venous thromboembolic disease in critically ill patients. *Medicina Intensiva*, 40 (8), 483–490, 2016.

[50] Peeters, J. F. W.; Basten, R. J. I.; Tinga, T. (2018). Improving failure analysis efficiency by combining fta and fmea in a recursive manner. *Reliability Engineering & System Safety*, 172, 36–44, 2018.

[51] Schuller, B. W.; Burns, A.; Ceilley, E. A.; King, A.; Letourneau, J.; Markovic, A.; Sterkel, L.; Taplin, B.; Wanner, J.; Albert, J. M. (2017). Failure mode and effects analysis: A community practice perspective, *Journal of Applied Clinical Medical Physics*, 18 (6), 258–267, 2017.

[52] Seiti, H.; Hafezalkotob, A. (2018). Developing pessimistic-optimistic risk-based methods for multi-sensor fusion: An interval-valued evidence theory approach. *Applied Soft Computing*, 72, 609–623, 2018.

[53] Seiti, H.; Hafezalkotob, A.; MartĂnez, L. (2019). R-numbers, a new risk modeling associated with fuzzy numbers and its application to decision making, *Information Sciences*, 483, 206–231, 2019.

[54] Seiti, H.; Hafezalkotob, A.; Najafi, S.; Khalaj, M. (2018). A risk-based fuzzy evidential framework for FMEA analysis under uncertainty: An interval-valued DS approach, *Journal of Intelligent & Fuzzy Systems*, 35 (2), 1419–1430, 2018.

[55] Shafer, G. (1976). *A Mathematical Theory of Evidence*, Princeton University Press, Princeton, 1976.

[56] Shankar, R.; Choudhary, D.; Jharkharia, S. (2018). An integrated risk assessment model: A case of sustainable freight transportation systems, *Transportation Research Part D: Transport and Environment*, 63, 662–676, 2018.

[57] Smets, P.; Kennes, R. (1994). The transferable belief model. *Artificial Intelligence*, 66 (2), 191–234, 1994.

[58] Song, Y.; Deng, Y. (2019). A new method to measure the divergence in evidential sensor data fusion. *International Journal of Distributed Sensor Networks*, 15 (4), DOI: 10.1177/1550147719841295, 2019.

[59] Song, Y.; Deng, Y. (2019). Divergence measure of belief function and its application in data fusion. *IEEE Access*, 7 (1), 107465–107472, 2019.

[60] Stojkovic, T.; Marinkovic, V.; Jaehde, U.; Manser, T. (2016). Using failure mode and effects analysis to reduce patient safety risks related to the dispensing process in the community pharmacy setting. *Research in Social & Administrative Pharmacy Rsap*, 13 (6), 1159–1166, 2016.

[61] Su, X.; Li, L.; Shi, F.; Qian, H. (2018). Research on the fusion of dependent evidence based on mutual information. *IEEE Access* 6, 71839–71845, 2018.

[62] Sun, L.; Liu, Y.; Zhang, B.; Shang, Y.; Yuan, H.; Ma, Z. (2016). An Integrated Decision-Making Model for Transformer Condition Assessment Using Game Theory and Modified Evidence Combination Extended by D Numbers, *Energies*, 9 (9), 697, 2016.

[63] Sun, R.; Deng, Y. (2019a). A new method to identify incomplete frame of discernment in evidence theory. *IEEE Access* 7 (1), 15547–15555.

[64] Sun, R.; Deng, Y. (2019b). A new method to determine generalized basic probability assignment in the open world. *IEEE Access*, 7 (1), 52827–52835, 2019.

[65] Tooranloo, H. S.; Ayatollah, A. S. (2016). Pathology the internet banking service quality using failure mode and effect analysis in interval-valued intuitionistic fuzzy environment. *International Journal of Fuzzy Systems*. 19 (1), 1–15, 2016.

[66] Wang, N.; Liu, X.; Wei, D. (2018). A Modified D Numbers' Integration for Multiple Attributes Decision Making. *IEEE Transactions on Fuzzy Systems*, 20 (1), 104–115, 2018.

[67] Wang, N.; Wei, D. (2018). A Modified D Numbers Methodology for Environmental Impact Assessment. *Technological and Economic Development of Economy* 24 (2), 653–669, 2018.

[68] Wang, Y.; Zhang, K.; Deng, Y. (2019). Base belief function: an efficient method of conflict management. *Journal of Ambient Intelligence and Humanized Computing*, 10 (9), 3427–3437, 2019.

[69] Wang, Z.; Gao, J.-M.; Wang, R.-X.; Chen, K.; Gao, Z.-Y.; Zheng, W. (2018). Failure mode and effects analysis by using the house of reliability-based rough vikor approach. *IEEE Transactions on Reliability*, 67 (1), 230–248, 2018.

[70] Xia, J.; Feng, Y.; Liu, L.; Liu, D.; Fei, L. (2019). On entropy function and reliability indicator for D numbers. *Applied Intelligence*, 49 (9), 3248–3266, 2019.

[71] Xiao, F. (2019). EFMCDM: Evidential fuzzy multicriteria decision making based on belief entropy. *IEEE Transactions on Fuzzy Systems*, DOI: 10.1109/TFUZZ.2019.2936368, 2019.

[72] Xiao, F.; Zhang, Z.; Abawajy, J. (2019). Workflow scheduling in distributed systems under fuzzy environment. *Journal of Intelligent & Fuzzy Systems*, DOI: 10.3233/JIFS–190483, Pre-press, 1–11, 2019.

[73] Xu, X.; Xu, H.; Wen, C.; Li, J.; Hou, P.; Zhang, J. (2018a). A belief rule-based evidence updating method for industrial alarm system design. *Control Engineering Practice*, 81, 73–84, 2018.

[74] Xu, X.; Zheng, J.; Yang, J.-B.; Xu, D.-L.; Chen, Y.-W. (2017). Data classification using evidence reasoning rule, *Knowledge-Based Systems*, 116, 144–151, 2017.

[75] Xu, X.-B.; Ma, X.; Wen, C.-L.; Huang, D.-R.; Li, J.-N. (2018b). Self-tuning method of pid parameters based on belief rule base inference. *Information Technology and Control*, 47 (3), 551–563, 2018.

[76] Yager, R. R. (2012). On Z-valuations using Zadeh's Z-numbers. *International Journal of Intelligent Systems*, 27 (3), 259–278, 2012.

[77] Yang, J.; Huang, H. Z.; He, L. P.; Zhu, S. P.; Wen, D. (2011). Risk evaluation in failure mode and effects analysis of aircraft turbine rotor blades using Dempster-Shafer evidence theory under uncertainty, *Engineering Failure Analysis*, 18 (8), 2084–2092, 2011.

[78] Yazdi, M.; Daneshvar, S.; Setareh, H. (2017). An extension to fuzzy developed failure mode and effects analysis (fdfmea) application for aircraft landing system. *Safety Science*, 98, 113–123, 2017.

[79] Zadeh, L. A. (1965). Fuzzy sets, *Information & Control*, 8 (3), 338–353, 1965.

[80] Zhang, J.; Zhong, D.; Zhao, M.; Yu, J.; Lv, F., (2019). An Optimization Model for Construction Stage and Zone Plans of Rockfill Dams Based on the Enhanced Whale Optimization Algorithm. *Energies*, 12 (3), 466, 2019.

[81] Zhang, W.; Deng, Y. (2019). Combining conflicting evidence using the DEMATEL method. *Soft computing*, 23 (17), 8207–8216, 2019.

[82] Zhao, J.; Deng, Y. (2019). Performer selection in Human Reliability analysis: D numbers approach. *International Journal of Computers Communications & Control*, 14 (3), 437–452, 2019.

[83] Zhou, M.; Liu, X.; Yang, J. (2017). Evidential reasoning approach for MADM based on incomplete interval value. *Journal of Intelligent & Fuzzy Systems* 33 (6), 3707–3721, 2017.

[84] Zhou, M.; Liu, X.-B.; Chen, Y.-W.; Yang, J.-B. (2018). Evidential reasoning rule for MADM with both weights and reliabilities in group decision making. *Knowledge-Based Systems*, 143, 142–161, 2018.

[85] Zhou, M.; Liu, X.-B.; Yang, J.-B.; Chen, Y.-W.; Wu, J. (2019). Evidential reasoning approach with multiple kinds of attributes and entropy-based weight assignment, *Knowledge-Based Systems*, 163, 358–375, 2019.

INTERNATIONAL JOURNAL OF COMPUTERS COMMUNICATIONS & CONTROL
ISSN 1841-9836, e-ISSN 1841-9844, 14(5), 692-710, October 2019.

A Robust Adaptive Control using Fuzzy Neural Network for Robot Manipulators with Dead-Zone

D.H. Vu, S. Huang, T.D. Tran, T.Y. Vu, V.C. Pham

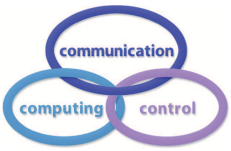

D. Ha Vu*
College of Electrical and Information Engineering
Hunan University, Changsha, China
*Corresponding author: vuhadhsd@hnu.edu.cn

Shoudao Huang
College of Electrical and Information Engineering
Hunan University, Changsha, China
hsd1962@hnu.edu.cn

T. Diep Tran
College of Electrical and Information Engineering
Hunan University, Changsha, China
phuongdiep222@hnu.edu.cn

T. Yen Vu
Faculty of Electrical Engineering
Saodo University, Chilinh, Vietnam
havi2203@hnu.edu.cn

V. Cuong Pham
Faculty of Electrical Engineering
Hanoi University of Industry, Hanoi, Vietnam
cuongpv0610@haui.edu.vn

Abstract: Abstract: In this paper, a robust-adaptive-fuzzy-neural-network controller (RAFNNs) bases on dead zone compensator for industrial robot manipulators (RM) is proposed to dead the unknown model and external disturbance. Here, the unknown dynamics of the robot system is deal by using fuzzy neural network to approximate the unknown dynamics. The online training laws and estimation of the dead-zone are determined by Lyapunov stability theory and the approximation theory. In this proposal, the robust sliding-mode-control (SMC) is constructed to optimize parameter vectors, solve the approximation error and higher order terms. Therefore, the stability, robustness, and desired tracking performance of RAFNNs for RM are guaranteed. The simulations and experiments performed on three-link RM are provided in comparison with neural-network (NNs) and proportional-integral-derivative (PID) to demonstrate the robustness and effectiveness of the RAFNNs.
Keywords: adaptive control, fuzzy neural networks, robot manipulators, unknown dead-zone.

1 Introduction

In fact, Robot manipulators are multi-input multi-output (MIMO) non-linear systems. In working process, robot system always bear the external disturbance, nonlinear fiction, pay load, etc. to overcome this face. So many controller propose such as adaptive controller, robust adaptive controller, backstepping controller, and intelligent controller, etc [2,8,9,17,26,29]. Backstepping technique has been widely applied to design adaptive controller for nonlinear system [13]. Investigations base on Backstepping control method were provided a systematic framework for the design of tracking and regulation strategies, suitable for a large class of state feedback linearizable nonlinear systems [4,10,25,28]. However, there are some problems in the Backstepping design method. A major constraint is that certain functions must be "linear in the unknown parameters", which may not be satisfied in practice. Furthermore, some tedious analysis is needed to determine "regression matrices", and the problem of determining and computing the regression matrices become even more acute. To deal these problems, intelligent controllers based on fuzzy control for RM have been proposed. The Fuzzy logic technique is a successful implementation for the approximation of non-linear systems [1,5,11,12,15,16,22,27]. In [11], the intelligent controller based on fuzzy logic was proposed for robotic manipulators under uncertain environments. In this controller, the approximation capability of fuzzy logic was used to approximate the unknown dynamic of robot system. The parameters of the intelligent controller were adjusted online bases on the Lyapunov algorithm. In [15], the authors suggested an adaptive fuzzy sliding mode control with nonlinear observer (AFSMCO) for the robot manipulators with unknown external force. Here, by combining the advantages of fuzzy logic, sliding mode control and nonlinear observer, the performance of control system was improved. However, most proposed adaptive fuzzy controllers were difficult in building suitable fuzzy control rules, membership function, and how to guarantee the system stability was a challenge problem to be solved. To deal this difficult problem, the adaptive fuzzy neural networks were proposed [3, 18, 23, 24]. In [23], Rong-Jong Wai, and Rajkumar Muthusamy suggested an intelligent controller bases on fuzzy neural network control for robot manipulator in order to improve the control performance of position tracking. In this controller, sliding mode control was developed for position tracking of robot manipulator system. Moreover, the fuzzy neural network was employed to approximation the unknown dynamic of control system. The fuzzy neural network was designed bases on the SMC rules. The adaptive laws were determined by using the Lyapunov theorem. In [24], a fuzzy neural network combined with backstepping control was proposed for robot manipulator to achieve the robustness and stability. Here, the fuzzy neural network was inherited backstepping control to improve the robustness of backstepping control. The parameters of fuzzy neural network control were determined and adjusted online by the Lyapunov theorem. The robustness and stability of proposed controller were improved.

Recently years, one of the important subjects for robotic manipulator that has attracted many researchers is the compensation of dead-zone. In fact, deal-zone is a natural and nonlinear item. To deal with compensation of non-smooth nonlinearities, many researches were proposed [6,7,14,19–21]. In [21], an adaptive neural network is proposed to compensate the dead-zone of the hydraulic system. In this proposed controller, the RBF neural network is applied to identify the dead-zone parameters and a cost function is proposed to provide the best approximation of dead-zone. The parameters of the control system and the dead-zone are easier to calculate.

In this paper, to deal with the problem of compensation dead-zone with the unknown dynamic and external disturbance, an adaptive robust fuzzy neural network control based on backstepping technique has been proposed. This proposed proposal is combined the advantage of FNN, sliding mode control, adaptive control and backstepping technique. The unknown robot dynamics are approximated by the FNN and the tracking errors are compensated by using the

robust term. In addition, all the parameters of the proposed controller are adjusted by the stability Lyapunov theory. Thus, the robustness and effectiveness of RAFNNs control system are guarantee.

The paper is organized as follows. The preliminaries are described in section 2. Section 3 presented control design and stability analysis. The simulation and experimental results of three-link robot manipulators are provided in section 4. Finally, section 5 gives conclusion.

2 Preliminaries

2.1 Model of Robotic Manipulators

Consider the dynamics of an n-link robot manipulator with external disturbance:

$$M_{RM}\left(\Theta\right)\ddot{\Theta}+C_{RM}\left(\Theta,\dot{\Theta}\right)\dot{\Theta}+G_{RM}\left(\Theta\right)+F_{RM}\left(\dot{\Theta}\right)=\tau-\tau_0 \tag{1}$$

With $\Theta=[\Theta_1\ \Theta_2\dots\Theta_n]\in R^{n\times 1}$ is the joint position vector, $\dot{\Theta}=\left[\dot{\Theta}_1\ \dot{\Theta}_2\dots\dot{\Theta}_n\right]\in R^{n\times 1}$ is the velocity vector and $\ddot{\Theta}=\left[\ddot{\Theta}_1\ \ddot{\Theta}_2\dots\ddot{\Theta}_n\right]\in R^{n\times 1}$ is the acceleration vector. $M_{RM}\left(\Theta\right)$, $C_{RM}\left(\Theta,\dot{\Theta}\right)$ and $G_{RM}\left(\Theta\right)$ are $[n\times n]$ expressing the symmetric inertial matrix, Coriolis and Centripetal terms, and Gravity terms, respectively. $F_{RM}\left(\dot{\Theta}\right)$ represents the $n\times 1$ vector of the frictions. τ_0 represents the $n\times 1$ vector of the input unknown disturbances. And τ is the $n\times 1$ control input vector of joints torque. For designing controller, several properties of the robot dynamics (1) have been assumed as follows.

Property 1: M_{RM} is the symmetric inertial Matrix and bounded as:

$$\vartheta_1\|x\|^2\le x^T M_{RM}x\le\vartheta_2\|x\|^2,\forall x\in R^n \tag{2}$$

With ϑ_1 and ϑ_2 are known positive constants.

Property 2: $\dot{M}_{RM}-2C_{RM}$ is skew symmetry matrix, in which

$$x^T\left[\dot{M}_{RM}-2C_{RM}\right]x=0 \tag{3}$$

Property 3: C_{RM}, G_{RM} and F_{RM} are satisfied:

$$\|C_{RM}\dot{\Theta}\|\le C_{kRM}\|\dot{\Theta}\|^2,\|G_{RM}\|\le G_{kRM},F_{RM}\le F_{kRM}\|\dot{\Theta}\|+F_0 \tag{4}$$

With $C_{kRM},G_{kRM},F_{kRM},F_0$ are positive constants.

Property 4: $\tau_0\in R^n$ is the unknown disturbance and τ_0 is bounded as follows:

$$\|\tau_0\|\le\tau_k,\tau_k>0 \tag{5}$$

According to assumptions given in [19], the dead zone function shows Fig. 1, and which is expressed as follows:

$$\tau=D(u),\quad D(u)=\begin{cases}h_r(u-d_r) & \text{for}\quad u>d_r\\ 0 & \text{for}\quad d_l\le u\le d_r\\ h_l(u+d_l) & \text{for}\quad u<d_l\end{cases} \tag{6}$$

Here, $d_r>0$, $d_l<0$ are unknown constant parameters of dead zone. $h_l\left(u\right)$, $h_r\left(u\right)$ are the unknown smooth functions.

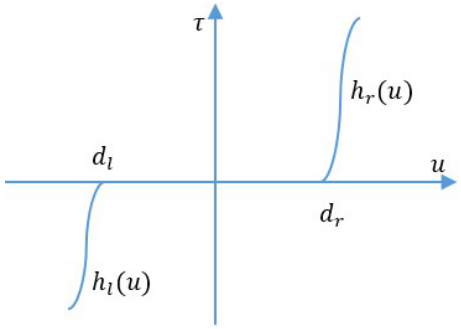

Figure 1: Dead zone model.

Where u is control input before entering the dead zone. τ is control input after entering the dead zone. Therefore (6) can be rewritten as:

$$\tau = D(u) = u - sat_D(u) \tag{7}$$

where the asymmetric saturation function is defined as:

$$sat_D(u) = \begin{cases} d_r & \text{for} \quad u > d_r \\ u & \text{for} \quad d_l \leq u \leq d_r \\ d_l & \text{for} \quad u < d_l \end{cases} \tag{8}$$

2.2 Backstepping controller

The conventional Backstepping controller for the dynamic of the RM is described as follows:
Step 1: the tracking error vector $Z_{\Theta 1}(t)$ and derivative of $Z_{\Theta 1}(t)$ are define as the follows:

$$Z_{\Theta 1}(t) = \Theta_d - \Theta \quad \text{and} \quad \dot{Z}_{\Theta 1}(t) = \dot{\Theta}_d - \dot{\Theta} \tag{9}$$

By using $\dot{\Theta}$ as the first virtual control input. Define an intermediate function as:

$$\alpha_{\Theta 1}(t) = \dot{\Theta}_d + \lambda_{\Theta 1} Z_{\Theta 1} \quad \text{and} \quad \dot{\alpha}_{\Theta 1}(t) = \ddot{\Theta}_d + \lambda_{\Theta 1} \dot{Z}_{\Theta 1}, \lambda_{\Theta 1} > 0 \tag{10}$$

Consider the first following Lyapunov function candidate $L_{\Theta 1}$ as:

$$L_{\Theta 1}(Z_{\Theta 1}(t)) = \frac{1}{2} Z_{\Theta 1}^T Z_{\Theta 1} \tag{11}$$

The tracking error vector $Z_{\Theta 2}(t)$ is define as the follows:

$$Z_{\Theta 2}(t) = \alpha_{\Theta 1}(t) - \dot{\Theta} = \dot{Z}_{\Theta 1} + \lambda_{\Theta 1} Z_{\Theta 1} \tag{12}$$

The derivative of $L_{\Theta 1}(Z_{\Theta 1}(t))$ is:

$$\dot{L}_{\Theta 1}(Z_{\Theta 1}(t)) = Z_{\Theta 1}^T \dot{Z}_{\Theta 1} = Z_{\Theta 1}^T (Z_{\Theta 2}(t) - \lambda_{\Theta 1} Z_{\Theta 1}) \tag{13}$$

Step 2: the derivative of $Z_{\Theta 2}(t)$ along to time, we have

$$\dot{Z}_{\Theta 2}(t) = \dot{\alpha}_{\Theta 1}(t) - \ddot{\Theta} \tag{14}$$

Where $\ddot{\Theta}$ used as the second virtual control input. Substituting (9, 10, 12, 14) into (1), we have:

$$M_{RM} \dot{Z}_{\Theta 2} = M_{RM} \dot{\alpha}_{\Theta 1} + C_{RM} \alpha_{\Theta 1} - C_{RM} Z_{\Theta 2} + G_{RM} + F_{RM} + \tau_0 - \tau \tag{15}$$

Consider the second Lyapunov function $L_{\Theta 2}$ as follows:

$$L_{\Theta 2}(Z_{\Theta 1}(t), Z_{\Theta 2}(t)) = L_{\Theta 1}(Z_{\Theta 1}(t)) + \frac{1}{2} Z_{\Theta 2}^T M_{RM} Z_{\Theta 2} \tag{16}$$

The derivative of $L_{\Theta 2} = (Z_{\Theta 1}(t), Z_{\Theta 2}(t))$ is:

$$\dot{L}_{\Theta 2} = Z_{\Theta 1}^T (Z_{\Theta 2}(t) - \lambda_{\Theta 1} Z_{\Theta 1}) + \frac{1}{2} Z_{\Theta 2}^T \dot{M}_{RM} Z_{\Theta 2} + Z_{\Theta 2}^T M_{RM} \dot{Z}_{\Theta 2} \tag{17}$$

Substituting (15) into (17) and use Property 2, we have:

$$\begin{aligned} \dot{L}_{\Theta 2} &= Z_{\Theta 1}^T (Z_{\Theta 2}(t) - \lambda_{\Theta 1} Z_{\Theta 1}) + \frac{1}{2} Z_{\Theta 2}^T \dot{M}_{RM} Z_{\Theta 2} \\ &\quad + Z_{\Theta 2}^T (M_{RM} \dot{\alpha}_{\Theta 1} + C_{RM} \alpha_{\Theta 1} - C_{RM} Z_{\Theta 2} + G_{RM} + F_{RM} + \tau_0 - \tau) \\ &= Z_{\Theta 1}^T Z_{\Theta 2}(t) - Z_{\Theta 1}^T \lambda_{\Theta 1} Z_{\Theta 1} + \frac{1}{2} Z_{\Theta 2}^T \left(\dot{M}_{RM} - 2C_{RM} \right) Z_{\Theta 2} + Z_{\Theta 2}^T (y + \tau_0 - \tau) \\ &= Z_{\Theta 1}^T Z_{\Theta 2}(t) - Z_{\Theta 1}^T \lambda_{\Theta 1} Z_{\Theta 1} + Z_{\Theta 2}^T (y + \tau_0 - \tau) \end{aligned} \tag{18}$$

With

$$y = M_{RM} \dot{\alpha}_{\Theta 1} + C_{RM} \alpha_{\Theta 1} + G_{RM} + F_{RM} \tag{19}$$

To continue our design, the adaptive control law is presented as:

$$\tau = y + \lambda_{\Theta 2} Z_{\Theta 2} + Z_{\Theta 1} + \tau_0, \ \lambda_{\Theta 2} > 0 \tag{20}$$

Substituting (20) into (18), we have:

$$\dot{L}_{\Theta 2} = -Z_{\Theta 1}^T \lambda_{\Theta 1} Z_{\Theta 1} - Z_{\Theta 2}^T \lambda_{\Theta 2} Z_{\Theta 2} \leq 0 \tag{21}$$

Since (21), $\dot{L}_{\Theta 2} < 0$, so $\dot{L}_{\Theta 2}(Z_{\Theta 1}(t), Z_{\Theta 2}(t)) < \dot{L}_{\Theta 2}(Z_{\Theta 1}(0), Z_{\Theta 2}(0))$. If $Z_{\Theta 1}(t), Z_{\Theta 2}(t)$ are bounded with $t > 0$. By defining $\Omega(t) = Z_{\Theta 1}^T \lambda_{\Theta 1} Z_{\Theta 1} + Z_{\Theta 2}^T \lambda_{\Theta 2} Z_{\Theta 2}$ so $\Omega(t) \leq \dot{L}_{\Theta 2}(Z_{\Theta 1}(t), Z_{\Theta 2}(t))$ and integrate the $\Omega(t)$ with respect to time as follows:

$$\int_0^t \Omega(\xi)\, d\xi \leq L_{\Theta 2}(Z_{\Theta 1}(t), Z_{\Theta 2}(t)) - L_{\Theta 2}(Z_{\Theta 1}(0), Z_{\Theta 2}(0)) \tag{22}$$

Because $L_{\Theta 2}(Z_{\Theta 1}(0), Z_{\Theta 2}(0))$ is a bounded function and $L_{\Theta 2}(Z_{\Theta 1}(t), Z_{\Theta 2}(t))$ is nonincreasing and bounded, we have:

$$\lim_{t \to \infty} \int_0^t \Omega(\xi)\, d\xi < \infty \tag{23}$$

According to Barbalat's Lemma [20], when $\dot{\Omega}(t)$ is bounded function. It can be shown that $\lim\limits_{t \to \infty} \int\limits_0^t \Omega(t)\, dt = 0$. From this result, we see that, $Z_{\mathfrak{L}1}(t), Z_{\mathfrak{L}2}(t)$ will converge to zero when $t \to \infty$ and the global stability of the control system for RM is guaranteed.

2.3 Structure of adaptive Fuzzy Neural Networks

A fuzzy logic system includes four parts: the knowledge base, the fuzzifier, the fuzzy inference engine working on fuzzy rules, and the defuzzifier. The knowledge base of the fuzzy logic system is a collection of fuzzy IF-THEN rules of the following form:

R^1: IF s_1 is R_1^l and s_2 is R_2^l and ... and s_2 is R_n^l, THEN y is G^l, $l = 1, 2, ..., N$

Where $s = (s_1, ..., s_n)^T$ and y are the fuzzy logic system input and output, respectively. F_i^l, G^l are associated with the fuzzy membership functions $\mu_{F_i^l}(s_i)$ and $\mu_{G^l}(y)$, respectively. N is the number of rules.

The output of the fuzzy system can be expressed as:

$$y(s) = \frac{\sum_{l=1}^{N} \delta_l \prod_{i=1}^{n} \mu_{F_i^l}(s_i)}{\sum_{l=1}^{N} \left[\prod_{i=1}^{n} \mu_{F_i^l}(s_i)\right]}$$

Where $\delta_l = \max_{y \in R} \mu_{G^l}(y)$ and $\delta = [\delta_1, \delta_2, ..., \delta_N]^T$.

The FNNs structure includes four - layer as shown in Fig. 2, which comprises the input, membership, rule and output layers.

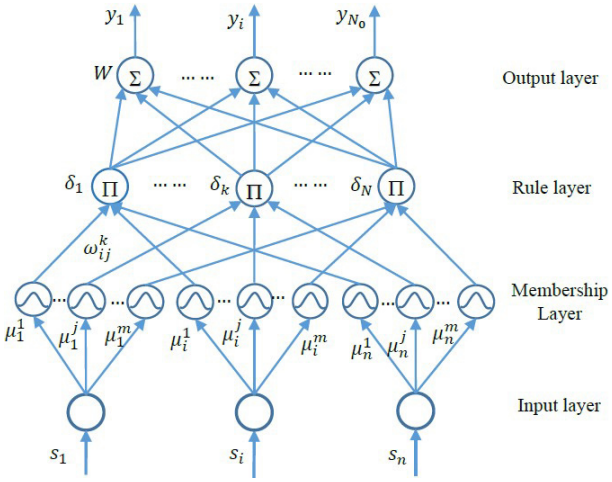

Figure 2: The FNNs structure.

Layer 1 (Input layer): Each node in this layer corresponds to one input linguistic variables s_i $(i = 1, 2, \ldots, n)$, and only transmits directly input values to the next layer.

Layer 2 (Membership layer): In this layer, each node represents the input values with the following Gaussian membership functions:

$$\mu_i^j(s_i) = exp\left[-\left(s_i - m_i^j\right)^2 / \left(b_i^j\right)^2\right] \tag{24}$$

Where m_i^j and b_i^j $(i = 1, 2, \ldots, n; j = 1, 2, \ldots, m)$ are, respectively, the center and standard deviation of the Gaussian membership function of the i^{th} input variable x_i to the node of this layer, and m denotes the total number of membership functions.

Layer 3 (Rule layer): Each node in this layer, which is described as a fuzzy rule, multiplies the inputs signal and the outputs result of the product. The output value of this layer is calculated:

$$\delta_k = \prod_{i=1}^{n} \omega_{ij}^k \mu_i^j(s_i), k = 1, 2, \ldots, N \tag{25}$$

Where δ_k is the k^{th} output of the rule layer, ω_{ji}^k is the weight between the membership layer and the rule layer, and N is the total number of rules.

Layer 4 (Output layer): In this layer, each node represents the output linguistic variables, and acts as a defuzzifier. The output can be represented as follows:

$$y_f = \sum_{1}^{N} w_k^f \delta_k \tag{26}$$

Moreover, (26) can be rewritten:

$$y = [y_1 y_2 \dots y_{N_0}]^T = W\delta = y_{FNNs}(s, W, m, b) \tag{27}$$

With

$$W = [w_1 w_2 \dots w_{N_0}]^T \tag{28}$$

$$\delta = [\delta_1 \delta_2 \dots \delta_N]^T \tag{29}$$

Where $w = \left[w_1^i \; w_2^i \dots w_N^i\right]^T$.

Next, we employ this FNNs as an approximator in our control design. Base on approximation error analysis, there exists an optimal FNNs with its optimal parameters:

$$y(s(t)) = W^{*T}\delta^*(s(t), m^*, b^*) + \Delta(s(t)) \tag{30}$$

Where W^*, m^*, b^* are the optimal parameters of W, m, b, respectively, $\Delta(s(t))$ is the approximation error vector.

Assumption 1: the bound of optimal FNNs parameters:

$$\|W^*\| \le \mathfrak{L}_w, \|m^*\| \le \mathfrak{L}_m, \|b^*\| \le \mathfrak{L}_b \tag{31}$$

Where $\mathfrak{L}_w, \mathfrak{L}_m, \mathfrak{L}_b$ are the positive real values.

Assumption 2: Error of approximation process is bounded:

$$\|\Delta^*\| \le \mathfrak{L}_\Delta \tag{32}$$

Where $\mathfrak{L}_\Delta$ is the positive real value. The output of the FNNs is the approximate value and is represented as the following:

$$\hat{y} = \hat{W}^T\hat{\delta}\left(s(t), \hat{m}, \hat{b}\right) \tag{33}$$

Where $\hat{y}, \hat{W}, \hat{m}, \hat{b}$ are the approximate values of y, W^*, m^*, b^*, respectively.

3 Control design and stability analysis

3.1 Control design

We recommend the RAFNNs to find an adaptive law of the suitable adaptive RAFNNs model that makes control system able to achieve the required approximation errors accuracy.

Architecture of the dead zone compensator is shown in Fig. 3.

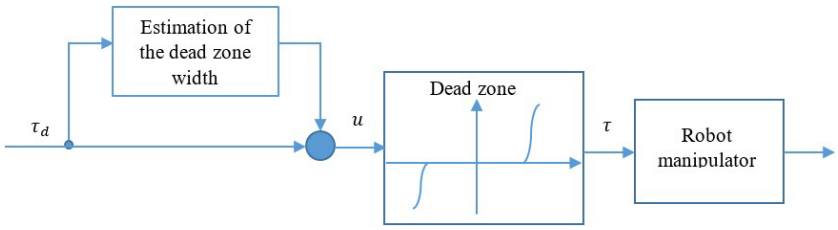

Figure 3: Adaptive dead zone compensation.

To compensate the effects of dead zone, the control input after passing the dead zone can be described in the following form [19]:

$$u = \tau_d + \eta\hat{d}_r + (I - \eta)\hat{d}_l \tag{34}$$

Where $\eta = I$ if $\tau_d \geq 0$, $\eta = 0$ if $\tau_d < 0$. The direct control input for robot manipulator can be expressed as follows:

$$\tau = \tau_d + \eta\hat{d}_r + (I - \eta)\,\hat{d}_l - E_D\left(\tau_d + \eta\hat{d}_r + (I - \eta)\,\hat{d}_l\right) = \tau_d - \tilde{D}^T\Xi + \tilde{D}^T\odot \tag{35}$$

Where $\tilde{D} = D - \hat{D}$, $\tilde{D} = diag\left\{\tilde{d}_1, \tilde{d}_2, \ldots, \tilde{d}_n\right\}$ and $\Xi = [\eta, \quad I - \eta]^T$ and the modelling mismatch $\odot$ satisfies the bound [7].

$$\|\odot\| \leq \sqrt{n} \tag{36}$$

Here, we proposed an intelligent controller which combines adaptive fuzzy neural networks control and Backstepping technique to suppress the effects of the uncertainties and approximation errors. Thus, the unknown functions of robot manipulator control system are estimated, and the stability can be guaranteed. The block diagram of RAFNNs is described in Fig. 4.

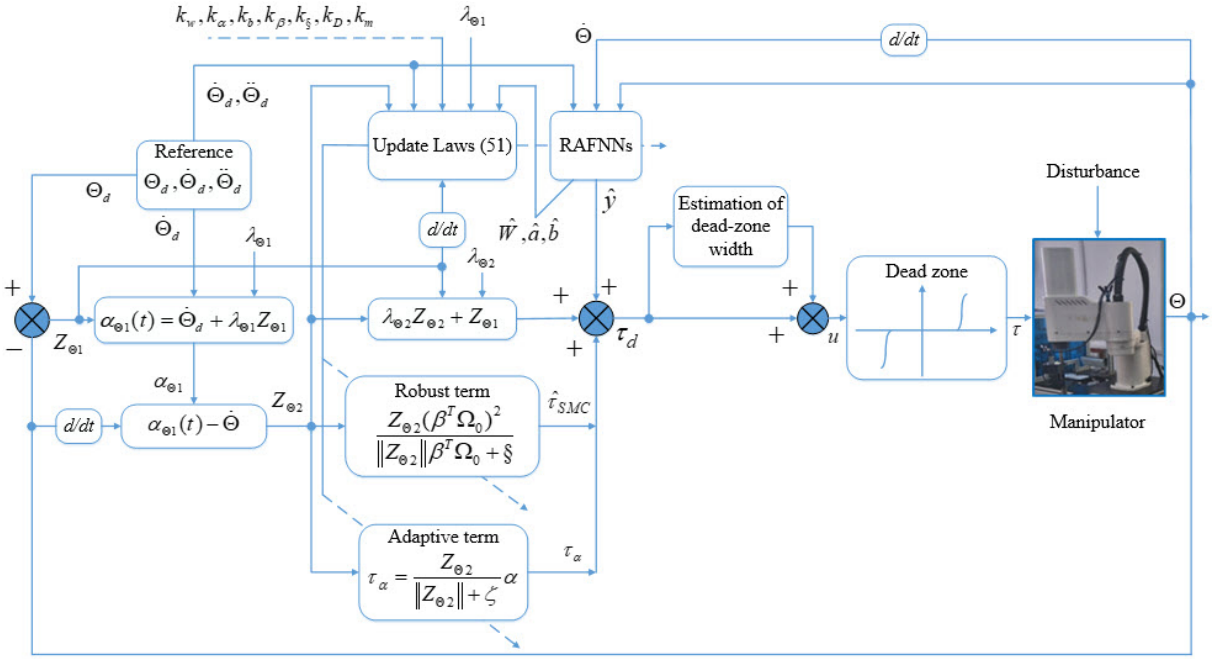

Figure 4: The block diagram of the adaptive control system.

The RAFNNs control law is presented as:

$$\tau_d = \hat{y} + \lambda_{\Theta 2} Z_{\Theta 2} + Z_{\Theta 1} + \tau_{SMC} + \tau_\alpha - \tilde{D}^T\Xi + \tilde{D}^T\odot \tag{37}$$

Where $\hat{y}$ is the approximation of y function, τ_{SMC} is a sliding control term, and τ_α is the adaptive control.

By using the RAFNNs control law (37) into (12), we can be rewritten as:

$$M_{RM}\dot{Z}_{\Theta 2} = \tilde{y} - (C_{RM} + \lambda_{\Theta 2})\,Z_{\Theta 2} - Z_{\Theta 1} + \tau_0 - \tau_{SMC} - \tau_\alpha - \tilde{D}^T\Xi + \tilde{D}^T\odot \tag{38}$$

With

$$\tilde{y} = y - \hat{y} = W^{*T}\delta^* - \hat{W}^T\hat{\delta} + \Delta \tag{39}$$

The parameter errors are defined as: $\tilde{W} = W^* - \hat{W}; \tilde{\delta} = \delta^* - \hat{\delta}; \tilde{m} = m^* - \hat{m}$ and $\tilde{b} = b^* - \hat{b}$. Thus, equation (39) is possible to be rephrased as:

$$\tilde{y} = W^{*T}\tilde{\delta} + \tilde{W}^T\hat{\delta} + \Delta \tag{40}$$

The function $\tilde{\delta}$ can be expanded in a Taylor series as:

$$\tilde{\delta} = \left[\frac{\partial\delta_1}{\partial m}, \frac{\partial\delta_2}{\partial m}, \ldots, \frac{\partial\delta}{\partial m}\right]_{m=\hat{m}} \tilde{m} + \left[\frac{\partial\delta_1}{\partial b}, \frac{\partial\delta_2}{\partial b}, \ldots, \frac{\partial\delta_n}{\partial b}\right]_{b=\hat{b}} \tilde{b} + H\left(\tilde{m}, \tilde{b}\right) \tag{41}$$

Or

$$\tilde{\delta} = \Upsilon^T \tilde{m} + \Gamma^T \tilde{b} + H\left(\tilde{m}, \tilde{b}\right) \tag{42}$$

where $H(\tilde{m}, \tilde{b}) \in R^n$ is the higher - order term vector:

$$\Upsilon^T = \left[\frac{\partial\delta_1}{\partial m}, \frac{\partial\delta_2}{\partial m}, \ldots, \frac{\partial\delta_n}{\partial m}\right]_{m=\hat{m}} \in R^{n\times(nm)};\ \ \Gamma^T = \left[\frac{\partial\delta_1}{\partial b}, \frac{\partial\delta_2}{\partial b}, \ldots, \frac{\partial\delta_n}{\partial b}\right]_{b=\hat{b}} \in R^{n\times(nm)}$$

Substitute (42) into (40), we have:

$$\begin{aligned}\tilde{y} + \tau_0 &= \tilde{W}^T\left[\hat{\delta} + \Upsilon^T(m^* - \hat{m}) + \Gamma^T\left(b^* - \hat{b}\right)\right] + \hat{W}\left(\Upsilon^T\tilde{m} + \Gamma^T\tilde{b}\right) \\ &\quad + W^{*T}H\left(\tilde{m}, \tilde{b}\right) + \Delta + \tau_0 \\ &= \tilde{W}^T\left(\hat{\delta} - \Upsilon^T\hat{m} - \Gamma^T\hat{b}\right) + \hat{W}^T\left(\Upsilon^T\tilde{m} + \Gamma^T\tilde{b}\right) + \omega\left(x, N\right)\end{aligned} \tag{43}$$

Where $\omega = [\omega_1, \omega_2, \ldots, \omega_n]^T \in R^n$ and using (42), we obtain

$$\begin{aligned}\omega &= \tilde{W}^T\left(\Upsilon^T m^* + \Gamma^T b^*\right) + W^{*T}H\left(\tilde{m}, \tilde{b}\right) + \Delta \\ &= \left(W^{*T} - \hat{W}^T\right)\left(\Upsilon^T m^* + \Gamma^T b^*\right) + W^{*T}\left(\tilde{\delta} - \Upsilon^T\tilde{m} - \Gamma^T\tilde{b}\right) + \Delta + \tau_0 \\ &= W^{*T}\left(\tilde{\delta} + \Upsilon^T\hat{m} + \Gamma^T\hat{b}\right) - \hat{W}^T\left(\Upsilon^T m^* + \Gamma^T b^*\right) + \Delta + \tau_0\end{aligned}$$

The bound of ω is determined as:

$$\begin{aligned}\|\omega\| &= \|W^{*T}\left(\tilde{\delta} + \Upsilon^T\hat{m} + \Gamma^T\hat{b}\right) - \hat{W}^T\left(\Upsilon^T m^* + \Gamma^T b^*\right) + \Delta + \tau_0\| \\ &= \|(W^{*T}\tilde{\delta} + \Delta + \tau_0) + W^{*T}\left(\Upsilon^T\hat{m} + \Gamma^T\hat{b}\right) - \hat{W}^T\left(\Upsilon^T m^* + \Gamma^T b^*\right)\|\end{aligned}$$

Since

$$\|W^{*T}\Upsilon^T\hat{m}\| \le \|W^{*T}\Upsilon^T\|\|\hat{m}\|; \|W^{*T}\Gamma^T\hat{b}\| \le \|W^{*T}\Gamma^T\|\|\hat{b}\|;$$
$$\|\hat{W}^T\left(\Upsilon^T m^* + \Gamma^T b^*\right)\| \le \|\hat{W}^T\|\|\Upsilon^T m^* + \Gamma^T b^*\|$$

Hence, we can infer:

$$\begin{aligned}\|\omega\| &\le \|W^{*T}\tilde{\delta} + \Delta + \tau_0\| + \|W^{*T}\Upsilon^T\|\|\hat{m}\|\|W^{*T}\Gamma^T\|\|\hat{b}\|\|\hat{W}^T\|\|\Upsilon^T m^* + \Gamma^T b^*\| \\ &\le \left[\|W^{*T}\tilde{\delta} + \Delta + \tau_0\|, \|W^{*T}\Upsilon^T\|, \|W^{*T}\Gamma^T\|, \left(\|\Upsilon^T m^* + \Gamma^T b^*\|\right)\right]^T \left[1, \|\hat{m}\|, \|\hat{b}\|, \|\hat{W}\|\right] \\ &\le \beta^{*T}\Omega_0\end{aligned} \tag{44}$$

Where

$$\beta^* = \left[\|W^{*T}\tilde{\delta} + \Delta + \tau_0\|, \|W^{*T}\Upsilon^T\|, \|W^{*T}\Gamma^T\|, \left(\|\Upsilon^T m^* + \Gamma^T b^*\|\right)\right]^T; \Omega_0 = \left[1, \|\hat{m}\|, \|\hat{b}\|, \|\hat{W}\|\right]^T$$

Follow above analysis, a sliding mode control term τ_{SMC} is designed by:

$$\tau_{SMC} = \frac{Z_{\Theta 2}\left(\beta^T\Omega_0\right)^2}{\|Z_{\Theta 2}\|\beta^T\Omega_0 + \mathcal{S}} \tag{45}$$

Where $\mathcal{S}$ is a positive scalar control gain

$$\dot{\mathcal{S}} = -k_{\mathcal{S}}\mathcal{S}, \mathcal{S}(0) > 0 \tag{46}$$

With $\beta = [\beta_1, \beta_2, \beta_3, \beta_4]^T$ is a bound of vector β^*.
To estimate the sliding control term τ_{SMC} we present adaptive term $\hat{\tau}_{SMC}$ as:

$$\hat{\tau}_{SMC} = \frac{Z_{\Theta 2}\left(\hat{\beta}^T \Omega_0\right)^2}{\|Z_{\Theta 2}\|\hat{\beta}^T\Omega_0 + \mathcal{S}} \tag{47}$$

Where $\hat{\beta}$ is the estimate of β^*.
The adaptive control τ_α is designed by:

$$\tau_\alpha = \frac{Z_{\Theta 2}}{\|Z_{\Theta 2}\| + \zeta}\alpha \tag{48}$$

Where $\zeta > 0$ and it is chosen such that $\int_0^\infty \zeta dt < \infty$.
With the adaptation law as follows:

$$\dot{\alpha} = \frac{\|Z_{\Theta 2}\|^2}{\|Z_{\Theta 2}\| + \zeta} \tag{49}$$

Applying (43) to (38), yields:

$$\begin{aligned} M_{RM}\dot{Z}_{\Theta 2} = \tilde{W}^T\left(\hat{\delta} - \Upsilon^T\hat{m} - \Gamma^T\hat{b}\right) + \hat{W}^T\left(\Upsilon^T\tilde{m} + \Gamma^T\tilde{b}\right) + \omega \\ - \left(C_{RM} + \lambda_{\Theta 2}\right)Z_{\Theta 2} - Z_{\Theta 1} - \tau_{SMC} - \tau_\alpha - \tilde{D}^T\Xi + \tilde{D}^T\odot \end{aligned} \tag{50}$$

Based on the aforementioned analysis, the online adaptive update laws of RAFNNs, adaptive control, and sliding control term parameters can be chosen as:

$$\begin{cases} \dot{\hat{W}} = k_W(\hat{\delta} - \Upsilon^T\hat{m} - \Gamma^T\hat{b})Z_{\Theta 2}^T \\ \dot{\hat{m}} = k_m\hat{W}\Upsilon^T Z_{\Theta 2} \\ \dot{\hat{b}} = k_b\hat{W}\Gamma^T Z_{\Theta 2} \\ \dot{\hat{\beta}} = k_\beta\|Z_{\Theta 2}\|\Omega_0 \\ \dot{\mathcal{S}} = -k_{\mathcal{S}}\mathcal{S} \\ \dot{\alpha} = \frac{k_\alpha\|Z_{\Theta 2}\|^2}{\|Z_{\Theta 2}\|+\zeta} \\ \dot{\hat{D}} = k_D\Xi Z_{\Theta 2}^T - k_D\alpha_D\hat{D}\|Z_{\Theta 2}\| \end{cases} \tag{51}$$

Here $k_w, k_m, k_b, k_\beta, k_{\mathcal{S}}, k_\alpha, k_D$ are positive adaptation rates.

3.2 Stability analysis

Theorem 1: Consider the RAFNNs adaptive control law of an n-link robot manipulator represented by (1) is designed in (37), and a sliding control term τ_{SMC} is given by (45), the adaptation control is defined in (48) and the parameters $\dot{\hat{W}}$, $\dot{\hat{m}}$, $\dot{\hat{b}}$, $\dot{\hat{\beta}}$, $\dot{\mathcal{S}}$, $\dot{\alpha}$, $\dot{\hat{D}}$ are adjusted by the adaptive algorithm (51). Then the position tracking error and all the system parameters converges to zero.

Proof: The Lyapunov function candidate is chosen as follows as:

$$L(t) = \frac{1}{2}\left[Z_{\Theta 1}^{T} Z_{\Theta 1} + Z_{\Theta 2}^{T} M_{RM} Z_{\Theta 2} + \frac{1}{k_w}\tilde{W}^T\tilde{W} + \frac{1}{k_m}\tilde{m}^T\tilde{m} + \frac{1}{k_b}\tilde{b}^T\tilde{b} + \frac{1}{k_\beta}\tilde{\beta}^T\tilde{\beta} + \frac{2}{k_{\mathcal{S}}}\mathcal{S} + \frac{1}{k_\alpha}\alpha^2 + \frac{1}{k_D} tr\left(\tilde{D}^T\tilde{D}\right)\right] \tag{52}$$

The derivative of $L(t)$ along to time, we have:

$$\dot{L}(t) = Z_{\Theta 1}^{T}\left(Z_{\Theta 2}(t) - \lambda_{\Theta 1} Z_{\Theta 1}\right) + \frac{1}{2} Z_{\theta 2}^{T}\dot{M}_{RM} Z_{\Theta 2} + Z_{\Theta 2}^{T} M_{RM}\dot{Z}_{\Theta 2} - \frac{1}{k_w}\tilde{W}^T\dot{\hat{W}} - \frac{1}{k_m}\tilde{m}^T\dot{\hat{m}} - \frac{1}{k_b}\tilde{b}^T\dot{\hat{b}} - \frac{1}{k_\beta}\tilde{\beta}^T\dot{\hat{\beta}} + \frac{1}{k_{\mathcal{S}}}\dot{\mathcal{S}} + \frac{1}{k_\alpha}\alpha\dot{\alpha} - \frac{1}{k_D} tr\left(\tilde{D}^T\dot{\hat{D}}\right) \tag{53}$$

Substitute (50) into (53) and using property 2, we obtain:

$$\begin{aligned}\dot{L}(t) = {} & -Z_{\Theta 1}^{T}\lambda_{\Theta 1} Z_{\Theta 1} - Z_{\Theta 2}^{T}\lambda_{\Theta 2} Z_{\Theta 2} + Z_{\Theta 2}^{T}\left[\tilde{W}^T\left(\hat{\delta} - \Upsilon^T\hat{m} - \Gamma^T\hat{b}\right)\right. \\ & \left. + \hat{W}^T\left(\Upsilon^T\tilde{m} + \Gamma^T\tilde{b}\right) + \omega - \tau_{SMC} - \tau_\alpha + \tilde{D}^T\Xi - \tilde{D}^T\odot\right] - \frac{1}{k_w}\tilde{W}^T\dot{\hat{W}} - \frac{1}{k_\upsilon}\tilde{m}^T\dot{\hat{m}} \\ & - \frac{1}{k_b}\tilde{b}^T\dot{\hat{b}} - \frac{1}{k_\beta}\tilde{\beta}^T\dot{\hat{\beta}} + \frac{1}{k_{\mathcal{S}}}\dot{\mathcal{S}} + \frac{1}{k_\alpha}\alpha\frac{k_\alpha\|Z_{\theta 2}\|^2}{\|Z_{\theta 2}\| + \zeta} - \frac{1}{k_D} tr\left(\tilde{D}^T\dot{\hat{D}}\right)\end{aligned} \tag{54}$$

Substituting the adaptive algorithm (51) to (54), we have:

$$\begin{aligned}\dot{L}(t) = {} & -Z_{\Theta 1}^{T}\lambda_{\Theta 1} Z_{\Theta 1} - Z_{\Theta 2}^{T}\lambda_{\Theta 2} Z_{\Theta 2} + Z_{\Theta 2}^{T}(\omega - \tau_{SMC} - \tau_\alpha) + Z_{\Theta 2}^{T}\left(\tilde{D}^T\Xi - \tilde{D}^T\odot\right) \\ & - \tilde{\beta}^T\|Z_{\Theta 2}\|\Omega_0 - \mathcal{S} + \alpha\frac{\|Z_{\Theta 2}\|^2}{\|Z_{\Theta 2}\| + \zeta} - tr\left(\tilde{D}^T\left(\Xi Z_{\Theta 2}^{T} - \alpha_D\hat{D}\|Z_{\Theta 2}\|\right)\right)\end{aligned} \tag{55}$$

By using (44), (45) and (48), it becomes:

$$\begin{aligned}\dot{L}(t) \le {} & -Z_{\Theta 1}^{T}\lambda_{\Theta 1} Z_{\Theta 1} - Z_{\Theta 2}^{T}\lambda_{\Theta 2} Z_{\Theta 2} - Z_{\Theta 2}^{T}\frac{Z_{\Theta 2}\left(\hat{\beta}^T\Omega_0\right)^2}{\|Z_{\Theta 2}\|\hat{\beta}^T\Omega_0 + \mathcal{S}} + Z_{\Theta 2}^{T}\beta^{*T}\Omega_0 \\ & - \tilde{\beta}^T\|Z_{\Theta 2}\|\Omega_0 - \mathcal{S} + tr\left(\tilde{D}^T Z_{\Theta 2}^{T}\left(\alpha_D\hat{D} - \odot\right)\right) \\ \le {} & -Z_{\Theta 1}^{T}\lambda_{\Theta 1} Z_{\Theta 1} - Z_{\Theta 2}^{T}\lambda_{\Theta 2} Z_{\Theta 2} + \frac{\mathcal{S}\|Z_{\Theta 2}\|\hat{\beta}^T\Omega_0}{\mathcal{S}\|Z_{\Theta 2}\|\hat{\beta}^T\Omega_0 + \mathcal{S}} - \mathcal{S} + tr\left(\tilde{D}^T Z_{\Theta 2}^{T}\left(\alpha_D\hat{D} - \odot\right)\right)\end{aligned} \tag{56}$$

Since the sum of the last two terms in (56) is always less than zero, we can place the new upper bound on $\dot{L}$.

$$\dot{L}(t) \le -Z_{\Theta 1}^{T}\lambda_{\Theta 1} Z_{\Theta 1} - Z_{\Theta 2}^{T}\lambda_{\Theta 2} Z_{\Theta 2} + tr\left(\tilde{D}^T Z_{\Theta 2}^{T}\left(\alpha_D\left(D - \tilde{D}\right) - \odot\right)\right) \tag{57}$$

By using $tr\tilde{D}^T\left(D - \tilde{D}\right) = \left(\tilde{D}, D\right) - \|\tilde{D}\|^2 \le \|\tilde{D}\|\|D\| - \|\tilde{D}\|^2$ and using (36) into the inequality (57) could be rewritten as follows:

$$\begin{aligned}\dot{L} & \le -Z_{\Theta 1}^{T}\Omega_{\Theta 1} Z_{\Theta 1} - Z_{\Theta 2}^{T}\Omega_{\Theta 2} Z_{\Theta 2} + \sqrt{n}\|Z_{\Theta 2}\|\|\tilde{D}\| + \alpha_D D_M\|Z_{\Theta 2}\|\|\tilde{D}\| - \alpha_D\|Z_{\Theta 2}\|\|\tilde{D}\|^2 \\ & \le -Z_{\Theta 1}^{T}\Omega_{\Theta 1} Z_{\Theta 1} - Z_{\Theta 2}^{T}\Omega_{\Theta 2} Z_{\Theta 2} + c_0\|Z_{\Theta 2}\|\tilde{D}\| - \alpha_D\|Z_{\Theta 2}\|\|\tilde{D}\|^2\|\end{aligned} \tag{58}$$

With $c_0 = \sqrt{n} + \alpha_D D_M$.

We see that to make sure $\dot{L} \leq 0$

$$-c_0\|Z_{\Theta 2}\|\|\tilde{D}\| + \alpha_D\|Z_{\Theta 2}\|\|\tilde{D}\|^2 > 0 \tag{59}$$

So, if we choose suitable constant vectors α_D, D_M which satisfy (59), $\dot{L}\left(Z_{\Theta 1}(t), Z_{\Theta 2}(t), \mathcal{S}(t), \tilde{W}, \tilde{a}, \tilde{b}, \tilde{\beta}\right) \leq 0$, $\dot{L}\left(Z_{\Theta 1}(t), Z_{\Theta 2}(t), \mathcal{S}(t), \tilde{W}, \tilde{a}, \tilde{b}, \tilde{\beta}\right)$ is a negative semidefinite function, $\dot{L}\left(Z_{\Theta 1}(t), Z_{\Theta 2}(t), \mathcal{S}(t), \tilde{W}, \tilde{a}, \tilde{b}, \tilde{\beta}\right) \leq \dot{L}\left(Z_{\Theta 1}(0), Z_{\Theta 2}(0), \mathcal{S}(0), \tilde{W}, \tilde{b}, \tilde{\beta}\right)$, if all parameters such as $Z_{\Theta 1}(t), Z_{\Theta 2}(t), \mathcal{S}(t), \tilde{W}, \tilde{a}, \tilde{b}, \tilde{\beta}$ are bounded with $t > 0$. By defining $\epsilon(t) = -Z_{\Theta 1}^T \Omega_{\Theta 1} Z_{\Theta 1} - Z_{\Theta 2}^T \Omega_{\Theta 2} Z_{\Theta 2}$ so $\epsilon(t) \leq -\dot{L}(t)$ and integrate the $\epsilon(t)$ with respect to time as follows:

$$\int_0^t (\xi)\, d\xi \leq L\left(Z_{\Theta 1}(0), Z_{\Theta 2}(0), \mathcal{S}(0), \tilde{W}, \tilde{a}, \tilde{b}, \tilde{\beta}\right) - L\left(Z_{\Theta 1}(t), Z_{\Theta 2}(t), \mathcal{S}(t), \tilde{W}, \tilde{a}, \tilde{b}, \tilde{\beta}\right) \tag{60}$$

Because $L\left(Z_{\Theta 1}(0), Z_{\Theta 2}(0), \mathcal{S}(0), \tilde{W}, \tilde{a}, \tilde{b}, \tilde{\beta}\right)$ is a bounded function, and $L\left(Z_{\Theta 1}(t), Z_{\Theta 2}(t), \mathcal{S}(t), \tilde{W}, \tilde{a}, \tilde{b}, \tilde{\beta}\right)$ is nonincreasing and bounded, we have

$$\lim_{t\to\infty} \int_0^t \epsilon(\xi)\, d\xi < \infty \tag{61}$$

According to Barbalat's Lemma [20], when $\dot{\epsilon}(t)$ is bounded function. It can be shown that $\lim_{t\to\infty} \int_0^t \epsilon(t)\, dt = 0$. From this outcome, we see that, $Z_\Theta(t)$ will converge to zero when $t \to \infty$ and the global stability of the control system for RM is assured by the updated law (37).

4 Simulation and experimental results

4.1 Simulation results

Here, a three-link RM is applied to confirm the efficiency of the suggested control method based on RAFNNs for illustrative purposes. The detailed system parameters of three-link RM model (Fig. 5) are given as follows:

$$M_{RM} = \begin{bmatrix} M_{RM11} & M_{RM12} & M_{RM13} \\ M_{RM21} & M_{RM22} & M_{RM23} \\ M_{RM31} & M_{RM32} & M_{RM33} \end{bmatrix}; C_{RM} = \begin{bmatrix} C_{RM11} & C_{RM12} & C_{RM13} \\ C_{RM21} & C_{RM22} & C_{RM23} \\ C_{RM31} & C_{RM32} & C_{RM33} \end{bmatrix};$$

$$G_{RM} = \begin{bmatrix} G_{RM1} \\ G_{RM2} \\ G_{RM3} \end{bmatrix};$$

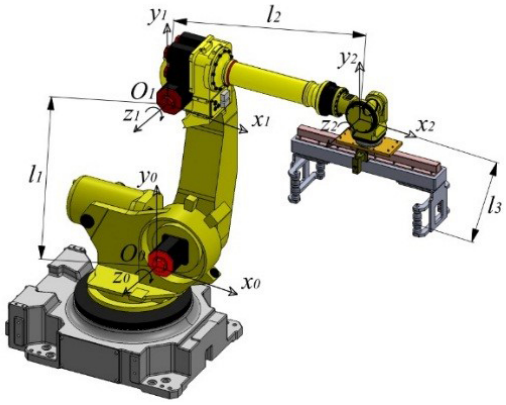

Figure 5: The model of three-joint RM.

$$
\begin{aligned}
M_{RM11} &= (m_1+m_2+m_3)\,l_1^2+(m_2+m_3)\,l_2^2+m_3l_3^2+2\,(m_2+m_3)\,l_1l_2\cos(\Theta_2)\,;\\
&\quad +2m_3l_1l_3\cos(\Theta_2+\Theta_3)+2m_3l_2l_3\cos(\Theta_3)\,;\\
M_{RM12} &= (m_2+m_3)\,l_2^2+m_3l_3^2+(m_2+m_3)\,l_1l_2\cos(\Theta_2)\\
&\quad +m_3l_1l_3\cos(\Theta_2+\Theta_3)+2m_3l_2l_3\cos(\Theta_3)\,;\\
M_{RM13} &= m_3l_3^2+m_3l_1l_3\cos(\Theta_2+\Theta_3)+m_3l_2l_3\cos(\Theta_3)\,;\ M_{RM21}=M_{RM12};\\
M_{RM22} &= (m_2+m_3)\,l_2^2+m_3l_3^2+2m_3l_2l_3\cos(\Theta_3)\,;\ M_{RM23}=m_3l_3^2+m_3l_2l_3\cos(\Theta_3)\,;\\
M_{RM31} &= m_3l_3^2+m_3l_1l_3\cos(\Theta_2+\Theta_3)+m_3l_2l_3\cos(\Theta_3)\,;\\
M_{RM32} &= M_{23};\ M_{RM33}=m_3l_3^2;\\
C_{RM11} &= -2\,(m_2+m_3)\,l_1l_2\sin(\Theta_2)\,\dot{\Theta}_2-2m_3l_1l_3\sin(\Theta_2+\Theta_3)\left(\dot{\Theta}_2+\dot{\Theta}_3\right)\\
&\quad -2m_3l_2l_3\sin(\Theta_3)\,\dot{\Theta}_3;\\
C_{RM12} &= -\,(m_2+m_3)\,l_1l_2\sin(\Theta_2)\,\dot{\Theta}_2-m_3l_1l_3\sin(\Theta_2+\Theta_3)\left(\dot{\Theta}_2\right)\\
&\quad -2m_3l_2l_3\sin(\Theta_3)\,\dot{\Theta}_3-2m_3l_1l_3\sin(\Theta_2+\Theta_3)\,\dot{\Theta}_3;\\
C_{RM13} &= -m_3l_2l_3\sin(\Theta_3)\,\dot{\Theta}_3-m_3l_1l_3\sin(\Theta_2+\Theta_3)\,\dot{\Theta}_3;\ C_{RM22}=-2m_3l_2l_3\sin(\Theta_3)\,\dot{\Theta}_3;\\
C_{RM23} &= -m_3l_2l_3\sin(\Theta_3)\,\dot{\Theta}_3;\ C_{RM32}=m_3l_2l_3\sin(\Theta_3)\,\dot{\Theta}_2;\ C_{RM33}=0;\\
G_{RM1} &= (m_1+m_2+m_3)\,gl_1sin(\Theta_1)+(m_2+m_3)\,gl_2sin(\Theta_1+\Theta_2)\\
&\quad +m_3gl_3sin(\Theta_1+\Theta_2+\Theta_3)\,;\\
G_{RM2} &= (m_2+m_3)\,gl_2sin(\Theta_1+\Theta_2)+m_3gl_3sin(\Theta_1+\Theta_2+\Theta_3)\,;\\
G_{RM3} &= m_3gl_3sin(\Theta_1+\Theta_2+\Theta_3)
\end{aligned}
$$

Where m_1, m_2, m_3 are links masses; l_1, l_2, l_3 are links lengths; The parameters of three link RM are given as follows: $m_1 = 5.4\,(kg)$, $m_2 = 4.4\,(kg)$, $m_3 = 2\,(kg)$, $l_1 = 520\,(mm)$, $l_2 = 420\,(mm)$, $l_3 = 260\,(mm)$; $g = 9.8\,(m/s^2)$.

The desired joint trajectories of the three link robot manipulator are chosen by:

$$\Theta_d = \begin{bmatrix} \Theta_{d1} & \Theta_{d2} & \Theta_{d3} \end{bmatrix}^T = \begin{bmatrix} 0.5\sin(2\pi t) & 0.5\sin(2\pi t) & 0.5\sin(2\pi t) \end{bmatrix}^T.$$

In addition, external disturbances and friction force in this simulation are selected as fol-

lowing:

$$\tau_0 = \begin{bmatrix} 3\sin(\pi t) \\ 3\sin(\pi t) \\ 3\sin(\pi t) \end{bmatrix}; \; F_{IRM}\left(\dot{\Theta}\right) = \begin{bmatrix} 5\dot{\Theta}_1 + 0.3sign\left(\dot{\Theta}_1\right) \\ 5\dot{\Theta}_2 + 0.3sign\left(\dot{\Theta}_2\right) \\ 5\dot{\Theta}_3 + 0.3sign\left(\dot{\Theta}_3\right) \end{bmatrix}.$$

The proposed controller parameter values are given as follows: $\lambda = diag(6,6,6)$; $K = diag(100\ ,\ 110\ ,100)$; $k_w = diag(60,\ 60,\ 60,\ 60,\ 60)$; $k_m = k_b = diag(50,40,50) \in R^{mp\times mp}$; $k_\beta = diag(0.001,0.001,0.001,0.001,0.001)$; $k_{\mathcal{S}} = 0.12$; $k_\alpha = 0.1$,$h_r(u) = u - d_r$; $h_l(u) = u + d_l$; $d_r = 10$; $d_l = -10$; $k_D = 10$; $\alpha_D = 0.2$.

The initial conditions are selected as follows: $\mathcal{S}(0) = 1$, $\Omega_0(0) = [1\ \ 1\ \ 1\ \ 1]$, $\zeta(0) = 1$.

In here, the proposed RAFNNs is applied to control the RM in comparison with the NNs [26] and PID. The simulation results of the NNs, PID and the proposed RAFNNs are shown in Fig. 6. Since the simulated results, we see that, the position tracking of three links with the RAFNNs, NNs, and PID can be guaranteed, and the tracking errors of the NNs, PID and the proposed intelligent controller are converged. However, the proposed intelligent control system converges faster than the NNs and PID systems. It means that all updated parameters in the dynamic structure RAFNNs and the amount of the rule nodes are adjusted, the approximation capability of the dynamics structure RAFNNs is also superior to the NNs and PID systems. Moreover, from Fig. 6 it can be observe that, the control force of the suggested RAFNNs is smoother and has smaller oscillation than the NNs and PID to attain the requested level of performance when the tracking errors reach the high value.

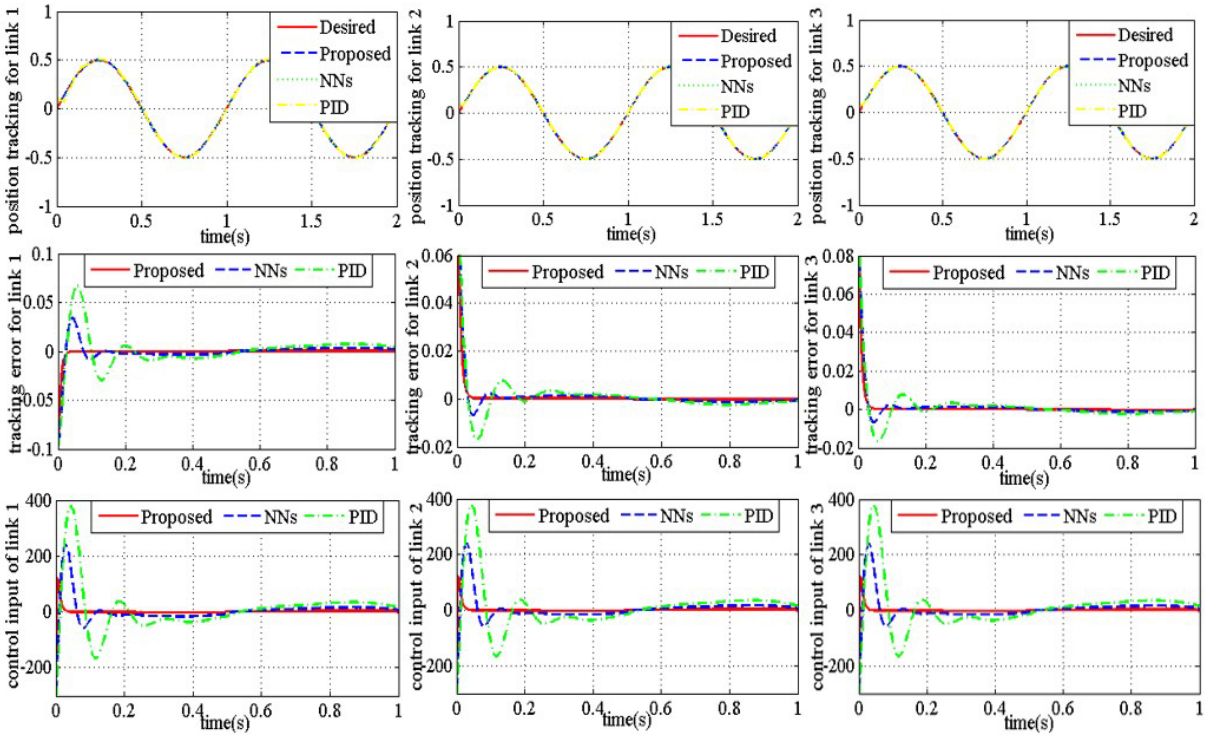

Figure 6: Simulated results of trajectory, tracking errors, and control efforts of the NNs, PID and proposed RAFNNs system.

4.2 Experimental results

Here, we implemented two experimental outcomes to prove the efficiency of the RAFNNs controller on a three-link robot manipulators. Fig. 7 illustrates the experimental control system model.

Figure 7: Experimental control system.

The first experimental example assumes that 0.5-kg payload is added in the masses of three links RM, and all parameters are the same as in the simulation model. The experimental results of joint trajectory, control torques and tracking errors are exposed in Fig. 8. From Fig. 8, we can easily see that the position tracking of RM are still obtained with PID, NNs, and RAFNNs. However the responses and the tracking error norm of the RAFNNs are quite better than the NNs and PID methods. Furthermore, from these results can see that the proposed intelligent controller torques are less and smooth than NNs in [26], and PID which still exist the chattering phenomena when a load of manipulators changed. Therefore, the position tracking performance of the recommended RAFNNs is better than the NNs and PID under parameters variation. It means that due to the dynamic structure, the proposed RAFNNs is less sensitive to the parameter variation than the NNs and PID.

The second experimental case, the external disturbance $d_e(t)$ is suddenly injected more into control system when the robot is tracking a trajectory. This occurred after the first 0.5s of the experimental period, and all other parameters are the same as in the simulation model. The external disturbance shapes are expressed as follows:

$$d_e(t) = [100\sin(100t) \quad 100\sin(100t) \quad 100\sin(100t)\ ]^T$$

.

The experimental outcomes of the second case are shown in Fig. 9. According to these results, it is easy to see that, the performance of the proposed RAFNNs is just slightly affected, while the performance of PID approach is seriously affected. Therefore, the control performance and robustness of the proposed RAFNNs under external disturbance are better than the NNs [26] and PID. It is obvious that the performance of the proposed RAFNNs is better than the NNs and PID system after a period of learning.

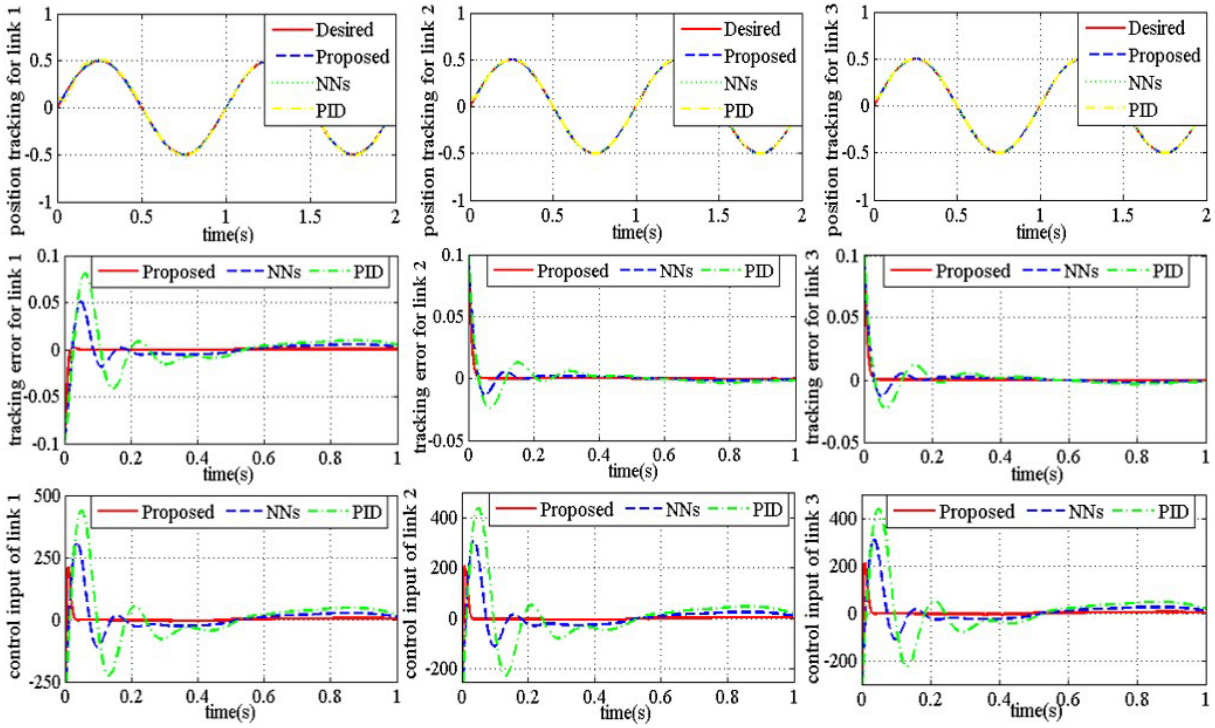

Figure 8: Trajectory, tracking errors, and control efforts of the NNs, PID and proposed RAFNNs system in the first experimental case.

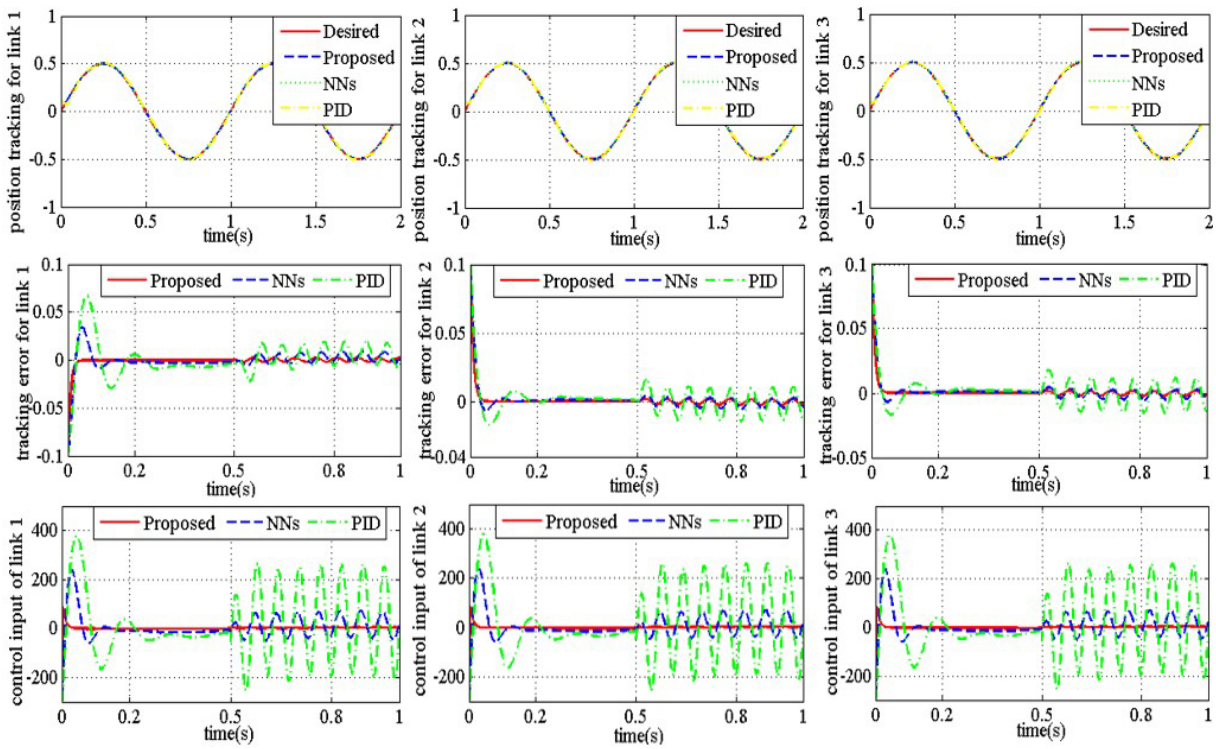

Figure 9: Trajectory, tracking errors, and control efforts of the NNs, PID and proposed RAFNNs system in the second experimental case.

5 Conclusions

In this paper, an adaptive robust control system based on structure FNN has been proposed, and the mathematical proof has been presented. It has been also successfully implemented to control the joints of three-link RM for achieving high precision position tracking and compensation dead-zone. By combining the FNN, Lyapunov stability theorem, the adaptive control laws are developed to tune all parameters of the network in order to reduce approximation error and improved control performance. In addition, the robust term is designed dealing with the approximation error, prime parameter vectors and higher order terms in Taylor series. Therefore, the proposed controller proved that this control system could achieve desired tracking performance. The stability and robustness of the closed-loop manipulators system are guaranteed. Simulation and experimental results of three-links RM via the proposed RAFNNs and NNs, PID also have provided in this study to compare and display. The proposed RAFNNs control systems can be applied to other systems, such as MMR, AC servo systems, and they can also be applied as a good alternative in the existing robot manipulator control system. This application could require further investigations.

Bibliography

[1] Baigzadehnoe, B.; Rahmani, Z.; Khosravi, A.; Rezaie, B. (2017). On position/force tracking control problem of cooperative robot manipulators using adaptive fuzzy backstepping approach, *ISA Transactions*, 70, 432–446, 2017.

[2] Bragina, A. A.; Shcherbakov, V. P.; Shiryaev, V. I. (2018). Synthesis of Adaptive Control of Robotic Manipulator by the Method of Lyapunov Functions, *IFAC-PapersOnLine*, 51, 298–303, 2018.

[3] Chen, C. (2011). Robust Self-Organizing Neural-Fuzzy Control With Uncertainty Observer for MIMO Nonlinear Systems, *IEEE Transactions on Fuzzy Systems*, 19, 694–706, 2011.

[4] Chung, C.; Chang, Y. (2013). Backstepping control of multi-input non-linear systems, *IET Control Theory & Applications*, 7, 1773–1779, 2013.

[5] He, J.; Luo, M.; Zhang, Q.; Zhao, J.; Xu, L. (2016). Adaptive Fuzzy Sliding Mode Controller with Nonlinear Observer for Redundant Manipulators Handling Varying External Force, *Journal of Bionic Engineering*, 13, 600–611, 2016.

[6] He, W.; Dong, Y.; Sun, C. (2015). Adaptive neural network control of unknown nonlinear affine systems with input deadzone and output constraint, *ISA Transactions*, 58, 96–104, 2015.

[7] Ik Han, S.; Lee, J. (2016). Finite-time sliding surface constrained control for a robot manipulator with an unknown deadzone and disturbance, *ISA Transactions*, 65, 307–318, 2016.

[8] Ishii, C.; Shen, T.; Tamura, K. (1997). Robust model-following control for a robot manipulator, *IEE ProcControl Theory Appl*, 144(1), 53–60, 1997.

[9] Jing, C.; Xu, H.; Niu, X. (2019). Adaptive sliding mode disturbance rejection control with prescribed performance for robotic manipulators, *ISA transactions*, 91, 41–51, 2019.

[10] Jing, Z.; Changyun, W.; Ying, Z. (2004). Adaptive backstepping control of a class of uncertain nonlinear systems with unknown backlash-like hysteresis, *IEEE Transactions on Automatic Control*, 49, 1751–1759, 2004.

[11] Karamali Ravandi, A.; Khanmirza, E.; Daneshjou, K. (2018). Hybrid force/position control of robotic arms manipulating in uncertain environments based on adaptive fuzzy sliding mode control, *Applied Soft Computing*, 70, 864–874, 2018.

[12] Khorashadizadeh S.; Sadeghijaleh, M. (2018). Adaptive fuzzy tracking control of robot manipulators actuated by permanent magnet synchronous motors, *Computers & Electrical Engineering*, 72, 100–111, 2018.

[13] Krstic, M.; Kanellakopoulos, I.; Kokotovic, P. V. (1995). *Nonlinear Adaptive Control Design*, New York, NY, USA: Wiley, 1995.

[14] Lewis, F. L.; Tim, K.; Wang, L. Z.; Li, Z. X. (1999). Deadzone compensation in motion control systems using adaptive fuzzy control system, *IEEE Trans. Control. Syst. Technol*, 7, 731–742, 1999.

[15] Peng, J.; Dubay, R. (2019). Adaptive fuzzy backstepping control for a class of uncertain nonlinear strict-feedback systems based on dynamic surface control approach, *Expert Systems with Applications*, 120, 239–252, 2019.

[16] Precup, R.; Tomescu, M.; Preitl, S. (2009). Fuzzy logic control system stability analysis based on Lyapunov's direct method, *International journal of computer, communication & control*, IV, 415–426, 2009.

[17] Rossomando, F. G.; Soria, C.; Carelli, R. (2014). Sliding mode control for trajectory tracking of a non- holonomic mobile robot using adaptive neural networks, *Control Engineering and Applied Informatics*, 16, 12–21, 2014.

[18] Sabahi, F. (2018). Introducing validity into self-organizing fuzzy neural network applied to impedance force control, *Fuzzy Sets and Systems*, 337, 113–127, 2018.

[19] Selmic R. R.; Lewis, F. L. (2000). Deadzone compensation in motion control systems using neural networks, *IEEE Transactions on Automatic Control*, 45, 602–613, 2000.

[20] Slotine J. J. E.; Li, W. (1991). *Applied Nonlinear Control*, Prentice-Hall, Hoboken, NJ, 1991.

[21] Tsai, C.-H.; Chuang, H.-T. (2004). Deadzone compensation based on constrained RBF neural network, *Journal of the Franklin Institute*, 341, 361–374, 2004.

[22] Vrkalovic, S.; Lunca, E.; Borlea, I. (2018). Model-free sliding mode and fuzzy controllers for reverse osmosis desalination plants, *International journal of Artificial intelligence*, 16, 208–222, 2018.

[23] Wai, R.; Muthusamy, R. (2013). Fuzzy-Neural-Network Inherited Sliding-Mode Control for Robot Manipulator Including Actuator Dynamics, *IEEE Transactions on Neural Networks and Learning Systems*, 24, 274–287, 2013.

[24] Wai, R.; Muthusamy, R. (2014). Design of Fuzzy-Neural-Network-Inherited Backstepping Control for Robot Manipulator Including Actuator Dynamics, *IEEE Transactions on Fuzzy Systems*, 22, 709–722, 2014.

[25] Wen, C.; Zhou, J.; Liu, Z.; Su, H. (2011). Robust Adaptive Control of Uncertain Nonlinear Systems in the Presence of Input Saturation and External Disturbance, *IEEE Transactions on Automatic Control*, 56, 1672–1678, 2011.

[26] Wu, Y.; Huang, R.; Li, X.; Liu, S. (2019). Adaptive neural network control of uncertain robotic manipulators with external disturbance and time-varying output constraints, *Neurocomputing*, 323, 108–116, 2019.

[27] Ying, H. (2005). Structure and stability analysis of general mamdani fuzzy dynamic Models, *International journal of intelligent systems*, 20, 103–125, 2005.

[28] Ying, Z.; Changyun, W.; Yeng Chai, S. (2000). Adaptive backstepping control design for systems with unknown high-frequency gain, *IEEE Transactions on Automatic Control*, 45, 2350–2354, 2000.

[29] Zhou, D.; Shi, M.; Chao, F.; Lin, C. M.; Yang, L.; Shang, C.; Zhou, C. (2018). Use of human gestures for controlling a mobile robot via adaptive CMAC network and fuzzy logic controller, *Neurocomputing*, 282, 218–231, 2018.

INTERNATIONAL JOURNAL OF COMPUTERS COMMUNICATIONS & CONTROL
ISSN 1841-9836, e-ISSN 1841-9844, 14(5), 711-732, October 2019.

Bibliometric Analysis on Research Trends of International Journal of Computers Communications & Control

X.X. Wang, Z.S. Xu, I. Dzitac

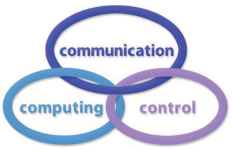

Xinxin Wang
Sichuan University
Business School
Chengdu 610064, China
wangxinxin_cd@163.com

Zeshui Xu*
Sichuan University
Business School
Chengdu 610064, China
*Corresponding author: xuzeshui@263.net

Ioan Dzitac
1. Aurel Vlaicu University of Arad
310330 Arad, Elena Dragoi, 2, Romania
ioan.dzitac@uav.ro
2. Agora University of Oradea
410526 Oradea, P-ta Tineretului 8, Romania,
idzitac@univagora.ro
3. University of Craiova
Department of Economic Informatics & Statistics
Str. A.I. Cuza, nr. 13, Craiova, Romania

Abstract: *International Journal of Computers Communications & Control* (*IJCCC*) is an international journal in the fields of automation control systems and computer science. According to Web of Science (WoS), the first document of *IJCCC* was published in 2006. In this paper, we study the research trends of publications in *IJCCC* by performing bibliometric analysis from 2006 to 2019. 982 publications are selected from WoS after data preprocessing by VOS viewer and CiteSpace. Firstly, fundamental information of publications is explored including the type, the annual trend and the most cited publications in *IJCCC*. Secondly, characteristics of countries/regions, institutions and authors are presented in terms of evaluation indicators. Next, landscape analysis is conducted to show the development of *IJCCC* at level of countries/regions, institutions, authors and references, such as co-authorship analysis, bibliographic coupling analysis, co-citation and burst detection analysis, co-occurrence and timeline view analysis. Based on which, discussions about current challenges and possible research trends of *IJCCC* are provided. Finally, some main findings are summarized. This paper offers a valuable reference for scholars to understand the research trends of *IJCCC* and grasp hot topics related to relative fields.
Keywords: *International Journal of Computers Communications & Control*; bibliometric analysis; Web of Science; landscape analysis; research trends.

1 Introduction

International Journal of Computers Communications & Control (*IJCCC*)is an international journal (ISSN: 1841-9836, e-ISSN 1841-9844) that is directed to the international communities of scientific researchers in computers, communications and control, from the universities, research units and industry. According to the homepage of the journal [32], *IJCCC* publishes 6 issues per year, and calls for topics which are integrated solutions in computer-based control and communications, computational intelligence methods and soft computing, and advanced decision support systems. The editors-in-chief of *IJCCC* are professor Ioan DZITAC and professor Florin Gheorghe FILIP, and the journal was founded in 2006, at Agora University, by Ioan DZITAC, Florin Gheorghe FILIP and Misu-Jan MANOLESCU. This journal is a member of the Committee on Publicatin Ethics (COPE) since 2012, and subscribes to the principles of COPE. *IJCCC* is indexed in Science Citation Index Expanded (SCIE) database from 2006 with an impact factor of 1.585 by Journal Citation Reports (2018), and is also indexed in Scopus database from 2008 with CiteScore (2018) of 1.56. In Web of Science (WoS), *IJCCC* ranks 38 and 108 among totally 62 and 155 academic journals in the fields of automation & control systems, and computer science, respectively. In the past decade, *IJCCC* was nominated by Elservier for Journal Excellence Award - "Scopus Awards Romania 2015" (SNIP2014=1.029), and has been in top 3 of 157 Romanian journals indexed by Scopus (in all fields) and No.1 in Computer Science field by Elservier/Scoupus. Therefore, it is meaningful to study research trends of *IJCCC* systematically and intuitively by bibliometric methods and visualization tools.

Bibliometrics is an important branch of intelligence science, and bibliometric methods have been effective tools so far to evaluate the merits of a given research direction or a certain journal [1,21,27]. On the one hand, the evolution of a research direction could be revealed by bibliometric methods, because bibliometrics is a discipline with the extensive intersection and combination of philology, information science and statistics in a specific area [8]. At present, bibliometrics has been applied to many research fields, such as fuzzy decision making [16], engineering [17], supply chain of renewable energy [2] and sustainable energy [7]. On the other hand, the development trend of a journal could be explored based on bibliometric analysis. For example, productivity and influence could be evaluated by some generally accepted bibliometric indicators, such as total number of publications (TP), total number of citations (TC), average number of citations per publication (AC), and H-index [10]. Bibliometric analysis has attracted more and more scholars to research journals, such as *European Journal of Operational Research* [14], *IEEE Transaction on Fuzzy Systems* [28], *Technological and Economic Development of Economy* [Yu1], *Information Sciences* [30] and *Knowledge-Based Systems* [31].

Visualization is one of the most important techniques in bibliometric analysis, because it helps scholars intuitively see the structure and the trend of a research field or a journal [5]. Due to that VoS viewer [22] and CiteSpace [4] have powerful user graphic-interface and mapping visualization capability, they have been the most popular tools to make landscape analysis. VoS viewer could present the structure of publications in the journal by co-authorship analysis, bibliographic coupling analysis and co-occurrence analysis, etc. CiteSpace could grasp hot topics and track development trend of the journal by burst detection analysis and timeline analysis. Until now, VoS viewer and CiteSpace have been widely used in many areas, such as food chemistry [12], computer and information ethics [9], emergency medicine [3], and information literacy assessment [19].

Since WoS is one of the most widely-used databases in academics, and provides many leading journals available and detailed information about publications around the world [6], we collect data using the name of the journal from WoS Core Collection database on September 18, 2019. All publications in *IJCCC* are exported in plain text format and Comma-Separated Values (CSV)

format, which contain bibliographic information, keywords information and citation information, etc. As a result, 982 publications are derived in WoS since first publication in 2006. Therefore, we make a bibliometric analysis to study the research trends of *IJCCC* from 2006 to 2019.

In this paper, the contributions lie in the following aspects:

(1) Fundamental information of publications is provided to describe the inner structure of *IJCCC*, which includes the type, the annual trend and the most cited publications.

(2) Characteristics of publications in *IJCCC* are presented at the level of countries/regions, institutions and authors by some bibliometric indictors.

(3) Landscape analysis is given by co-authorship analysis, bibliographic coupling analysis, co-citation and burst detection analysis, co-occurrence analysis and timeline view analysis.

(4) The current challenges and research trends of *IJCCC* are discussed according to the above-mentioned analysis.

The rest of this paper is organized as follows: Section 2 illustrates fundamental information. In Section 3, the characteristics of publications are given at level of countries/regions, institutions and authors. Section 4 makes landscape analysis. In Section 5, some discussions are provided about current challenges and research trends in *IJCCC*. Section 6 ends the paper with some conclusions.

2 Fundamental information of publications in *IJCCC*

In this section, we introduce the fundamental information of publications in *IJCCC* from 2006 to 2019, including the type of publications, the annual trend of publications, and the most cited publications in *IJCCC*.

2.1 Type of publications in IJCCC

Automation control systems and computer science are research directions of publications in *IJCCC*. In WoS, the publications in *IJCCC* are dived into six types, which are articles, proceeding papers, editorial materials, biographic items, corrections and reviews in order. Figure 1 shows the information in detail.

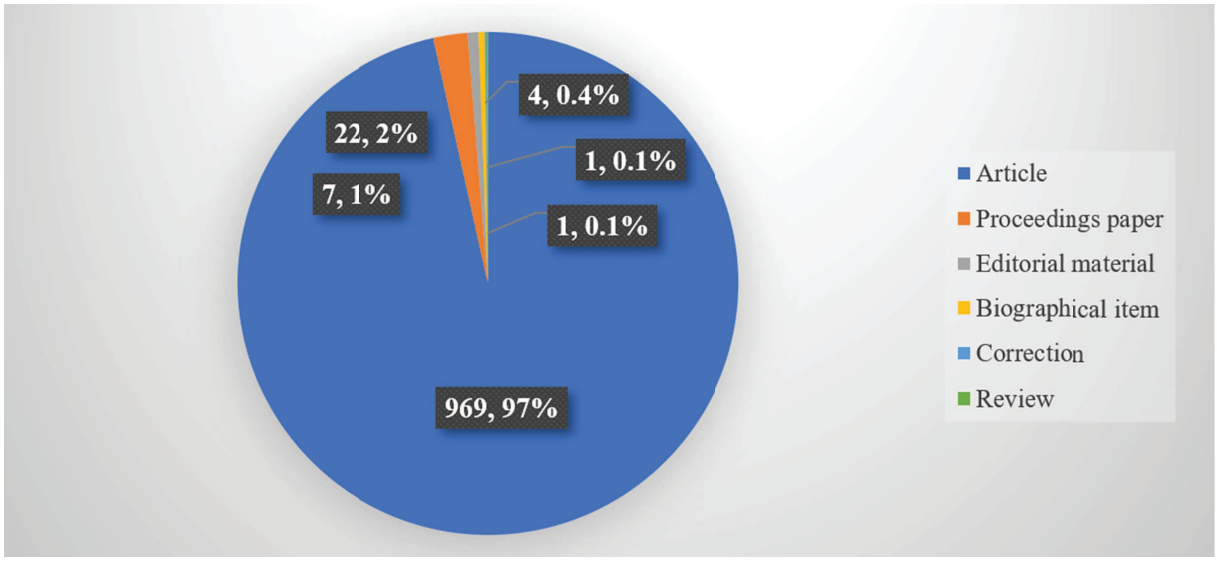

Figure 1: The type of publications in *IJCCC*

Table 1: Annual information of publications in *IJCCC* from 2006 to 2019

Year	TP	TC	AC	H-index
2006	85	88	1.04	5
2007	35	304	8.69	11
2008	**125**	**701**	5.61	**14**
2009	41	396	**9.66**	10
2010	92	436	4.74	10
2011	65	329	5.06	9
2012	85	341	4.01	9
2013	85	433	5.09	11
2014	73	261	3.58	9
2015	75	350	4.67	9
2016	64	235	3.67	7
2017	59	153	2.59	6
2018	59	116	1.97	4
2019	39	28	0.72	3

Obviously, articles are the most type of publications in *IJCCC* with the number of 969, which occupies a comparatively great proportion (97%) of all documents. The types are followed by proceeding papers (22, 2%), editorial materials (7, 1%), biographic items (4, 0.4%), corrections (1, 0.1%) and reviews (1, 0.1%).

2.2 Annual trend of publications in IJCCC

In order to describe the trend of publications in *IJCCC* from 2006 to 2019, Table 1 lists the annual information in terms of some evaluation indicators, i.e., TP, TC, AC and H-index.

Noted that the maximum value under each indicator is highlighted in bold. Obviously, 2008 is the most prominent year because of the highest TP (125), the highest TC (701) and the highest H-index (14). Besides, the publications in 2009 have the highest AC (9.66), followed by 2007 (8.69) and 2008 (5.61).

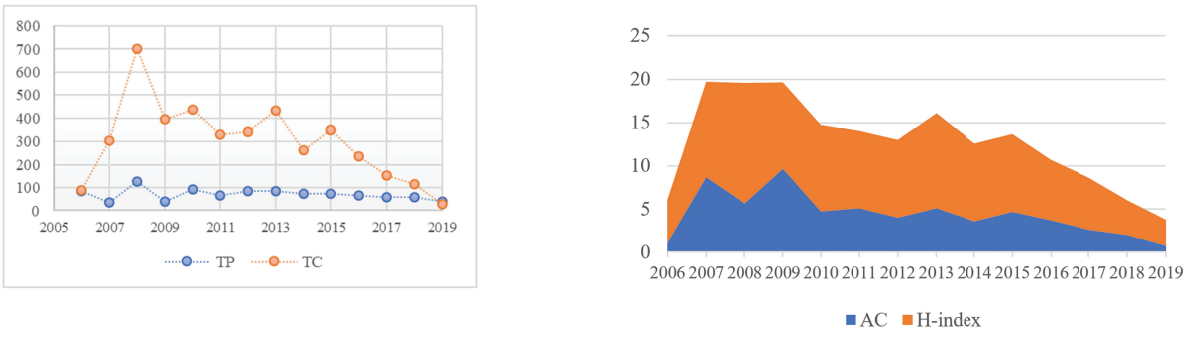

(a) (b)

Figure 2: The annual trends of publications in *IJCCC*: (a) The annual distributions of TP and TC; (b) The annual distributions of AC and H-index

Figure 2 shows the annual trends of publications in *IJCCC* with respect to TP, TC, AC and H-index, respectively. In Figure 2 (a), the distribution of TP shows a steady trend in the last

Table 2: The information of top 10 cited publications in *IJCCC*

Rank	Title (Type)	Author	Country	Year	Citation	AC
1	Spiking Neural P Systems with Anti-Spikes (Article)	Pan et al.	China	2009	99	9
2	Tissue P Systems with Cell Division (Article)	Paun et al.	Romania	2008	71	5.92
3	Generalized Ordered Propositions Fusion Based on Belief Entropy (Article)	Li et al.	China	2018	60	30
4	Extended EDAS Method for Fuzzy Multicriteria Decision-making: An Application to Supplier Selection (Article)	Keshavarz Ghorabaee et al.	Lithuania	2016	54	13.5
5	Determining Basic Probability Assignment Based on the Improved Similarity Measures of Generalized Fuzzy Numbers (Article)	Jiang et al.	China	2015	52	10.4
6	Ant Systems & Local Search Optimization for Flexible Job Shop Scheduling Production (Article)	Liouane et al.	Tunisia	2007	49	3.77
7	A Hybrid Model Based on Fuzzy AHP and Fuzzy WASPAS for Construction Site Selection (Article)	Turskis et al.	Lithuania	2015	48	9.6
8	Fuzzy Logic Control System Stability Analysis Based on Lyapunov's Direct Method (Article)	Precup et al.	Romania	2009	47	4.27
9	EECDA: Energy Efficient Clustering and Data Aggregation Protocol for Heterogeneous Wireless Sensor Networks (Article)	Kumar et al.	India	2011	44	4.89
10	Computing Nash Equilibria by Means of Evolutionary Computation (Article)	Lung et al.	Romania	2008	41	3.42

decade, while the trend of TC increases from 2006 to 2008, and has a certain fluctuation between 2009 and 2015, and has been decreasing from 2016 to 2019. Noted that it does not imply that no excellent contributions appeared since 2016, but rather that it always needs time for publications to be widely recognized and cited [18]. In Figure 2 (b), there are two peaks about AC, and one is in 2009, the other is in 2007. The trend of AC is steady from 2010 to 2016. In terms of H-index of publications, the highest H-index is 14 in 2008, followed by 11 in 2007 and 2013, respectively. The distribution of H-index shows a steady trend from 2007 to 2015.

2.3 The most cited publications in IJCCC

There are some highly publications in *IJCCC* since 2006, which have impact on the research field. Table 2 lists the information of top 10 cited publications in detail, including title, type, author, country, year, citation and AC.

The top 10 cited publications in IJCCC are all articles from China (3), Romania (3), Lithuania (2), Tunisia (1) and India (1). The publications by Pan et al. in 2009 and by Li et al. in 2018 have the highest citation (99), and the highest AC (30), respectively. The research content of the top 10 cited publications mainly contains P systems, information fusion and fuzzy theory. Specially, half of them made research based on fuzzy information, and applied to belief entropy [15], decision making [13], similarity measures [11], AHP and WASPAS [23], and logic control system [20], which indicates that fuzzy theory has been very popular and effective in both theoretical research [24, 26] and practical application [25].

Table 3: The top 10 prolific countries/regions of publications in *IJCCC*

Rank	Country	TP	TC	AC	≥50	≥30	≥20	≥10	%TP	H-index
1	Romania	**354**	**1531**	4.32	2	**10**	**12**	**39**	**36.05%**	**17**
2	China	199	889	4.47	**3**	4	8	24	20.26%	13
3	India	52	234	4.5	0	2	2	9	5.30%	9
4	France	49	304	6.2	0	1	3	11	4.99%	10
5	USA	49	200	4.08	0	0	2	3	4.99%	7
6	Chile	38	116	3.05	0	0	0	3	3.87%	6
7	Spain	33	357	**10.08**	2	3	4	8	3.36%	9
8	Serbia	30	135	4.5	0	1	1	2	3.05%	6
9	South Korea	29	46	1.59	0	0	0	1	2.95%	3
10	Tunisia	23	197	8.57	0	1	2	7	2.34%	4

3 Characteristics of countries/regions, institutions, and authors

Author(s) and the corresponding incidental information are important parts of each publication, and we further analyze the characteristics of publications in *IJCCC* at level of countries/regions, institutions, and authors, respectively.

3.1 Characteristic at level of countries/regions

So far, 71 countries/regions have published documents in *IJCCC* since 2006, and the distribution around the world in detail is shown in Figure 3.

Figure 3: Countries/regions' distribution of publications in *IJCCC*

It is noted that the redder the color is, the more publications the country/region has. As we can see, countries/regions cover five continents, especially in North America, Australia and Europe. Besides, the most publications are mainly from East Europe, East Asia and South Asia. Table 3 lists the top 10 prolific countries/regions of publications in *IJCCC*, considering evaluation indicators, i.e., TP, TC, AC, %TP, H-index and the numbers of citations no less than 50/30/20/10.

In Table 3, the maximum value under each indicator is also highlighted in bold. Romania is very prominent according to TP, TC, %TP and H-index, which indicates that Romania makes a great contribution to IJCCC. Spain has the highest AC (10.08), which denotes that the publications from Spain have received the highest recognition, followed by Tunisia (8.57), France (6.2) and India (4.5). Moreover, China has the most highly cited publications in IJCCC, because it ranks the first in terms of the number of citations no less than 50.

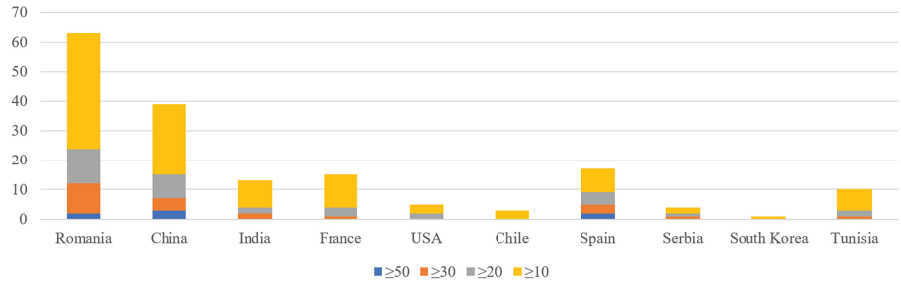

Figure 4: The number of citations no less than 50/30/20/10 in the top 10 prolific countries/regions

According to the number of citations no less than 50/30/20/10, Figure 4 shows the situation of the top 10 prolific countries/regions. The publications from three countries have been cited no less than 50, which are China, Romania and Spain, while Chile and South Korea do not have publication that is cited more than 20. In addition, Romania has the most publications that are cited no less than 30/20/10, followed by China. Overall, Romania is the most influential country in terms of publications in *IJCCC*, followed by China, Spain and France.

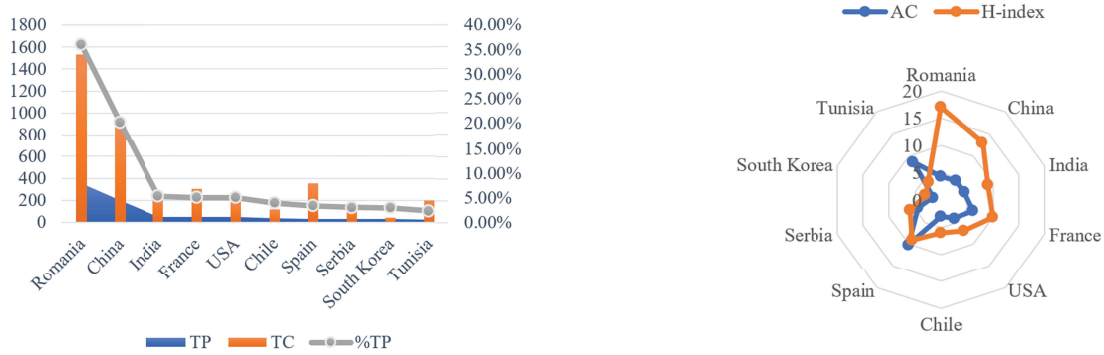

(a) (b)

Figure 5: The situation of TP, TC, %TP, AC and H-index in the top 10 prolific countries/regions: (a) The situation of TP, TC and %TP; (b) The situation of AC and H-index

In terms of TP, TC, %TP, AC and H-index, Figure 5 shows the situation of the top 10 prolific countries/regions. In Figure 5 (a), more than half of the total publications are from Romania and China. Although Spain is the seventh for TP, it ranks the third as far as TC is concerned. In Figure 5 (b), the radar map of AC and H-index is drawn. Spain does well in AC, and Romania is prominent in H-index. The gap of H-index is wider than the gap of AC among the top 10 prolific countries/regions.

3.2 Characteristic at level of institutions

In the following, we investigate the prolific institutions among totally 763 institutions in *IJCCC*. Table 4 lists the top 10 prolific institutions of publications in detail.

In Table 4, top 9 prolific institutions are from Romania, and the rest is from China, which indicates that the institutions in Romania have strong interest in *IJCCC*. BABES BOLYAI UNIVERSITY is the most prolific institution considering TP, followed by UNIVERSITY OF ORADEA and LUCIAN BLAGA UNIVERSITY OF SIBIU. According to TC, AC and H-index,

Table 4: The top 10 prolific institutions of publications in *IJCCC*

Rank	Institution	Country	TP	TC	AC	H-index
1	BABES BOLYAI UNIVERSITY	Romania	**49**	151	3.08	7
2	UNIVERSITY OF ORADEA	Romania	47	215	4.57	8
3	LUCIAN BLAGA UNIVERSITY OF SIBIU	Romania	39	138	3.54	6
4	AUREL VLAICU UNIVERSITY OF ARAD	Romania	35	232	6.63	8
5	ROMANIAN ACADEMY OF SCIENCES	Romania	31	**404**	**13.03**	**10**
6	TECHNICAL UNIVERSITY OF CLUJ NAPOCA	Romania	24	41	1.71	3
7	POLYTECHNIC UNIVERSITY OF BUCHAREST	Romania	23	51	2.22	5
8	TRANSYLVANIA UNIVERSITY OF BRASOV	Romania	23	52	2.26	4
9	AGORA UNIV ORADEA	Romania	21	110	5.24	7
10	BEIJING JIAOTONG UNIVERSITY	China	20	49	2.45	4

ROMANIAN ACADEMY OF SCIENCES ranks the first, which represents that the publications of the institution in *IJCCC* have won wide recognition in the field of research.

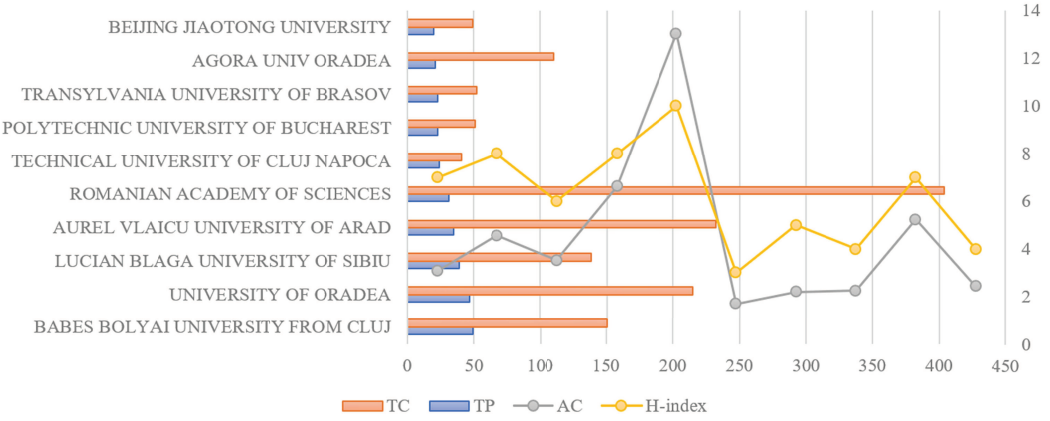

Figure 6: The situation of TC, TP, AC and H-index in the top 10 prolific institutions

Figure 6 depicts the situation of TC, TP, AC and H-index in the top 10 prolific institutions. The difference of TC is more significant than the difference of TP among the top 10 prolific institutions, and ROMANIAN ACADEMY OF SCIENCES performs well in terms of TC, followed by AUREL VLAICU UNIVERSITY OF ARAD and UNIVERSITY OF ORADEA. In addition, the range of AC is bigger than the range of H-index, and the trends of AC and H-index are basically consistent among the top 10 prolific institutions in *IJCCC*.

3.3 Characteristic at level of authors

At present, 2,049 authors around the world have publication(s) in *IJCCC*, and Table 5 lists the top 10 prolific authors of publications in detail.

In the top 10 prolific authors of publications in *IJCCC*, four authors from Romania, and two authors from Chile, and Colombia, France, USA, and Tunisia have one author, respectively. According to TP, TC and H-index, DZITAC I. (Romania) is the leading author, and BORNE P.

Table 5: The top 10 prolific authors of publications in *IJCCC*

Rank	Author	Country	TP	TC	AC	H-index
1	DZITAC I.	Romania	**23**	**149**	6.48	**7**
2	DONOSO Y.	Colombia	16	41	2.56	4
3	BORNE P.	France	12	136	**11.33**	**7**
4	DUMITRESCU D.	Romania	11	59	5.36	3
5	DZITAC S.	Romania	11	62	5.64	5
6	ANDONIE R.	USA	10	36	3.6	3
7	LEFRANC G.	Chile	9	17	1.89	3
8	MANOLESCU M.J.	Romania	9	62	6.89	3
9	BENREJEB M.	Tunisia	8	63	7.88	4
10	CUBILLOS C.	Chile	8	16	2	2

(France) ranks the first in terms of AC and H-index.

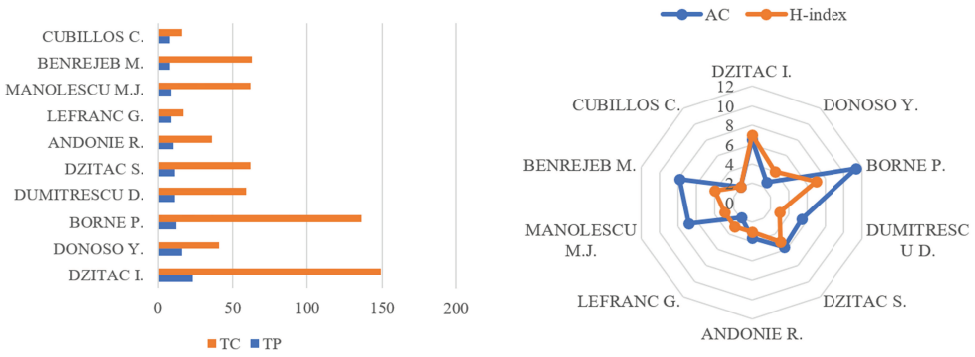

(a) (b)

Figure 7: The situation of TC, TP, AC and H-index in the top 10 prolific authors: (a) The situation of TC and TP (b) The situation of AC and H-index

Figure 7 shows the situation of the top 10 prolific authors with respect to TC, TP, AC and H-index. In Figure 7 (a), there is a greater gap with TC compared with TP among the top 10 prolific authors, and DZITAC I. (Romania) ranks the first according to TC, followed by BORNE P. (France) and BENREJEB M. (Tunisia). In Figure 7 (b), BORNE P. (France), BENREJEB M. (Tunisia) and MANOLESCU M.J. (Romania) are prominent in order according to AC. DZITAC I. (Romania) and BORNE P. (France) are leading authors in terms of H-index. Moreover, the difference of AC is bigger than the difference of H-index among the top 10 prolific authors of publications in *IJCCC*.

4 Landscape analysis

With the help of VoS viewer and CiteSpace, we make landscape analysis of publications in *IJCCC* from 2006 to 2019. Specifically, we do bibliometric analysis from four aspects, which are co-authorship analysis, bibliographic coupling analysis, co-citation and burst detection analysis, and co-occurrence and timeline view analysis, respectively.

4.1 Co-authorship analysis

In order to reflect the collaboration relationship clearly of publications in *IJCCC* during the whole time period, overlay visualization of co-authorship is described at level of countries/regions, institutions and authors by VoS viewer. It is noted that a node represents a country/region/institution/author, and the size of the node means the number of cooperation in overlay visualization. A link between two nodes indicates a collaboration relationship, and the thicker the link is, the more cooperation they have. The color of a node or a link mans the overlay time of co-authorship about countries/regions, institutions and authors.

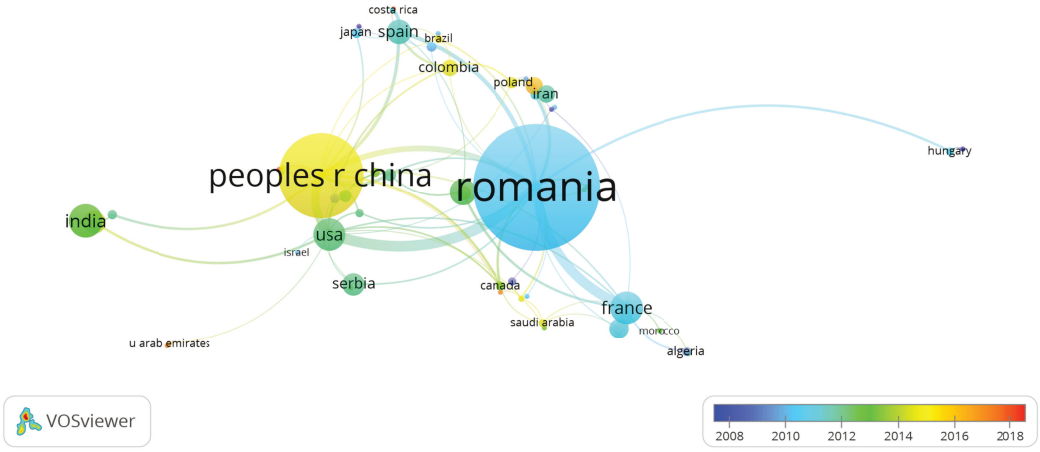

Figure 8: Overlay visualization of co-authorship at level of countries/regions in *IJCCC*

Figure 8 shows the overlay visualization about countries/regions of publications in *IJCCC*, where 71 countries/regions are selected when the minimum number of publications is set as 1. Overall, Romania and China are highlight, which indicates that they have many co-authorship publications in *IJCCC* from 2010 to 2012, and from 2014 to 2016, respectively. During each interval of timeline, the most prominent countries are Algeria, Romania, India and China in order. In addition, Romania and France have more cooperation between 2010 and 2012, while Romania and USA have closer cooperation between 2012 and 2014.

According to the institutions of publications in *IJCCC*, Figure 9 shows the overlay visualization of co-authorship where 50 institutions are selected among totally 812 institutions set the minimum number of publications as 5. UNIVERSITY OF ORADEA (Romania) and LUCIAN BLAGA UNIVERSITY OF SIBIU (Romania) are prominent in co-authorship from 2010 to 2012. VILNIUS GEDIMINAS TECHNICAL UNIVERSITY (Lithuania) and UNIVERSITY OF ELECTRONIC SCIENCE AND TECHNOLOGY OF CHINA (China) have more co-authorship publications in *IJCCC* in recent years.

Similarly, Figure 10 describes the overlay visualization of authors' co-authorship in *IJCCC*, where 338 authors are selected among totally 2,250 authors set the minimum number of publications as 2. As we can see, the authors between 2014 and 2018 have more co-authorship publications in *IJCCC* than the authors between 2008 and 2014. Besides, DONOSO Y. (Colombia) and DZITAC I. (Romania) perform better about co-authorship from 2014 to 2016.

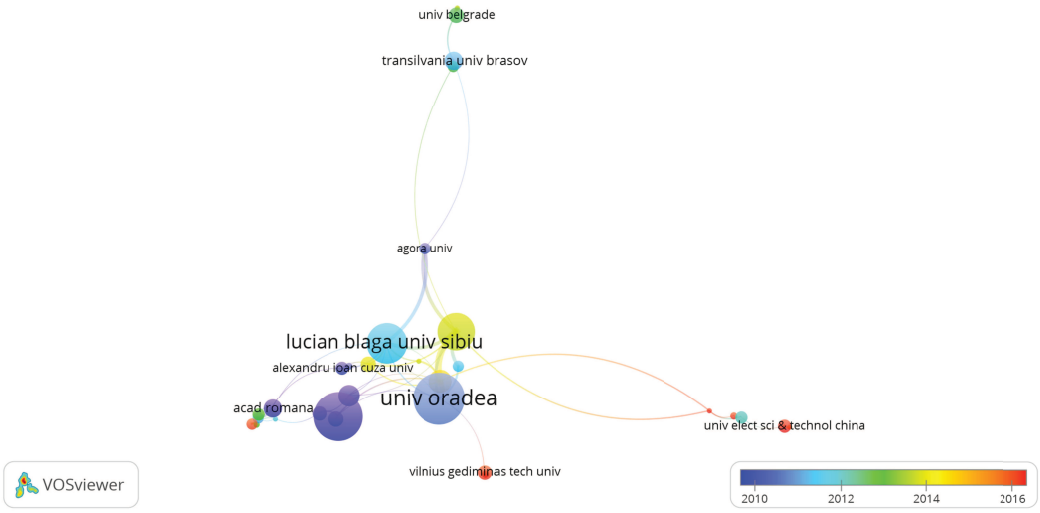

Figure 9: Overlay visualization of co-authorship at level of institutions in *IJCCC*

4.2 Bibliographic coupling analysis

In order to describe a similarity relationship of relative information in *IJCCC* from 2006 to 2019, we make density visualization of bibliographic coupling analysis by VoS viewer in terms of publications, authors, institutions and countries/regions. The redder the publication/author/institution/country/region is in the map of density visualization, the higher the coupling degree is, which indicates that the closer the subject content and professional nature of the two publications/authors/institutions/countries/regions are.

Figure 11 depicts the density visualization of bibliographic coupling analysis with respect to publications and authors in *IJCCC*. In Figure 11 (a), 118 publications are selected among totally 982 publications when the minimum number of publications is set as 10. There are two hotspots, and the highest coupling degree publication is Pan (2009), followed by Li (2018) and Keshavarz Ghorabaee (2016). In Figure 11 (b), we set the minimum number of publications as 5, and 29 authors meet the threshold among totally 2,250 authors. The number of authors is more than publications in terms of hotspot, and DONOSO Y. (Colombia) and DZITAC I. (Romania) are most prominent in bibliographic coupling.

According to institutions and countries/regions, Figure 12 shows the density visualization of bibliographic coupling analysis. When the minimum number of publications is set as 5, 50 institutions meet the threshold among totally 812 institutions, and 33 countries/regions meet the threshold among totally 71 countries/regions. In Figure 12 (a), UNIVERSITY OF ORADEA (Romania) is the most prominent institution and has the high connection degree with other institutions. In Figure 12 (b), Romania has the highest coupling degree, which represents that scholars prefer to cite publications in *IJCCC* from Romania, followed by China and India.

4.3 Co-citation and burst detection analysis

Considering the cited authors/journals/references in *IJCCC*, we make co-citation analysis by CiteSpace and VoS viewer. In the co-citation network by CiteSpace, a node indicates an author/journal/reference, and the size of the node means the number of citations with which the author/journal/reference is cited. A link between two nodes represents a co-citation relationship. The thicker the link is, the more citations the author/journal/reference has, and the top of them

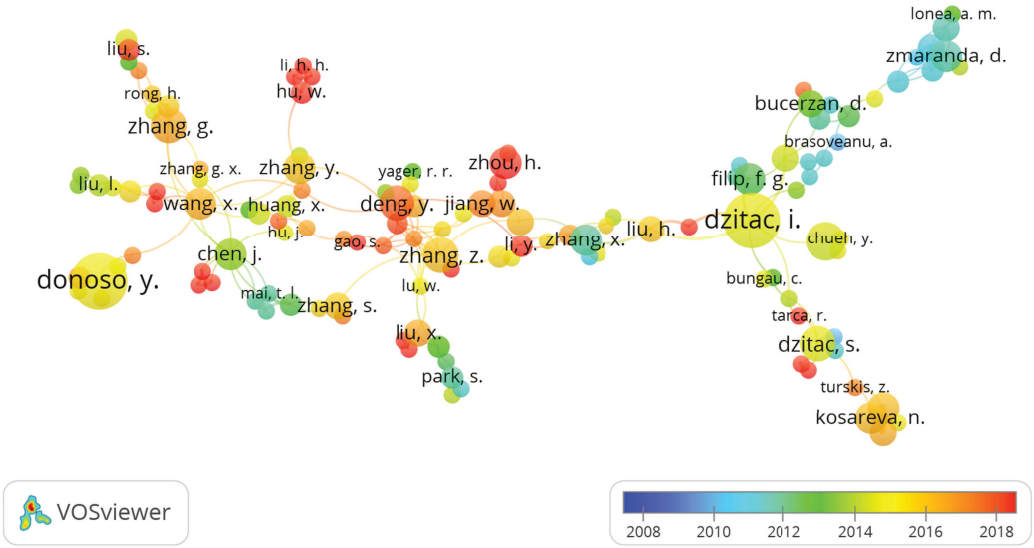

Figure 10: Overlay visualization of co-authorship at level of authors in *IJCCC*

are labeled in the networks.

According to the cited authors and the cited journals, Figure 13 shows the co-citation networks of publications in *IJCCC* by CiteSpace. There are 12,122 nodes and 19,910 edges about authors in Figure 13 (a), and 9,216 nodes and 30,760 edges about journals in Figure 13 (b). As we can see, high cited authors are more dispersive in their cooperative relationship, while high cited journals are relative concentration. Table 6 and Table 7 list the top 12 cited authors/journals with strongest citation bursts from 2006 to 2019, respectively.

In Table 6, DZITAC I. ranks the first with the maximum burst strength of 3.9746. The publications by WANG J. and ZHANG G. X. have made a far-reaching impact, because they own the longest citation burst duration with five years from 2015 to 2019. The citation bursts of six authors (DZITAC I., WANG J., WANG T., ZHANG G. X., DEMPSTER A. P. and CHEN

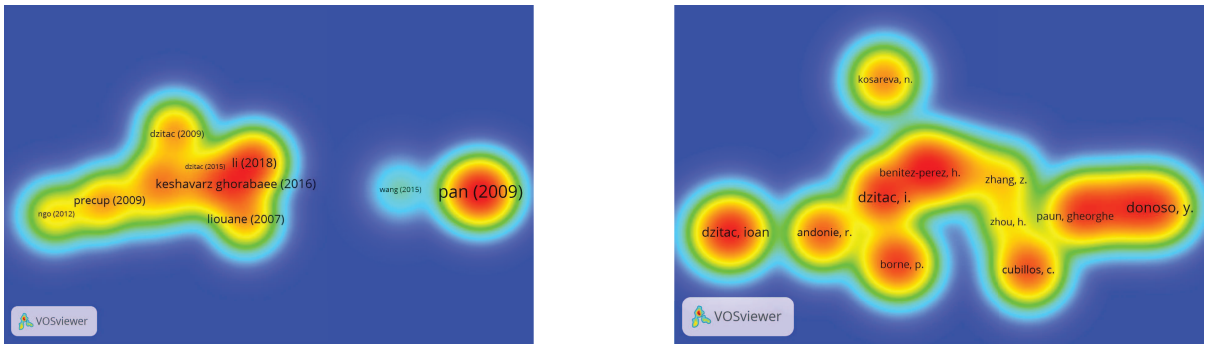

(a) (b)

Figure 11: Density visualization of bibliographic coupling analysis at level of publications and authors in *IJCCC*: (a) Publications' bibliographic coupling analysis; (b) Authors' bibliographic coupling analysis

Table 6: The top 12 cited authors with the strongest citation bursts from 2006 to 2019

Rank	Cited Authors	Year	Strength	Begin	End	2006-2019
1	DZITAC I	2006	**3.9746**	2017	2019	
2	NADABAN S	2006	**3.7872**	2015	2017	
3	AKYILDIZ IF	2006	**3.7701**	2012	2015	
4	WANG J	2006	**3.7064**	2015	2019	
5	WANG T	2006	**3.4668**	2017	2019	
6	LI M	2006	**3.4269**	2016	2017	
7	ZHANG GX	2006	**3.4152**	2015	2019	
8	CHEN SM	2006	**3.3259**	2014	2015	
9	CIOBANU G	2006	**3.1619**	2009	2010	
10	DEMPSTER AP	2006	**3.0792**	2017	2019	
11	CHEN X	2006	**3.0752**	2016	2019	
12	BARBAT BE	2006	**3.0331**	2008	2010	

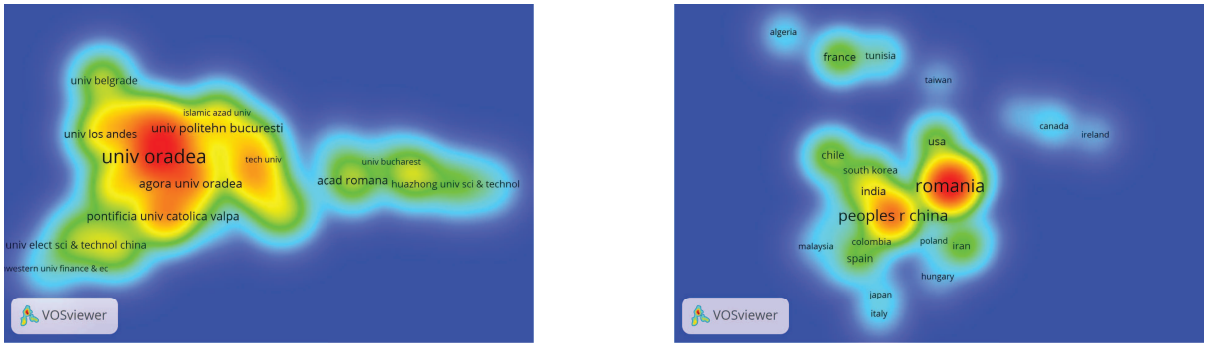

(a) (b)

Figure 12: Density visualization of bibliographic coupling analysis at level of institutions and countries/regions in *IJCCC*: (a) Institutions' bibliographic coupling analysis;(b) Countries/regions' bibliographic coupling analysis

X.) are close to 2019, which indicates that their work may have formed a popular topic at present.

In Table 7, *LECT. NOTES. COMPUTER*, which is an important branch about computer sciences in Springer, has the strongest strength with the value of 8.6363, followed by *MEMBRANE COMPUTING I.* and *IEEE ACM. T. NETWORK*. The citation burst of *THEOR. COMPUT. SCI.* has the longest duration with six years from 2006 to 2011. In addition, *LECT. NOTES. COMPUTER* and *THEOR. COMPUT. SCI.* began earlier from 2006, which illustrates that the publications in IJCCC cited them earlier and explosively.

Considering the cited references in *IJCCC*, Figure 14 shows the co-citation density visualization by VoS viewer. There are totally 16,675 cited references in *IJCCC*, and two cited references are very prominent, which are PAUN G. (2000) and DZITAC I. (2009). Table 8 lists the detailed information of two references with the strongest citation bursts from 2006 to 2019.

There are only two cited references with strongest citation bursts, which both began from 2009 and ended to 2010. To be specific, PAUN G. (2000) has the strongest strength with the value of 7.6022, followed by DZITAC I. (2009) with the value of 5.8144.

4.4 Co-occurrence and timeline view analysis

Keywords are important information to understand the knowledge structure and the research trend in the journal. In the following, we make a keyword co-occurrence analysis of publications in *IJCCC* by VoS viewer. There are 3,842 keywords of publications in *IJCCC* from 2006 to 2019, and 98 keywords are selected when the minimum number of occurrences of a keyword is set as 5, shown in Figure 15.

Similarly, a node with a color represents a keyword in a cluster, and the bigger the node is, the more citations the keyword has. A link between two nodes means the co-occurrence of two keywords, and the thicker the line is, the more co-occurred times they have. In Figure 15, "systems", "algorithm", "membrane computing", "networks" and "machine learning" are highlight in each cluster. In order to understand the characteristic of each cluster, we describe a cluster visualization of keywords in *IJCCC* by CiteSpace, shown in Figure 16. When the minimum number of citations of a keyword is set as 10, 11 associated clusters are summarized among totally 34 clusters according to all keywords of publications in *IJCCC*. To be specific, the clusters are "fuzzy control", "routing", "citation of books", "wireless sensor networks", "Dempster-Shafer evidence theory", "forest policy", "membrane computing", "semantic web", "system development life circle model", "machine learning", "knowledge management" and "petri nets" in order.

Table 7: The top 12 cited journals with the strongest citation bursts from 2006 to 2019

Rank	Cited Authors	Year	Strength	Begin	End	2006-2019
1	LECT NOTES COMPUTER	2006	**8.6363**	2006	2010	
2	MEMBRANE COMPUTING I	2006	**8.0721**	2009	2010	
3	IEEE ACM T NETWORK	2006	**5.0765**	2011	2015	
4	COMPUT COMMUN	2006	**5.0340**	2012	2013	
5	IEEE T NEURAL NETWOR	2006	**4.9156**	2010	2013	
6	J PROCESS CONTR	2006	**4.0303**	2007	2008	
7	IEEE INFOCOM SER	2006	**3.9476**	2012	2016	
8	IEEE COMMUN LETT	2006	**3.8981**	2011	2014	
9	THEOR COMPUT SCI	2006	**3.7852**	2006	2011	
10	INT J COMPUTERS COMM	2006	**3.5514**	2007	2008	
11	WIREL NETW	2006	**3.5024**	2011	2012	
12	LECT NOTES ARTIF INT	2006	**3.3479**	2008	2011	

(a) (b)

Figure 13: Co-citation networks at level of authors and journals in *IJCCC*: (a) Authors' co-citation network (b) Journals' co-citation network

Table 8: The top 2 cited references with the strongest citation bursts from 2006 to 2019

Rank	Reference	Year	Strength	Begin	End	2006-2019
1	PAUN G, MEMBRANE COMPUTING I	2000	**7.6022**	2009	2010	
2	DZITAC I, INT J COMPUT COMMUN	2009	**5.8144**	2009	2010	

In order to depict the trend of the keywords of publications in *IJCCC* from 2006 to 2019, Figure 17 shows the timeline view of keywords by CiteSpace. Five stages are presented during the whole time period. Firstly, it focused more on "architecture", "genetic algorithm", and "multi-agent system" between 2006 and 2007. Secondly, the keywords of "combinational optimization", "fuzzy set", "fuzzy logic" and "human-computer interaction" occurred most from 2007 to 2010. Next, it paid more attention to "adaptive control", "performance analysis", "sensor networks" and "machine learning" between 2010 and 2013. Then, the publications preferred to occur keywords like "space", "priority", "similarity measure" and "multidimensional scaling" from 2013 to 2016. Finally, the publications have focused more on "group decision making", "big data model", "representation" and "dependence assessment" in recent four years. Over time, the keywords of publications in *IJCCC* have changed continually, and *IJCCC* has focused more on fuzzy group decision making in the fields of automation control systems and computer science in the age of big data.

Figure 14: Co-citation density visualization of references in *IJCCC*

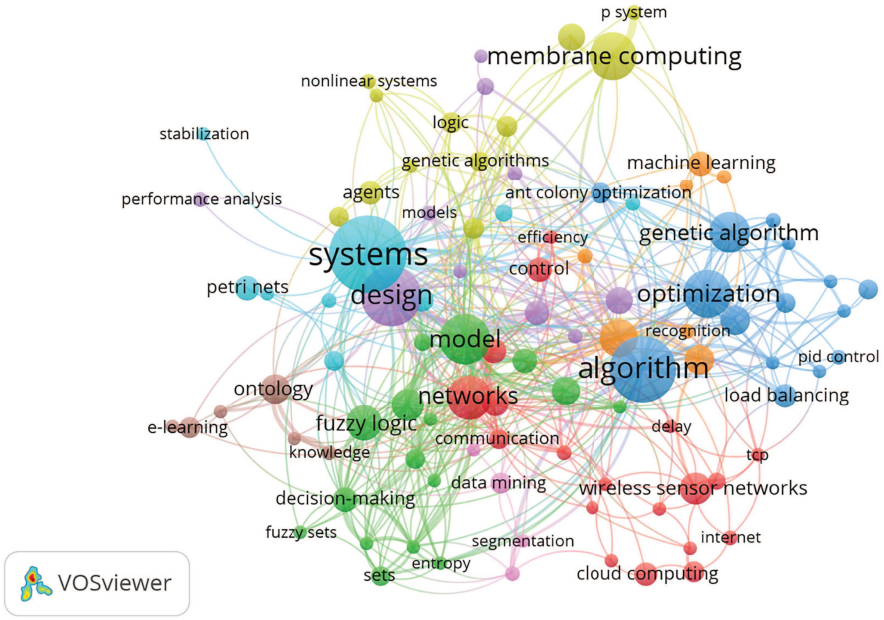

Figure 15: The keyword co-occurrence network of publications in *IJCCC*

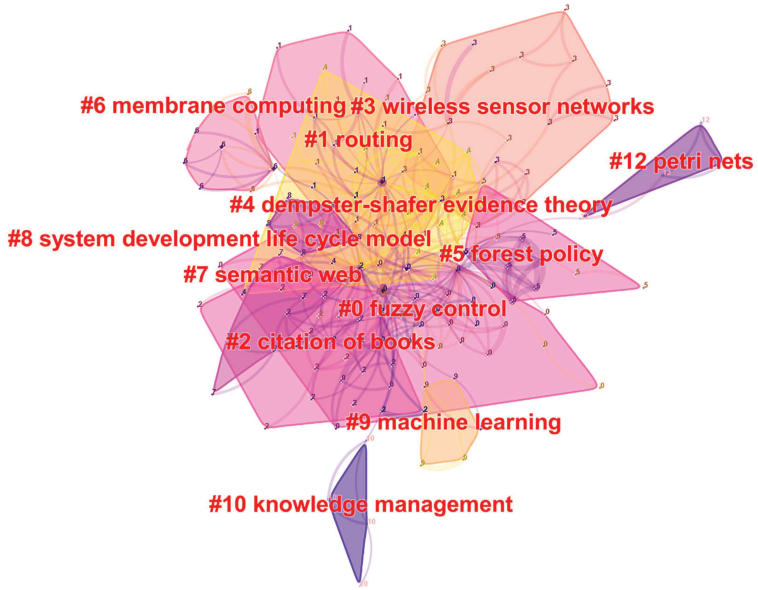

Figure 16: The cluster visualization of keywords in *IJCCC*

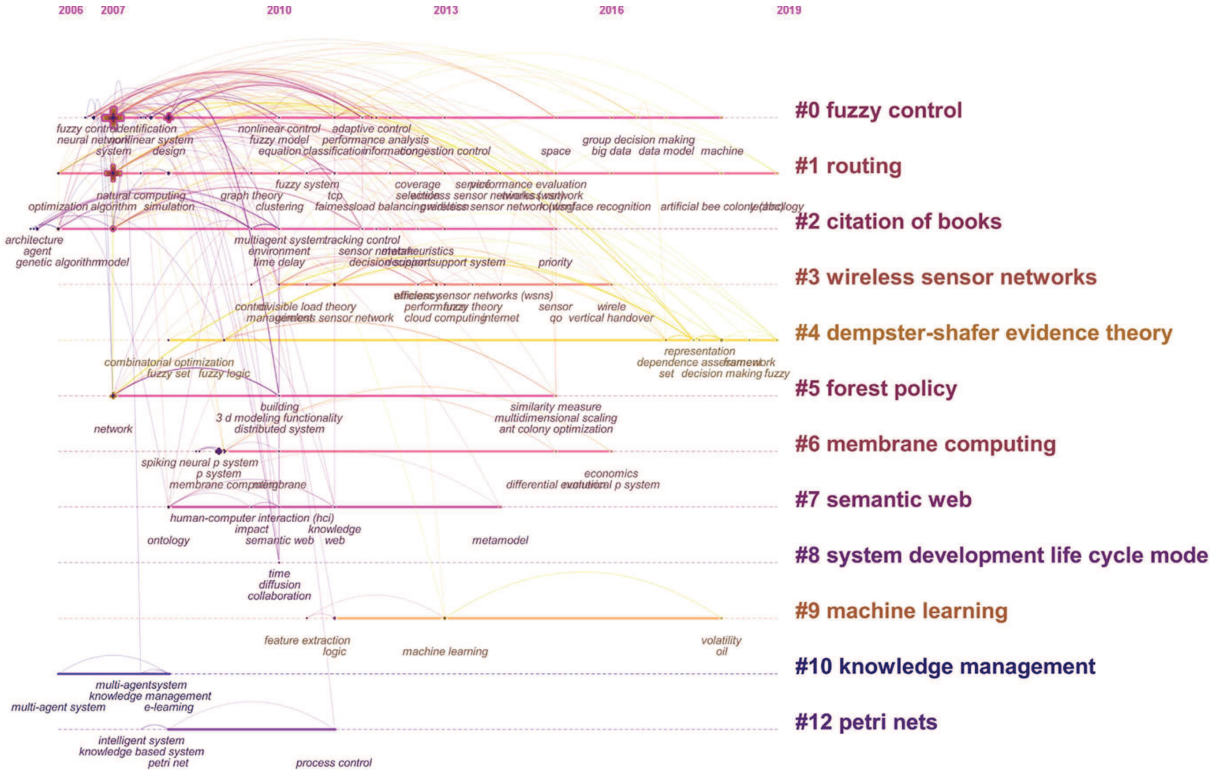

Figure 17: The timeline view of keywords in *IJCCC*

5 Discussion

International Journal of Computers Communications & Control has contributed to the fields of automation control systems and computer science since 2006. According to analysis results about fundamental information of publications, characteristics of countries/regions, institutions and authors, and landscape view, we give some discussions about current challenges and possible research trends of *IJCCC*.

(1) Since the number of publications has been steady during the last decade, *IJCCC* has a certain requirement about theme and quality of publications. Considering the number of citations, the trend increases from 2006 to 2008, and has a certain fluctuation between 2009 and 2015, which indicates that *IJCCC* has created the influence in the relative fields. Besides, half of the top 10 cited publications are related to fuzzy theory, which represents that the research in *IJCCC* does well in fuzzy logic and fuzzy information applied to computers, communications and control.

(2) According to characteristics of countries/regions, institutions and authors, most countries/regions are from East Europe, East Asia and South Asia. In addition, 9 institutions are all from Romania and one from China in the top 10 prolific institutions, and four authors from Romania in the top 10 prolific authors, followed by Chile. Therefore, it is an opportunity and challenge for *IJCCC* to increase scientific influence so that authors and institutions from other countries/regions prefer to publish relative documents in the journal.

(3) On the basis of landscape analysis, we further discuss some interesting phenomena. Institutions and authors are not obvious in the co-authorship networks, and their hotspots are relatively sparse in the density visualization of bibliographic coupling analysis, where the same situation exists at level of countries/regions, expect for Romania and China. It may be a good way for *IJCCC* to develop scientific research by international communication and cooperation with various institutions and authors. In burst detection analysis, there are only two cited references with strongest citation bursts, which indicates that there is a development space for *IJCCC* to increase the attention among academic journals. In terms of co-occurrence analysis and timeline view analysis, the trend of hot topics in *IJCCC* has turned to group decision making and big data model under complex and uncertain environment. Therefore, *International Journal of Computers Communications & Control* provides an important and valuable platform for scholars to research decision making methods and big data model of automation control systems and computer science.

6 Conclusions

This paper studies research trends of *International Journal of Computers Communications & Control* from 2006 to 2019 by performing bibliometric analysis. Depending on data from WoS, the work is conducted by VoS viewer and CiteSpace from three aspects, which are fundamental information of publications, characteristics of countries/regions, institutions and authors, and landscape analysis. Specifically, type, annual trend and the most cited publications are explored in *IJCCC*, and the number of publications has almost been steady since 2009. Romanian is the most prolific and influential country, and publications from Spain has the highest citations per year. The top 3 prolific institutions are BABES BOLYAI UNIVERSITY, UNIVERSITY OF ORADEA and LUCIAN BLAGA UNIVERSITY OF SIBIU, respectively. DZITAC I. (Romanian) is the most prolific author, followed by DONOSO Y. (Colombia) and BORNE P. (France). Landscape analysis is presented including co-authorship analysis, bibliographic coupling analysis, co-citation and burst detection analysis, co-occurrence and timeline view analysis. Furthermore, we discuss the current challenges and possible research trends according to the above-

mentioned analysis. The work is valuable for scholars to understand the trend and grasp hot topics related to automation control systems and computer science. In the future, we will further study bibliometric methods in depth and focus on the development of *International Journal of Computers Communications & Control*.

Acknowledgments

The work was supported by the National Natural Science Foundation of China (Nos. 71571123, 71771155 and 71801174).

Bibliography

[1] Andonie, R. ; Dzitac, I. (2010). How to Write a Good Paper in Computer Science and How Will It Be Measured by ISI Web of Knowledge, *International Journal of Computers Communications & Control*, 5(4), 432-446, 2010.

[2] Azevedo, S. G.; Santos, M.; Antón, J. R. (2019). Supply chain of renewable energy: A bibliometric review approach, *Biomass and Bioenergy*, 70-83, 2019.

[3] Chan, T. M.; Kuehl, D. R. (2019). On lampposts, sneetches, and stars: a call to go beyond bibliometrics for determining academic value, *Academic Emergency Medicine*, 688-694, 2019.

[4] Chen, C. M. (2006). CiteSpace II: Detecting and visualizing emerging trends and transient patterns in scientific literature, *Journal of the American Society for Information Science and Technology*, 359-377, 2006.

[5] Cobo, M. J.; Lopez-Herrera, A. G.; Herrera-Viedma, E.; Herrera, F. (2011). Science mapping software tools: Review, analysis, and cooperative sudy among tools, *Journal of the American Society for Information Science and Technology*, 1382-1402, 2011.

[6] Falagas, M. E.; Pitsouni, E. I.; Malietzis, G. A.; Pappas, G. (2008). Comparison of PubMed, Scopus, Web of Science, and Google Scholar: strengths and weaknesses, *Faseb Journal*, 338-342, 2008.

[7] Hache, E.; Palle, A. (2019). Renewable energy source integration into power networks, research trends and policy implications: A bibliometric and research actors survey analysis, *Energy Policy*, 23-35, 2019.

[8] He, X. R.; Wu, Y. Y.; Yu, D. J.; Merigo, J. M. (2017). Exploring the ordered weighted averaging operator knowledge domain: A bibliometric analysis, *International Journal of Intelligent Systems*, 1151-1166, 2017.

[9] Heersmink, R.; Van den Hoven, J.; Van Eck, N. J.; Van den Berg, J. (2011). Bibliometric mapping of computer and information ethics, *Ethics and Information Technology*, 241-249, 2011.

[10] Hsieh, P. N.; Chang, P. L. (2009). An assessment of word-wide research productiveity in production and operations management, *International Journal of Production Economics*, 540-551, 2009.

[11] Jiang, W.; Yang, Y.; Luo, Y.; Qin, X. Y. (2015). Determining basic probability assignment based on the improved similarity measures of generalized fuzzy numbers, *International Journal of Computers Communications and Control*, 333-347, 2015.

[12] Kamdem, J. P.; Duarte, A. E.; Lima, K. R. R.; Rocha, J. B. T.; Hassan, W.; Barros, L. M.; Roeder, T.; Tsopmo, A. (2019). Research trends in food chemistry: A bibliometric review of its 40 years aniversary (1976-2016), *Food Chemistry*, 448-457, 2019.

[13] Keshavarz Ghorabaee, M.; Zavadskas, E. K.; Amiri, M.; Turskis, Z. (2016). Extended EDAS method for fuzzy multi-criteria decision-making: An application to supplier selection, *International Journal of Computers Communications and Control*, 358-371, 2016.

[14] Laengle, S.; Merigo, J. M.; Miranda, J.; Slowinski, R.; Bomze, I.; Borgonovo, E.; Dyson, R.G.; Oliveira, J. F.; Teunter, R. (2017). Forty years of the European Journal of Operational Research: A bibliometric overview, *European Journal of Operational Research*, 803-816, 2017.

[15] Li, Y.; Deng, Y. (2018). Generalized ordered propositions fusion based on belief entropy, *International Journal of Computers Communications and Control*, 792-807, 2018.

[16] Liu, W. S.; Liao, H. C. (2017). A bibliometric analysis of fuzzy decision research during 1970-2015, *International Journal of Fuzzy Systems*, 1-14, 2017.

[17] Maditati, D. R.; Munim, Z. H.; Schramm, H. J.; Kummer, S. (2018). A review of green supply chain management: From bibliometric analysis to a conceptual framework and future research directions, *Resources Conservation and Recycling*, 150-162, 2018.

[18] Pilkington, A.; Meredith, J. (2009). The evolution of the intellectual structure of operations management-1980-2006: A citation/co-citation analysis, *Journal of Operational Management*, 185-202, 2009.

[19] Pinto, M. (2015). Viewing and exploring the subject area of information literacy assessment in higher education (2000-2011), *Scientometrics*, 227-245, 2015.

[20] Precup, R. E.; Tomescu, M. L.; Preitl, S. (2009). Fuzzy logic control system stability analysis based on lyapunov's direct method, *International Journal of Computers Communications and Control*, 415-426, 2009.

[21] Shang, G. Z.; Saladin, B.; Fry, T.; Donohue, J. (2015). Twenty-six years of operations management research (1985-2010): authorship patterns and research constituents in eleven top rated journals, *International Journal of Production Research*, 6161-6197, 2015.

[22] Stopar, K.; Bartol, T. (2019). Digital competences, computer skills and information literacy in secondary education: mapping and visualization of trends and concepts, *Scientometrics*, 479-498, 2019.

[23] Turskis, Z.; Zavadskas, E. K.; Antucheviciene, J.; Kosareva, N. (2015). A hybrid model based on fuzzy AHP and fuzzy WASPAS for construction site selection, *International Journal of Computers Communications and Control*, 873-888, 2015.

[24] Wang, X. X.; Xu, Z. S.; Gou, X. J. (2019). Nested probabilistic-numerical linguistic term sets in two-stage multi-attribute group decision making, *Applied Intelligence*, 2582-2602, 2019.

[25] Wang, X. X.; Xu, Z. S.; Gou, X. J.; Trajkovic, L. (2019). Tracking a maneuvering target by multiple sensors using extended kalman filter with nested probabilistic-numerical linguistic information, *IEEE Transaction on Fuzzy Systems*, DOI: 10.1109/TFUZZ. 2019.2906577.

[26] Wang, X. X.; Xu, Z. S.; Gou, X. J; Xu, M. (2019). Distance and similarity measures for nested probabilistic-numerical linguistic term sets applied to evaluation of medical treatment, *International Journal of Fuzzy Systems*, 1306-1329, 2019.

[27] White, H. (2018). Pennants for Garfield: bibliometrics and document retrieval, *Scientometrics*, 757-778, 2018.

[28] Yu, D. J.; Xu, Z. S.; Kao, Y. S.; Lin, C. T. (2018). The structure and citation landscape of IEEE Transactions on Fuzzy Systems (1994-2015), *IEEE Transactions on Fuzzy Systems*, 430-442, 2018.

[29] Yu, D. J.; Xu, Z. S.; Pedrycz, W.; Wang, W. R. (2017). Information sciences 1968-2016: A retrospective analysis with text mining and bibliometric, *Information Sciences*, 619-634, 2017.

[30] Yu, D. J.; Xu, Z. S.; Saparauskas, J. (2019). The evolution of "Technological and Economic Development of Economy": a bibliometric analysis, *Technological and Economic Development of Economy*, 369-385, 2019.

[31] Yu, D. J.; Xu, Z. S.; Wang, W. R. (2018). Bibliometric analysis of fuzzy theory research in China: A 30-year perspective, *Knowledge-Based Systems*, 188-199, 2018.

[32] http://univagora.ro/jour/index.php/ijccc/.

INTERNATIONAL JOURNAL OF COMPUTERS COMMUNICATIONS & CONTROL
ISSN 1841-9836, e-ISSN 1841-9844, 14(5), 733-752, October 2019.

Design, Modeling and Control of Bionic Knee in Artificial Leg

H.L. Xie, Y. Xie, F. Li

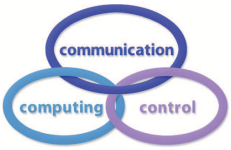

Hualong Xie*
Department of Mechanical Engineering and Automation,
Northeastern University, Shenyang 110819, China
hlxie@mail.neu.edu.cn

Yao Xie
Department of Mechanical Engineering and Automation,
Northeastern University, Shenyang 110819, China
1870220@stu.neu.edu.cn

Fei Li
Department of Information Science and Engineering,
Shenyang University of Technology, Shenyang 110870, China
lifeisut@163.com

Abstract: The biped robot with heterogeneous legs (BRHL) greatly facilitates the development of intelligent lower-limb prosthesis (ILLP). In the BRHL, the remaining leg of the amputee is simulated by an artificial leg, which provides the bionic leg with the precise gait following trajectory. Therefore, the artificial leg must closely mimic the features of the human leg. After analyzing the motion mechanism of the human knee, this paper designs a four-link bionic knee in light of the coexistence of rolling and sliding between the femur, the meniscus and the tibia. Drawing on the driving mechanism of leg muscles, two pneumatic artificial muscles (PAMs) were adopted to serve as the extensor and flexor muscles on the thigh. The two PAMs move in opposite direction, driving the knee motions in the artificial leg. To overcome the complexity of traditional PAM modelling methods, the author set up a PAM feature test platform to disclose the features of the PAMs, and built static and dynamic nonlinear mathematical models of the PAMs based on the test data. Next, a proportional-integral-derivative (PID) closed loop controller and sliding mode controller was designed for the bionic knee, referring to the kinetics equation of the knee. Through experimental simulation, it is confirmed that the proposed controller can accurately control the position of the four-link bionic knee, and that the designed bionic knee and PAM driving mode are both correct.
Keywords: Bionic knee, biped robot with heterogeneous legs (BRHL), pneumatic artificial muscle (PAM), high-speed on-off valve, sliding mode control

1 Introduction

Millions around the world have lost their lower extremities due to varied reasons, ranging from wars, earthquakes, diseases, work-related injuries, traffic accidents to accidental injuries. In 2006, China launched the second national sample survey on disabled people [4]. The survey results show that 29.07% (24.12 million) of Chinese with disabilities suffered from extremity disability; about 8% (2.26 million) of them had one or more of their limbs amputated, including

1.58 million of lower extremity amputees. In the US, around 1.60 million have lost some or all their limbs, and the majority (97%) of amputations caused by vascular complications target the lower extremities. A good chunk (25.8%) of these lower extremity amputations removes the leg above the knee [7].

Currently, there is not yet any biomedical technology capable of regenerating human tissues. In this case, the intelligent lower-limb prosthesis (ILLP) [6, 10, 19] is the most desirable way to compensate for the walking function of lower extremity amputees. This paper designs a novel biped robot with heterogeneous legs (BRHL) [15, 17, 21], laying a solid basis for the R&D of the ILLP. For example, the BRHL can be applied in prosthesis tests to disclose the walking features of the disabled wearing the ILLP, eliminating the need for the disabled to walk repeatedly in prosthesis, the physical and mental pains of the disabled in the tests, and the human interference in the test results.

As shown in Figure 1, our BRHL consists of an artificial leg, a bionic leg and a robotic upper body. The artificial leg and the bionic leg correspond to the remaining good leg and the ILLP of the amputee, respectively. The artificial leg is required to simulate the normal gait of the remaining leg in an accurate manner, and provide the bionic leg with the precise gait following trajectory. Therefore, the control of the artificial leg is critical to the development of the entire BRHL [16, 18].

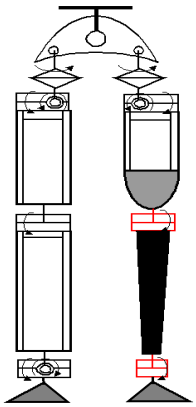

Figure 1: The structure of the BRHL

To satisfy the requirements on the artificial leg, this paper adopts the PAMs based on high-speed on-off valve control to replace the "flexor and extensor muscle groups"of the biceps and quadriceps of the human leg, and drives the joint movement. Compared with traditional robot driving modes (e.g. motor, hydraulic unit and cylinder), the two-PAMs driving mode bears great resemblance with the driving mode of human knee in motion mechanism and smoothness.

During the normal motions of human knee, rolling and sliding coexist between the femur, the meniscus and the tibia; the trajectory of the instant center of rotation (ICR) is in the form of a J-shape curve. In our design, the J-shape ICR trajectory of the knee is achieved through a four-link bionic mechanism, which also enhances the system flexibility and stability [8].

It is a complex task to establish a model for the PAMs, due to their various nonlinear uncertainties, including but not limited to the friction of the woven mesh, gas compression and irregular deformation. The flow of the high-speed on-off valve is also hard to simulate, adding to the difficulty in system control. Many attempts have been made to overcome the difficulty.

For instance, Jouppila et al. [5] designed a full-state observer based on the smooth variable structure filter (SVSF) and the sliding mode control (SMC), which regulates the PAM position via the SMC, and verified the robustness of the observer in controlling the PAM stretching

system for pulling reciprocating masses. Using hysteresis compensation, Vo-Minh et al. [12] improved the control precision with two closed loops for feedforward compensation: the inner loop compensates for the nonlinear pressure within the PAM, while the outer loop makes up for the nonlinear dynamics of the PAM. Chen and Ushijima et al. from Tokyo University of Science [1] improved the precision of the PAM model based on Chou's theoretical model [2], but the improved model is too complex to applied in actual control.

In this paper, a PAM feature testing platform is constructed, following the PAM modelling theories proposed by Shaofei Wang from Tokyo University of Technology [14], Shameek Ganguly from Indian Institute of Technology [3] and many other scholars [13, 22]. Then, the author fitted the test data by polynomial function, and created a desirable static model for the PAMs. Considering the actual control scenarios, two opposite pulse-width modulation (PWM) signals were applied simultaneously on the high-speed on-off valve bank, respectively acting on the on-off valves of the two PAMs. On this basis, a valve port flow model was established, in light of Sanville's valve flow formula [9]. After that, a proportional-integral-derivative (PID) closed loop controller was designed, referring to the Lagrangian-Eulerian kinetics equation of the knee. Finally, the position control of the four-link bionic knee was achieved successfully through a simulation on MATLAB Simulink.

2 Design of bionic knee on the artificial leg

The human skeleton is a masterpiece of evolution. It is the most suitable biological mechanism for walking on both legs. The knee, a critical joint in two-legged walking, mainly encompasses the medial and lateral condyles of the femur, the tibia, the meniscus, cruciate ligaments, muscles and nerves [**?**, 20]. The cruciate ligaments refer to the anterior cruciate ligament (ACL) and posterior cruciate ligament (PCL) of knee joint. As shown in Figure 2, the interface between the lower end of the femur and the meniscus, and that between the meniscus and the upper end of the tibia, are both irregular in shape. During walking, both rolling and sliding motions occur on the two interfaces.

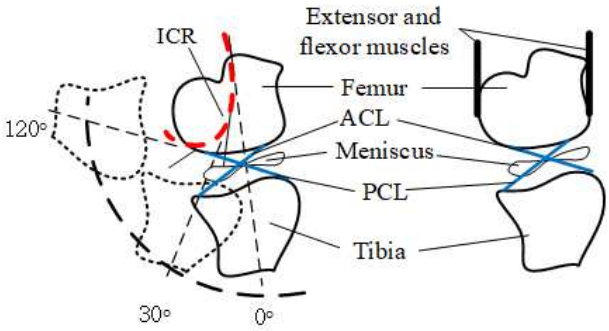

Figure 2: Structure of human knee

In flexion and extension, the horizontal axis of the knee is not fixed, and the ICR trajectory is in the form of a J-shape curve. The ICR motion adjusts the torque of the ground reaction force to the knee, and affects the knee's following of hip motion, exerting a direct impact on the walking stability and energy consumption. Therefore, whether the ICR trajectory exists in J-shape is an important criterion to evaluate the design of bionic knee.

The single-axis bionic knee is highly flexible, but lacks stability. Meanwhile, the four-link bionic knee can output a J-shape ICR trajectory, and ensure the motion flexibility and stability. The ICR trajectory enables the artificial leg to have a higher height from the ground and better

obstacle avoidance ability during swing phase. In addition, the ICR trajectory allows the artificial leg to effectively use the ground reaction to maintain stability during support phase [6]. This explains the popularity of the four-link mechanism in the design of intelligent prothesis.

In view of the human knee mechanism, three plans were prepared for the design of bionic knee on the artificial leg (Figure 3). In the first plan, the artificial leg takes up too much space, which may interfere in the motion of the bionic leg. Thus, this plan was abandoned. Despite the rational space arrangement, the second plan has a common defect with the first plan: excessively long PAMs are required for the bionic knee to complete the normal gait (at least 0∼90°)); the PAMs, coupled with the driving chain, will not match the length of the thigh. Hence, the second plan was also discarded. The third plan was formulated based on these two plans. In the third plan, a multiplying wheel (gear ratio: 2.5) was introduced to increase the knee rotation angle per unit of PAMs'contraction length and effectively reduce the length of PAM. In addition, the third plan increases the transverse distance between the two PAMS, effectively avoiding interference caused by the inflation of PAMS.

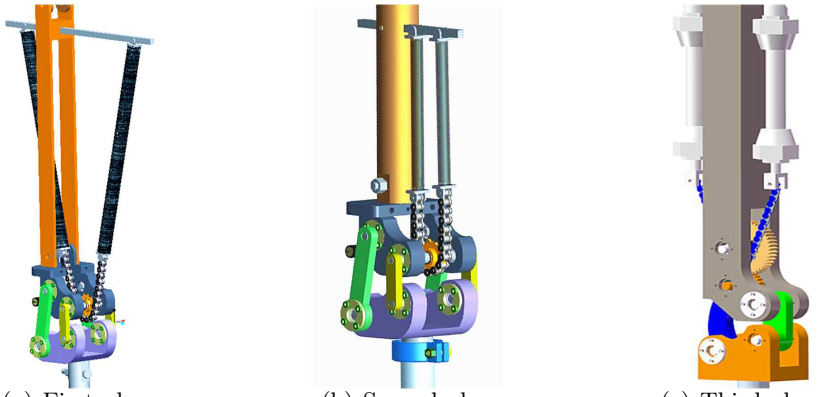

(a) First plan (b) Second plan (c) Third plan

Figure 3: Design plans for bionic knee on the artificial leg

3 Motion analysis and dynamic modeling of knee joint

3.1 Analysis of the four-link mechanism

The ICR trajectory is the key criterion to evaluate the bionic performance of the four-link mechanism. Therefore, the analysis of the four-link mechanism focuses on two issues: the correspondence between the rotation angle of the knee (the angle between the thigh and the shank) and that of the chain wheel, and the ICR trajectory. For convenience, a Cartesian coordinate system was set up as in Figure 4(b), where the origin O lies at the center of the driving shaft.

According to the closed chain vector equation of the four-link mechanism, the links must satisfy the following constraint:

$$l_1 e^{i\theta_1} + l_2 e^{i\theta_2} - l_3 e^{i\theta_3} - l_4 = 0 \tag{1}$$

where θ_i is the rotation angle of the linkage i; $l_i(i{=}1,2,\ldots,4)$ is linkage length of the four-link bionic knee; θ is the rotation angle of the chain wheel on the transmission chain; φ is the rotation angle of the bionic knee; α and β are initial values of θ_1 and θ_2; $\theta_1 = \alpha - \lambda\theta$, $\theta_2 = \varphi + \beta$. The rotation angle of the bionic knee can be computed by the two constants by:

$$\varphi = 2\arctan\left(\frac{a \pm \sqrt{a^2+b^2-c^2}}{b-c}\right) - \beta \tag{2}$$

where $a = -2l_1l_2\sin(\alpha-\lambda\theta)$; $b = 2l_2\left(l_1\cos(\alpha-\lambda\theta) - l_4\right)$; $c = l_1^2+l_2^2-l_3^2+l_4^2-2l_1l_4\sin(\alpha-\lambda\theta)$.

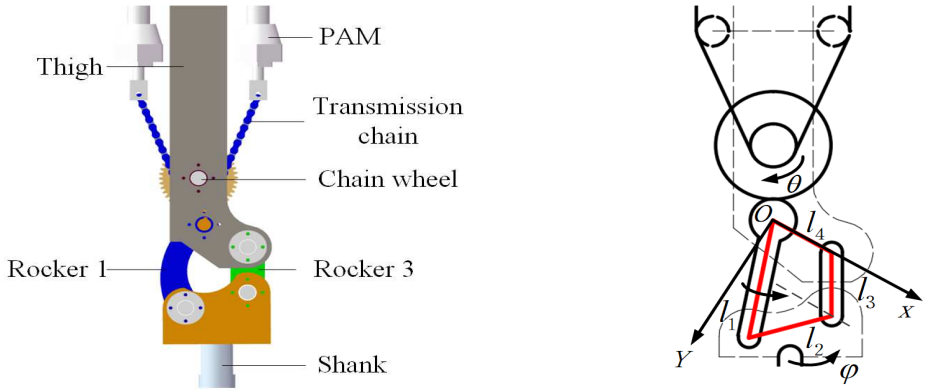

(a) Knee joint model (b) Knee joint diagram

Figure 4: Structure of the bionic knee on the artificial leg

According to Kennedy's theorem, the ICR of the links, the shank and the load lies in the intersection between the extension lines of rockers 1 and 3. Thus, the value of the ICR can be derived from the slopes of the extension lines. The coordinates of each point were solved in light of the coordinate system in Figure 4. Next, the ICR trajectory of the four-link mechanism was drawn using the plot commands in MATLAB. As shown in Figure 5, the obtained ICR trajectory was obviously a J-shape curve.

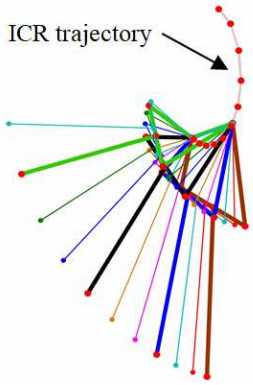

Figure 5: ICR trajectory of the bionic knee

3.2 Kinetics modelling of the bionic knee on the artificial leg

The movement analysis diagram of artificial leg is shown in Figure 6. The bionic knee on the artificial leg is a single-degree of freedom (1 DOF) system. Based on the coordinate system in Figure 6, the kinetics equation of the system was established by the Lagrangian-Eulerian method as:

$$L = K - E = \sum_{i=1}^{3}\left(\frac{1}{2}m_i\left(\dot{x}_i^2 + \dot{y}_i^2\right)\right) + \sum_{i=1}^{3}\left(\frac{1}{2}J_i\dot{\theta}_i^2\right) - \sum_{i=1}^{3}\left(m_i g l_i \cdot \xi\left(\theta_i\right)\right) \tag{3}$$

where K is the kinetic energy term; E is the potential energy term; θ_i are the rotation angles of rocker 1, rocker 3, the shank (connected to link 2) and the load on the ankle; $\xi\left(\theta_i\right)$ is the vertical motion component; J_i is the equivalent moment of inertia; m_i is the equivalent mass; (x_i, y_i) are the centroid coordinates of each link.

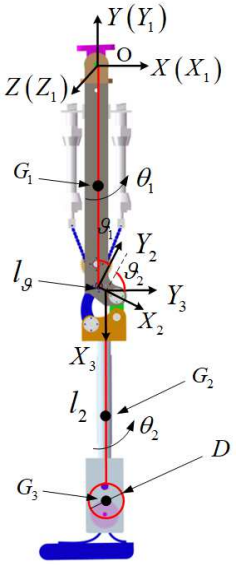

Figure 6: Movement analysis diagram of artificial leg

The kinetic equation of knee joint of artificial leg can be written as:

$$\begin{aligned}
T &= \frac{d}{dt}\left(\frac{\partial L}{\partial \dot{\theta}_2}\right) - \frac{\partial L}{\partial \theta_2} \\
&= \begin{bmatrix} \frac{1}{3}\mathrm{m}_2 l_2^2 + \frac{1}{2}\mathrm{m}_2 l_2 l_\vartheta \sin\left(\theta_2 + \vartheta_1\right) + \frac{1}{2}\mathrm{m}_2 l_1 l_2 \cos\theta_2 + \frac{1}{2}\mathrm{m}_3\left(l_2 + \frac{D}{2}\right)^2 \\ \frac{1}{2}\mathrm{m}_3\left(l_2 + \frac{D}{2}\right) l_\vartheta \sin\left(\theta_2 + \vartheta_1\right) + \frac{1}{2}\mathrm{m}_3 l_1\left(l_2 + \frac{D}{2}\right)\cos\theta_2 + \frac{1}{4}\mathrm{m}_3 D^2 \end{bmatrix} \ddot{\theta}_1 \\
&+ \left[\frac{1}{3}\mathrm{m}_2 l_2^2 + \frac{1}{4}\mathrm{m}_3\left(l_2 + \frac{D}{2}\right)^2 + \frac{1}{4}\mathrm{m}_3 D^2\right]\ddot{\theta}_2 \\
&+ \begin{bmatrix} -\frac{1}{2}\mathrm{m}_2 l_2 l_\vartheta \cos\left(\theta_2 + \vartheta_1\right) + \frac{1}{2}\mathrm{m}_2 l_1 l_2 \sin\theta_2 \\ -\frac{1}{2}\mathrm{m}_3\left(l_2 + \frac{D}{2}\right) l_\vartheta \cos\left(\theta_2 + \vartheta_1\right) + \frac{1}{2}\mathrm{m}_3 l_1\left(l_2 + \frac{D}{2}\right)\sin\theta_2 \end{bmatrix} \dot{\theta}_1^2 \\
&+ \frac{1}{2}m_2 g l_2 \sin\left(\theta_1 + \theta_2\right) + m_3 g\left(l_2 + \frac{D}{2}\right)\sin\left(\theta_1 + \theta_2\right) \\
&= \mathrm{M}_{21}\ddot{\theta}_1 + \mathrm{M}_{22}\ddot{\theta}_2 + \mathrm{C}_{21}\dot{\theta}_1^2 + \mathrm{G}_2
\end{aligned} \tag{4}$$

where $\vartheta_1 = \frac{\pi}{6}$ and $\vartheta_2 = \frac{\pi}{3}$ are transformation angles of coordinate system; l_ϑ is coordinate offset; D is equivalent cylinder diameter of load; M_{21} is coupling inertia of the knee joint; M_{22} is effective inertia of shank and load; C_{21} is centripetal acceleration coefficient; G_2 is gravity item of shank and load.

During the calculation, the masses of rockers 1 and 3 were neglected, for they are much smaller than the loads on the shank, the ankle and the artificial foot. Then, the Lagrangian-Eulerian equation can be simplified as:

$$T = \frac{d}{dt}\left(\frac{\partial L}{\partial \dot{q}}\right) - \frac{\partial L}{\partial q} = M(q)\ddot{q} + G(q) = (F_{\mathrm{A}} - F_{\mathrm{B}})\, r \tag{5}$$

where q is generalized coordinate vector; F_A and F_B are the output forces of extensor and flexor PAMs, respectively; r is the reference radius of the chain wheel.

4 Experimental modeling of the PAMs

Due to a series of nonlinear factors, such as elastic deformation of rubber tube, friction between woven mesh and gas compression, the modeling of the PAMs is very difficult. Firstly, the static characteristics modeling of PAMs is established by experiment. Then, by referring to the Sanville flow formula, the functional relationship between the gas mass flow of the PAMs and the PWM signal is analyzed, and then the dynamic equation of PAM charging and discharging is solved.

4.1 Static characteristics modeling of PAMs

In our design, the bionic knee is driven by two PAMs, which works similar to a spring with variable stiffness. When the PAM is inflated, the diameter increases and the length is shortened, outputting an axial tensile force. It is obvious that the output force F of the PAMs depends on the internal pressure P and the shrinkage ratio ε. Currently, the PAMs are usually modelled based on their stress-induced deformation, using the law of conservation of energy. However, this modelling approach is relatively complex, and inconvenient in actual application. To solve the problem, this paper establishes a PAM testing platform (Figure 7) to disclose the isobaric and isometric features of the PAMs, and sets up the PAM model based on the test results. The workflow of the isobaric and isometric test is presented in Figure 8. The bionic knee on the artificial leg uses the MAS-20-100N-AA-MC PAMs (Festo AG, Germany), whose initial length l_0 is 100mm and the maximum shrinkage ratio is 20$\sim$ 25% (no pressure, no load).

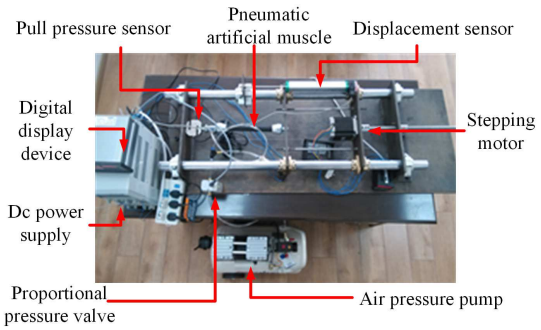

Figure 7: PAM feature testing platform

With the aid of the Curve Fitting toolbox of MATLAB, the data of the isobaric and isometric test were fitted by the least squares method, using the polynomial function. The fitting results can be expressed as:

$$F = P\,(a_0 + a_1\varepsilon) + a_2\varepsilon^3 + a_3\varepsilon^2 + a_4\varepsilon + a_5 \tag{6}$$

where a_i is the polynomial coefficient and its value is shown in Table 1.

Table 1: Parameters value of a_i

a_0	a_1	a_2	a_3	a_4	a_5
2314	-7455	-151900	56710	-6699	-70.64

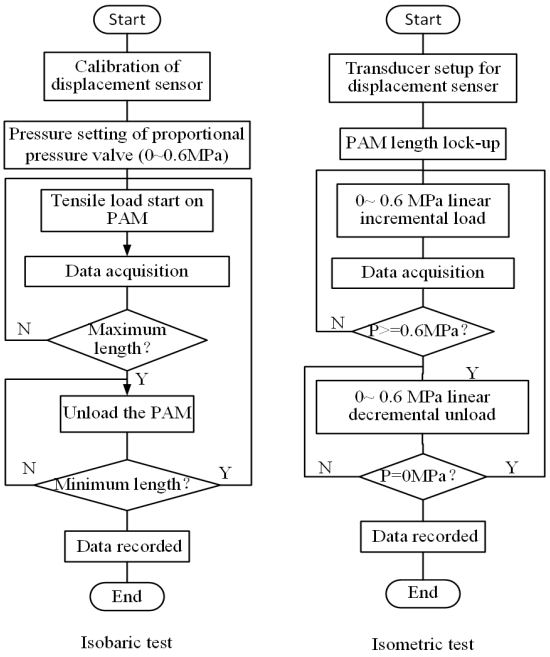

Figure 8: Workflow of isobaric and isometric test

According to formula (6), the relationship of PAM output force F with internal pressure P and shrinkage rate ε is shown in Figure 9. The contour shows the function relationship between internal pressure P and shrinkage ε under different loads.

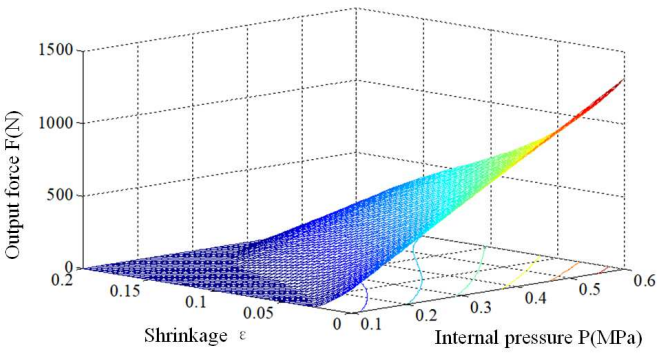

Figure 9: Fitting model of PAM

The comparison of PAM fitting value with isobaric and isometric experimental value is shown in Figure 10 and 11. It can be known that the experimental modeling method can accurately express the static characteristics of PAM, which is simpler than analytical modeling method and can be used for simulation and controller design.

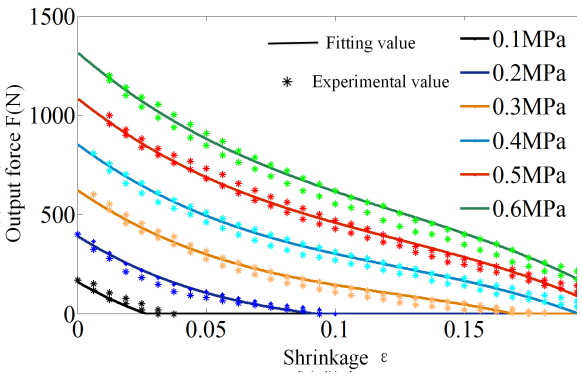

Figure 10: Comparison of fitting value and isobaric experimental value of PAM

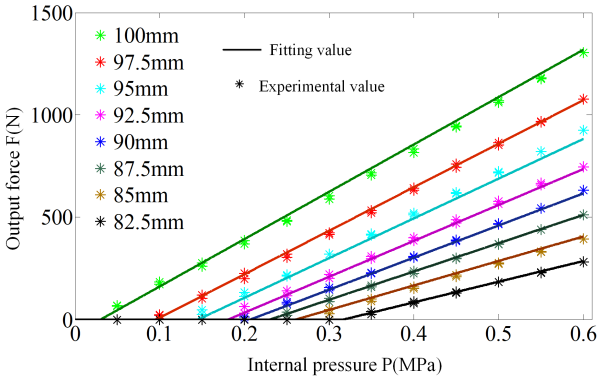

Figure 11: Comparison of fitting value and isometric experimental value of PAM

4.2 Dynamic characteristics modeling of PAMs

The charging and discharging process of PAMs is realized by controlling the valve port flow of a group of high-speed on-off valves through pulse width modulation (PWM) signal. In the process of dynamic characteristics modeling of PAMs, it is assumed that the whole pneumatic system is in an ideal state.

The pressure change rate $\dot{P}$ of the PAMs can be illustrated as:

$$\dot{P} = \frac{\gamma R T \dot{m}}{V} - \frac{\gamma P \dot{V}}{V} \tag{7}$$

where $\dot{m}$ is the mass flow at the valve port; R is the ideal gas constant; γ is the isentropic index (γ=1.4 for the air); T is the thermodynamic temperature of the gas; V is the internal volume, which is approximately linear with the shrinkage ratio.

In this paper, charging and discharging experiments were carried out on the PAMs under no load. The working diagram of PAM is shown in Figure 12. The variation of its internal volume was obtained by actual test, as shown in Figure 13. The internal volume was approximately proportional to the shrinkage rate, and the test data was approximately fitted by a linear curve, that is:

$$V = b_1 \varepsilon + b_2 \tag{8}$$

Where b_1 and b_2 are the fitting parameters, $b_1 = 1.9e-4$, $\quad b_2 = 3.21e-5$.

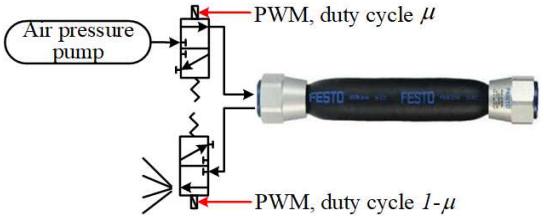

Figure 12: Charging and discharging processes of the high-speed on-off valve

Based on Sanville's valve flow formula, the total valve port flow of a single PAM under simultaneous charging and discharging can be established as:

$$\begin{aligned}\dot{m} &= \dot{m}_{in}\left(A_{in}, P, \mu\right) - \dot{m}_{out}\left(A_{out}, P, 1-\mu\right) \\ &= \begin{cases} \mu P_{up}\Gamma_1 - (1-\mu)P\Gamma_2 & P < 0.189 \\ \mu P_{up}\Gamma_1 - (1-\mu)P\Gamma_1 & 0.189 \le P \le 0.317 \\ \mu P_{up}\Gamma_3 - (1-\mu)P\Gamma_1 & P > 0.317 \end{cases}\end{aligned} \tag{9}$$

where $\Gamma_1 = \frac{A_{\max}}{\sqrt{RT}}\sqrt{\gamma\left(\frac{2}{\gamma+1}\right)^{\frac{\gamma+1}{\gamma-1}}}$, $\Gamma_2 = \frac{A_{\max}}{\sqrt{RT}}\sqrt{\frac{2\gamma}{\gamma-1}\left[\left(\frac{P_{atm}}{P}\right)^{\frac{2}{\gamma}} - \left(\frac{P_{atm}}{P}\right)^{\frac{\gamma+1}{\gamma}}\right]}$, $\Gamma_3 = \frac{A_{\max}}{\sqrt{RT}}\sqrt{\frac{2\gamma}{\gamma-1}\left[\left(\frac{P}{P_{up}}\right)^{\frac{2}{\gamma}} - \left(\frac{P}{P_{up}}\right)^{\frac{\gamma+1}{\gamma}}\right]}$; P_{up} is the stabilized pressure outputted by the air pump, P_{up}=0.6MPa; P_{atm} is the atmospheric pressure, P_{atm}=0.1MPa; A_{max} is the maximum opening area of the valve.

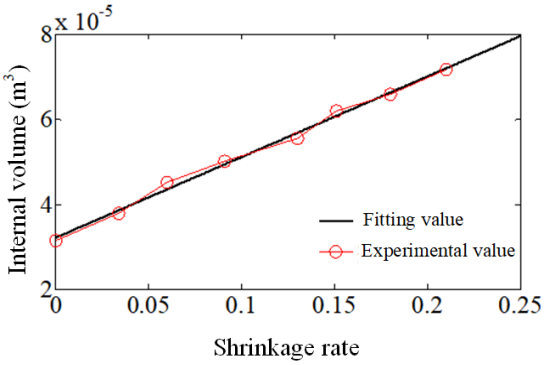

Figure 13: Relationship between internal volume and shrinkage rate of PAMs

The simulation results of the gas mass flow model inside a single PAM are shown in Figure 14. Through lateral comparison and analysis, with the increase of internal pressure, the gas flow of the charging valve port becomes smaller and smaller, while the gas flow of the discharging valve port increases. Through longitudinal comparison and analysis, the gas flow of the charging valve port increases and the discharging valve port decreases when the duty ratio of PWM signal is increased. The value of gas mass flow is consistent with the rated value 100L/min of high-speed switching valve, indicating that the modeling of gas mass flow inside PAM is correct.

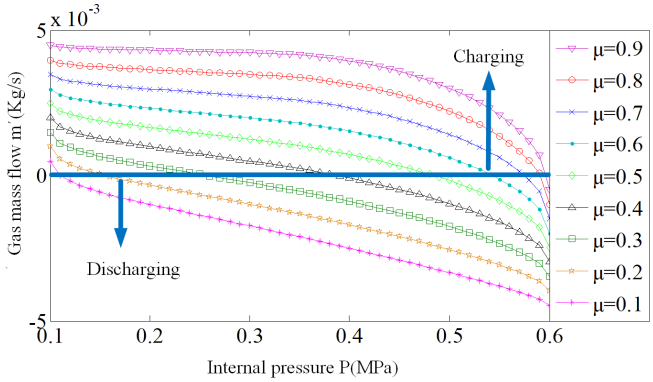

Figure 14: Valve port flow of PAM

To sum up, the function relationship between internal pressure of PAMs and PWM signal can be described as:

$$\begin{cases} P_A = \int \left(\mu_A, P_A, \theta, \dot{\theta}\right)\Big|_{P_{A0}=0.1MPa} \\ P_B = \int \left(\mu_B, P_B, \theta, \dot{\theta}\right)\Big|_{P_{B0}=0.6MPa} \end{cases} \tag{10}$$

Assuming that the internal volume of PAM is fixed at the initial value, the change curve of the internal pressure of PAM A and B with duty ratio of PWM signal can be obtained, as shown in Figure 15. As can be seen from the figure, when the duty ratio is equal to 0.9, the PAM reaches a stable pressure value at a faster rate, and the stable value is roughly the same as the upstream pressure source of 0.6 MPa. On the contrary, the stable pressure value of the PAM is similar to the atmospheric pressure of 0.1 MPa. Thus by adjusting the duty ratio of PWM signal, the control of internal pressure value and charging and discharging rate of PAM is realized.

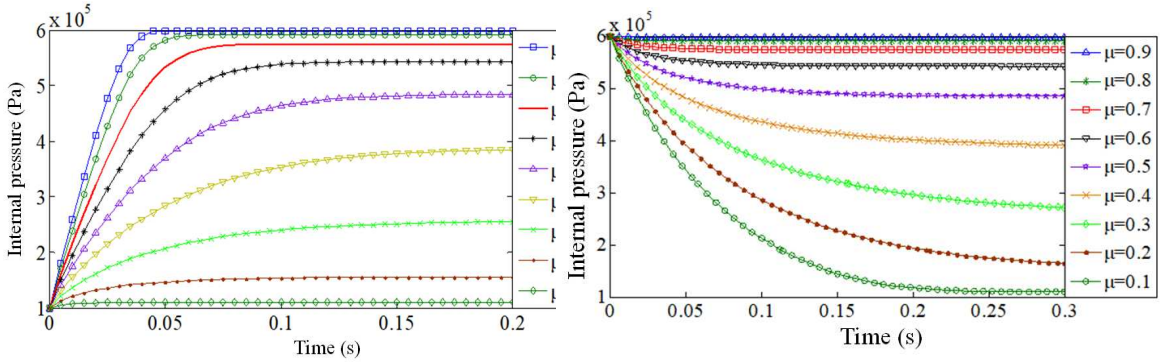

(a) Internal pressure change of PAM A

(b) Internal pressure change of PAM B

Figure 15: Change curve of the internal pressure of PAMs

5 Control simulation and analysis

5.1 Simulation based on PID control

The PID control is one of the most popular automatic control strategies. Besides strong robustness and adaptability, the PID control operates on a simple philosophy: adjusting the system response through proportional, integral and derivative corrections of error. The design of a PID controller does not require the solving of an accurate mathematical model of the object.

The functional relationship between the rotation angle of the chain wheel and the shrinkage ratio of the PAMs can be described as:

$$\begin{cases} \varepsilon_A = \theta \cdot r / l_0 \\ \varepsilon_B = \varepsilon_0 - \theta \cdot r / l_0 \end{cases} \tag{11}$$

where $\varepsilon_0 = 0.2$ is the preload shrinkage ratio of the PAM B.

By combining equations (6), (10) and (11), the functional relationship between the output force of PAM and the PWM signal can be obtained:

$$\begin{cases} F_A = f_A\left(\mu_A, \theta, \dot{\theta}\right) \\ F_B = f_B\left(\mu_B, \theta, \dot{\theta}\right) \end{cases} \tag{12}$$

Based on the solution of the dynamic equation of the artificial leg and the motion analysis of the four-bar knee joint, the functional relationship between the knee torque and the rotation angle of the chain wheel can be obtained:

$$T = M_{21\theta}\ddot{\theta}_1 + M_{22\theta}\ddot{\theta} + C_{21\theta}\dot{\theta}_1^2 + G_{2\theta}\left(\theta_1, \theta\right) = F_A\left(\mu_B, \theta, \dot{\theta}\right) \cdot r - F_B\left(\mu_B, \theta, \dot{\theta}\right) \cdot r \tag{13}$$

In order to simplify the control simulation, during the control of the knee joint, fix the hip joint, i.e. $\theta_1 = 0$, equations (13) can be converted into the general form:

$$\ddot{\theta} = \frac{1}{M_{22\theta}}\left[F_A\left(\mu_A, \theta, \dot{\theta}\right) \cdot r - F_B\left(\mu_B, \theta, \dot{\theta}\right) \cdot r - G_{2\theta}(\theta)\right] \tag{14}$$

The PID control law and transfer function can be respectively expressed as:

$$u(t) = K_p\left(e(t) + \frac{1}{T_i}\int_0^t e(t)dt + T_d\frac{de(t)}{dt}\right) \tag{15}$$

$$G_{(s)} = \frac{U_{(s)}}{E_{(s)}} = K_p\left(1 + \frac{1}{T_i s} + T_d s\right) \tag{16}$$

where K_p, $K_i = K_p/T_i$ and $K_d = K_p \times T_d$ are the gain parameters of the proportional, integral and derivative operations, respectively; T_i and T_d are the time constants of the integral and derivative operations, respectively. The PID controller for the bionic knee with valve signal is presented in Figure 16. The block "Knee - Sprocket"is a switch from knee angle to sprocket angle and the block "Sprocket - Knee"is a switch from sprocket angle to knee angle. The block "Model of Knee"represents the knee dynamics model of the artificial leg. For PAM B, PWM signal contrary to ideal angle information is given, and PWM signal duty ratio of PAM A is adjusted by PID controller. The angle information of sprocket is collected by the encoder for feedback, which is used for solution of control error.

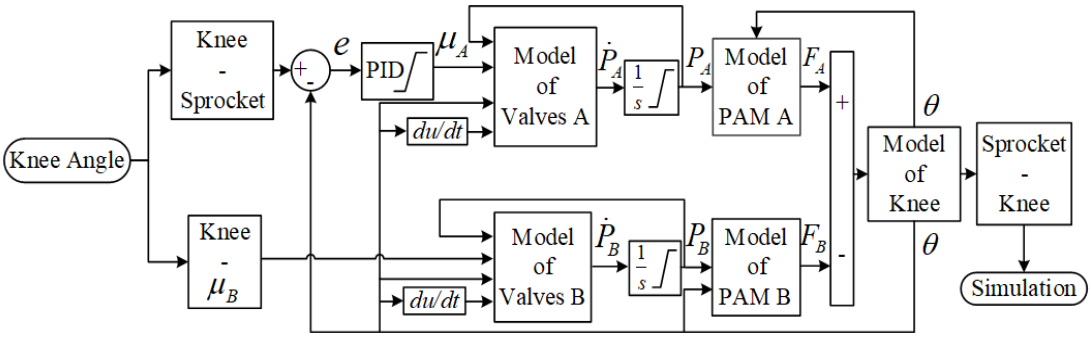

Figure 16: Structure of the PID controller of the bionic knee

To verify the four-link bionic knee and the model of the PAMs driving mode, a simulation model was set up on MATLAB Simulink, and adopted to simulate how the bionic knee followed the ideal trajectories under irregular square wave signal and sinusoidal signal, respectively.

The PID controller parameters were configured through trial and error: $K_p = 3.9$; $K_i = 5.88$; $K_d = 2.05$; N (differential filter coefficient) = 100. Considering the actual response time of high-speed on-off valve under continuous working mode ((< 0.2ms)), the step length was fixed at 0.01s; the duty cycle range of the PWM control signal was set to 0.12∼ 0.88; the integrator output range of the internal pressure of the PAMs was set to 0.1∼ 0.6MPa; the initial pressure of

the two PAMs were set to $P_A = 0.1$Mpa and $P_B = 0.6$Mpa, respectively. The simulation results are shown in Figures 17 $\sim$ 22.

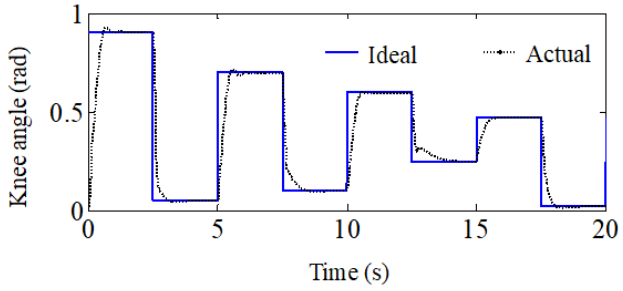

Figure 17: Following curve under irregular square wave signal

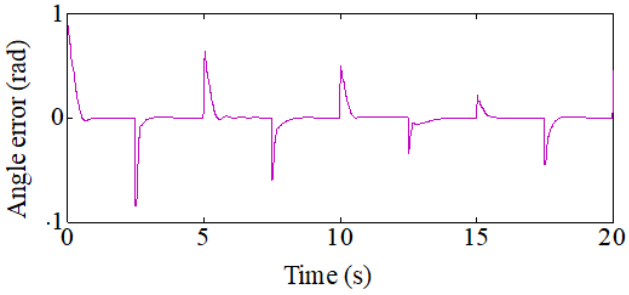

Figure 18: Angle error under irregular square wave signal

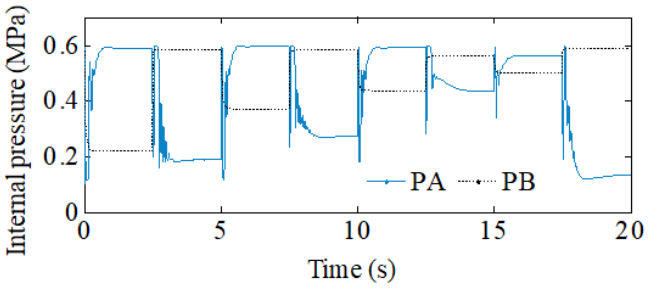

Figure 19: Internal pressure variation under irregular square wave signal

As shown in Figures 17 $\sim$ 19, under the PID control, the different positions of the bionic knee rotated quickly by the required angles, following the ideal trajectory under irregular square wave signal, and the internal pressure of the PAMs changed between 0.1 and 0.6MPa. Thus, the PID controller can satisfy the requirements for actual application.

As shown in Figures 20$\sim$ 22, for the sinusoidal signal, the bionic knee can achieve ideal follow on the whole under the PID control, but the tracking error was about 0.06 rad. It can be seen that the PID controller basically meets the control requirements for the linear system, but has little capacity for the nonlinear system. Due to the strong nonlinear of the electric-pneumatic system of the knee joint, the design of nonlinear controller needs to be considered.

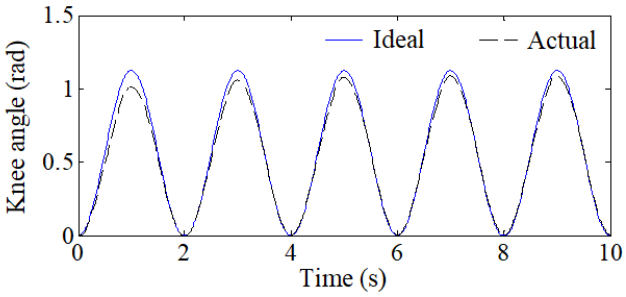

Figure 20: Following curve under sinusoidal signal

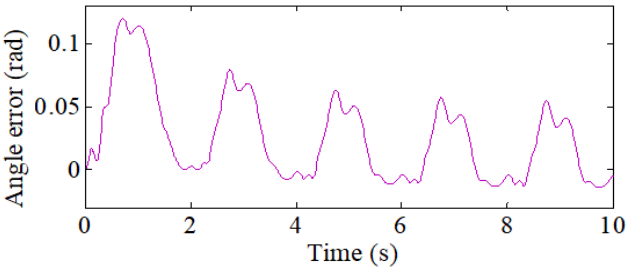

Figure 21: Angle error under sinusoidal signal

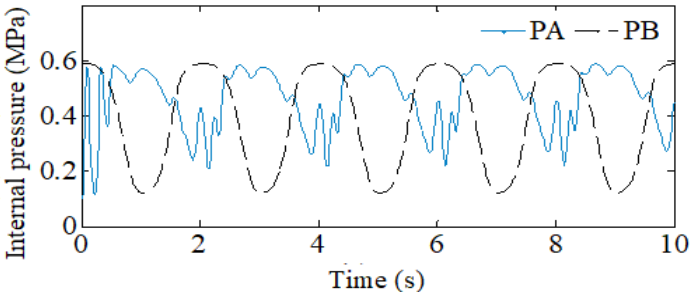

Figure 22: Internal pressure variation under sinusoidal signal

5.2 Simulation based on sliding mode control

Sliding mode control is essentially a nonlinear control. Compared with other control methods, the structure of the sliding mode control system is not fixed and purposefully changing according to the current state of the system (such as deviation) during the dynamic process, forcing the system to move in accordance with the predetermined sliding mode state trajectory. This method has the advantages of rapid response and insensitivity to parameter change and disturbance, and is suitable for the control of electric-pneumatic system of bionic knee joint.

Considering that the bionic knee system of artificial leg is a second-order equation about angle θ of sprocket wheel, the designed sliding mode function is:

$$s(t) = \lambda_1 e + \dot{e} \tag{17}$$

where $\lambda_1 > 0$ and meets Hurwitz conditions. The angle tracking error of the knee joint system is:

$$e = \theta_d - \theta \quad \dot{e} = \dot{\theta}_d - \dot{\theta} \tag{18}$$

Where θ_d is the angle of sprocket wheel in ideal movement of knee joint. The derivative of the sliding mode function is:

$$\dot{s} = \lambda_1 \dot{e} + \ddot{e} = \lambda_1 \left(\dot{\theta}_d - \dot{\theta} \right) + \left(\ddot{\theta}_d - \ddot{\theta} \right) \tag{19}$$

In order to ensure the stability of the control system of the knee joint, the motion points in the area around the sliding mode surface should eventually tend to the sliding mode surface $s = 0$. Therefore, Lyapunov function is defined as follows:

$$V_1 = \frac{1}{2} s^2 \tag{20}$$

According to Lyapunov stability criterion, there should be:

$$\lim_{s \to 0} \dot{V}_1 = \lim_{s \to 0} s\dot{s} \leq 0 \tag{21}$$

Weighing the approaching speed and stability of the control system, this paper adopts the exponential approaching law:

$$\dot{s} = -\delta_1 \cdot \text{sign}(s) - \delta_2 s \quad \delta_1 > 0 \quad \delta_2 > 0 \tag{22}$$

Exponential term $-\delta_2 s$ can guarantee that the system state can approach the sliding mode with a large speed when s is large. However, when s is small, its approach speed is slow and cannot guarantee to arrive in a finite time. Therefore, an isokinetic approach term $-\delta_1 \cdot \text{sign}(s)$ is added. Combined with the knee system model of artificial leg, the sliding mode controller based on the approach law is obtained:

$$\begin{aligned} F_A \left(\mu_A, \theta, \dot{\theta} \right) &= \frac{M_{22\theta}}{r} \left(\lambda_1 \left(\dot{\theta}_d - \dot{\theta} \right) + (\delta_1 \cdot \text{sign}(s) + \delta_2 s) + \ddot{\theta}_d \right) + \frac{G_{2\theta}(\theta)}{r} + F_B \left(\mu_B, \theta, \dot{\theta} \right) \\ &= P_A \left(\mu_A, \dot{\theta}, \theta \right) \cdot \kappa_{A1}(\theta) + \kappa_{A2}(\theta) \end{aligned} \tag{23}$$

Where κ_{A1} and κ_{A2} are polynomials about shrinkage in the static model of PAM.

According to the charging and discharging dynamic model of PAM, and combining the functional relationship between the angle of sprocket wheel and the shrinkage rate of PAM, the functional relationship between the internal pressure P_A of flexor and the duty ratio μ_A of PWM, the control signal of high-speed switching valve group, is established.

$$\mu_A = \begin{cases} \frac{\overline{V} + P_A \Gamma_{2A}}{P_{up} \Gamma_{1A} + P_A \Gamma_{2A}} & P_A < 0.189 \\ \frac{\overline{V} + P_A \Gamma_{1A}}{P_{up} \Gamma_{1A} + P_A \Gamma_{1A}} & 0.189 \leq P_A \leq 0.317 \\ \frac{\overline{V} + P_A \Gamma_{1A}}{\Gamma_{3A} + P_A \Gamma_{1A}} & P_A > 0.317 \end{cases} \tag{24}$$

where $\overline{V} = \frac{V\dot{P}_A + \gamma P_A \dot{V}}{\gamma A_{\max} \sqrt{RT}}$, $\Gamma_{1A} = \sqrt{\gamma \cdot \left(\frac{2}{\gamma+1} \right)^{\frac{\gamma+1}{\gamma-1}}}$, $\Gamma_{2A} = \sqrt{\frac{2\gamma}{\gamma-1} \cdot \left[\left(\frac{P_{atm}}{P_A} \right)^{\frac{2}{\gamma}} - \left(\frac{P_{atm}}{P_A} \right)^{\frac{\gamma+1}{\gamma}} \right]}$ and $\Gamma_{3A} = \sqrt{\frac{2\gamma}{\gamma-1} \cdot \left[\left(\frac{P_A}{P_{up}} \right)^{\frac{2}{\gamma}} - \left(\frac{P_A}{P_{up}} \right)^{\frac{\gamma+1}{\gamma}} \right]}$.

The simulation system of artificial knee joint based on sliding mode control is shown in Figure 23. In the simulation process, the step size setting is consistent with the PID simulation. $\lambda_1 = 8$, $\delta_1 = 5.88$, , $\delta_2 = 2.05$ and the setting range of duty cycle output of high-speed switching

valve is 0.12∼0.88. The initial values of internal pressure inside the PAM is also set as PA= 0.1 MPa and PB= 0.6 MPa. The simulation results are shown in Figures 24∼31.

It can be seen from Figures 24∼26 that, for irregular square wave signals, the sliding mode control system can achieve better tracking, with smaller error and faster response time than the PID controller. The internal pressure of the PAM varies within 0.1∼0.6 MPa and is reasonable.

It can be seen from Figures 27 and 29 that, for the trajectory curve of sinusoidal signal, the sliding mode controller can achieve ideal following, with the error range controlled within 0.03 rad and a fast response time, which fully meets the precision requirements of knee motion control. As shown in Figures 30∼31, the sliding mode controller can realize the ideal following of human normal gait, which proves the correctness of the structure design and system modeling in this paper.

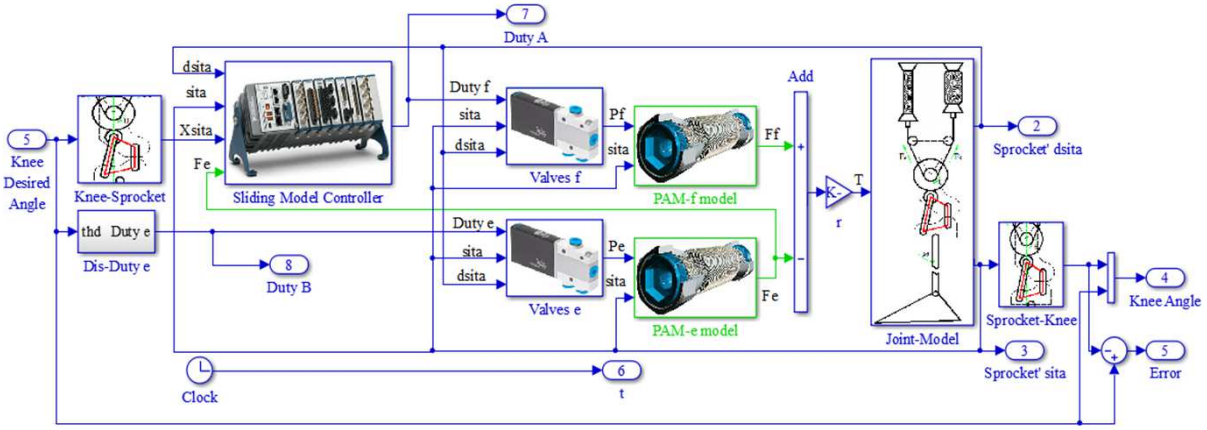

Figure 23: Simulation system of artificial knee joint based on sliding mode control

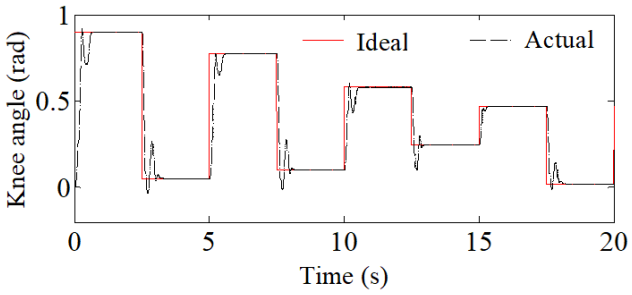

Figure 24: Following curve under irregular square wave signal

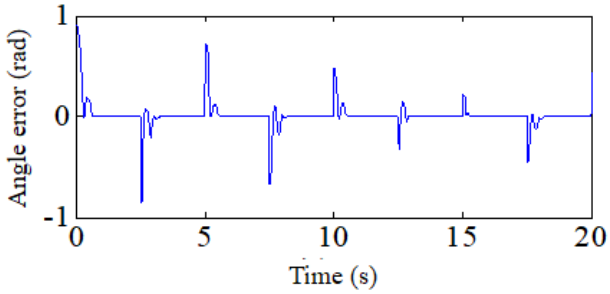

Figure 25: Angle error under irregular square wave signal

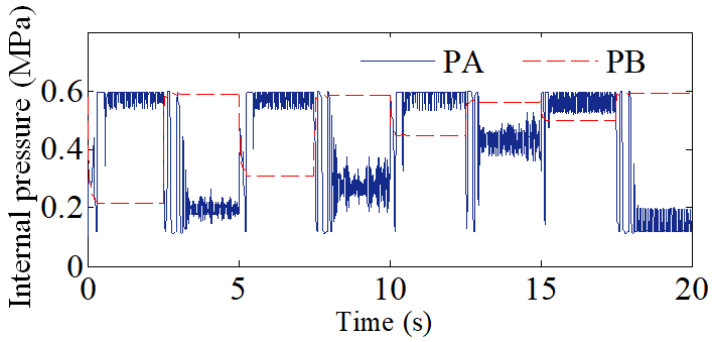

Figure 26: Internal pressure variation under irregular square wave signal

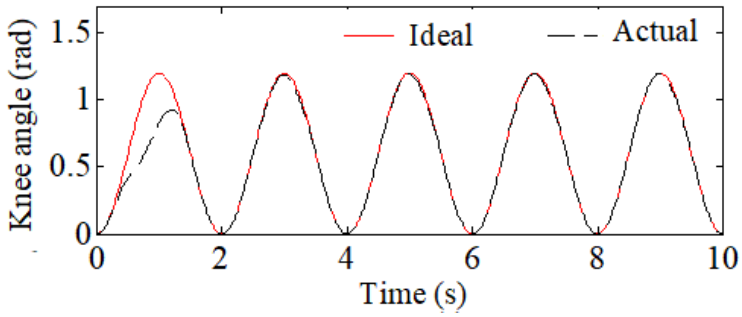

Figure 27: Following curve under sinusoidal signal

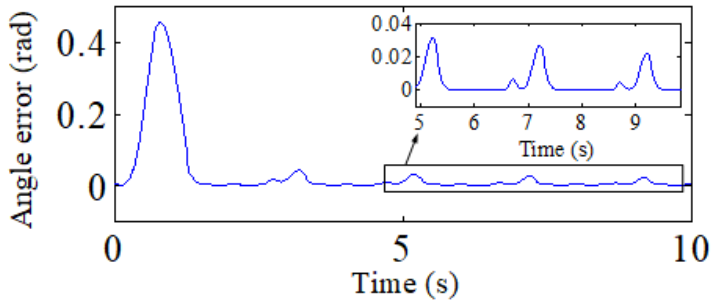

Figure 28: Angle error under sinusoidal signal

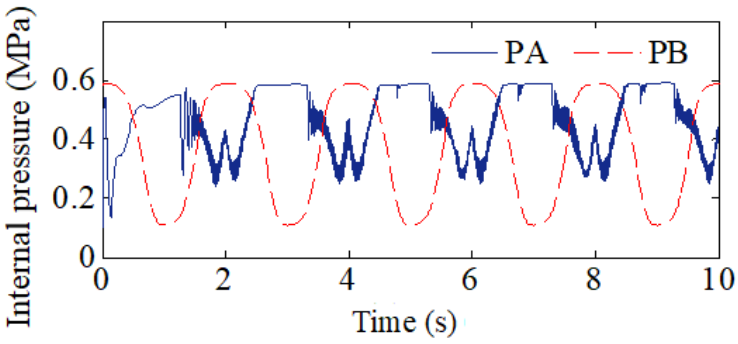

Figure 29: The internal pressure variation under sinusoidal signal

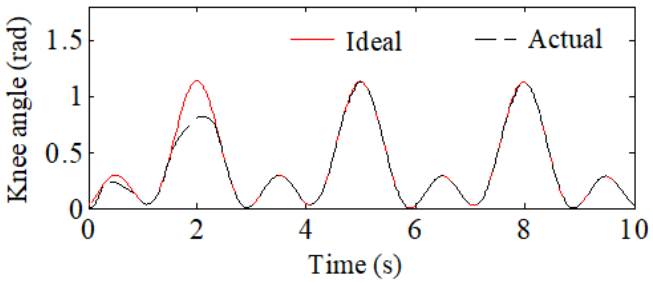

Figure 30: Following curve under human normal gait

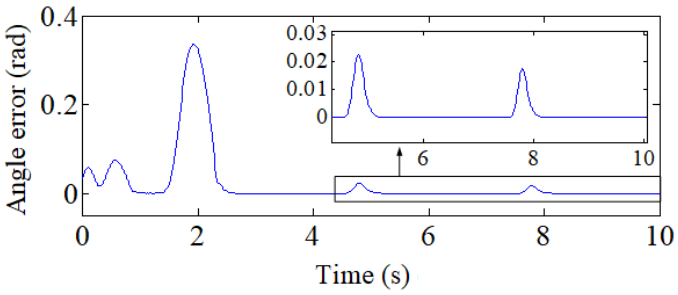

Figure 31: Angle error under human normal gait

6 Conclusions

In this paper, the authors propose a new prosthesis platform and design a bionic artificial leg that simulates the healthy leg of human body.

Based on the analysis of human knee motion, this paper designs a four-link bionic knee, and simulates the flexor and extensor muscles as two PAMs. The two PAMs move in opposite direction, driving the knee motions in the artificial leg. In this way, the artificial leg can move similarly to a human leg.

After testing the PAM features, a static model was developed for the PAMs based on the test results, using the least squares method. Based on Sanville's valve flow formula, a dynamic model was constructed for the total valve port flow of each PAM under simultaneous charging and discharging.

Finally, the PID closed loop controller and sliding mode controller were designed for the bionic knee. The simulation results show that compared with the PID closed-loop controller, the sliding mode controller can significantly improve ideal track following effect and realize the ideal track following of the human normal gait, which indicates the correctness of the structural design and system modeling in this paper.

Acknowledgment

Financial supports from the Fundamental Research Funds for the Central Universities (ID N170313025) and Scientific Study Project of Liaoning Province Education Department (ID LQGD2017029) are highly appreciated.

Bibliography

[1] Chen, D.H.; Ushijima, K. (2013); Prediction of the mechanical performance of mcKibben artificial muscle actuator, *International Journal of Mechanical Science*, 78(1), 183-192, 2013.

[2] Chou, C.P.; Hannaford, B. (1996); Measurement and modeling of mcKibben pneumatic artificial muscles, *IEEE Transactions on Robotics and Automation*, 12(1), 90-102, 1996.

[3] Ganguly, S.; Garg, A.; Pasricha, A.; Dwivedy, S.K. (2012); Control of pneumatic artificial muscle system through experimental modelingm, *Mechatronics*, 22(8), 1135-1147, 2012.

[4] Gong, S.Y.; Yang, P.; Song, L.; Chen, L.L. (2011); Simulation of swing phase dynamics in trans-femoral prostheses based on MATLAB, *Journal of Hebei University of Technology*, 40(2), 6-9, 2011.

[5] Jouppila, V.; Gadsden, S.A.; Ellman, A. (2014); Experimental comparisons of sliding mode controlled pneumatic muscle and cylinder actuators, *Journal of Dynamic Systems Measurement&Control*, 136(4), 543-552, 2014.

[6] Pandit, S.; Godiyal, A.K.; Vimal, A.K.; Singh, U.; Joshi, D.; Kalyanasundaram, D. (2018); An affordable insole-sensor-based trans-femoral prosthesis for normal gait, *Sensors*, 18(3), 2018.

[7] Pillai, M.V.; Kazerooni, H.; Hurwich, A. (2001); Design of a semi-active knee-ankle Prosthesis, *Proceedings of IEEE International Conference on Robotics and Automation*,IEEE, Shanghai, China, 5293-5300, 2001.

[8] Radcliffe, C.W. (2003); Biomechanics of knee stability control with four-bar prosthetic knees, *ISPO Australia Annual Meeting*, 2003.

[9] Sanville, F.E. (1971); Van Brussel, H. (1971); New method of specifying the flow capacity of pneumatic fluid power valves, *Hydraulic Pneumatic*, 17(195), 120-126, 1971.

[10] Su, B.Y.; Wang, J.; Liu, S.Q.; Sheng, M.; Jiang, J.; Xiang,K. (2019); A CNN-Based Method for Intent Recognition Using Inertial Measurement Units and Intelligent Lower Limb Prosthesis, *IEEE Transactions on Neural Systems and Rehabilitation Engineering*, 27(5), 1032-1042, 2019.

[11] Tian, H.; Ma, L.; Zhu, X.; Dang, X. (2019); Grinding method, trajectory planning and simulation of a 3 DOF knee grinding robot, *International Journal of Simulation Modelling*, 18(1), 150-162, 2019.

[12] Vo-Minh, T.; Tjahjowidodo, T.; Ramon, H.; Van Brussel, H. (2011); A new approach to modeling hysteresis in a pneumatic artificial muscle using the maxwell-slip model, *IEEE/ASME Transactions on Mechatronics*, 16(1), 177-186, 2011.

[13] Vo-Minh, T.; Tjahjowidodo, T.; Ramon, H.; Van Brussel, H. (2010); Cascade position control of a single pneumatic artificial muscle-mass system with hysteresis compensation, *Mechatronic*, 20(3), 402-414, 2010.

[14] Wang, S.F., Sato, K.; Kagawa, T. (2014); Precise positioning of pneumatic artificial muscle systems, *Journal of Flow Control, Measurement&Visualization*, 2(4), 138-153, 2014.

[15] Xie, H.L.; Chen, K.L.; Li, F. (2015) ; Bionic artificial leg design and control simulation based on fuzzy PID control algorithm, *Proceedings of IEEE International Conference on Cyber Technology in Automation, Control and Intelligent Systems*, IEEE, Shenyang, China, 2097-2102, 2015.

[16] Xie, H.L.; He, N.; Li, F.; ieYang, J.Y. (2015); The bionic design and system identification of intelligent bionic leg with magneto-rheological damper, *Tehnicki Vjesnik,*, 22(5), 1093-1098, 2015.

[17] Xie, H.L.; Liang, Z.Z.; Li, F.; Guo, L.X. (2010); The Knee Joint Design and Control of above Knee Intelligent Bionic Leg Based on Magneto-rheological Damper, *International Journal of Automation and Computing*, 7(3), 277-282, 2010.

[18] Xie, H.L.; Liu, Z.B.; Yang, J.Y. (2016); Modelling of Magnetorheological Damper for Intelligent Bionic Leg and Simulation of Knee Joint Movement Control, *International Journal of Simulation Modelling*, 15(1), 144-156, 2016

[19] Young, A.; Hargrove, L. (2016); A classification method for userindependent intent recognition for transfemoral amputees using powered lower limb prostheses, *IEEE Transactions on Neural Systems and Rehabilitation Engineering*, 24(2), 217-225, 2016.

[20] Zhang, X.F.; Fu, H.Q.; Wang, X.T.; Li, G.L.; Yang, R.; Liu, Y. (2016); Design of a novel bionic prosthetic knee joint, *Assembly Automation*, 36(4), 398-404, 2016.

[21] Zhang, Z.H.; Hu, C. (2015); Multi-model stability control method of underactuated biped robots based on imbalance degrees, *International Journal of Simulation Modelling*,14(4), 647-657, 2015.

[22] Zhu, J.M.; Huang, C.Y.; Lei, J.T.; Qi, B.C. (2017); Position/Stiffness Control of Antagonistic Bionic Joint Driven by Pneumatic Muscles Actuators, *Journal of Mechanical Engineering*, 53(13), 64-74, 2017.

INTERNATIONAL JOURNAL OF COMPUTERS COMMUNICATIONS & CONTROL
ISSN 1841-9836, e-ISSN 1841-9844, 14(5), 753-771, October 2019.

DCM: D Number Extended Cognitive Map. Application on Location Selection in SCM

L. Zhao, F. Xiao

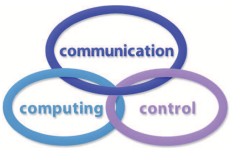

Lian Zhou
Computer and Information Science
Southwest University, Chongqing, China

Fuyuan Xiao*
Computer and Information Science
Southwest University, Chongqing, China
*Corresponding author: xiaofuyuan@swu.edu.cn, doctorxiaofy@hotmail.com

Abstract: Offshore outsourcing is a widely used management technique for performing business functions with the aim of reducing labor and transportation costs. The selection of locations has a significant influence on the supply chain's resilience and qualities, but the influence of multiple external factors on the supply chain's performance in local places in a complex and uncertain environment has not been examined. In this study, we investigated the influence of external factors in a highly uncertain and complicated situation in which relationships between external factors and supply chain resilience are complicated. Furthermore, we proposed a novel model to select locations from a comprehensive perspective. Specifically, the fuzzy cognitive map (FCM) is utilized to simulate the dynamic influence process where the adjacency is aggregated by D numbers. The weights of different resilience capabilities are considered from the perspective of maximizing benefits by using the decision-making trial and evaluation laboratory-analytic network processes (DEMATEL-ANP) model. By comparing the distance to the ideal solutions, we selected the best alternative location. Our results differ from the general case, which reveals that the weights of different capabilities influence selections.
Keywords: Offshore outsourcing, supply chain resilience, location selection; FCM, D number, DEMATEL-ANP, multicriteria decision making (MDM).

1 Introduction

In recent years, the globalization of the economy and competition has led to low consumption, and thus, the offshore outsourcing process has attracted extensive attention as one of the most adaptive strategies [9, 13]. Offshoring allows for firms to focus on core competencies to improve their productivity, efficiency, and flexibility. The core competencies release a range of expertise that crosses traditional functions horizontally and adapts to changes in the long-term demands of clients, thus continuing domination over competitors [21]. A comparatively successful offshore outsourcing strategy can significantly assist a firm in improving its production efficiency, productivity, and flexibility to improve total profits and tackle emergency situations [22]. However, factors limiting the extensive application of offshore outsourcing remain, and outsourcing may elicit some potential threats to client firms by extending their supply chains (SCs) [6].

Offshore outsourcing also has the potential to transfer specific ownership of the business

activities and resources to low-cost providers overseas. Comparing the keyword offshore outsourcing to a similar keyword, outsourcing, we usually consider offshore outsourcing to involve a vendor located in a country other than that of the buyer. Therefore, only the location of the seller differentiates the above two keywords. The core of offshore outsourcing is the practice of using a supplier rather than in-house employees to perform a function [2]. The following question to be solved is where to outsource [7]. The selected provider will participate in increasing integration of the SC. Previous research has shown that the supply chain network is vulnerable to disruptions, and the failure of elements within the SC may cause the failure of the whole network. We assumed that an ideal offshore outsourcing location would satisfy the requirements of employers in terms of both economic and political aspects to enhance the performance of the whole SC. However, an erroneous choice may cause a significant negative effect on the entire SC network [20].

To realize competitive advantages of supply chains, the priority is to develop 'agility', 'self-alignment', and 'adaptation' (triple A's). Supply chain 'agility' indicates an instant response to short-term perturbations caused by uncertainties in the upstream and downstream supply chains. With respect to offshore outsourcing supply chains, agility is related to the capabilities of the supply chain to deal with unexpected changes in market demand, which can transform from challenges into opportunities and lead the supply chain to gain competitive advantages in a volatile and turbulent environment [33]. Supply chain 'alignment' refers to the integration process of several members in the supply chain to achieve better performance [25]. The necessity of the attribute has been highlighted in many studies and requires further investigation [35]. Finally, the adaptability of the supply chain enables the supply chain to evolve based on market changes in strategies [15]. Recent researches have shown the importance of supply chain adaptability as a dynamic capability. In summary, the reviewed capabilities could be denoted by the keyword 'resilience', and more specifically, the best way to improve a supply chain's competitiveness in an offshore outsourcing scenario is to maximize its resilience.

Most client firms are offshoring core competencies with global suppliers, with a focus on the selection of key value-creating competencies. This situation increases SC complexity and interdependency, leading to a risk of SC vulnerability. Therefore, SC resilience is very crucial to minimize property losses in disruptions. Recent research has revealed that the Tohoku earthquake affected supply chains in the Philippines in 2017. Specifically, due to the lack of resilience in supply chains, many properties and client firms suffered from destructive natural disasters [1].The above event suggests that a resilient supply chain is important for minimizing the negative effects of disruptions and allowing for the SC to recover normal activity in a short time [9].If a corporation has a responsive SC, SC resilience can return to a normal or even better state [10]. Furthermore, an offshore outsourcing process also involves unexpected outer disruptions and accidental events, and incoming potential risks would cause damage to SC systems. Moreover, due to the complexity and interdependence of entities in SC, a minor failure within the SC may cause a failure cascade in the whole system. Therefore, SC resilience is considered an important indicator in the offshore outsourcing process.

Despite these challenges, previous research has not made progress in investigating the relationship between locational decisions in offshore outsourcing and SC resilience. Few studies have employed SC resilience as an indicator when selecting offshore outsourcing locations. Thus, we assumed that an ideal offshore outsourcing location has positive effects on SC resilience to prevent accidental disruptions and ensure SC robustness. To bridge the gap between offshore outsourcing and SC resilience, this study proposed a combined method based on the analytic network process (ANP) [12], decision-making trial and evaluation laboratory (DEMATEL) method [11], fuzzy cognitive map (FCM) [12], and technique for order preference by similarity to an ideal solution (TOPSIS) [16]. Specifically, FCM can represent all connections with the considered

abilities to evaluate alternative locations and address the imprecise and fuzzy weights of links. DEMATEL and ANP are combined to determine the weights of FCM, and TOPSIS is implemented in alternative locations specific to outcomes gathered from FCM.

In this study, FCM can predict the impacts of alternative locations on SC resilience by simulating scenarios over time, and the executive functions can select an optimal offshore outsourcing location. Furthermore, ANP-DEMATEL is used to determine the weights of links by inputting evaluations from experts. In addition, TOPSIS is considered an efficient tool for ranking alternative offshore outsourcing locations with respect to SC resilience. The aim is to maximize SC resilience by choosing an ideal offshore outsourcing location. In addition, to avoid subjectivity and fuzziness of experts assessments, multiple experts are invited to evaluate the project, and their opinions are aggregated by D numbers The rest of this paper is organized as follows. The background of our study is overviewed in Section 2. In Section 3, some related preliminaries related to our study are introduced. In Section 4, we present our hybrid integration approach for selecting the best alternative outsourcing locations with respect to supply chain resilience.we present a DCM based integration decision model for selecting the best alternative outsourcing locations with respect to supply chain resilience. Section 5 presents an empirical application of the proposed model. The verification and discussion of our approach's rationality and superiority are described in Section 6. Section 7 conducts a sensitivity analysis. In the final section, we present the conclusions of our study.

2 Preliminaries

2.1 D number theory

In the real world, uncertainty modeling and optimization are difficult to quantify because knowledge and information are imprecise and incomplete [14]. Dempster-Shafer evidence theory (also known as D-S theory or evidence theory) is an efficient tool for dealing with the information fusion issue [3, 4, 17, 28]. However, some inherent drawbacks limit the broader application of the D-S theory. First, D-S theory requires a strong hypothesis that elements in the discerning frame are mutually exclusive, which is very difficult to satisfy, especially in linguistic assessments. Second, a norm basic probability assignment (BPA) must follow a completeness constraint in D-S theory, which means that the sum of all focal elements in a BPA must be equal to 1 [6]. However, the experts do not have access to the overall knowledge, and the assessment is based only on partial information, potentially resulting in an incomplete BPA [32, 33]. To address this issue, D numbers are presented [8, 18–20, 29].

2.2 Fuzzy cognitive maps

Political scientist Robert Axelrod introduced cognitive maps in the 1970s to represent social scientific knowledge [23]. The fuzzy cognitive map (FCM), an extension of the cognitive map, is a causal description of a model of the behavior of a system [24]. FCM is an interactive structure of concepts, each of which interacts with the rest, and reveals the dynamics and different behaviors of the system. Each concept is described by a number A_i that represents its value and results from the transformation of the fuzzy real value of the system's variable, for which this concept stands, in the interval [0,1]. There are three types of causal interactions between concepts that represent the type of influence from concepts to the others.

2.3 DEMATEL

The methodology of the Decision Making Trial and Evaluation Laboratory (DEMATEL) was developed initially by the Battelle Memorial Association in Geneva [5] and is an effective method for analyzing the direct and indirect relationships between components in the system with respect to severity and type [34]. DEMATEL is widely applied in supply chain management and service quality evaluation. By utilizing this method, we can extract a better understanding of the structural relationships, and thus, this method is an ideal way to solve complicated system problems. The procedure for implementing DEMATEL to solve dependent evidence consists of four steps namely 1) Define the quality feature and establish the measurement scale 2) Extract the DRM of influential factors 3) Normalized DRM 4) Calculate TRM.

2.4 ANP

Network analysis is a very useful tool to model real application [31, 36, 37]. The analytic network process (ANP) is capable of tackling dependence among components in a system. It is a generation of the analytic hierarchy process (AHP) and allows for more complicated interrelationships among decision elements by replacing the hierarchy in the AHP [26] with a network. The network structure of ANP includes the control level and network level. The control level consists of goal and independent criteria whose weights can be obtained by AHP. There is at least one goal at the control level. At the network control level, the network spreads out in all directions and involves arrows between clusters or loops within the same cluster. These arrows and loops indicate the relations among clusters or within a cluster. ANP is also applied to prioritize factors or criteria in the decision-making problem. In this paper, we only consider one goal, and criteria are omitted at the control level.

2.5 TOPSIS

The technique for Order Preference by Similarity to Ideal Solution (TOPSIS), which was developed by Hwang and Yoon in 1981 [38], is a method for ranking alternatives in applications and concepts [30, 39]. The core ideal of TOPSIS is to choose alternatives that simultaneously have the shortest distance from the positive ideal solution and the farthest distance from the negative ideal solution. The positive ideal solution maximizes the benefit criteria and minimizes the cost criteria, whereas the negative ideal solution maximizes the cost criteria and minimizes the benefit criteria.

3 Selecting offshore outsourcing location considering supply chain resilience

As shown above, supply chain resilience (SCRE) is a crucial factor in offshore outsourcing and should receive close attention when selecting an outsourcing location. The main thrust of this paper is to rank some alternative locations and select the most suitable one from the perspective of SCRE. However, in the real world, multiple factors influence SCRE, and these factors interact with SCRE under changing conditions in foreign locations. Thus, the interacting behaviors among SCRE and these external factors should be regarded as a dynamic mechanism in a highly complex and uncertain manner. In addition, the SCRE could be divided into various capabilities (e.g., flexibility, visibility, anticipation, etc.). These different capabilities have weights corresponding to different criteria under one goal of maximizing total benefits. All of these issues should be taken into consideration via a comprehensive perspective. In summary, the issue

of selecting the best offshore outsourcing location is a typical multi-criteria decision-making (MCDM) problem. Since most existing research has researches have regarded the issue as a static problem or focused on one aspect of it, we propose a comprehensive perspective to tackle this complicated problem. First, we use a fuzzy cognitive map extended by the D number to identify the influencing mechanism of outer factors on SCRE in an offshore outsourcing location. Then, an ANP-DEMATEL model is utilized to assign weights to different capabilities of SCRE in the benefit perspective. Finally, we rank alternative locations with disparate outer factors by using the TOPSIS method. The details are introduced below.

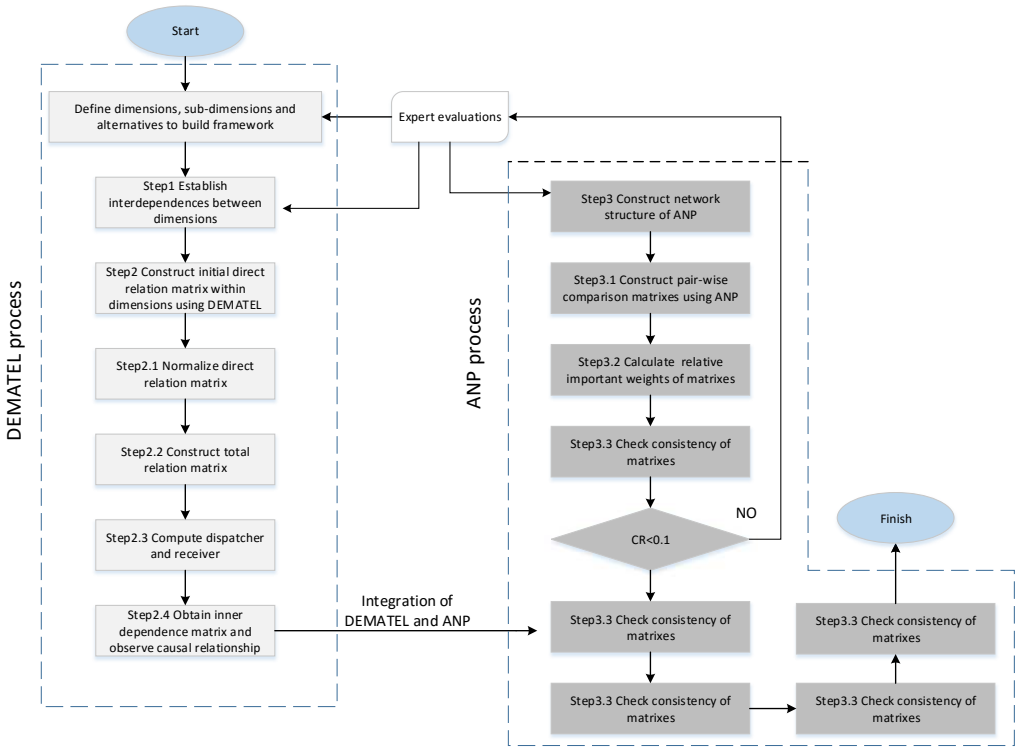

Figure 1: An overview of the weight assignment framework

3.1 Identify the impacts of outer factors on SCRE

To determine the impact of outer factors on SCRE in offshore outsourcing, the FCM is introduced to simulate the process in a complicated and uncertain environment. The procedure is presented below.

1) Expert evaluation: Some authorities on outsourcing will be invited to define crucial outer factors that are closely related to SCRE. They may use their experience, knowledge and some interactive techniques such as the Delphi method or affinity diagrams to identify these factors for further research. Similarly, the different aspects of SCRE capability are addressed in this step. These outer factors and the SCRE capabilities will be regarded as the nodes in the FCM that describe the real problem or general system.

2) Identify the causal connections between nodes ($w_i \to w_j$). The type of relation (positive or negative) and its intensity should be taken into consideration and defined. The preliminary means of conducting this procedure is to define intensity scales. All evaluations should be mapped on the interval $[0, 1]$. We use AHP to quantify the degree of intensity. The scientific evaluations

are transformed into a quantitative range by implementing the AHP method.

3) Aggregate the multiple experts' opinions in different groups. In the real world, the interactions between external factors and SCRE capabilities are very uncertain due to their complexity. To address this problem, multiple experts with different backgrounds will be invited to decrease uncertainty and obtain a relatively precise result. D number theory is introduced to fuse these evaluations due to its superiority in representing incomplete and imprecise information.

4) FCM inference. FCM can not only represent causal relations but also predict future implications through dynamic simulations. At the initial stage, each FCM node is assigned a value $[0, 1]$, and the initial state vector $V_{s_i}^0 = (v_1^0 \quad v_2^0 \quad \cdots \quad v_{n-1}^0 \quad v_n^0)$ is obtained. Then, using Eq. (7), the behavior of the influencing mechanism will be revealed.

In this stage, the impacts of external factors on SCRE can be identified, and the evolutionary process of FCM can quantify these impacts.

3.2 Weight different resilience capability

An overview of the integrated DEMATEL and ANP approach for assigning different weights to SCRE capabilities is given in Fig. 1.

Briefly, the values are gathered from a computer database and questionnaires. The DEMATEL method is employed to deal with the inner dependency by gathering pairwise comparisons. The inner dependency is then structured, and ANP is implemented to perform further calculations. The details are listed as follows:

Step 1: Define the criteria, objective, sub-criteria, and alternatives of the ANP model. The criteria and sub-criteria are acquired from experts' knowledge, experience, and other appropriate approaches. In this paper, the objective is to maximize the offshore outsourcing practitioners' benefits, and the alternatives are different SCRE capabilities.

Step 2: Construct a direct-relation matrix using DEMATEL: Decision makers are required to compare the criteria pairwise with respect to influence and direction. The comparison scale is defined at 5 levels: (0) no influence, (1) low influence, (2) medium influence, (3) high influence, and (4) extreme influence.

Step 2.1: Normalize the direct-relation matrix. The direct-relation matrix is transformed to the normalized matrix.

Step 2.2: Calculate the total relation matrix. The total relation matrix could be obtained via the normalized direct-relation matrix.

Step 2.3: To visualize the relations among factors, we calculate the dispatcher and receiver groups. The dispatcher is estimated from $D-R$, which has positive values and a greater influence on other factors. They are assumed to exhibit higher priority and are called dispatcher groups, where R is the sum of the columns and D is the sum of rows in the matrix T. The other values with negative values of $D - R$ receive more influence from one another and are considered to have lower priority; these are called receiver groupers. The value $D + R$ here shows the relation degree of each factor with others. Those factors with higher $D + R$ have more of a relationship with each other, and those with lower $D + R$ have less of a relationship with each other.

Step 2.4: Obtain the inner dependence matrix: The sum of each column is 1 in the total relationship matrix.

Step 3: Use ANP to construct the network for the problem and access the different SCRE capabilities.

Step 3.1: Calculate the relative weights of different criteria in offshore outsourcing benefits. The AHP method is utilized to calculate their weight. A scale of 9 from equal importance to extreme importance is used to measure the relative importance of criteria. A decision maker would judge the relative dominance between each pair of criteria, and the results will be turned

into values of 1, 3, 5, 7, and 9, which represent equal importance, moderate importance, strong importance, demonstrated importance, and extreme importance, respectively, whereas values of 2, 4, 6, and 8 indicate intermediate importance. Through the process of AHP, the relative weights of criteria are obtained.

Step 3.2: The supermatrix can be acquired by entering the vectors derived from DEMATEL, and then, the normalized weighted matrix is transferred from the supermatrix by multiplying the relative weights of criteria from step 3.1., in which every column's sum is 1. The weighted matrix then converges to a stable value after it is raised by its limiting power.

Step 4 Determine the relative weights of the SCRE capabilities: the final weights are found in the corresponding row in the limit of the supermatrix; these weights should be taken into consideration when we select optimal offshore outsourcing locations.

3.3 Rank alternative locations and select optimal one in SCRE perspective

Some alternative locations for offshore outsourcing are discussed and compared at this stage. Since these alternatives have different outer factors, they have different values for each outer factor. We input these initial vectors into the FCM, and after the FCM reaches an equilibrium stage, various SCRE capabilities will be activated. The TOPSIS method is then used to quantify the distance of alternative locations to the ideal solution considering the relative weights of each SCRE capability. The location with the greatest value according to Eq. (18) will be chosen as the suitable location for offshore outsourcing.

4 Empirical case study

In this section, we present an empirical case to illustrate the effectiveness of our method for location selection considering SCRE. Four alternative locations are considered in our study. This study pursues a generalized finding and proves the proposed method's effectiveness. In this study, we have been required to select the best offshore outsourcing location considering SCRE capability in the background of a single and explanatory case study. The chosen case is highly representative and valuable because it evaluates the global supply chain of spirit drinks with geographically remote locations worldwide. The supply chain is so complicated that only the focal producer has more than 30 production facilities. We will use the proposed method to select the most suitable locations step by step.

4.1 Identify the impacts of outer factors on RSCRE

1) Expert evaluation: Some experts are invited to describe outer factors that influence the resilience of the supply chain as well as the detailed capabilities of SCRE. The results are shown in the Appendix. More specifically, the nodes in the FCM will be acquired.

2) In this step, the experts judge the causal relations among the nodes as well as their intensity. AHP is implemented to make pairwise comparisons, and quantitative intensities are obtained. All experts have the same weights; thus, the outcome will be the average of all experts. The consistency ratio should be less than 0.1, and all numbers map into $[0, 1]$. The intensity levels are shown in Table 1.

3) Aggregate experts' opinions from different groups. Since the causal relations among nodes are highly complicated and uncertain in practice, multiple experts are invited to assess the causal relations among those external factors and capabilities. In this case, three groups of experts are invited to evaluate the causal relations between them. These three groups have different backgrounds, and they will give their opinions from different perspectives. The impact

Table 1: Intensity levels and their associated quantities from AHP

Intensity level	Quantity(expert1)	Quantity(expert2)	Quantity(expert3)	Average
None	0	0	0	0
Very Weak	0.03	0.055	0.026	0.037
Weak	0.06	0.062	0.076	0.066
Moderate	0.117	0.143	0.121	0.127
Strong	0.225	0.264	0.256	0.248
Very Strong	0.568	0.477	0.521	0.522
Consistency Ratio	0.07	0.07	0.07	0.045

of F12 (technological infrastructure) on Cap9 (collaboration) can be considered as an example. In the first group, seven experts conclude that technological infrastructure has a strong positive relationship with collaboration; two experts believe the relationship is solid, and only one thinks it is moderate. In the second group, six experts assign a strong relation between F12 and Cap9; one holds the view of a moderate relationship. And the results are shown in Table 2 and Table 3. See also in Appendix the interactions between the criteria and SC resilience capabilities.

Table 2: The adjacency matrix (Part A)

ID	F1	F2	F3	F4	F5	F6	F7	F8	F9	F10	F11	F12	F13	F14	F15	F16
F1	0	0	0	0	0	0	0	0	0	0	0	0	0	0	0	0
F2	0	0	0	0	-0.533	0	0	0	0.251	0	0	0	0	0	0	0
F3	0	0	0	0	0	0	0	0	0	0	0	0	0	0.523	0	0.248
F4	0	0	0	0	0	0	0	0	0	0	0	0	0	0	0	0
F5	0	0	0	0	0	0	0	0	0	0	0	0	0	0	0	0
F6	0	0	0.254	0	0	0	0	0	0	0	0	0	0	0	0	0
F7	0	0	0	0	0	0	0	0	0	0	0	0	0	0	0	0
F8	0	0	0	0	0	0	0	0	0	0	0	0	0	0	0	0
F9	0	0	0	0	0	0	0	0.067	0	0.248	0	0	0	0.251	0	0
F10	0	0	0	0	0	0	0	0	0	0	0	0	0	0	0	0
F11	0	0	0	0	0	0	0	0	0	0	0	0	0	0	0	0
F12	0	0	0	0	0	0	0	0	0	0	-0.067	0	0	0	0	0
F13	0	0	0	0	0	0	0	0	0	0.071	0	0	0	0.251	0	0
F14	0	0	0	0	0	0	0	0	0	0	0	0	0	0	0	0
F15	0	0	0	0	0	0	0	0	0	0	-0.067	0	0	0	0	0
F16	0	0	0	0	0	0	0	0	0	0	0	0	0	0	0	0
Cap1	0	0	0	0	0	0	0	0	0	0	0	0	0	0	0	0
Cap2	0	0	0	0	0	0	0	0	0	0	0	0	0	0	0	0
Cap3	0	0	0	0	0	0	0	0	0	0	0	0	0	0	0	0
Cap4	0	0	0	0	0	0	0	0	0	0	0	0	0	0	0	0
Cap5	0	0	0	0	0	0	0	0	0	0	0	0	0	0	0	0
Cap6	0	0	0	0	0	0	0	0	0	0	0	0	0	0	0	0
Cap7	0	0	0	0	0	0	0	0	0	0	0	0	0	0	0	0
Cap8	0	0	0	0	0	0	0	0	0	0	0	0	0	0	0	0
Cap9	0	0	0	0	0	0	0	0	0	0	0	0	0	0	0	0

Table 3: The adjacency matrix (Part B)

ID	Cap1	Cap2	Cap3	Cap4	Cap5	Cap6	Cap7	Cap8	Cap9
F1	0	0	0	0	0	0	0	0.531	0
F2	0	0.251	0	0.133	0	0	0	0	0
F3	0	0	0	0	0	0	0	0	0
F4	0	0	0	0	0	0	0	0	0
F5	-0.127	0	0	-0.253	0	0	0	-0.131	0
F6	0	0	0	0	0	0	0	0	0
F7	0	0	0.252	0	0.526	0	0	0	0
F8	0	0	0	0	0	0	-0.071	0	0
F9	0	0	0	0	0	0	0	0	0
F10	-0.388	0	0	-0.251	0	0	-0.131	0	-0.04
F11	0	-0.066	-0.127	0	0	0	0	0	0
F12	0.248	0.248	0.248	0	0.129	0	0	0	0.279
F13	0	0	0	0	0	0	0	0	0
F14	0	0	0	-0.068	0	0	-0.131	0	0
F15	0	0	0	0	0	0.068	0	0	0.131
F16	-0.525	0	0	0	0	0	0	0	0
Cap1	0	0	0	0	0	0	0	0	0
Cap2	0	0	0	0	0	0	0	0	0
Cap3	0	0	0	0	0	0	0	0	0
Cap4	0	0	0	0	0	0	0	0	0
Cap5	0	0	0	0	0	0	0	0	0
Cap6	0	0	0	0	0	0	0	0	0
Cap7	0	0	0	0	0	0	0	0	0
Cap8	0	0	0	0	0	0	0	0	0
Cap9	0	0	0	0	0	0	0	0	0

4) FCM inference. The FCM nodes' values are assigned to $[0, 1]$ to simulate the impacts of outer factors on SCRE capabilities. In this study, we set the initial state vector $V_{s_i}^0 = (0 \quad 0 \quad \cdots \quad 1 \quad \cdots \quad 0) \quad (n = 1, 2, \cdots, 16)$. The number in the initial state vector represents the external factors, and our one factor is given a value of 1; the outer factors are assigned to 0. The activation value of the SCRE capabilities can be obtained. In this way, a better perspective of the impact of each outer factor on the SCRE capabilities is provided. In Appendix can be see the impact of each outer factor on the 9 SCRE capabilities and the influence of each outer factor on the SCRE capabilities. F12 (technological infrastructure) has the most positive effects on SCRE, whereas F9 (tax rate) significantly impairs the whole resilience of the supply chain. The conclusion drawn from the table is that the offshore outsourcing practitioner should select locations with great technical infrastructure and a lower tax rate.

4.2 Weight different resilience capability

Step 1: The objective, criteria, sub-criteria, and alternatives of the decision-making problem are introduced in Section 3.2. Finally, 5 criteria, as well as 21 of their sub-criteria, are identified:

Technical aspects: (C1) Efficiency, (C2) Security, (3) Energy sustainability, (4) Circulation of capital, (5) Advanced technology, and (6) Technical innovation

Economic aspects: (C7) Operation cost, (C8) Investment cost, (C9) Production cost, (C10) Return on investment, and (C11) Maintenance cost

Political aspects: (C12) Foreign dependency, (13) Capability with respect to the national political and legislative situation, (14) Capability with respect to national energy policy objectives, and (15) Public policy and financial support

Social aspects: (C16) Social benefits, (17) Social acceptability, and (18) Job creation

Environmental aspects: (C19) Greenhouse emissions, (20) Land requirements, and (21) Impact on the ecosystem

Step 2: Construct direct relation matrixes according to the 4-level scale, which features inner dependence. Taking C7-C11 as an example, the initial relations among them are listed in

the Appendix. Not all direct relation matrixes are listed here due to space limitations.

Steps 2.1-2.2: The direct relation matrixes can be transformed into total relation matrixes to reveal their comprehensive relations. Still taking C7-C11 as an example, the overall relation matrix is shown in the Appendix.

Step 2.3: The impact diagram is constructed as introduced in Section 3. The horizontal axis refers to R+D, and the vertical axis is D-R. The impact diagram visualizes the direct and indirect relations, where D+R is the sum of relations among the elements and shows the importance of each element. D-R indicates the causal relations; $D - R > 0$ indicates that the element affects other elements to a greater extent than it is affected by them. The impact diagram of C7-C11 is shown in Appendix.

Step 2.4: The results reveal a strong inner dependence among the sub-criteria of the economic aspect. Thus, the inner dependence matrix is calculated. Table 8 in the appendix shows the inner dependence matrix of the economic aspect.
Taking $C7 - C9$ as an example, the total relation of C7-C9 is 0.101, and $R_{C7} = 0.101 + 0.243 + 0.088 + 0.111 + 0.119 = 0.661$. Therefore, the inner dependence of C7-C9 is $0.101/0.661 = 0.152$

Step 3: Now, DEMATEL and ANP are integrated to assign weights to different SCRE capabilities.

Step 3.1: First, we calculate the values of different criteria with respect to offshore outsourcing benefits. This step is processed by the AHP method using the 5-level scale. The following results are obtained:

Technical aspects: 0.41, Economical aspects: 0.18, Social aspects: 0.18, Environmental aspects: 0.11, and Political aspects: 0.12

Step 3.2: The initial unweighted supermatrix of ANP can be acquired by entering the vectors derived from DEMATEL and Step 2. The results are shown in the Appendix.
Multiplying the unweighted supermatrix by the criteria relative weights from Step 3.1 produces the normalized supermatrix. The supermatrix is then increased to a sufficiently large power until convergence occurs to obtain the limited supermatrix.

Step 4: The relative weights of the SCRE capabilities are determined with respect to benefits. The final priority values are found in the corresponding columns of the limited supermatrix. The results are shown in the Appendix.

4.3 Rank alternative locations and select optimal one in SCRE perspective

In this section, the optimal alternative locations for offshore outsourcing are selected by using TOPSIS based on the existing experts' evaluations. First, a group discussion is conducted in which the experts evaluate 4 potential alternative locations: L1, L2, L3, and L4. In this way, scores are acquired that represent how a location fulfills outer factors. A five-point scale is developed in the Appendix.

The scores of each outer factor for the locations consist of an initial vector, which is then input into the FCM to determine the adjacency as in Section 4.1. After several iterations, the FCM presents an equilibrium state that reflects the level of SCRE capabilities. The concrete process of the evolutionary process is shown in Appendix. In this study, the equilibrium state emerges after more than 4800 iterations. The equilibrium values generally reflect the final SCRE capability: the higher the value, the more elastic the supply chain will be. The sign $(+, -)$ indicates that the supply chain resilience will be enforced or damaged. For example, capability 8 (market position) reaches -0.6990 in location 1, which indicates that Cap8 will be impaired in location 1 with a degree of 0.699. Cap3 (anticipation) is 0.4296 in location 3 after many iterations. Therefore, Cap3 will be activated to some extent in location 3. The detailed results

are shown in the Appendix. In this way, the mechanism of evolutionary processes is revealed, and the SCRE capabilities in each location are presented for further decision-making.

Once the equilibrium values of the different capabilities in the 4 locations are obtained, the TOPSIS method is utilized to analyze the consistency of each alternative location with respect to the ideal solution from the resilience perspective. The weights of each capability from Section 4.2 will be considered.

First, we construct a decision matrix $D = (x_{mm})$ from Table 13. Then, we normalize the decision matrix by Eq. (12). The weights of each capability are considered in this step, and using Eqs. (14)-(18), the results are calculated and listed in Appendix. The most suitable location considering supply chain resilience is location 3, whose value is 0.6866. The different values of the SCRE capabilities in the four locations are shown in Fig. 2.

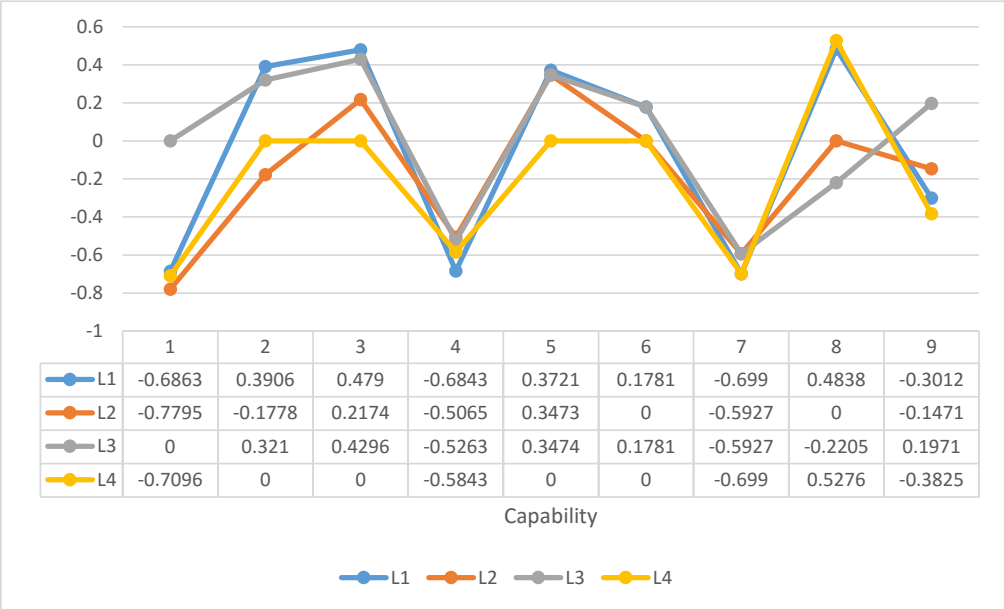

	1	2	3	4	5	6	7	8	9
L1	-0.6863	0.3906	0.479	-0.6843	0.3721	0.1781	-0.699	0.4838	-0.3012
L2	-0.7795	-0.1778	0.2174	-0.5065	0.3473	0	-0.5927	0	-0.1471
L3	0	0.321	0.4296	-0.5263	0.3474	0.1781	-0.5927	-0.2205	0.1971
L4	-0.7096	0	0	-0.5843	0	0	-0.699	0.5276	-0.3825

Figure 2: Comparison of the 4 locations

5 Sensitivity analysis

To investigate the impact of the SCRE's weights (developed by W_{Capi} for capability Capi, where $i = 1, 2, \cdots, 9$) on the selection of offshore outsourcing locations with the best benefits, we conduct a sensitivity analysis. Eleven experiments were conducted. In the Appendix can bee see the details of these experiments.

As shown in the Appendix, in the first nine experiments, the weight of each SCRE capability is set as the highest one by one, and the others are set at low and equal values. For example, in experiment 1, the weight of Cap1 is 0.5, and the weights of the remaining SCRE capabilities (Cap2-Cap9) are 0.0625. The highest weight is computed as 0.5 as follows. Since there are a total of 9 capabilities, 8 are assumed to be of equal importance and are allocated equal weights of 0.0625. This leaves the weight of Cap1 as 0.5, which ensures that the sum of all weights of the capabilities is 1. Similarly, in the next 8 experiments, we set each capability as the most important one by giving it a weight of 0.5 and leaving equal weights of 0.0625 for the remaining

capabilities. In experiment 10, the weights of each SCRE capability are equal to 0.111. In experiment 11, the real case in our study is shown.

As shown in the Appendix, location 4 has the highest score in 7/11 experiments (including the case study). Therefore, based on the assessments obtained, our offshore outsourcing location is comparatively insensitive to weights, with location 4 emerging as the winner in the majority of cases (7/11). However, in this study, the best option for practitioners is L3. This could be regarded as a special case that reveals that the selection in the real situation may be different than that in the theoretical analysis.

6 Results of the simulation of four alternative locations

In this section, we further investigate the acquired results and discuss some implications of the analyzed data. The supply chain resilience values are presented in Table 13. The results are gathered from the FCM dynamic process, which reveals the future trends of supply chain resilience. Although the optimal solution is identified by comparing its distance to the ideal solution, we explore some special cases by using the results of our proposed model.

6.1 Results of simulation of location 1

The results show that 5 resilience capabilities will be enforced and 4 resilience capabilities will be damaged. The final values range from -0.6990 to 0.4838. Visibility (Cap2), anticipation (Cap3) and adaptability (Cap6) are the highest in this location among the four alternatives, which indicates that these three capabilities will be increased to different extents. However, recovery capability (Cap4) and financial strength (Cap7) are significantly impaired compared with the other three alternatives.

6.2 Results of simulation of location 2

In location 2, the supply chain's adaptability (Cap4) and market position (Cap8) will not be influenced and thus will remain at a stable level. The anticipation capability (Cap3) and security (Cap5) will increase slightly (+0.2174 and +0.3473, respectively) in location 2. In addition, other capabilities will be damaged to different extends extents. Among these damaged capabilities, flexibility (Cap1) is greatly impaired, even compared with other places. Companies seeking flexibility in their supply chain should avoid choosing this location.

6.3 Results of simulation of location 3

In location 3, the flexibility of the supply chain will be stable and will not be influenced. Five capabilities (Cap2, Cap3, Cap5, Cap6, and Cap9) will be improved. Among those capabilities, adaptability (Cap6) and collaboration (Cap9) have their highest values at this location among the four alternatives, whereas the market position of this location has the lowest value compared with the other alternatives. Companies that are concerned with adaptability and collaboration should pay more attention to this location.

6.4 Results of simulation of location 4

The supply chain's capabilities of visibility (Cap2), anticipation (Cap3), security (Cap5), and adaptability (Cap6) are not influenced in location. It has a comparatively good market position among the four alternatives (the value is 0.5276). However, other resilience capabilities will be impaired.

Since offshore outsourcing refers to the transfer of some specific ownership business activities or resources to low-cost providers outside of the client company's country of origin, a new provider will be a new player in the SC network. The offshore outsourcing process can exert some impacts on SC resilience compared to in-home production. Many capabilities of SC resilience are enhanced, while some capabilities are weakened. In this part, we discuss the differences between offshore outsourcing and in-home production with respect to SC resilience. Hence, if a manager seeks to preserve or even improve some capabilities of SC resilience, they should consider whether or not to select offshore outsourcing; if they choose offshore outsourcing, they should also consider which location to select.

7 Conclusions and future works

Offshore outsourcing is a heated issue that has received extensive attention. However, the impacts of complicated and diverse environments on supply chain resilience may minimize the ability of supply chains to defend against risks. To overcome this problem, we propose to select a suitable location where the supply chain's resilience will be maximized based on an integrated MCDM method. The main contributions and innovations of this research paper could be summarized as follows. Firstly, this paper combines FCM and D number theory to the concept development if DCM that not only remains the abilities to represent uncertainty but also contributes to aggregating knowledge from different sources (experts/commanders). Since uncertain information fusion has been studied for many years, indicating that D number theory is an effective framework to represent and fuse uncertain information. The combination of D number theory and FCM is shown to be valuable approaches through illustration. Secondly, DEMATEL-ANP is implemented to quantify the weight in context of offshore outsourcing problem. From sensitivity analysis, we conclude that a concise result could be obtained. Overall, The proposed method can support practitioners while evaluating alternative outsourcing locations according to their impacts on the SC resilience. Experts perceived the main advantage of the proposed method in the ability to predict effects due to indirect implications, which are otherwise very difficult to predict, especially for large models. In fact, in our case, one location would improve resilient capabilities and two locations would rather damage it. Such location behavior could not been predicted without our simulation. For academics, this paper provides a groundwork for further studies because it is the first time that a research shows how offshore outsourcing location decision-making can improve, preserve or damage SC resilience. Looking to the future, empirical works would validate the influences detected. In addition, the developed hybrid method is generic, flexible and easily adaptable. Therefore, it could be applied easily to other sectors to represent messy problems with causalities and predict future outcomes.

Our future work involves the validation of the proposed model results by comparison with other techniques available in the literature for the selection of outsourcing locations.

Funding

This research is supported by the Fundamental Research Funds for the Central Universities(No. XDJK2019C085) and Chongqing Overseas Scholars Innovation Program(No. cx2018077).

Author contributions

L.Z designed, performed experiments and wrote the paper. F.X developed the method, conceived the experiments and revised the paper.

Conflict of interests

The authors declare no conflict of interest.

Bibliography

[1] Ali, S.; Hongqi, L.; Khan, S.U.; Zhongguo, Y.; Liping, Z. (2017. Success factors for software outsourcing partnership management: An exploratory study using systematic literature review. *IEEE Access*, 5, 23589–23612, 2017.

[2] Dekkers, R.(2000). Decision models for outsourcing and cor competencies in manufacturing. *International Journal of Production Research*, 38(17), 4085–4096, 2000.

[3] Dempster, A.P. (1967). Upper and lower probabilities induced by a multivalued mapping. *The annals of mathematical statistics*, 325–339, 1967.

[4] Dong, Y.; Zhang, J.; Li, Z.; Hu, Y.; Deng, Y.(2019). Combination of evidential sensor reports with distance function and belief entropy in fault diagnosis. *International Journal of Computers Communications & Control*, 14(3), 293–307, 2019.

[5] Fontela, E.; Gabus, A.(1976). *The dematel observer*, Battelle Geneva Research Center, Geneva, 1976.

[6] Gao, X.; Deng, Y. (2019). The generalization negation of probability distribution and its application in target recognition based on sensor fusion. *International Journal of Distributed Sensor Networks*,15(5), 381, 2019.

[7] Giret, A.; Julián, V.; Corchado, J.M.; Fernández, A.; Salido, M.A.; Tang, D.(2018). How to choose the greenest delivery plan: A framework to measure key performance indicators for sustainable urban logistics. *IFIP International Conference on Advances in Production Management Systems*, 181–189, 2018.

[8] Guan, X.; Liu, H.; Yi, X.; Zhao, J.(2018). The Improved Combination Rule of D Numbers and Its Application in Radiation Source Identification, *Mathematical Problems in Engeneering*, Article ID 6025680, 2018.

[9] Gurtu, A.; Searcy, C.; Jaber, M. (2016). Effects of offshore outsourcing on a nation. *Sustainable Production and Consumption*, 7, 94–105, 2016.

[10] Gylling, M.; Heikkilä, J.; Jussila, K.; Saarinen, M. (2015). Making decisions on offshore outsourcing and backshoring: A case study in the bicycle industry. *International Journal of Production Economics*, 162, 92–100, 2015.

[11] Han, Y.; Deng, Y.(2018). An enhanced fuzzy evidential dematel method with its application to identify critical success factors. *Soft computing*, 22(15), 5073–5090, 2018.

[12] Han, Y.; Deng, Y. (2018). An evidential fractal ahp target recognition method. *Defence Science Journal*, 68(4), 367–373, 2018.

[13] Han, Y.; Deng, Y.(2018). A hybrid intelligent model for assessment of critical *Ambient intelligence*, 9(6), 1933–1953, 2018.

[14] Han, Y.; Deng, Y. (2019). A novel matrix game with payoffs of maxitive belief structure, *International Journal of Intelligent Systems*, 34(4), 690–706

[15] Han, Y.; Deng, Y.; Cao, Z.; Lin, C.(2019). An interval-valued pythagorean prioritized operator-based game theoretical framework with its applications in multicriteria group decision making, *Neural Computing and Applications*, 1–19, 2019.

[16] Lai, Y.J.; Liu, T.Y.; Hwang, C.L.(1994). Topsis for modm. *European journal of operational research*, 76(3), 486–500, 1994.

[17] Li, Y.; Deng, Y.(2019). TDBF: Two Dimension Belief Function. *International Journal of Intelligent Systems*, 34(8), 1968–1982, 2019.

[18] Lin, S.; Li, C.; Xu, F.; Liu, D.; Liu, J. (2018). Risk identification and analysis for new energy power system in China based on D numbers and decision-making trial and evaluation laboratory (DEMATEL), *Journal of Cleaner Production*,180, 81–96, 2018.

[19] Liu, P.; Zhang, X.(2019). A multicriteria decision-making approach with linguistic D numbers based on the Choquet integral, *Cognitive Computation*, 11(4), 560–575, 2019.

[20] Mo, H.; Deng, Y.(2019). An evaluation for sustainable mobility extended by D numbers, *Technological and Economic Development of Economy*, 25(5), 802-819, 2019.

[21] Mousavi, S.M.; Antuchevičienė, J.; Zavadskas, E.K.; Vahdani, B.; Hashemi, H.(2019). A new decision model for cross-docking center location in logistics networks under interval-valued intuitionistic fuzzy uncertainty, *Transport*, 34(1), 30–40, 2019.

[22] Mukherjee, D.; Gaur, A.S.; Datta, A.(2013). Creating value through offshore outsourcing: An integrative framework, *Journal of International Management*, 19(4), 377–389, 2013.

[23] O'keefe, J.; Nadel, L.(1978). *The hippocampus as a cognitive map*, Clarendon Press, Oxford, 1978.

[24] Papageorgiou, E.; Stylios, C.; Groumpos, P.(2003). Fuzzy cognitive map learning based on nonlinear hebbian rule, *Australasian Joint Conference on Artificial Intelligence*, 256–268, 2003.

[25] Pereira, V.; Anderson, V.(2012). A longitudinal examination of hrm in a human resources offshoring (hro) organization operating from india. *Journal of World Business*, 47(2), 223–231, 2012.

[26] Saaty, T.L.(1980). *The analytic hierarchy process: planning. Priority Setting. Resource Allocation*, MacGraw-Hill, New York International Book Company, 1980.

[27] Saaty, T.L.(1996). *Decision making with dependence and feedback. The analytic network process*, Rws Publications, 1996.

[28] Shafer, G., et al.(1976). *A mathematical theory of evidence*, vol. 1. Princeton university press, Princeton, 1976.

[29] Shankar, R.; Choudhary, D.; Jharkharia, S.(2018). An integrated risk assessment model: A case of sustainable freight transportation systems, *Transportation Research Part D: Transport and Environment*, 63, 662–676, 2018.

[30] Shukla, A.; Agarwal, P.; Rana, R.; Purohit, R.(2017). Applications of topsis algorithm on various manufacturing processes: A review. *Materials Today: Proceedings*, 4(4), 5320–5329, 2017.

[31] Singh, P.; Agrawal, R.(2018). A customer centric best connected channel model for heterogeneous and iot networks, *Journal of Organizational and End User Computing*, 30(4), 32–50, 2018.

[32] Sun, R.; Deng, Y.(2019). A new method to identify incomplete frame of discernment in evidence theory, *IEEE Access*, 7, 15547–15555

[33] Sun, R.; Deng, Y.(2019). A new method to determine generalized basic probability assignment in the open world, *IEEE Access*, 7, 52827–52835, 2019.

[34] Tsai, S.B.; Zhou, J.; Gao, Y.; Wang, J.; Li, G.; Zheng, Y.; Ren, P.; Xu, W.(2017). Combining fmea with dematel models to solve production process problems. *Plos One*, 12(8), e0183, 634, 2017.

[35] Yadlapalli, A.; Rahman, S.; Gunasekaran, A.(2018). Socially responsible governance mechanisms for manufacturing firms in apparel supply chains. *International Journal of Production Economics*, 196, 135–149, 2018.

[36] Yang, H.; Deng, Y. (2019). A bio-inspired optimal network division method, *Physica A: Statistical Mechanics & Its Applications*, 527, 210–219

[37] Yang, H.; Deng, Y.; Jones, J. (2018). Network division method based on cellular growth and physarum-inspired network adaptation, *International Journal of Unconventional Computing*, 13(6), 477–491, 2018.

[38] Yoon, K.; Hwang, C.L. (1981). *Multiple attribute decision making: methods and applications*, Springer-Verlag, Berlin, 1981.

[39] Yoon, K.P.; Kim, W.K.(2017). The behavioral topsis. *Expert Systems with Applications*, 89, 266–272, 2017.

APPENDIX

Table 4: Outer factors influencing SCRE

Factors	Description
F1	Quality of the final production
F2	Transport infrastructure
F3	Government regulation
F4	Culture distance
F5	Delivery time
F6	Political risks
F7	Facility security
F8	Management cost
F9	Tax rates
F10	Transport cost
F11	Monitoring cost
F12	Technological infrastructure
F13	Exchange rates
F14	Labour cost
F15	Technical and language skills of employees
F16	Origin denomination regulatory compliance

Table 5: Outer factors influencing SCRE

Capability	Description
Cap1	Flexibility
Cap2	Visibility
Cap3	Anticipation
Cap4	Recovery
Cap5	Security
Cap6	Adaptability
Cap7	Financial strength
Cap8	Market position
Cap9	Collaboration

Table 6: The adjacency matrix

ID	Cap1	Cap2	Cap3	Cap4	Cap5	Cap6	Cap7	Cap8	Cap9	Sum
F1	0	0	0	0	0	0	0	0.29520	0	0.2952
F2	-0.6919	0	0	-0.5923	0	0	-0.6878	0.4607	-0.3758	-1.887
F3	-0.6442	0	0	-.3766	0	0	-0.4607	0	0	-1.4814
F4	0	0	0	0	0	0	0	0	0	0
F5	-0.1864	0	0	-0.2320	0	0	0	-0.1864	0	-0.6048
F6	-0.7849	0	0	-0.4784	0	0	-0.5787	0	0	-1.8421
F7	0	0	0.2320	0	0.2952	0	0	0	0	0.5272
F8	0	0	0	0	0	0	-0.1503	0	0	-0.1503
F9	-0.5931	0	0	-0.5601	0	0	-0.5511	0	-0.2902	-1.9945
F10	-0.2676	0	0	-0.2320	0	-0.1864	0	0	-0.1242	-0.8102
F11	0	-0.1503	-0.1864	0	0	0	0	0	0	-0.3367
F12	0.2320	0.3410	0.3986	0	0.1864	0	0	0	0.2320	1.3901
F13	-0.5241	0	0	-0.5096	0	0	-0.4798	0	-0.2523	-1.7838
F14	0	0	0	-0.1503	0	0	-0.1864	0	0	-0.3367
F15	0	0.3040	0.3742	0	0	0.1503	0	0	0.1864	1.015
F16	-0.2952	0	0	0	0	0	0	0	0	-0.2952

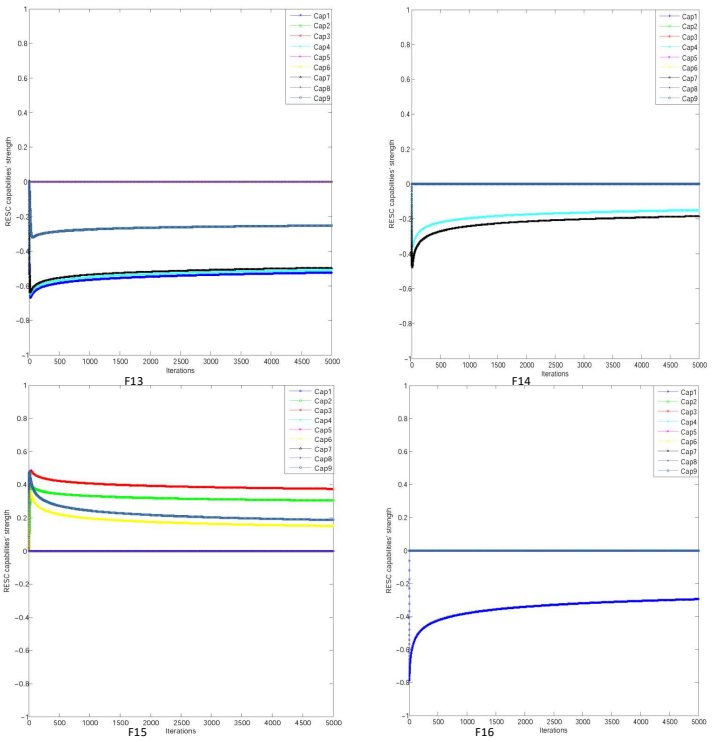

Figure 3: The impact of each outer factor on the 9 SCRE capabilities

Table 7: The adjacency matrix

I	C7	C82	C9	C10	C11
C7	0.122	0.305	0.101	0.494	0.304
C8	0.344	0.167	0.243	0.586	0.476
C9	0.309	0.203	0.088	0.458	0.368
C10	0.132	0.129	0.111	0.133	0.160
C11	0.075	0.125	0.119	0.317	0.095

Table 8: The inner dependence matrix corresponding to the economic aspect

	C7	C8	C9	C10	C11
C7	0.124	0.328	0.152	0.249	0.217
C8	0.350	0.180	0.367	0.295	0.339
C9	0.315	0.219	0.133	0.231	0.262
C10	0.135	0.138	0.168	0.067	0.114
C11	0.076	0.135	0.180	0.160	0.067

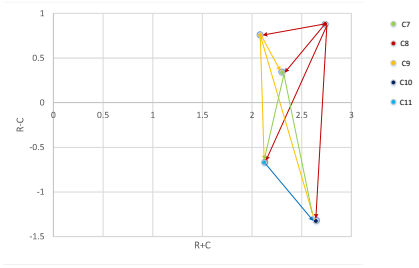

Figure 4: The inner dependence of economic aspects

Author index